# Safely Building New Houses in the Geul Catchment:

## How to mitigate the impact on flooding?

D.W. Idsinga

# Safely Building New Houses in the Geul Catchment:

## How to mitigate the impact on flooding?

by

D.W. Idsinga

to obtain the degree of Master of Science in Water Management
at the Delft University of Technology,
to be defended publicly on Tuesday February 6, 2024 at 11:00 a.m.

| | | |
|---|---|---|
| Student number: | 4918630 | |
| Project duration: | March 1, 2023 – February 6, 2024 | |
| Thesis committee: | Dr. ir. Rolf Hut | TU Delft (Chair) |
| | Dr. Marcus Hrachowitz | TU Delft |
| | Mark de Weerd MSc | Royal HaskoningDHV |
| | Rinske Hutten MSc | Deltares |
| | Joost Buitink PhD | Deltares |

An electronic version of this thesis is available at http://repository.tudelft.nl/.

Cover Image: Confluence of the Geul and the mill branch at the downstream end of Valkenburg, photo taken July 28, 2023.

# Preface

This report is my final work as a student. This research is conducted to obtain the Master of Science degree in Civil Engineering with the track Water Management. I spent the last 11 months investigating the hydrology in the Geul catchment and modelling the impact of housing on the July 2021 flood event. It resulted in a workflow for provinces to investigate the impact of housing on the catchment hydrology.

After a period of searching for the research goal and overcoming software problems, I could apply my gained hydrological knowledge. It gave me more insight into the workfield of hydrology and its problems. Hydrology is not as strict, catchable, and straightforward as math problems and the truth is not known. I learned to handle these uncertainties to give a substantiate conclusion. This research showed that solving problems by one hydrological model is not desirable. This model can give the right results for the wrong reasons, is designed for only a short period, or is not capable to solve a problem. Working with multiple models improves the certainty, but the most important thing is to know why a hydrological model gives certain results. All these things I learned during this research and I am going to use and expand in my career as an engineer.

First of all, I want to thank RoyalHaskoningDHV for the opportunity to do my master thesis at this company. I also want to thank my main supervisors Rolf Hut and Mark de Weerd for their help every week. The advices, positivity, and critical and open minded thinking helped me during this research. In addition, I want to thank Rineke Hulsman and Rinske Hutten for their help with D-HYDRO, which sometimes made me hopeless. I also thank Angela Klein and Joost Buitink for their help with Wflow_sbm. Further, I thank Markus Hrachowitz for his hydrological knowledge and his supervising. In addition, I want to thank Jerom Aerts for his time during his PhD for questions about the eWaterCycle and the Geul catchment. Last but not least, I thank all the RoyalHaskoningDHV colleagues who helped me along the way.

Lastly, I want to thank family, friends, and my wife Janniek for the support in these study years. Especially Janniek, to whom I married in the meantime, for her critical thinking, and keeping track of my freetime.

Enjoy reading!

*D.W. Idsinga*
*Waardenburg, January 2024*

# Abstract


In July 2021 severe flooding occurred in the South of Limburg, Belgium, and Germany due to heavy precipitation. Extreme precipitation events like this are expected to occur more often in our changing climate. Urbanization is thought to be another contributing factor to the July 2021 flood event. The Netherlands is expected to increase urbanization as a solution to its housing shortage. To make room for urbanization, while minimizing the effect of climate change, the government wants to make ”water and soil leading”, *Water en Bodem Sturend*, in the decision-making about the layout of the Netherlands.

Therefore, the goal of this research is to investigate the best suitable subcatchment for the construction of new residential houses within the Geul catchment, in terms of flooding. The July 2021 flood event is used as a reference. The first step was to investigate the hydrological response of the Geul catchment. Secondly, this hydrological response was modelled by the semi-distributed hydrological models HBV coupled to D-RR and by the distributed model Wflow_sbm. HBV and D-RR are set up in this research, while Wflow_sbm is adopted from Klein (2022) and Bouaziz (2022). The hydrological models are coupled to the Geul hydrodynamic model D-HYDRO of Hulsman, Weijers, Verstegen, and Goedbloed (2023). The building plans in the Geul catchment were investigated and scenarios were constructed. These scenarios were simulated in the hydrological models. This method resulted in a workflow that can be found in Idsinga (2024). The workflow can be applied on analyses of different land cover types.

The modelled hydrographs showed differences between the hydrological models. Each model better describes one part of the hydrological response compared to the other. HBV and D-RR better represent the subsurface flow and describe the hydrological response during consecutive precipitation events. Wflow_sbm represents the overland flow flux better and therefore describes the hydrological response during the July 2021 flood event. The modelled flood extents during the July 2021 flood event are also compared to the estimated extent by Slager, de Moel, and de Jong (2021). Wflow_sbm showed better similarity to the measured flood extent than HBV and D-RR.

The Province of Limburg wants to build 18,730 new houses in the South of Limburg. This results in an increase of 6 $km^2$ paved area. In this research, this increase is applied to different locations in the Geul catchment. Next, the impact of completely paved subcatchments was investigated. The relatively small 6 $km^2$ increase in paved area did not result in different discharge behaviour and the total area of the flood extent showed a small difference. However, it impacted the flooded paved area. Building far from the river on the hills resulted in no increase in the flooded paved area. New houses in the valleys, close to the river, are more exposed to flooding. In the Meerssen subcatchment, the added paved area was responsible for 95% of the total increase in the flooded paved area. This was also the case in the Gulp subcatchment, where about 90% of the increase in flooded paved area came from the added paved area.

The Meerssen subcatchment is the most vulnerable to flooding. This subcatchment contains the most paved area and more runoff will result in a more flooded paved area. A completely paved Gulp subcatchment results in a less flooded paved area than building 6 $km^2$ close to the Geul in the Meerssen subcatchment. When the Belgians build new houses in the Sippenaeken subcatchment, the Netherlands will receive more water during an extreme event such as in July 2021.

The letter *Water en Bodem Sturend* states that new houses must be built in sensible locations. In this research, the location of new houses is found to be important for the hydrological response. Building close to the river results in a more flooded paved area than building far from the river. The Gulp subcatchment is the least vulnerable to flooding and can be considered the best building location for new houses among the three investigated subcatchments.

# Samenvatting

In juli 2021 zorgde extreme regenval voor een grote overstroming in Zuid-Limburg, België en Duitsland. De verwachting is dat extreme buien als deze vaker zullen voorkomen in ons veranderend klimaat. Een andere belangrijke factor tijdens de overstroming in juli 2021 is de verstedelijking. Nederland gaat meer huizen bouwen vanwege het huizentekort. Om meer huizen te kunnen bouwen én rekening te houden met klimaatverandering, wil het Kabinet *Water en Bodem Sturend* maken in ruimtelijke plannen.

Daarom is het doel van dit onderzoek om het beste deelgebied te vinden om nieuwe huizen te bouwen in het Geul gebied, aangaande overstromingen. De overstroming in juli 2021 is de referentie. De hydrologie in het Geul gebied is onderzocht in de eerste stap. Vervolgens is dit gemodelleerd met het semi-gedistribueerde hydrologische model HBV, gekoppeld met D-RR, en met het gedistribueerde model Wflow_sbm. HBV en D-RR zijn opgezet in dit onderzoek en Wflow_sbm is overgenomen en aangepast van Klein (2022) en Bouaziz (2022). De hydrologische modellen zijn gekoppeld aan het Geul hydrodynamische model D-HYDRO van Hulsman et al. (2023). De bouwplannen in het Geul gebied zijn onderzocht en scenario's zijn opgezet om het effect te beoordelen. Deze scenario's zijn gesimuleerd in de gekoppelde hydrologische modellen. Deze methode resulteerde in een workflow die beschreven staat in Idsinga (2024). De workflow kan worden toegepast in analyses van andere typen landgebruik.

De gemodelleerde debieten lieten verschillen zien tussen de hydrologische modellen. Elk model beschrijft een deel van de hydrologie beter dan het andere model. HBV en D-RR simuleren de ondergrondse afstroming beter en beschrijven daardoor de hydrologie tijdens opeenvolgende buien beter. Wflow_sbm simuleert de oppervlakkige afstroming beter en beschrijft daardoor de hydrologie tijdens de overstroming in juli 2021 beter. Verder zijn de gemodelleerde overstromingsvlakten vergeleken met de bepaalde overstromingsvlakte door Slager et al. (2021). De overstromingsvlakte van Wflow_sbm komt beter overeen met de werkelijke juli 2021 overstroming dan die van HBV en D-RR.

De Provincie Limburg wil 18,730 nieuwe huizen gaan bouwen in Zuid-Limburg. Dit resulteert in 6 $km^2$ meer bebouwing. In dit onderzoek is deze toename toegepast op verschillende locaties in het Geul gebied. Daarnaast is het effect onderzocht van compleet bebouwde deelgebieden. De relatief kleine toename van 6 $km^2$ aan bebouwd gebied veranderde het afvoergedrag niet. De totale overstromingsvlaktes veranderden licht, maar de bebouwde overstromingsvlaktes veranderden significant. Het bouwen van nieuwe huizen op de heuvels, ver van de Geul, zorgde niet voor een toename van het overstroomde bebouwde gebied. Nieuwe huizen in de dalen, vlakbij de Geul, zijn meer blootgesteld aan overstromingen. De extra bebouwing zorgde voor 95% van de totale toename aan overstroomd bebouwd gebied in het Meerssen deelgebied. Dit was ook het geval in het Gulp deelgebied, waar 90% van de toename in overstroomd bebouwd gebied kwam door de extra bebouwing.

Het deelgebied Meerssen wordt het meest blootgesteld aan overstromingen. Dit deelgebied bevat de meeste bebouwing en meer afvoer zal leiden tot meer overstroomd bebouwd gebied. Een compleet bebouwd Gulp deelgebied zorgt voor minder overstroomd bebouwd gebied dan 6 $km^2$ bebouwing vlakbij de Geul in Meerssen. Wanneer de Belgen meer huizen bouwen in het Sippenaeken deelgebied, zal Nederland meer water ontvangen tijdens extreme neerslag als in juli 2021.

De Kamerbrief *Water en Bodem Sturend* stelt dat gebouwd moet worden op verstandige locaties. In dit onderzoek is gevonden dat de locatie van nieuwe huizen inderdaad uitmaakt voor de hydrologie. Het bouwen van nieuwe huizen dicht bij de Geul zorgt voor meer overstroomd bebouwd gebied dan bij het bouwen ver van de Geul. Het Gulp deelgebied is het minst kwetsbaar voor overstromingen en kan daardoor worden gezien als het beste deelgebied voor het bouwen van nieuwe huizen, van de drie onderzochte deelgebieden.

# Contents

# 1

# Introduction

## 1.1. Introduction

In July 2021 severe flooding occurred in the South of Limburg, Belgium, and Germany due to heavy precipitation. More than 150 mm of rain fell in the South of Limburg on Tuesday 13 and Wednesday 14 July 2021 (KNMI, 2021). The amount of precipitation on these two days was more than two times the normal value for July. The subsequent flooding led to at least 433 million Euros damage and at least 220 persons who sadly passed away in Belgium and Germany (NOS Nieuws, 2021; RTL Nieuws, 2023). Intense rainfall like this is expected to occur more often in our changing climate (KNMI, 2021).

Another driver of the July 2021 flood event is urbanization. According to Yang, Ni, Tian, and Niyogi (2021), the impact of cities and climate warming together on the rainfall anomaly is 50% larger than the impacts alone. The Netherlands is expected to increase urbanization as a solution to its housing shortage (NOS Nieuws, 2023; Rijksoverheid.nl, 2023). This is the result of population growth as older people live longer at home, fewer people per home, and migration. The House of Representatives has set the goal to build 961.000 houses before 2030, to address this problem. Increased urbanization results in more impervious areas, leading to increased surface runoff during a precipitation event (Ruby, 2006). Increased urbanization in combination with heavier precipitation events due to climate change is a major challenge that requires proper spatial planning (van Hattum, Blauw, Jensen, & de Bruin, 2016).

To make room for urbanization, while minimizing the effect of climate change, the government wants to make water and soil the leading factors (*Water en Bodem Sturend*) in decision-making about the layout of the Netherlands (Rijksoverheid, 2022). Minister Harbers and Secretary of State Heijen of the Ministry of Infrastructure and Watermanagement wrote a letter to the House of Representatives (Harbers & Heijnen, 2022). The main goal of the letter is to improve the spatial planning of the Netherlands by achieving sufficient clean water and healthy soil now and in the future (Harbers & Heijnen, 2022). Measures are recommended to be more resilient to droughts and floods. Creating more space for holding, storing, and draining water in the spatial planning, land use, and land management of the Netherlands improves flood resilience. This may seem a contradiction to the large building plans of the same House of Representatives; however, the plans should go hand in hand (Westenbrink, 2022). The *Water en Bodem Sturend* letter suggests building in 'sensible locations' (H2O ACTUEEL, 2022). This means that building should not be allowed in locations where the water function is leading.

In the Netherlands, the primary entities working on spatial decisions are municipalities and provinces, with the waterboards having more of an advisory role (Klostermann & Veraart, 2022). To connect these organizations, the *Omgevingswet* will contain a *Weging van waterbelang* (Weighing of water importance) (Klostermann & Veraart, 2022; Rijksoverheid, 2023). The municipalities and provinces have to take into account the view of the waterboard in the new spatial planning process (Informatiepunt Leefomgeving, 2023). However, the *Weging van waterbelang* occurs on the scale of the spatial plan. For example, compensation is determined for an increase in paved surface, or water extraction makes the location of the building not desirable.

## 1.2. Modelling

Changes in the hydrological response can be modelled with a hydrological model. A hydrological model calculates the runoff to a river for a catchment for a given precipitation event (Devia, Ganasri, & Dwarakish, 2015). The model is a simplified representation of the hydrologic processes in reality, which are shown in Figure 1.1. Many different hydrological models are used for rainfall-runoff modelling (Sitterson et al., 2017). They are often not reproducible as the code and data are often not made available regularly (Horton, Schaefli, & Kauzlaric, 2022; Hutton et al., 2016). Hut et al. (2022) built the eWaterCycle platform to tackle this problem. The platform provides access to preexisting models and data sources, which are open and FAIR (Findable, Accessible, Interoperable, and Reproducible). The eWaterCycle platform makes it possible for hydrologists to do hydrological experiments and focus on the hydrology, and not on the computer science behind the models. This leads to a shorter cycle time between an idea and an experiment, and the platform supports fully reproducible experiments.

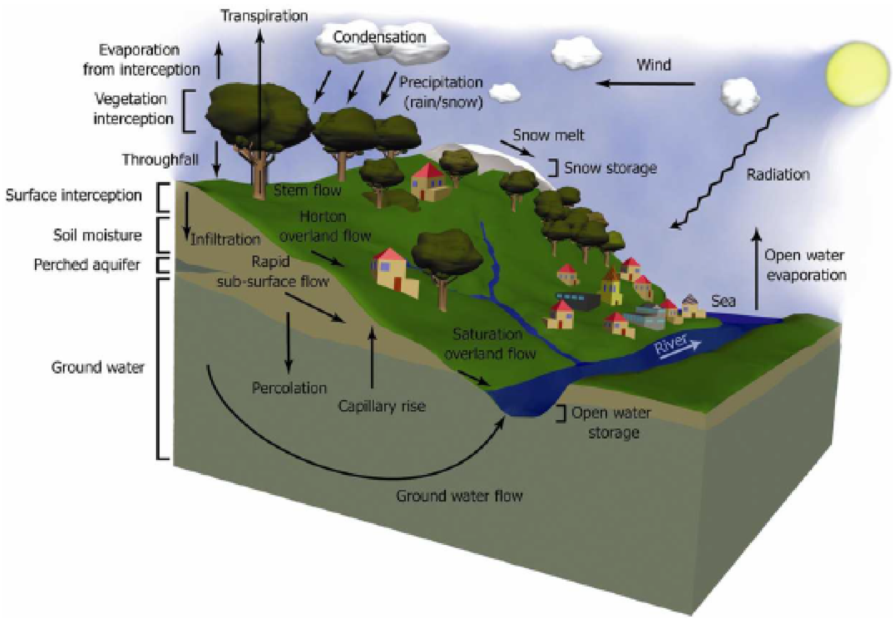


Figure 1.1: An example of the main hydrological processes in a catchment (Savenije, 2009).

The calculated runoff by the hydrological model is the input for a hydrodynamic model. A hydrodynamic model calculates the movement of water in a stream by solving fluid motion equations (Pasquier, He, Hooton, Goulden, & Hiscock, 2019). The most used and simplest hydrodynamic model type is a one-dimensional (1D) model. This model calculates the flow in and along a stream. The water does not leave the stream, so flood mapping is not possible. A two-dimensional model (2D) deals with flood-plains, however it is computationally more extensive than the 1D model. 1D-2D coupled hydrodynamic models combine the strengths of the 1D and 2D models. A 1D-2D model contains flood mapping and has less calculation time than a 2D model. The 1D part simulates the movement of water in the stream, and the 2D part simulates the flow outside the stream. An example of a 1D-2D simulation with the D-HYDRO Suite 1D2D, developed by Deltares, is shown in Figure 1.2. D-HYDRO, known internationally as Delft3D, is an example of a 1D-2D hydrodynamic modelling software. It is the successor of SOBEK2, which is also developed by Deltares and allows for integrated surface water modelling (Deltares, n.d.-a).

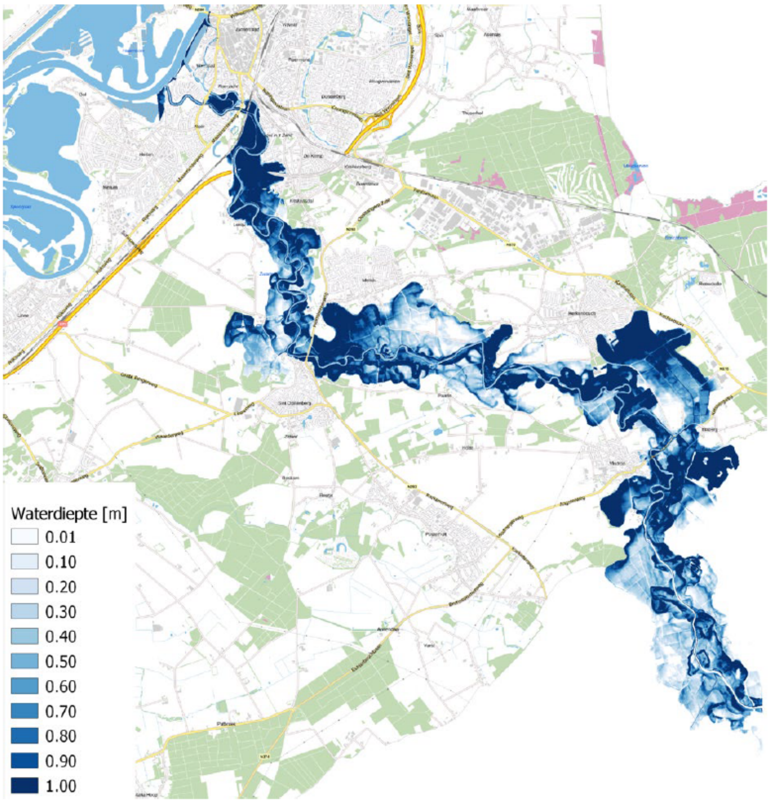


Figure 1.2: An example of a hydrodynamic simulation of the Rur river, in the North of Limburg (Elmensdorp, 2023).

The models are as complete, accurate, and detailed as possible approximations of reality, within the limits of data availability, model runtime, and model limitations. The models are calibrated and validated for historical extreme precipitation events.

## 1.3. Research Objective

The goal of this research is to investigate the best suitable subcatchment for the construction of new residential houses within the Geul catchment, in terms of flooding. By doing so, the housing shortage and the policy *Water en Bodem Sturend* are linked for this catchment. The July 2021 flood event is used as a reference for this research. This results in the following research question:

*Where can new houses be build in the Geul catchment, with the least amount of impact on peak discharge of the July 2021 flood?*

The research consists of four steps to answer the research question. Each step is described by a subquestion. The subquestions are elaborated in detail below, and an overview is given in Figure 1.3 afterward.

1. *What is the current hydrological response of the Geul catchment?*

The first step of the research is understanding the hydrology in the Geul catchment. This is needed to understand the underlying processes of the response of the catchment to a precipitation event and the flood event on 13 and 14 July 2021. The better the understanding, the better the hydrological models can be set up. The July 2021 flood event is used as reference for the simulation of scenarios for spatial development. Understanding the hydrological response to the event results in a better interpretation of the simulation results.

2. *How well do HBV + D-RR - D-HYDRO and Wflow_sbm - D-HYDRO describe the hydrological response of the Geul catchment?*

Two types of hydrological models are investigated in this research. The models are (re)calibrated and should provide the best possible representation of the hydrological response of the Geul catchment. The first model type consists of the semi-distributed HBV and D-Rainfall Runoff (D-RR). HBV calculates the runoff of the unpaved area, and D-RR calculates the runoff of the paved areas. The Waterboard of Limburg currently uses the HBV-96 of Bergström (1976) with the software of SMHI (n.d.). However, this model is not FAIR (Findable, Accessible, Interoperable, and Reproducible). The software does not allow to investigate the underlying processes. Because of this, it is chosen to build a new, FAIR, HBV model. The distributed Wflow_sbm model is the second type of model and calculates the runoff per grid cell. This model is built by Klein (2022) and further developed by Bouaziz (2022). Both hydrological models are coupled to the D-HYDRO model of the Geul, built by Royal HaskoningDHV (RHDHV) (Hulsman et al., 2023). The model results are assessed and the models are compared.

3. *What are the building plans in the Geul catchment?*

The third step provides insight in the building plans of the Province of Limburg. Based on these plans, scenarios are constructed to investigate the impact of building new houses and their locations on the hydrological response. Each scenario generates a new parameterset for the hydrological models, based on the original parameterset and meteorological data. Next, the parameter set is applied to each hydrological model.

4. *How does the hydrological response of the Geul catchment change by building additional houses?*

The constructed scenarios and the corresponding parametersets in step 3 are executed in D-HYDRO. Each building scenario has a different impact on the hydrological response. The change in hydrological response is investigated by changes in the hydrographs and flood extents.

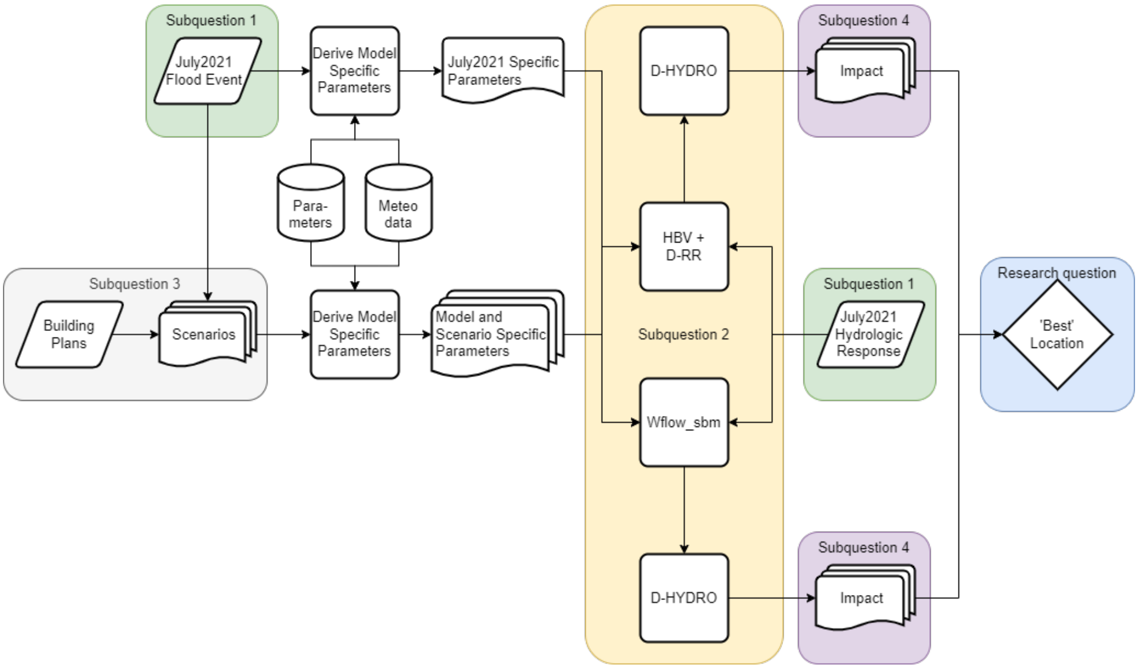


Figure 1.3: Setup of the conducted research.

## 1.4. Structure

This research is divided in seven chapters. The study area and hydrological response are described in Chapter 2. The method and model representations of this research are given in Chapter 3. Chapter 4 presents the results. Chapter 5 gives the discussion about the research. Last but not least, Chapter 6 gives the conclusion and Chapter 7 gives the recommendations of this research.

# 2

# Study Area

Chapter 2 describes the characteristics of the Geul catchment. Section 2.1 contains the topography of the catchment. Section 2.2 describes the hydrologic response of the Geul catchment. The hydrogeology is described in Section 2.3. The land cover is given in Section 2.4. Section 2.5 contains the definition of the subcatchments and their main characteristics. Lastly, the Geul river system is explained in Section 2.6, including control structures and water retention basins.

## 2.1. Topography

The Geul is a tributary of the river Meuse and is located in the South of Limburg. The Geul catchment is shown in Figure 2.1 and has a size of 340 $km^2$. The Geul springs in the Belgian Ardennes and flows into the Meuse at Bunde. Around Gulpen, the tributaries Eyserbeek, Gulp, and Selzerbeek flow into the Geul. The main part of the catchment, 52%, is in the Netherlands. 42% of the catchment is in Belgium and 6% in Germany (Klein, 2022). The Geul catchment has a hilly landscape with altitudes ranging from 17 to 374 meters (Dautrebande, Leenaars, Schmitz, & Vanthournout, 2000; European Environment Agency, 2017).

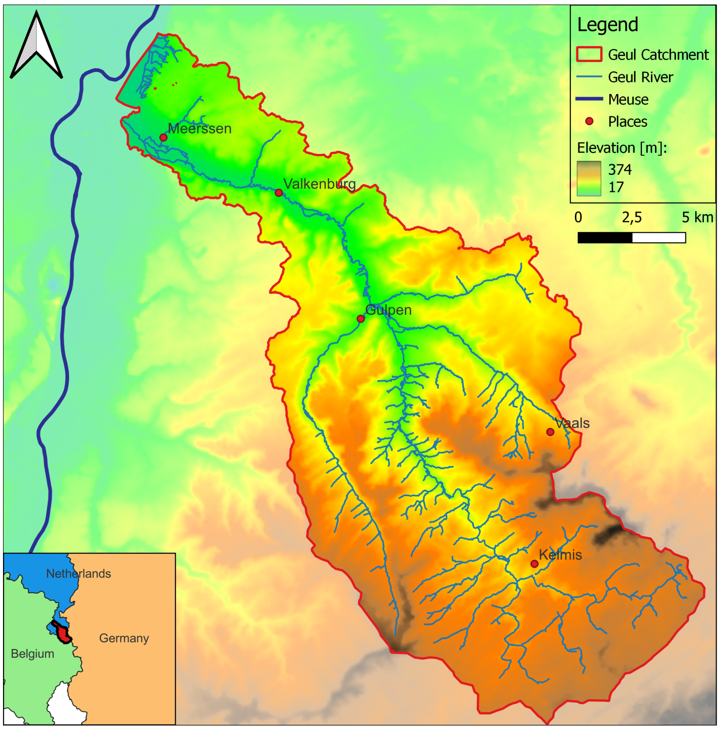


Figure 2.1: Elevation map of the Geul catchment, based on data from the European Environment Agency (2017).

## 2.2. Hydrological Response

A schematic view of the hydrological processes that result in river flow is presented in Figure 2.2. The hydrological response of the Geul catchment is explained on the basis of this figure. The hydrological processes became more extreme during the July 2021 flood event.

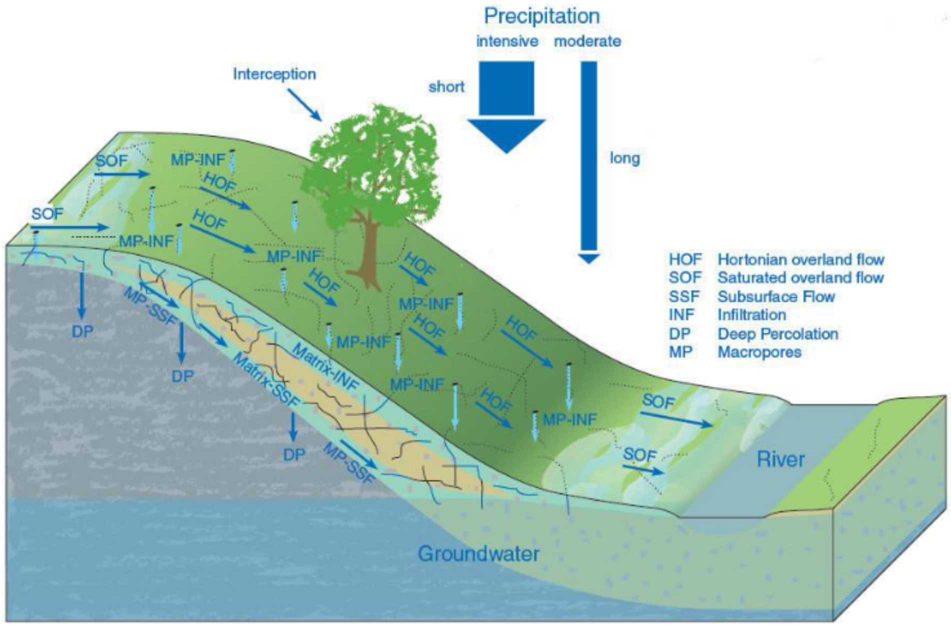


Figure 2.2: Schematic view of the hydrological processes wich result in river flow in the Geul catchment (Bureau Stroming, 2022).

When it starts to rain, the precipitation will partly infiltrate into the soil. The amount and speed of infiltration depends on the infiltration capacity and the degree of saturation of the soil (Elmensdorp, 2023). The infiltration capacity is determined by the type of subsoil and soil cover. The subsoil determines the amount of water that can be stored in the soil. The type of subsoil varies over the catchment, as is explained in Section 2.3. The infiltration also depends on the permeability of the soil cover. There is for example more infiltration in a forest than in agricultural land. The smallest amount of infiltration is in paved areas, where the precipitation runs off to the sewers and streams. The variability of the soil cover in the catchment is explained in Section 2.4. Each subcatchment reacts differently to a precipitation event. The differences are explained in Section 2.5

A part of the infiltrated water flows just below the soil surface. The infiltrating precipitation encounters an impermeable layer and flows down the slope over this layer, this is called subsurface flow (Bureau Stroming, 2022). The water is released in the stream in the valley, at the end of the slope. The remaining water flows to the groundwater, which is several meters up to 40 meters below the surface. The overal direction of flow is to the northwest. The groundwater flow contributes to the streams and the Meuse. As the groundwater flow is very slow, the water takes several months from infiltration to outflow (Elmensdorp, 2023).

When the precipitation intensity is larger than the infiltration capacity, hortonian overland flow occurs (Bureau Stroming, 2022). This plays an important role in paved areas and on steeply sloping agricultural fields, where the most of the water can not infiltrate into the soil. When the temporal storages are filled and the soil is saturated, saturation overland flow occurs. The excess water runs off from the hills to the streams. Lastly, barren fields generate fast runoff, as there are no crops that can slow down the overland flow. The difference in infiltration capacity can be seen between the Dutch and Belgian part of the Geul catchment. As is explained in Section 2.3, the Belgian part has a thin soil and contains impermeable rocks. This results in less storage and a faster response to precipitation than the Dutch part. The Dutch area acts like a sponge, because of the chalk layers (Elmensdorp, 2023).

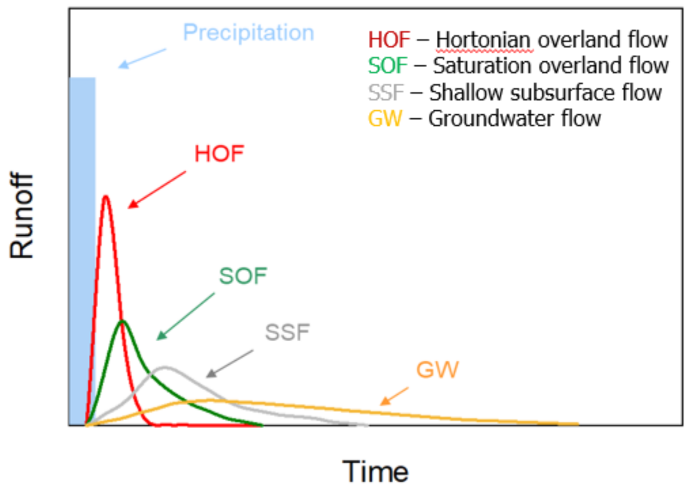


Figure 2.3: Schematic view of the hydrological processes wich result in river flow in the Geul catchment (Hrachowitz, 2021).

The hydrological processes have different timescales, as can be seen in Figure 2.3 (Hrachowitz, 2021). Hortonian overland flow is the fastest hydrological process and generates the peak discharge. Saturation overland flow is also a fast process, but happens when the soil is saturated and is slower generated. Saturation overland flow and subsurface flow determine together how fast the discharge is dropped to the base flow. Subsurface flow has some delay, because the water travels slower in the ground than over the surface. Lastly, groundwater flow is slowly generated and does not contribute to peak discharges.

Finally, the water is accumulated in the river system of the Geul and is transported to the Meuse. The river system is explained in Section 2.6. According to Klein (2022), the travel time during high discharge is 2-3 hours from Kelmis to Cottessen, 5-7 hours from Cottessen to Valkenburg, and 5-7 hours from Valkenburg to Meerssen. High discharges due to extreme precipitation lead to overflowing banks and ultimately to fluvial flooding. The water level of the Meuse plays an important role in the Geul catchment. There is a high chance of coincidence between high water levels in the streams and Meuse. In this case, the water level in the Meuse slows down the runoff from the Geul to the Meuse. This can result in a further risk of flooding (Elmensdorp, 2023).

## 2.3. Hydrogeology

The geohydrology in the Geul catchment has a large impact on the runoff processes in the catchment (Schaminée et al., 2009). The hilly landscape and chalk subsoil are unique in the Netherlands. The subsoil of the Geul catchment can be divided into four categories, shown Figure 2.4. The subsoil of the northwest part of the catchment is characterized by thick layers of loess loam and a thick layer of tertiary deposits in the subsoil. The subsoil of the middle part of the catchment is characterized by limestone. The subsoil of the southeast part is characterized by flint luvium. These geohydrologic properties of the catchment have a large impact on the runoff behaviour. The upstream flint luvium area in Belgium generates fast runoff peaks, because of less storage in the subsoil. The downstream loess area in the Netherlands causes more spread out runoff peaks, because of more storage in the subsoil (Elmensdorp, 2023).

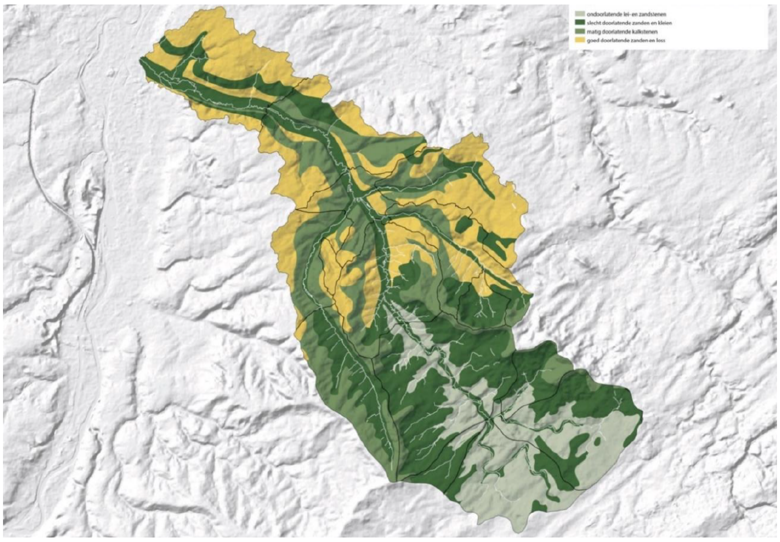

Figure 2.4: Permeability map of the subsoil of the Geul catchment (Bureau Stroming, 2022). Grey: Impermeable slate and sandstones. Dark green: Poorly permeable sands and clays. Light green: Moderately permeable limestones. Yellow: Well drained sands and loess.

## 2.4. Land Cover

Land cover partly determines the hydrologic response, as is explained in Section 2.2. The Geul catchment was subjected to major land cover changes over the last centuries (Dautrebande et al., 2000). Grasslands became agricultural lands and the catchment became more densely populated (Stam, 2002; Tsiokanos, 2022).

Klein (2022) estimated the land cover using the Coordination of Information on the Environment (CORINE) land cover, which is often used for hydrologic analyses in Europe. However, according to Slager, Becker, Bouaziz, and Kwadijk (2022), the dataset was inconsistent with more detailed land cover maps, topographic maps and recent aerial photographs. During the research, Openstreetmap data is found to be more consistent. The constructed land cover map of the Geul catchment is shown in Figure 2.5.

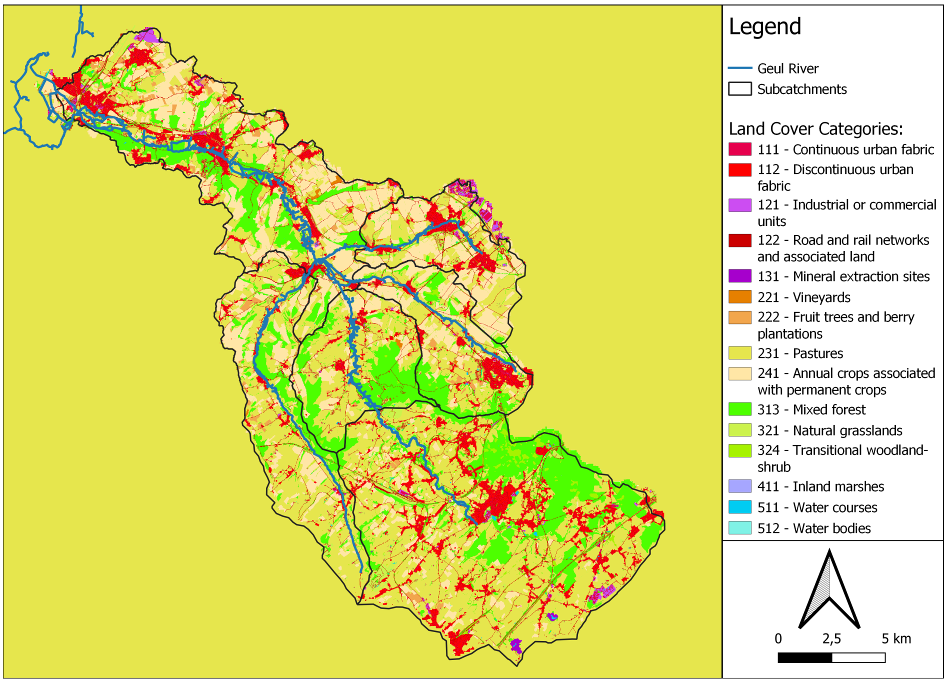


Figure 2.5: Land cover map, based on Openstreetmap data with CORINE land cover classes (Slager et al., 2022).

Poppelier (2023) stated that land cover is heterogeneously distributed over the Geul catchment. Data from Slager et al. (2022), shown in Table 2.1, shares this conclusion. There are large differences between the countries within the catchment. Germany contains the most agriculture (41%), while Belgium (55%) and the Netherlands (38%) contain the most grasslands. The Netherlands has more agriculture (28%) than Belgium (8%). Overall, the Geul catchment is mainly characterized by grasslands (46%), followed by agriculture (19%) and forests (20%). The remaining area is paved or water.

| | Agriculture | Forest | Grass | Infrastructure | Buildings | Urban | Water |
|---|---|---|---|---|---|---|---|
| **Geul Catchment** | 19% | 20% | 46% | 5% | 2% | 7% | 1% |
| **Gulp** | 23% | 15% | 55% | 3% | 0% | 4% | 0% |
| **Eyserbeek** | 39% | 5% | 37% | 7% | 1% | 11% | 0% |
| **Selzerbeek** | 28% | 20% | 37% | 6% | 0% | 9% | 0% |
| **Sippenaeken** | 6% | 22% | 55% | 5% | 1% | 11% | 0% |
| **Hommerich** | 16% | 33% | 44% | 3% | 0% | 4% | 0% |
| **Meerssen** | 34% | 19% | 30% | 6% | 1% | 10% | 0% |

Table 2.1: Land cover percentages in the Geul catchment and per subcatchment. Estimated with Openstreetmap data by Slager et al. (2022).

The land cover determines how fast precipitation runs off and partly how much water infiltrates into the soil (Bureau Stroming, 2022). The runoff to the Geul river mostly originates from urban areas. Also agriculture generates fast runoff, especially when the croplands are barren or partly vegetated (Slager et al., 2022). On the other hand, forest areas reduce the runoff by interception and infiltration. Grassland does not generate runoff when the infiltration capacity is smaller than the precipitation intensity. This was the case during the July 2021 flood event, otherwise the runoff peak would have increased (Bureau Stroming, 2022).

## 2.5. Subcatchments

The Geul catchment is divided in six subcatchments, which are displayed in Figure 2.6. The subcatchments are based on the discharge stations of the Waterboard Limburg (Klein, 2022). The Geul is divided in three subcatchments, Sippenaeken, Hommerich, and Meerssen. The three other subcatchments are the tributaries Gulp, Selzerbeek, and Eyserbeek. Table 2.2 summarises the main characteristics of the subcatchments. The subcatchments are elaborated by literature and the observed hyetographs.

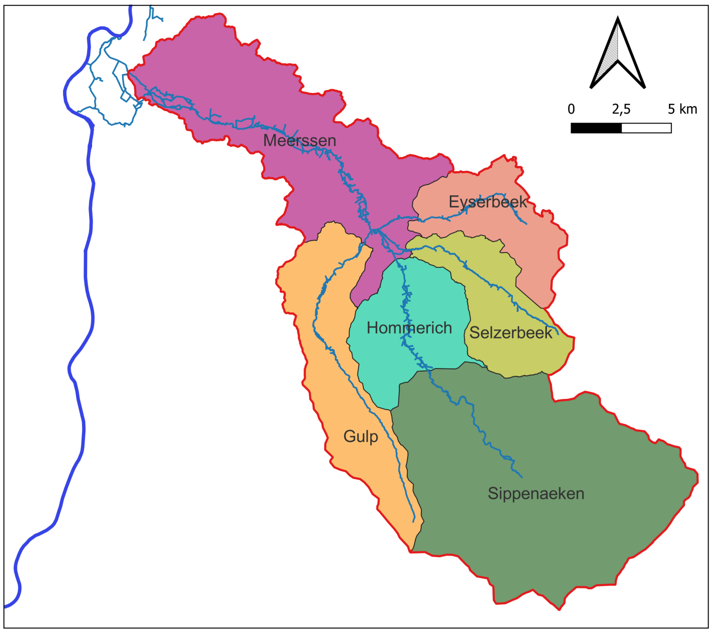


Figure 2.6: The subcatchments in the Geul catchment.

| Subcatchment | Size [km$^2$] | Slope [m/km] | River Length [km] | Average Discharge [m$^3$/s] | Response Time [h] | Thickness Groundwater Aquifer [m] |
|---|---|---|---|---|---|---|
| Gulp | 46 | 12 | 18 | 0.36 | 2 | 40 - 100 |
| Eyserbeek | 27 | 6 | 12 | 0.11 | 1 | 40 - 100 |
| Selzerbeek | 29 | 10 | 14.5 | 0.15 | 1 | 10 - 100 |
| Sippenaeken | 123 | 7 | 20 | 1.1 | 2 - 4 | 0 - 20 |
| Hommerich | 31 | 3 | 12 | 1.5 | | 10 - 80 |
| Meerssen | 82 | 2 | 24.5 | 2.8 | 4 - 10 | 40 - 100 |

Table 2.2: Overview of the characteristics per subcatchment (Klein, 2022).

### 2.5.1. Gulp

The Gulp is the largest tributary of the Geul and springs in Henri-Chapelle in Belgium (Klein, 2022; Nota & van de Weerd, 1978). The river flows 18 kilometers to Gulpen, where it joins the Geul. Section 2.3 shows that the Gulp catchment is characterized by chalk and moderately permeable limestones. This leads to a high water storage capacity downstream and a more flashier response upstream, which can be seen in Figure 2.7. The discharge reacts fast to the precipitation, when the soil is saturated. The discharge does not react at the start of the event, but the discharge increases when the precipitation intensity increases and exceeds the infiltration capacity. This can be explained by the relatively large area of grasslands. Grasslands start to generate runoff when the precipitation capacity exceeds the infiltration intensity, as is explained in Section 2.4. Nota and van de Weerd (1978) showed that back in 1978, 70% of the total discharge consisted of base flow. This results in a higher average discharge value compared to the other tributaries Eyserbeek and Selzerbeek.

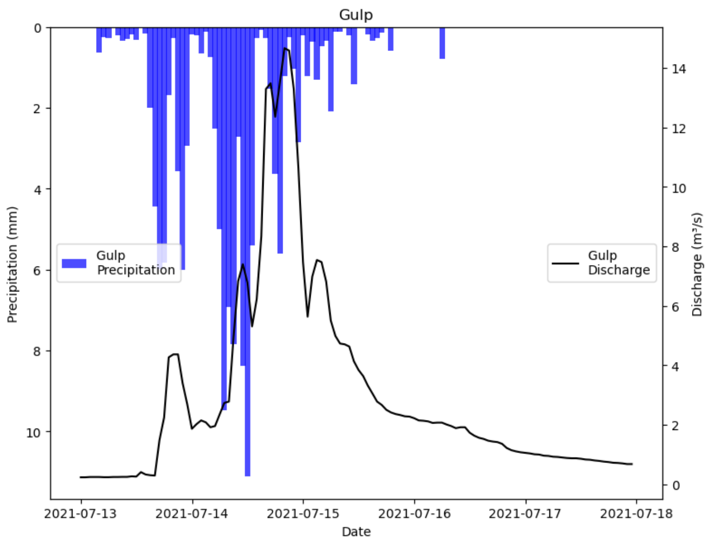


Figure 2.7: Discharge response of the Gulp subcatchment to the precipitation during the July 2021 flood event.

### 2.5.2. Eyserbeek

The Eyserbeek springs in Bocholtz and flows into the Geul at Gulpen (Wikipedia, 2022). The tributary has a length of 12 kilometers and an average slope of 5.9 m/km. The Eyserbeek subcatchment differs over the area. The upstream part is characterized by the impermeable Vaals formation and a canalized Eyserbeek. The downstream part is characterized by a chalk subsoil and a more natural flowing stream (Klein, 2022). Section 2.4 shows that he upstream part contains a high amount of urbanization. This results into short response times and high peak discharges in the river, as can be seen in Figure 2.8. The hortonian overland flow is dominant by the sharp shape of the peaks. The discharge fluctuates between 0.026 m$^3$/s and 10 m$^3$/s.

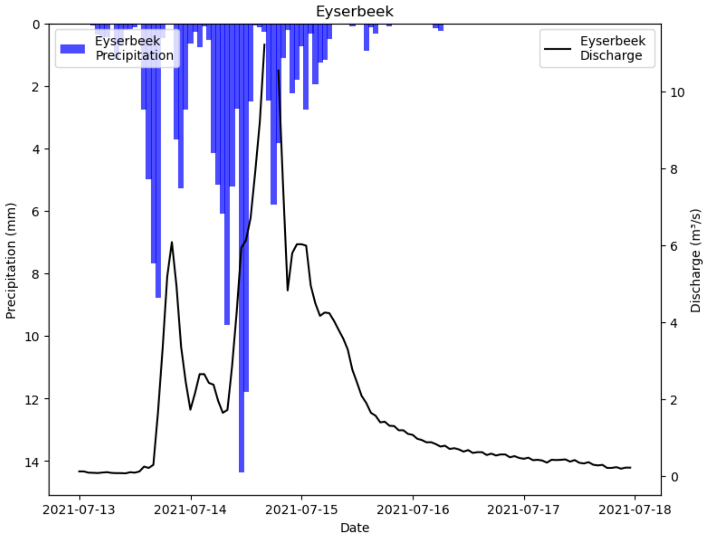


Figure 2.8: Discharge response of the Eyserbeek subcatchment to the precipitation during the July 2021 flood event.

### 2.5.3. Selzerbeek

The Selzerbeek springs near Aachen, just across the border in Germany and flows into the Geul at Gulpen. The Selzerbeek has a length of 14.5 kilometers and average slope of 10 m/km. The upstream part of the river has a low storage capacity, because of the Aken Formation (Klein, 2022). This results in short response times and high discharge peaks as can be seen in Figure 2.9. Section 2.4 shows that the Selzerbeek subcatchment contains less urban area than the Eyserbeek subcatchment, so the Selzerbeek has less flashy response. The discharge varies between 0.02 $m^3/s$ and 6 $m^3/s$.

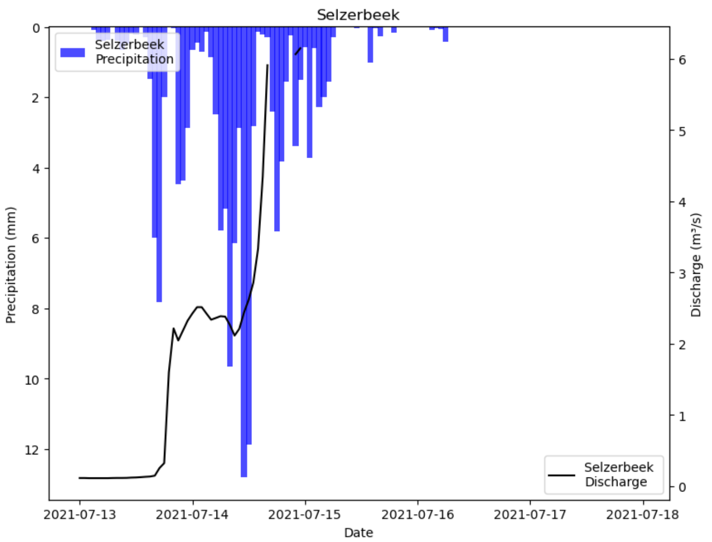


Figure 2.9: Discharge response of the Selzerbeek subcatchment to the precipitation during the July 2021 flood event.

### 2.5.4. Sippenaeken

The Sippenaeken subcatchment contains the Belgian part of the Geul catchment and has a size of 123 km$^2$ (Klein, 2022). This area is characterized by thin soils and a low storage capacity, as is explained in Section 2.3. This results in flashy behaviour with response times of 2-4 hours, as can be seen in Figure 2.10. The discharge response of Sippenaeken is less flashy than the Eyserbeek and Selzerbeek. This is caused by the grass flood plains along the Geul river, which delays and spreads the discharge peak. The flood plains are further elaborated in Section 2.6.2.

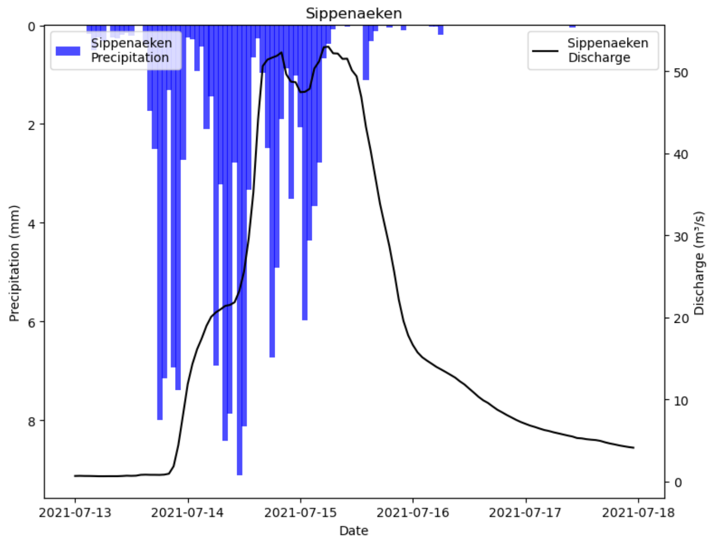


Figure 2.10: Discharge response of the Sippenaeken subcatchment to the precipitation during the July 2021 flood event.

### 2.5.5. Hommerich

Hommerich is the smallest subcatchment and has a size of 31 km$^2$. The subcatchment contains the area between the Belgian border and the village Hommerich (Klein, 2022). Section 2.3 shows that the soil type changes from thin soils to chalk plateaus in this area. This results in more storage capacity and a less flashy response, as can be seen in Figure 2.11. The first precipitation peak results in a small discharge peak, as the most of the precipitation is stored. Thereafter, the discharge from the Sippenaeken subcatchment enters Hommerich and the discharge increases.

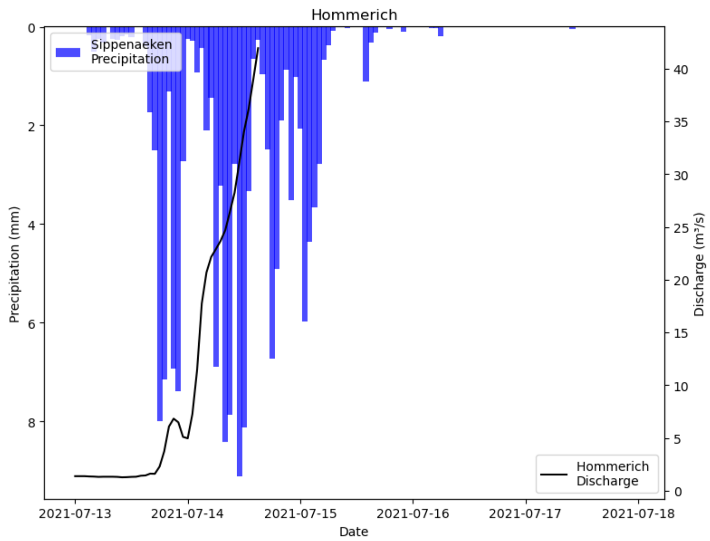


Figure 2.11: Discharge response of the Hommerich subcatchment to the precipitation during the July 2021 flood event.

### 2.5.6. Meerssen

The Meerssen subcatchment is located between the villages Hommerich and Meerssen and has a size of 82 km$^2$. This area contains the lower Geul part with a length of 24.5 kilometers (Klein, 2022). Section 2.3 explains that Meerssen is characterized by a chalk subsoil and a high infiltration capacity. Therefore, the area downstream of Valkenburg hardly contributes to the discharge in the Geul. The discharge is mainly generated by the other subcatchments (Elmensdorp, 2023; Klein, 2022). Figure 2.12 shows that the peak discharge occurs around 20 hours after the precipitation peak in the Sippenaeken subcatchment. The flow is delayed by the flood plains along the Geul and flooding of upstream villages.

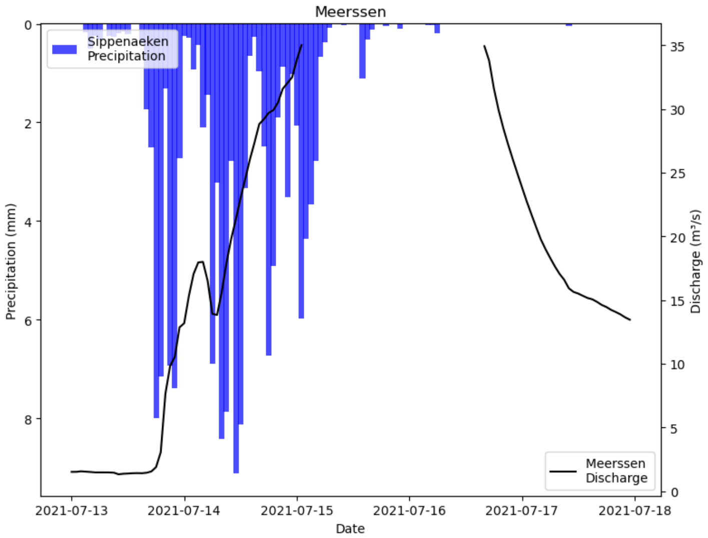


Figure 2.12: Discharge response of the Meerssen subcatchment to the precipitation during the July 2021 flood event.

## 2.6. River System

The Geul River, shown in Figure 3.8, is a very unique river in the Netherlands. It is a fast flowing stream, with a steep gradient and it meanders actively (de Moor & Verstraeten, 2008). The Geul has a length of 58 kilometers and has a fall of 250 meters. The slope decreases in downstream direction, with an average of 4.3 m/km. The Geul has a highly varying discharge, which mainly depends on the amount of precipitation (de Moor, Kasse, van Balen, Vandenberghe, & Wallinga, 2008). The mean discharge of the Geul is 4 m$^3$/s (Elmensdorp, 2023). High water peaks in the Geul are not rare. Many cities and villages are located in the Geul valley. The Geul has to flow trough the narrow centers of these places, which makes them sensitive to flooding (Elmensdorp, 2023). One of the bottlenecks of the Geul is the city of Valkenburg. Here, the river flows through tight flow profiles. Almost every year, local floods occur and some grasslands along the river are flooded (de Moor et al., 2008). For example in 2022, when a high water peak passed the city of Valkenburg, only one year after the July 2021 flood event, but the banks of the Geul were just not flooded (RTL Nieuws, 2022).

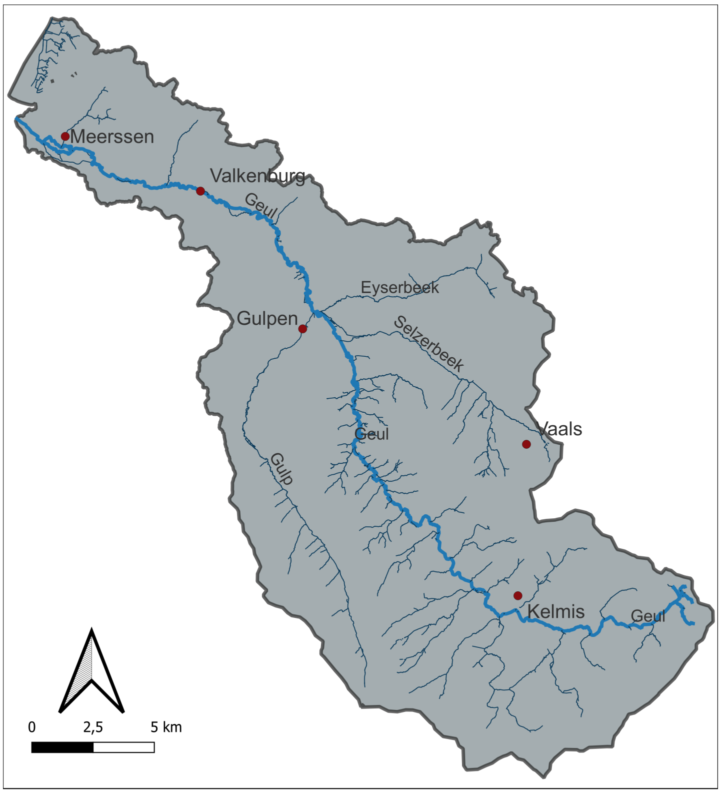


Figure 2.13: Overview of the river system of the Geul River.

### 2.6.1. Control Structures

The river system is characterized by the presence of water mills (Hulsman et al., 2023). The Geul and its tributaries contain 28 water mills, of which 14 water mills are located in the Geul valley (Winteraeken, 2017). Today, the water mills are used for electricity generation, e.g. Volmolen, for grain grinding, e.g. Oude Molen, or by the hospitality industry, e.g. IJzeren Molen (Wikipedia, 2021, 2023a, 2023b). The water mills, which distribute water between the main branch and the mill branch, have been replaced by automatic weirs over the years. A water mill usually consist of four parts, which are displayed in Figure 2.14:

- Distribution weir: controls the distribution of the water between the main branch and the mill branch. The water level is controlled together with the lossluis and maalsluis;
- Lossluis (Release lock): when the water level exceeds the maximum level, the excess water is released via a spillway or a gate;
- Maalsluis (Mill lock): controls the discharge to the waterwheel with a gate. At high discharges, the gate is closed to protect the waterwheel;
- Fish passage: ensures that fishes can pass the water mill.

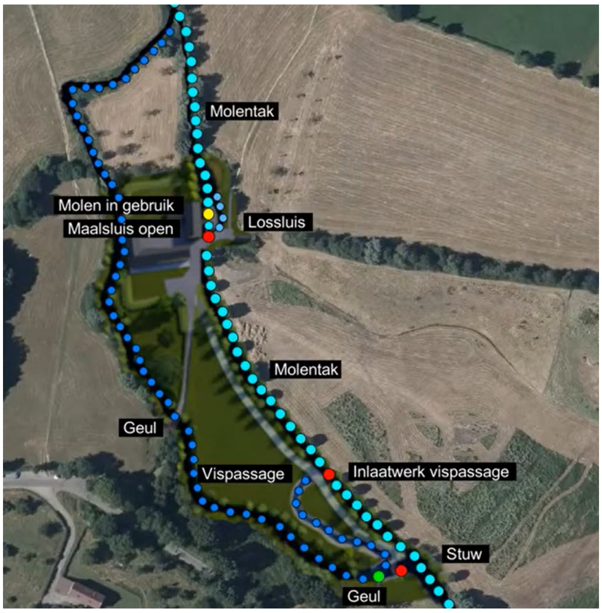


Figure 2.14: Overview of the water system around the Volmolen in Epen, screenshot taken from Waterschap Limburg (n.d.-b).

### 2.6.2. Water Retention Basins

More than 500 water retention basins are constructed in the Geul catchment (van Wel, 2021). Water is guided to the basins to store local heavy precipitation (Elmensdorp, 2023). The basins reduce and spread out the discharge peaks, which results in a lower flood risk (van Heeringen, Asselman, Beersma, Overeem, & Philip, 2022). The water retention basins are constructed in the tributaries, dry valleys, and on the slopes in the higher parts of the catchment. The basins are uncontrolled, except for the large water retention basins in Nijswiller (62.550 $m^3$) and Rolduckerweg (84.000 $m^3$) (Klein, 2022; van Heeringen et al., 2022). The outflow of these two basins is controlled by a gate, Figure 2.15 (Hulsman et al., 2023). The uncontrolled water retention basins are designed in a way that a full basin is empty within 24 hours. This is achieved by a so called 'spindelschuif' (gate), which has a fixed opening with a maximum outflow rate. This maximum can only be exceeded when the basin is full and spills.

Figure 2.15: The controlled outflow gate of the Buffer Nijswiller in the Selzerbeek (Waterschap Limburg, n.d.-a).

The water retention basins are not evenly distributed throughout the Geul catchment. There are no retention basins in the Belgian part of the catchment (Klein, 2022). Most of the storage volume in the Geul catchment is located in the most downstream subcatchment Meerssen (38%). The least amount of storage is located in the Gulp (7%) and Hommerich (6%), as they are more densely populated in comparison to the other subcatchments. Lastly, the Eyserbeek (30 %) and Selzerbeek (19%) contain the Rolduckerweg and Nijswiller basins, and have therefore a high storage volume. An overview of the subcatchments is given in Section 2.5.

Next to the water retention basins, the floodplains along the Geul function as a natural buffer (Klein, 2022). For example in the Belgian part of the Geul, shown in Figure 2.16. Here, the banks are characterized by flat surfaces, covered by grass. When the water level exceeds the bank level, the water flows to the floodplains. These floodplains delay and spread out the discharge peak. ”When the floodplains upstream are full, the floodplains downstream are not flooded yet and when the downstream ones start flooding, the upstream parts are empty again”, according to personal communication of Klein (2022) with Helena Pavelkova of the Waterboard of Limburg.

Figure 2.16: Floodplains in the Sippenaeken subcatchment, Belgium. Characterized by flat surfaces, covered by grass.

# 3
# Method

## 3.1. Overview

The hydrological response of the Geul catchment is captured in two different kinds of hydrological models, which are coupled to a hydrodynamic model. The first hydrological model is a combination of HBV for unpaved areas and D-RR for paved areas. HBV and D-RR are conceptual and semi-distributed models, which are elaborated in Section 3.2. The second hydrological model is a physically based, distributed Wflow_sbm model, explained in Section 3.3. The hydrological models for the Geul catchment are compared in Section 3.4. Both hydrological models are coupled to a D-HYDRO Suite 1D2D model of the Geul, in which the hydro-dynamical response is reviewed. The D-HYDRO model is explained in Section 3.5 and the coupling with the hydrological models in Section 3.6. The models are calibrated with measured data of the Geul and its tributaries. The forcing and measurement data are described in Section 3.7. Section 3.8 describes the calibration strategy. Lastly, the various spatial development scenarios in the Geul catchment are described in Section 3.9. The workflow and results obtained from the conducted research are summarized and visualized in Figure 3.1. The corresponding Jupyter Notebooks and scripts can be found in Idsinga (2024).

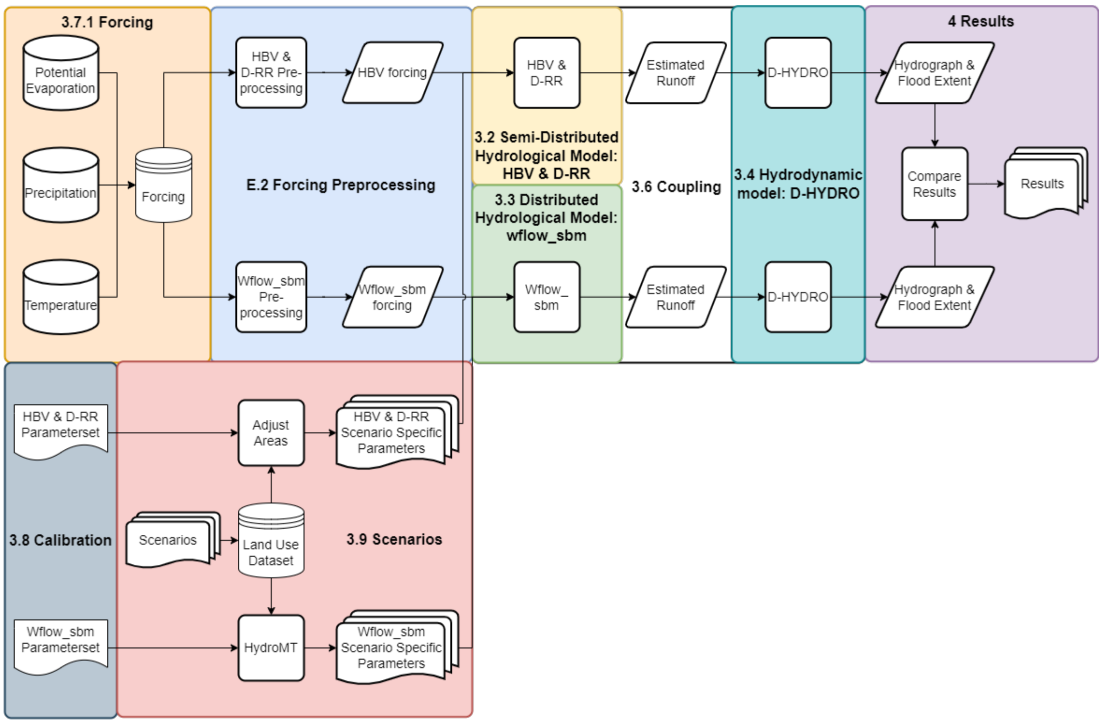


Figure 3.1: Overview of the used models and method of this research.

## 3.2. Semi-Distributed Hydrological Model: HBV & D-RR

The semi-distributed hydrological model in this research consists of an HBV model for unpaved areas and a D-RR model for paved areas. This section describes both models and their limitations.

### 3.2.1. HBV

The HBV (Hydrologiska Bryåns Vattenbalansavdelning) model is developed by Bergström (1976). The HBV model is widely used and many HBV concepts have been built over the years (Savenije, 2009; Seibert & Bergström, 2022). For this research, the HBV model built by Hrachowitz (2021) is chosen. This model has a relatively simple structure and therefore has a fast calibration. From now on, this version of HBV will be called HBV in this research. The HBV structure is presented in Figure 3.2 and is elaborated in more detail in Appendix B. HBV will be applied on subcatchment scale, so each subcatchment has its own parameters.

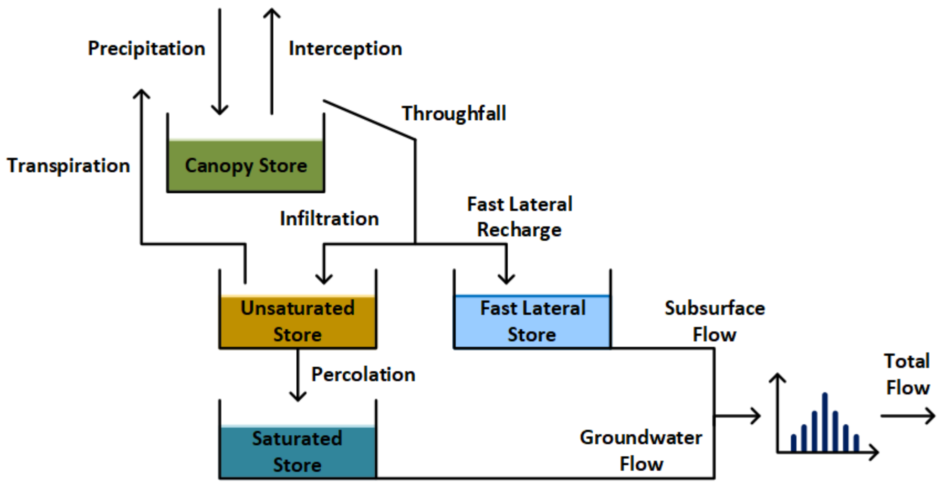


Figure 3.2: Schematization of the semi-distributed HBV model.

### 3.2.2. D-RR

D-RR (Rainfall Runoff) is an module in the D-HYDRO Suite (Deltares, 2022c). D-RR is build at the end of the 20th century and is widely used in the Netherlands for rainfall runoff modelling (Prinsen, Hakvoort, & Dahm, 2009). In this research, the paved areas are modelled as mixed sewer systems. The schematization of a D-RR mixed sewer system is presented in Figure 3.3. D-RR is explained in more detail in Appendix A.

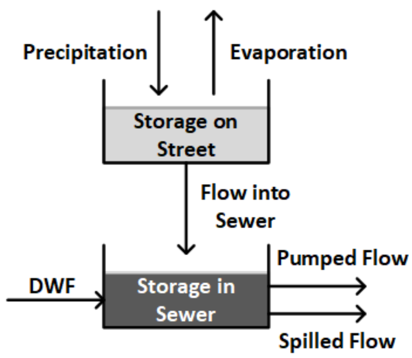


Figure 3.3: Schematization of the semi-distributed D-RR paved model, for a mixed sewer system.

### 3.2.3. Model Representation

In this research, D-RR represents the sewerage areas in the Geul catchment and HBV represents the remaining unpaved areas. The model areas are retrieved from the Waterboard of Limburg and are visualized in Figure 3.4a. The paved areas in D-RR are retrieved from the existing sewerage areas (Hulsman et al., 2023). A part of each sewerage area is connected to a sewer, this is called the paved area. Each sewer is connected to the Geul river by a sewer overflow. A pump pumps the water to a wastewater treatment plant and the water leaves the model. When the sewer is completely full, the excess water flows via the sewer overflow into the Geul.

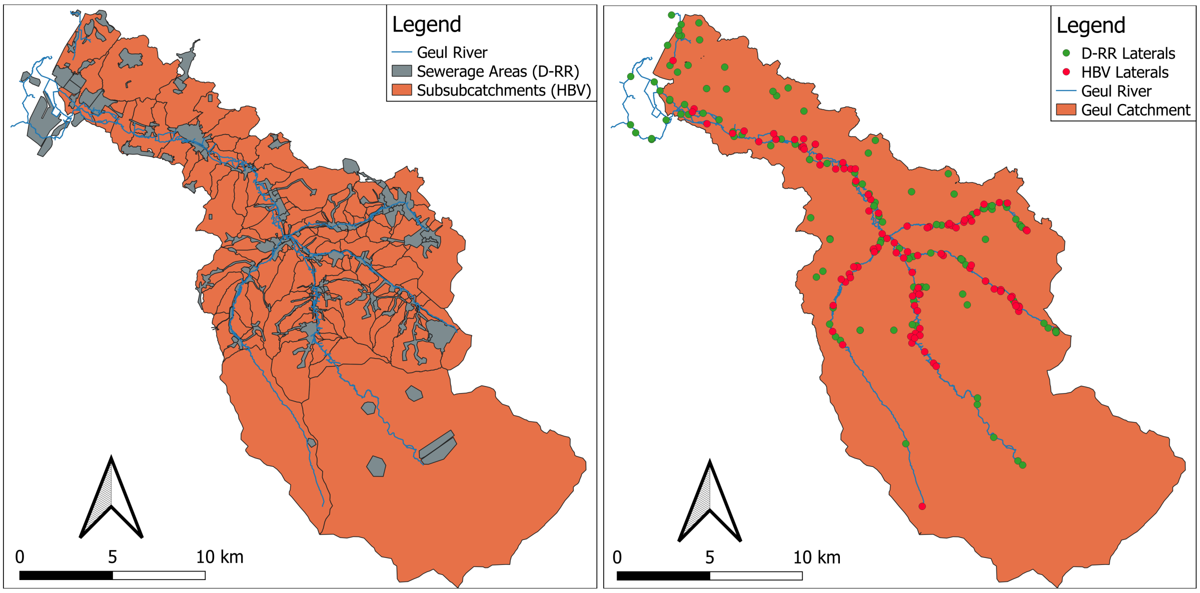


(a) Representation of HBV and D-RR.

(b) The defined laterals of HBV and D-RR.

Figure 3.4: The model representation of HBV and D-RR.

Hulsman et al. (2023) manually added the paved area of Aken (Aachen) to the D-RR model. Next to Aken, a number of villages in Belgium are added to D-RR. There are no sewerage areas defined in Belgium in the original model of Hulsman et al. (2023), because there was no data of these areas. Therefore in this research, the villages Gemmenich, Kelmis, Montzen, and Plombieres are manually added to the Sippenaeken subcatchment for this research. The village Hombourg in the Gulp subcatchment is also manually added. It is assumed that Kelmis has the same size of paved area as Vaals, based on Google Maps. The villages Gemmenich, Hombourg, Montzen, and Plombieres are assumed equal to Epen, based on Google Maps. It is assumed that these paved areas contain no sewer. This assumption led to more realistic results than the assumption of an improved combined sewer system. The assumption is elaborated in more detail in Appendix D.1. The paved areas are added via the workflow in Idsinga (2024). More information about the paved and unpaved areas is given in Appendix D.2.

### 3.2.4. Limitations

A disadvantage of a conceptual model is equifinality. Different combinations of parameters can give similar results (Savenije, 2009). It could be case that a parameter combination is not possible in reality (Hrachowitz, 2021). After calibration, it is important to check if the parameterset reflects the physics in reality. Another limitation of a conceptual model is capturing the heterogeneity in a subcatchment (Savenije, 2009). One value will not represent all processes and subcatchment properties.

## 3.3. Distributed Hydrological Model: Wflow_sbm

The Wflow_sbm (simple bucket model) is a physically based, spatially distributed hydrological model (Van Verseveld et al., 2022). The model concept is available in the open-source distributed modelling framework Wflow of Deltares (Deltares, n.d.-b). Wflow_sbm is largely based on Topog_SBM (Vertessy & Elsenbeer, 1999). The main difference between the concepts is that Topog_sbm is designed to simulate fast runoff processes in small catchments, while Wflow_sbm can also be applied on a large scale. Figure 3.5 presents the fluxes and storages of the Wflow_sbm model for each grid cell. The kinematic wave for river flow will be replaced by the D-HYDRO model in Chapter 5. The more detailed description of the Wflow_sbm model can be found in Appendix C.

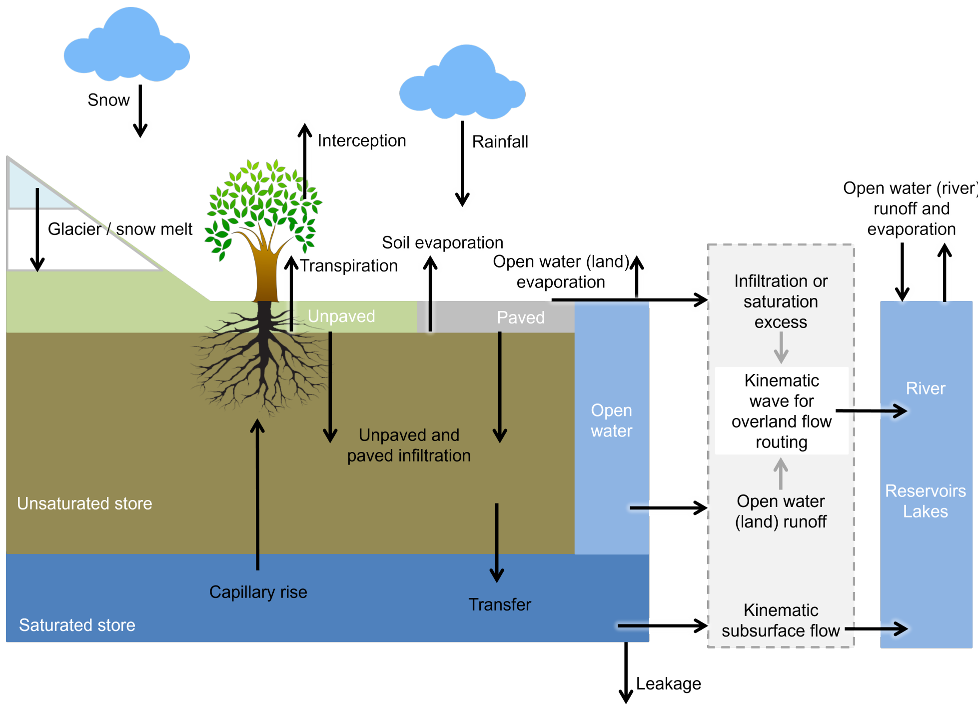


Figure 3.5: Schematization of the Wflow_sbm model (Schellekens, 2022).

An advantage of Wflow_sbm model is a well suited run time performance for large-scale, high-resolution modelling. Another advantage is that the most of the parameters are based on physical characteristics. Wflow_sbm has six remaining calibration parameters (Klein, 2022; Schellekens, 2022):

- **SoilThickness:** The depth of the soil. Increasing the soil depth increases the storage capacity of the soil, which decreases the discharge peaks.
- **KsatVer:** The vertical saturated hydraulic conductivity. Increasing KsatVer lowers the baseflow and flattens the discharge peaks.
- **f:** Determines the decrease of KsatVer with depth. The parameter f controls the baseflow recession and a part of the stormflow curve.
- **N and N_River:** The Manning N parameter controls the shape of the hydrograph. The parameter is not reviewed, because D-HYDRO determines the flow in the river.
- **KsatHorFrac:** Determines the horizontal saturated hydraulic conductivity by multiplying with KsatVer. Increasing KsatHorFrac increases the base flow and decreases the peak discharges.
- **MaxLeakage:** The maximum amount of water per timestep that leaves the saturated zone and is therefore out of the model. The amount of water that leaves the model can be adjusted.

### 3.3.1. Model Representation

The Wflow_sbm Geul parameterset is set up by Klein (2022) and is adjusted by Bouaziz (2022). The paved and unpaved areas are both defined in Wflow_sbm and are based on the land cover map as presented in Section 2.4. The Geul parameterset is derived with the Python package HydroMT Wflow (Eilander et al., 2023). This package is used to build or adjust a Wflow_sbm parameterset. The HydroMT Wflow package is also used to set up the subsubcatchments. Idsinga (2024) contains the Python code to set up the subsubcatchments. The result is shown in Figure 3.6.

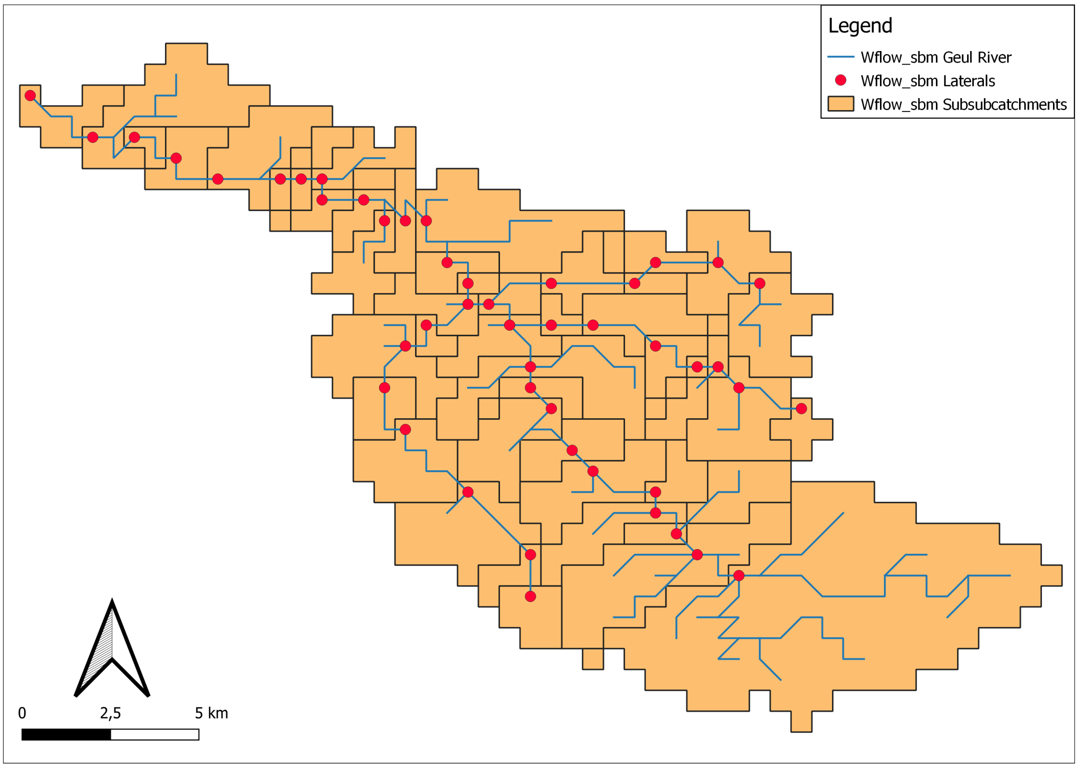


Figure 3.6: Model representation of Wflow_sbm, containing the Geul River, laterals, and subsubcatchments of Wflow_sbm.

### 3.3.2. Limitations

The hydrological Wflow_sbm model has several limitations. The model assumes that topography mostly controls the water flow (Schellekens, 2022). This assumption holds for steep terrain, but not for less steep terrain. In less steep terrain, the pressure differences and inertial momentum cannot be neglected. This assumption results in wrong estimations of channel flow, to a lesser degree overland flow, and lateral movement of groundwater. The results for soils deeper than 2 metres will be unrealistic. Another limitation is that the simple numerical solution gives different results for a daily timestep than for a hourly timestep.

## 3.4. Hydrological Model Comparison

HBV and D-RR are conceptual and semi-distributed models. Wflow_sbm is a physical, distributed Wflow_sbm model. The main differences are explained in Table 3.1. In theory, the distributed models are expected to outperform the semi-distributed models, as they contain more physical input, however this is not always the case in reality (Khakbaz, Imam, Hsu, & Sorooshian, 2012). Coupling the hydrological models to the hydrodynamic D-HYDRO model reduces the differences between the models. This makes HBV & D-RR a more physical model, because of the addition of momentum equations. Wflow_sbm becomes less distributed and physical, because of the definition of the subsubcatchments, shown in Figure 3.6. The water stays within the boundaries of a subsubcatchments and does not leave them. The models are qualitatively and quantitatively compared for the Geul. This section contains the qualitative hydrological model comparison. The results of the quantitative comparison are given in Chapter 4.

| HBV & D-RR | Wflow_sbm |
|---|---|
| Semi-distributed: estimates the runoff on sub-catchment scale (Coron, Thirel, Delaigue, Perrin, & Andréassian, 2017). | Distributed: accounts for spatial variability in the input variables and model parameters (Clarke, 1973). |
| Conceptual: consists of mathematically described processes and stores modelled as reservoirs, requires calibration (Savenije, 2009). | Physical: based on scientific principles of energy, water, and momentum fluxes (Hrachowitz, 2021; Islam, 2011). |

Table 3.1: The semi-distributed, conceptual hydrological models HBV and D-RR versus the distributed, physically based hydrological model Wflow_sbm.

The schematizations of the HBV and D-RR and Wflow_sbm are shown in Figure 3.7 next to eachother. Each type of storage has its own color. It can be seen that Wflow_sbm contains more storages than HBV and D-RR. This also results in more internal and external fluxes. The differences in model setup are given in Table 3.2. The differences between the fluxes in the models are given in Table 3.3.

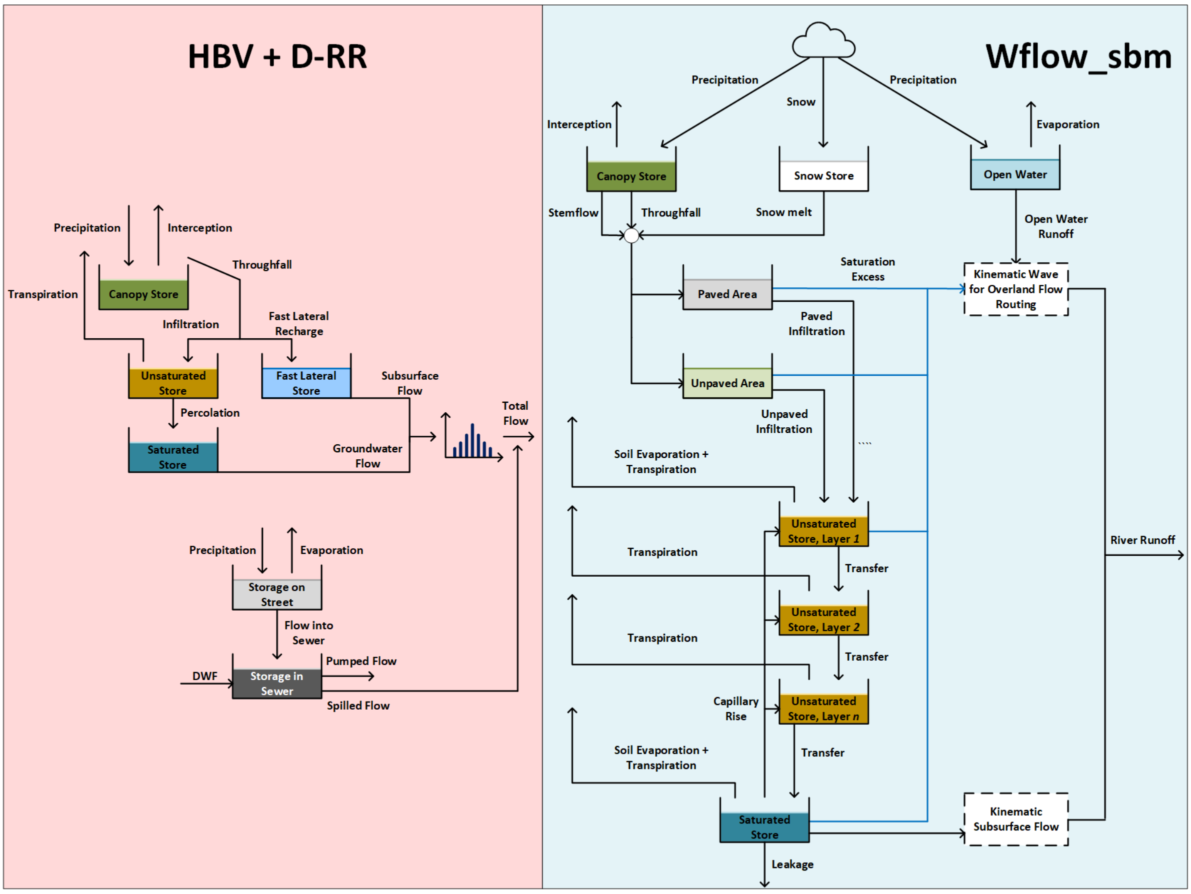


Figure 3.7: The schematizations of the hydrological models HBV + D-RR in red and Wflow_sbm in blue, next to eachother. Wflow_sbm a more complex model than HBV + D-RR and contains therefore more fluxes and storages.

| **Differences in Model Setup** |
|---|
| D-RR and HBV represent the paved and unpaved areas, Wflow_sbm represents both; |
| Wflow_sbm contains a snow module, HBV does not; |
| HBV generates subsurface flow from the Fast Lateral Store, Wflow_sbm from the Saturated Store; |
| D-RR contains a sewer, Wflow_sbm does not; |
| Wflow_sbm contains an Open Water store, HBV does not; |
| HBV contains less parameters than Wflow_sbm; |
| The soil in Wflow_sbm can have multiple layers, HBV contains one soil layer. |

Table 3.2: The differences in the hydrological model setup between HBV and D-RR and Wflow_sbm.

| **Differences in Fluxes** |
|---|
| Wflow_sbm contains a Stemflow flux, HBV does not; |
| Wflow_sbm contains a Saturation Excess flux, HBV does not; |
| Wflow_sbm contains a Overland Flow flux, HBV does not; |
| Wflow_sbm contains a Soil Evaporation flux, HBV does not; |
| Wflow_sbm contains a Capillary Rise flux, HBV does not; |
| HBV contains a Groundwater flux, Wflow_sbm contains a Leakage flux, where water leaves the model; |
| HBV contains a lag function to account for routing, Wflow_sbm contains kinematic wave equations. |

Table 3.3: The differences between the fluxes in HBV and D-RR and in Wflow_sbm.

In Section 2.2 is explained that the two main hydrological processes in the Geul catchment are overland flow and subsurface flow. HBV does not contain a flux for overland flow and Wflow_sbm does. Both models do contain a subsurface flux. HBV will compensate for the absence of an overland flow flux in the subsurface flow flux, which has to represent both main processes. This means that the HBV subsurface flow flux will likely not match reality.

Wflow_sbm contains overland flow and subsurface flow and will be able to capture both processes. However, Wflow_sbm assumes a constant infiltration rate for paved areas and does not contain sewers like in D-RR. Therefore, sewer overflows are not captured, influencing the hydrological response in urban areas. On the other hand, Wflow_sbm does contain a saturation excess flux for paved areas, while all the water flows enter the sewer in D-RR. A large part of the overland flow is generated in urban areas, so the Wflow_sbm overland flow flux will likely better match the reality than HBV and D-RR.

## 3.5. Hydrodynamic Model: D-HYDRO

The hydrodynamic modelling software used in this research is the D-HYDRO Suite 1D2D, internationally known as DELFT3D, developed by (Deltares, 2022a). This software simulates hydrodynamic flow, waves, water quality, and ecology. The D-HYDRO Suite integrates these computations by using modules for the different processes. A 1D2D model of the Geul river built by Royal HaskoningDHV (RHDHV), with the D-HYDRO Suite (Hulsman et al., 2023). The modelled river system in the D-HYDRO model of the Geul is shown in Figure 3.8. The modelled area is based on the main watercourses and the flooded areas. This model simulates the discharges and water depths in the Geul river and inundation in areas around the Geul. The roughness values in the model are calibrated for both low discharge and waves with inundation. Validation is done for low discharges up to the extreme July 2021 event. Hulsman et al. (2023) contains a detailed description of the model building process.

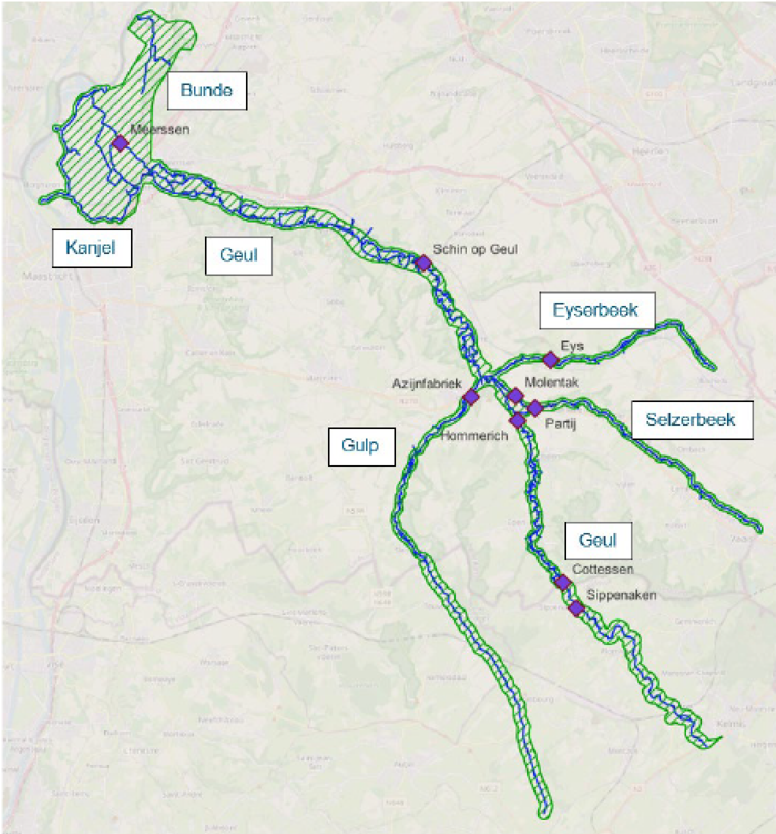


Figure 3.8: Modelled river system of the Geul River, including discharge measurement locations, by Royal HaskoningDHV (Hulsman et al., 2023).

The D-HYDRO model of the Geul uses three modules of the D-HYDRO Suite. The hydrodynamic simulation is done by the D-FLOW Flexible Mesh (D-FLOW FM) module (Deltares, 2022b). This module calculates the non-steady flow and transport phenomena on unstructured grids. The earlier mentioned D-RR module in Section 3.2.2 describes the paved areas in the Geul catchment and calculates the spilling to the open water from these areas (Deltares, 2022c). Lastly, D-RTC (Real Time Control) is used to model the control structures mentioned in Section 2.6.1. D-RTC determines the control actions of the structures, based on measured water levels in the D-FLOW FM module (Deltares, 2022d).

## 3.6. Coupling

The HBV and Wflow_sbm are offline coupled to D-HYDRO. First the HBV and Wflow_sbm are calculated, after which the output timeseries becomes the input of D-HYDRO. D-RR is online coupled with the FM module of D-HYDRO. This goes through the de Deltares Integrated Model Runner (DIMR) (Deltares, 2022b). The DIMR connects the modules and transfers data from one module to another. First, the water level is read from the FM module and is transferred to D-RR. Next, D-RR is calculated for the timestep. The discharge output is than transferred to the FM module and FM is run for the timestep.

The coupling of the hydrological models with D-HYDRO goes through laterals. The calculated discharge of a subsubcatchment is collected at the lateral and is inserted in D-HYDRO at that location. The laterals of HBV and D-RR are described in Section 3.2.3. The laterals of Wflow_sbm are described in Section 3.3.1. The procedure of coupling the hydrological models to D-HYDRO can be found in Idsinga (2024).

## 3.7. Data

The forcing of the hydrological models consists of precipitation, potential evaporation, and temperature (only Wflow_sbm) data. The distributed Wflow_sbm model requires spatially distributed data, whereas the semi-distributed HBV model requires one value per subcatchment. The forcing is described in Section 3.7.1. The D-HYDRO output is compared to discharge measurements, which are described in Section 3.7.2.

### 3.7.1. Forcing

Radardata from the Nationale Regenradar (NRR) of Schuurmans and van Vossen (2013) is used as precipitation input. The NRR product is based on composite radarimages of the KNMI (the Netherlands), WRD (Germany), and Jabekke (Belgium) and is calibrated on ground stations. The Geul catchment is well covered by these radars, as can be seen in Figure 3.9. The combination of the three different radar sources and ground measurements increases the accuracy of a large precipitation event as in July 2021. The coverage and quality make the precipitation data from the NRR well suited for this research.

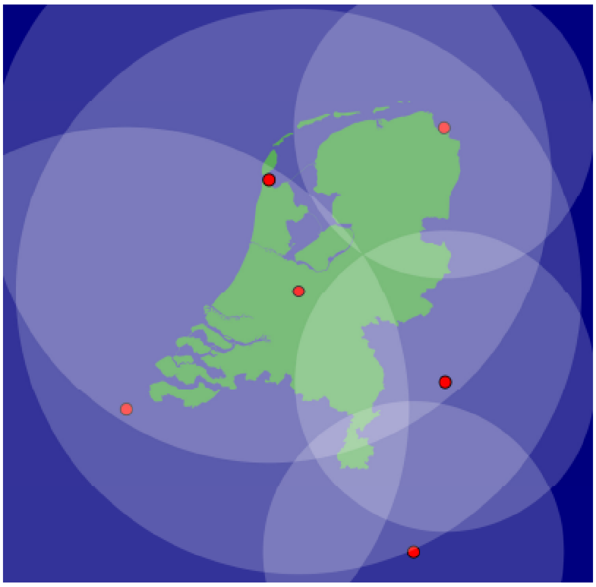

Figure 3.9: Coverage of the precipitation radars that are in the NRR data product (Schuurmans & van Vossen, 2013). The Geul catchment is located in the most south-east part of the Netherlands and is covered by multiple precipitation radars.

The ERA5-Land reanalysis is used for temperature data (Muñoz Sabater, 2019). ERA5-Land is the land component of the ERA5 climate reanalysis, with a finer resolution. However, the resolution is too large to capture the July 2021 flood event, as the precipitation occurred locally. ERA5 estimates a large number of atmospheric, land, and oceanic climate variables, by combining observations into global estimates using modelling and data assimilation (ECMWF, 2023). See the analysis in Appendix E.1.2 why the ERA5-Land is not used for the potential evaporation. The estimated values exceed the physical limit of 7 millimeters per hour (KNMI, n.d.). Instead, the calculated potential evaporation at the KNMI Maastricht weather station is used for the potential evaporation (KNMI, 2023a).

The HBV model requires one forcing value per time step for an entire subcatchment. This value should be representative for the forcing of the subcatchment. Different forcing types are analysed to find the most representative precipitation source for the HBV model in Appendix E.1. On the basis of the analysis, the mean NRR precipitation per subcatchment and the potential evaporation at the KNMI Maastricht weather station are used as input for the HBV model. Applying the data sources to hydrological models requires preprocessing. The steps to preprocess the forcing for HBV + D-RR and Wflow_sbm are presented in Appendix E.2.

### 3.7.2. Gauging Data

The D-HYDRO model of the Geul is calibrated on discharge and water level measurements of the Geul river. The coupled hydrological-hydrodynamic models are compared to the discharge measurements. Measurements provided by the Waterboard of Limburg for the Netherlands and L'hydrométrie en Wallonie for Belgium. The discharge measurement locations are shown in Figure 3.10. Information about discharge measurement locations and their uncertainty range is given in section E.3.

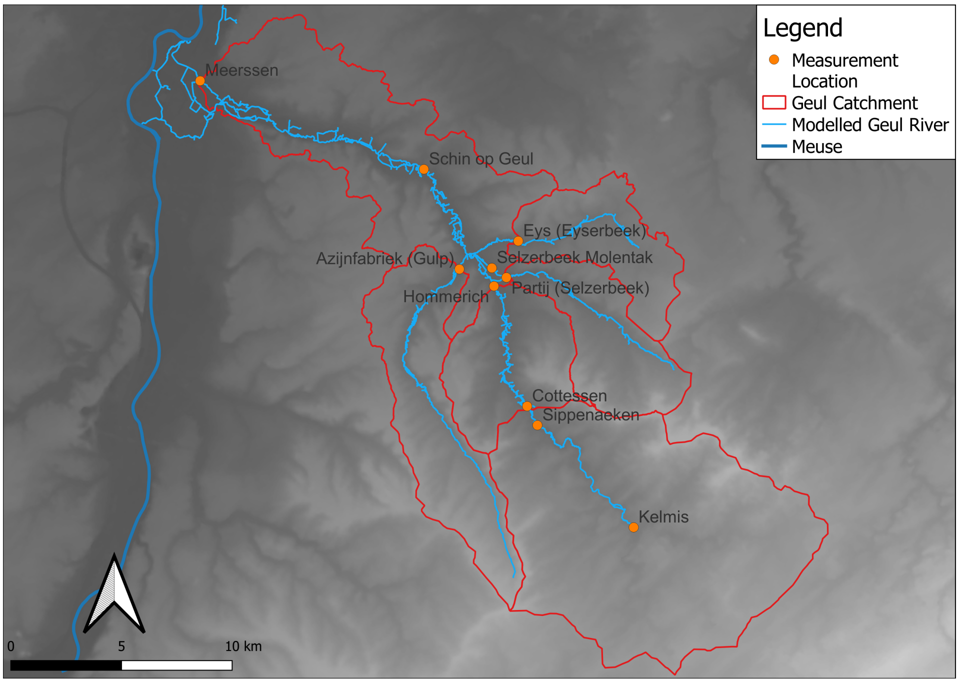


Figure 3.10: Map of the discharge measurement locations in the Geul catchment.

## 3.8. Calibration

The hydrological models are calibrated to the measured discharge in the Geul River. D-RR is based on the existing sewerage areas and is set up by Hulsman et al. (2023). The HBV calibration strategy is described in Section 3.8.1. The Wflow_sbm Geul parameterset is calibrated by Klein (2022) and Bouaziz (2022) and is slightly adjusted as explained in Section 3.8.2. The performance of the hydrological models is evaluated using the objective function in Section 3.8.3.

### 3.8.1. HBV

HBV is a conceptual model, where the fluxes are described by mathematical equations (Savenije, 2009). This requires calibration of the corresponding parameters. In Figure 3.10, it can be seen that there is a discharge measurement location at the downstream end of each subcatchment. So, HBV is calibrated on subcatchment scale and each subcatchment has its own parameterset as in Figure 3.11.

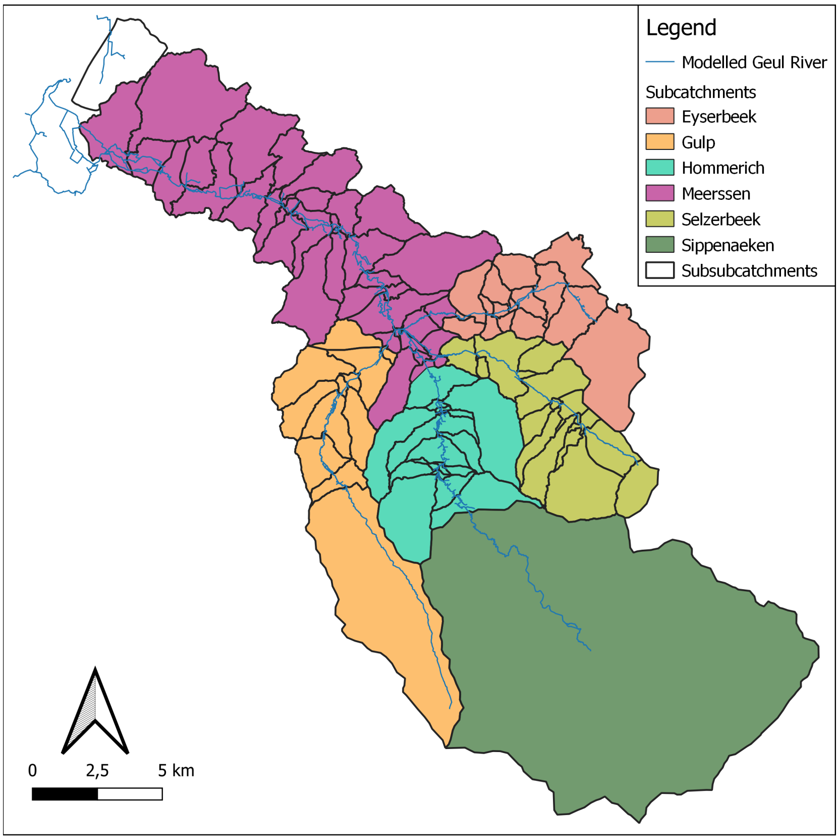


Figure 3.11: Overview of the subcatchments and subsubcatchments. The subsubcatchments in a subcatchment have been assigned the parameterset of that subcatchment.

The HBV parametersets are determined without coupling to D-HYDRO to reduce runtime. The parametersets are optimized by the Monte Carlo sampling method. This method randomly selects a parameter value between a predefined parameter range. At each Monte Carlo run, a random value between 0 and 1 is selected, after which this value is applied to the parameter range and a parameter value is calculated. This is done for each of the 8 parameters in HBV and results in a random selected parameterset. This is done 10.000 times and HBV is run for each random selected parametersets. Before the performance is evaluated, the D-RR output is combined with HBV output. D-RR is first calculated by D-HYDRO. The output is then added to the HBV lag function of the corresponding subcatchment to account for spatial variability in D-RR. The subcatchments Meerssen and Hommerich are downstream of other subcatchments. For this subcatchments, the observed upstream discharge is added to the HBV and D-RR output. In this case, HBV will not correct for uncertainty of the modelled discharge of the upstream subcatchments. The combining of D-RR and HBV output and the upstream observed discharge is visualized in Figure 3.12.

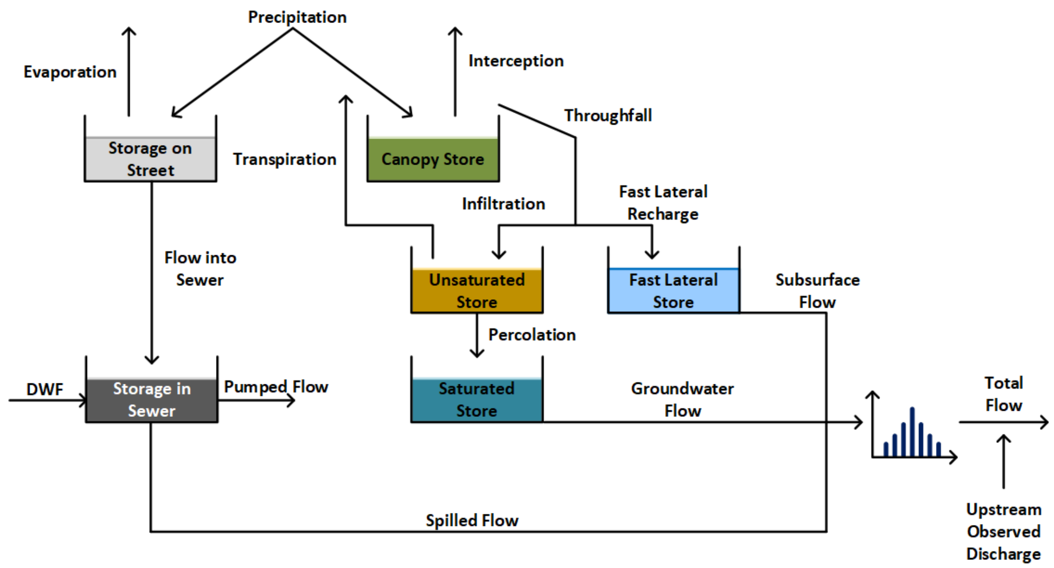


Figure 3.12: HBV calibration schematization. D-RR output is added to the HBV lag function, to account for routing in D-RR. The upstream observed discharge is added to the output, so HBV will not correct for upstream modelling uncertainty.

The combined output of a subcatchment is evaluated to the observed discharge by an objective function for the periods in Table 3.4 as explained in Section 3.8.3. The chosen periods are the same as in the research of Klein (2022), which allows to compare HBV + D-RR and Wflow_sbm for the same time period. Finally, the HBV + D-RR and Wflow_sbm parametersets are tested in D-HYDRO. This is done for a short period within the calibration and validation. The D-HYDRO calibration period is 31.01.2020 - 18.03.2020 and the D-HYDRO validation period is 26.01.2021 - 10.02.2021. Discharges during calibration periods are visualized in Appendix F.1.

| Name | Period |
|---|---|
| Calibration warm-up | 01.01.2019 - 31.12.2019 |
| Calibration | 01.01.2020 - 30.06.2020 |
| Validation warm-up | 01.07.2020 - 31.12.2020 |
| Validation | 01.01.2021 - 30.06.2021 |

Table 3.4: The calibration periods for the hydrological models. The periods are the same as in Klein (2022).

The Monte Carlo sampling method requires an interval per parameter. This parameter interval can be based on definitions, literature, or observations and can be further optimized by the objective function. The HBV parameters $I_{max}$, $S_{u,max}$, $T_{lag}$, and $K_s$ are constraint by literature and observations. The derivation of the intervals is given in Appendix F.3. First the parameter constraints by literature and observations are applied. The intervals are adjusted, when the modelled discharge behaviour of these intervals do not match the observed discharge, as explained in Appendix F.3.5. The other parameters are constraint by the result of the objective function, until an optimum is reached.

### 3.8.2. Wflow_sbm

The Wflow_sbm Geul parameterset is first calibrated by Klein (2022) on the parameters SoilThickness, Maximum Leakage, and KsatHorFrac. The soil thickness is adjusted to have a correct representation of the soil layers in the catchment. The water balance of the model is closed by adjusting the Maximum Leakage parameter. Lastly, the KsatHorFrac is adjusted to get a better representation of high flows during the July 2021 flood event. Next, the Wflow_sbm Geul parameterset is adjusted by Bouaziz (2022). The delineation of the river cells is adjusted, the land use map is changed; as explained in Section 2.4, and the KsatHorFrac is adjusted. This adjusted model is coupled to a Sobek model of the Geul catchment in Slager et al. (2022). As a D-HYDRO model is used in this research, the KsatHorFrac parameter is adjusted. The KsatHorFrac parameter is multiplied by 1.4 in the original parameterset. This multiplication factor is removed to increase the peak flows during the July 2021 flood event.

### 3.8.3. Objective Function

The performance of each HBV run is quantified by the Nash Sutcliff Efficiency (NSE) (Nash & Sutcliffe, 1970) in Equation (3.1). The goal is to find the HBV parametersets that represent the observed discharge the best.

$$NSE = 1 - \frac{\sum_{t=1}^{T} \left(Q_{mod}(t) - Q_{obs}(t)\right)^2}{\sum_{t=1}^{T} \left(Q_{obs}(t) - \overline{Q_{obs}}\right)^2} \tag{3.1}$$

The calculated NSE value determines how well the model corresponds to the observed discharge. A NSE value smaller than 0, indicates that the mean of the observed discharge estimates the observed discharge better than the modelled discharge. A NSE value of 1 indicates that the modelled discharge equals the observed discharge. This NSE value will not occur due to sources of uncertainty (Savenije, 2009). Uncertainty in the precipitation radar observations will effect the modelled discharge. The observed discharge is not the ”truth”, because measurement devices have an uncertainty, as in Appendix E.3. Another source is the model uncertainty. Parameters can compensate for errors in the precipitation input and observed discharge or for errors in other parameters. Lastly, the applied intervals by the parameter observations in Appendix F.3 contain uncertainty. This uncertainty comes through measurement errors and the derivation methods.

## 3.9. Scenarios

The Geul catchment is located in the South of Limburg. This part of the province of Limburg contains 292.306 houses and there are plans to build 18,730 new houses in the coming years (Provincie Limburg, 2021a, 2021b). The building plans in the Geul catchment for the Dutch part are visualized in Figure 3.13. It can be seen that the most of the new houses are planned in the villages close to the Geul river. In this research, different scenarios are constructed to check the consequences of building new houses to the hydrological response and flooding. This is done by changing the amount of new houses and their locations.

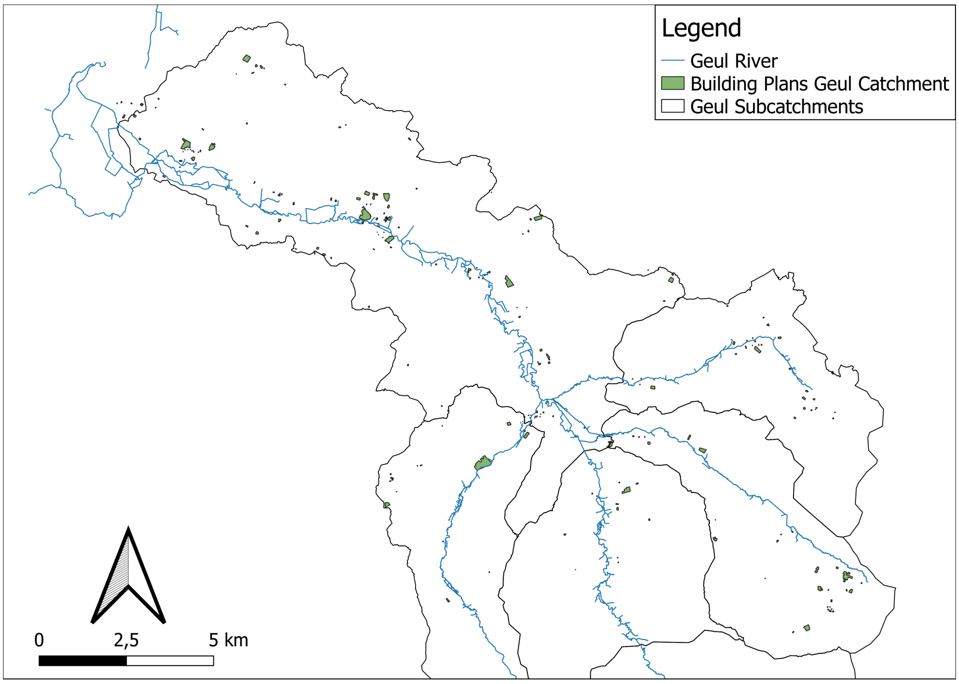


Figure 3.13: Building plans in the Geul catchment. Data by *Plancapaciteitsmonitor Limburg* (n.d.).

A house in the province of Limburg has a mean area of 158 $m^2$ (Provincie Limburg, 2022). Applying this to the building plans of the South of Limburg, results in an area of 3.0 $km^2$ for the 18,730 new houses. The total increase in paved area is twice the area of new houses, because new houses require infrastructure and services, as roads, schools, and stores. This is assumed to be equal to the area of the new houses. So, in total, 6.0 $km^2$ paved area is planned to be added to the South of Limburg. In this research, this new paved area will be applied to the Geul catchment at different locations. Next to these plans, the change in hydrological response is investigated for a completely paved subcatchment to investigate the subcatchment behaviour. This results in 8 scenarios, which are explained in the next subsections.

The scenarios are applied to the hydrological models through the scenario building process in Idsinga (2024). The land cover map in Section 2.4 is adjusted by changing the land cover categories of the pixels. The new paved areas get the category *112: Discontinous Urban Fabric*, this means that each pixel is 70% paved (Buitink, 2022). In this case, the large gardens and *Water en Bodem sturend* are taken into account. The changes in the land cover map are processed in the scenario builder notebook for the D-RR and HBV areas.

### 3.9.1. Scenario 1

The building plans are known for the Netherlands, but what happens to the hydrological response if Belgium and Germany start to increase their villages a lot? The Netherlands are downstream of these countries and has to deal with the changed response. Sippenaeken is the largest subcatchment in the Geul catchment and determines the downstream discharge for a large part (Elmensdorp, 2023). The change in the hydrological response is investigated for two building scenarios outside the Netherlands, which are visualised in Figure 3.14:

- Scenario 1a: The planned 6 $km^2$ increase of paved area, divided over the villages Aken (Germany), Hombourg, and Kelmis (Belgium);
- Scenario 1b: Completely paved Sippenaeken subcatchment;

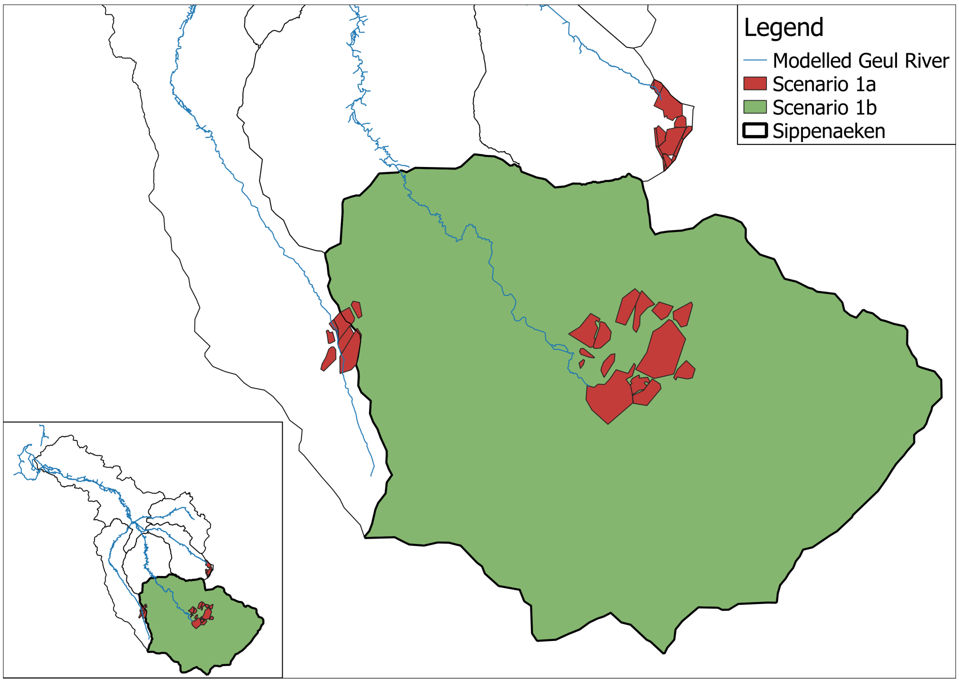


Figure 3.14: Visualization of the increased paved area for Scenario 1. Scenario 1a contains a 6 $km^2$ increase of paved area in the villages Hombourg, Kelmis, and Aken; from left to right. Scenario 1b contains a completely paved Sippenaeken subcatchment.

### 3.9.2. Scenario 2

The impact of the building plans are investigated per subcatchment in the Dutch part of the Geul catchment. Each subcatchment will react differently to an increase of the paved area. The planned increase of the paved area by 6 km$^2$ is added to the Meerssen (2a) and Gulp (2b) subcatchment, as they are the largest in the Dutch part. The difference of impact is investigated between building close to or far from the Geul river. Scenario 2a for the Meerssen subcatchment is visualized in Figure 3.15:

- Scenario 2a1: The planned 6 km$^2$ increase of paved area, divided over areas close to the Geul river in the Meerssen subcatchment;
- Scenario 2a2: The planned 6 km$^2$ increase of paved area, divided over areas far from to the Geul river in the Meerssen subcatchment;
- Scenario 2a3: Completely paved Meerssen subcatchment;

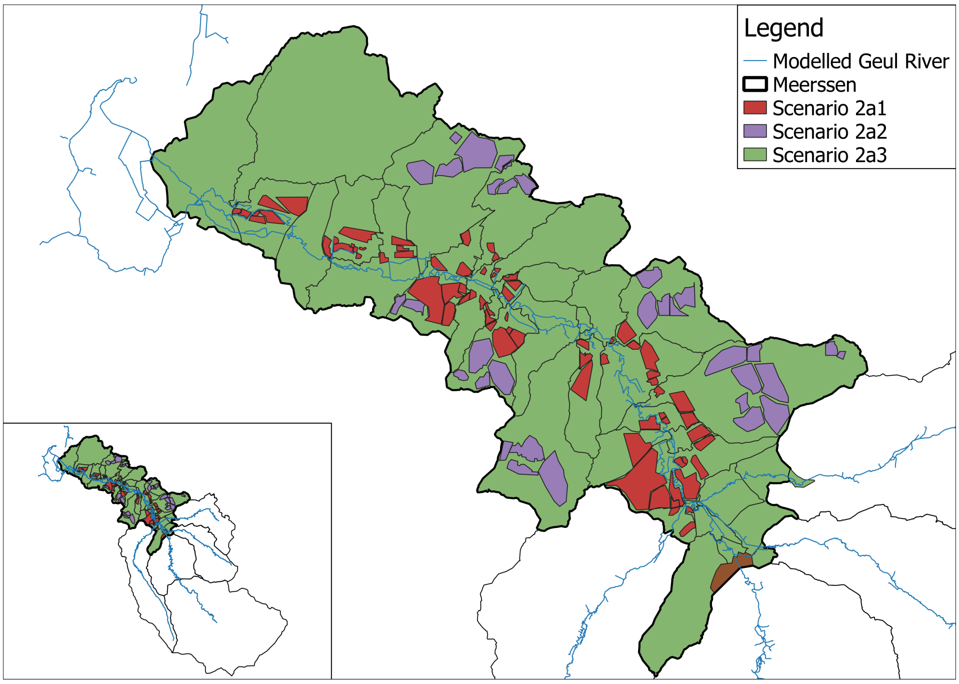


Figure 3.15: Visualization of the increased paved area for Scenario 2a in the Meerssen subcatchment. Scenario 2a1 contains a 6 km$^2$ increase of paved area close to the Geul river. Scenario 2a2 contains a 6 km$^2$ increase of paved area far from the Geul river. Scenario 2a3 contains a completely paved Meerssen subcatchment.

Scenario 2b for the Gulp subcatchment is visualized in Figure 3.16:

- Scenario 2b1: The planned 6 $km^2$ increase of paved area, divided over areas close to the Gulp tributary in the Gulp subcatchment;
- Scenario 2b2: The planned 6 $km^2$ increase of paved area, divided over areas far from to the Gulp tributary in the Gulp subcatchment;
- Scenario 2b3: Completely paved Gulp subcatchment.

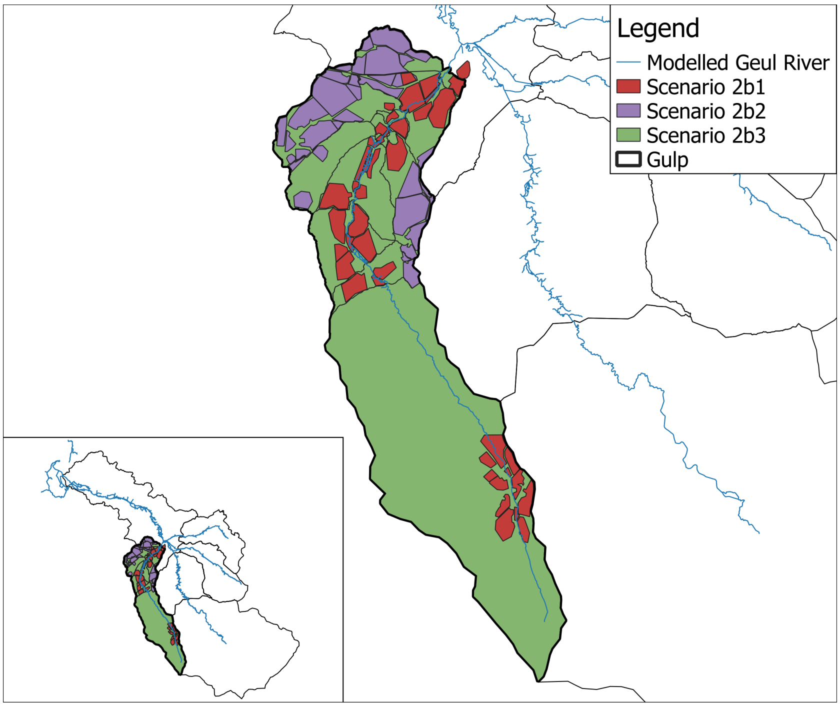


Figure 3.16: Visualization of the increased paved area for Scenario 2b in the Gulp subcatchment. Scenario 2b1 contains a 6 $km^2$ increase of paved area close to the Gulp tributary. Scenario 2b2 contains a 6 $km^2$ increase of paved area far from the Gulp tributary. Scenario 2b3 contains a completely paved Gulp subcatchment.

### 3.9.3. Impact Evaluation

The impact of each scenario is evaluated by the modelled hydrographs and flood extent. A scenario changes the discharge behaviour at a measurement location. The magnitude and timing of the peak discharge can change. The area of the flood extent can be larger or the water levels in the floodplains increase. The flood extent is determined by D-HYDRO and is defined by the maximum water depth level of at least 1 centimeter outside the Geul. This is analyzed by calculating the total area of the flood extent, the flooded paved area, and the flooded new paved area. The changes in discharge behaviour and flood extents are compared for the scenarios in Chapter 4. The steps to produce this results can be found in Idsinga (2024).

# 4
# Results

The hydrological models are calibrated according to the strategy described in Section 3.8. The results of the calibration of HBV are given in Appendix F. The calibrated hydrological models are coupled to D-HYDRO. The hydrographs of the results for the calibration period, validation period, and the July 2021 flood event are presented in Section 4.1. The modelled flood extents of the July 2021 flood event are presented in Section 4.2. The results of the scenarios are presented in Section 4.3 and Section 4.4, containing the hydrographs and flood extents respectively.

## 4.1. Calibration

The first D-HYDRO run contains the wet period in the calibration period from 31.01.2020 until 18.03.2020. The results of the hydrological models in that period in D-HYDRO are given in Figure 4.1. The second D-HYDRO run is presented in Figure 4.2, which contains the period 26.01.2021 - 10.02.2021 in the validation period. The results of the hydrological models in D-HYDRO for the July 2021 event are presented in Figure 4.3. In the figures it can be seen that the hydrological models show different behaviour for the three periods. The performance of the HBV and D-RR and Wflow_sbm are evaluated to the observed discharge for the NSE values and the shapes of the hydrographs.

HBV and D-RR perform better in the calibration period, while Wflow_sbm performs a little better in the validation period and better in the July 2021 flood event. HBV and D-RR performs better in the calibration period, because it is calibrated on that period. On the other hand, Wflow_sbm is adjusted to increase the representability of the July 2021 flood event. This results in a better performance for that event. The different calibration approaches explains the difference in the model results. Wflow_sbm is calibrated on a large precipitation event after a dry period, while HBV and D-RR are calibrated on a period with consecutive precipitation events. Therefore Wflow_sbm represents the peaks in the validation period better than HBV and D-RR, but overestimates the most of them.

Based on the hydrographs, Wflow_sbm represents the overland flow better than HBV and D-RR. Wflow_sbm follows the quick increase in most of the cases. For example at Azijnfabriek, Cottessen, and Sippenaeken in the validation period in Figure 4.2, while HBV and D-RR do not get the first discharge peak right. HBV and D-RR also show delay in the discharge peaks at Meerssen and Sippenaeken, compared to Wflow_sbm. This can also be seen for the July 2021 flood event in Figure 4.3. Wflow_sbm follows the observations in the discharge generation at Cottessen and Sippenaeken and shows flashy behaviour at Eys, Azijnfabriek, and Partij. On the other hand, HBV and D-RR do not represent the overland flow in Eys, Azijnfabriek, and Partij, where the discharge is underestimated by the model. HBV and D-RR, also show no flashy behaviour at the measurement locations along the Geul. At Sippenaeken, one delayed peak is generated instead of two peaks. The estimated discharge peak flattens more upstream as can be seen at Hommerich, Schin op Geul, and Meerssen. The timing of the discharge peak is later than the observations.

HBV and D-RR do represent the subsurface flow better than Wflow_sbm. This can mainly be seen in the calibration period in Figure 4.1. The saturation of the soil is very important in this period, because of the consecutive precipitation events. It can be seen that Wflow_sbm underestimates the discharge, except for Azijnfabriek and Partij. The lowering of the KsatHorFrac parameter, described in Section 3.8.2, is the reason for this discharge behaviour. This adjustment leads to increased peak discharges and less base flow. HBV and D-RR follow the observations better for the discharge after the peaks and the base flow. This can be seen for example at Meerssen and Sippenaeken. However, some discharge peaks are overestimated or are incorrectly timed during the lower flows. The subsurface flow is not fully correct represented by HBV and D-RR, but better than Wflow_sbm. This can also be seen in the validation period in Figure 4.2. After the first two discharge peaks, the generated discharge by Wflow_sbm quickly drops to the base flow at Sippenaeken. HBV and D-RR follow the observations more in this period, however for the next two discharge peaks, the discharge does not drop quick enough. This can be explained by the fact that subsurface flow is dominant in the second precipitation event, while overland flow is dominant during the third and fourth precipitation events. Lastly, the difference between the hydrological models can be seen for the July 2021 flood event in Figure 4.3. HBV and D-RR are closer to the observations after the discharge peak for all the measurement locations. The decrease in discharge is one day faster for Wflow_sbm than HBV and D-RR at Sippenaeken and the difference increases to two days downstream at Meerssen.

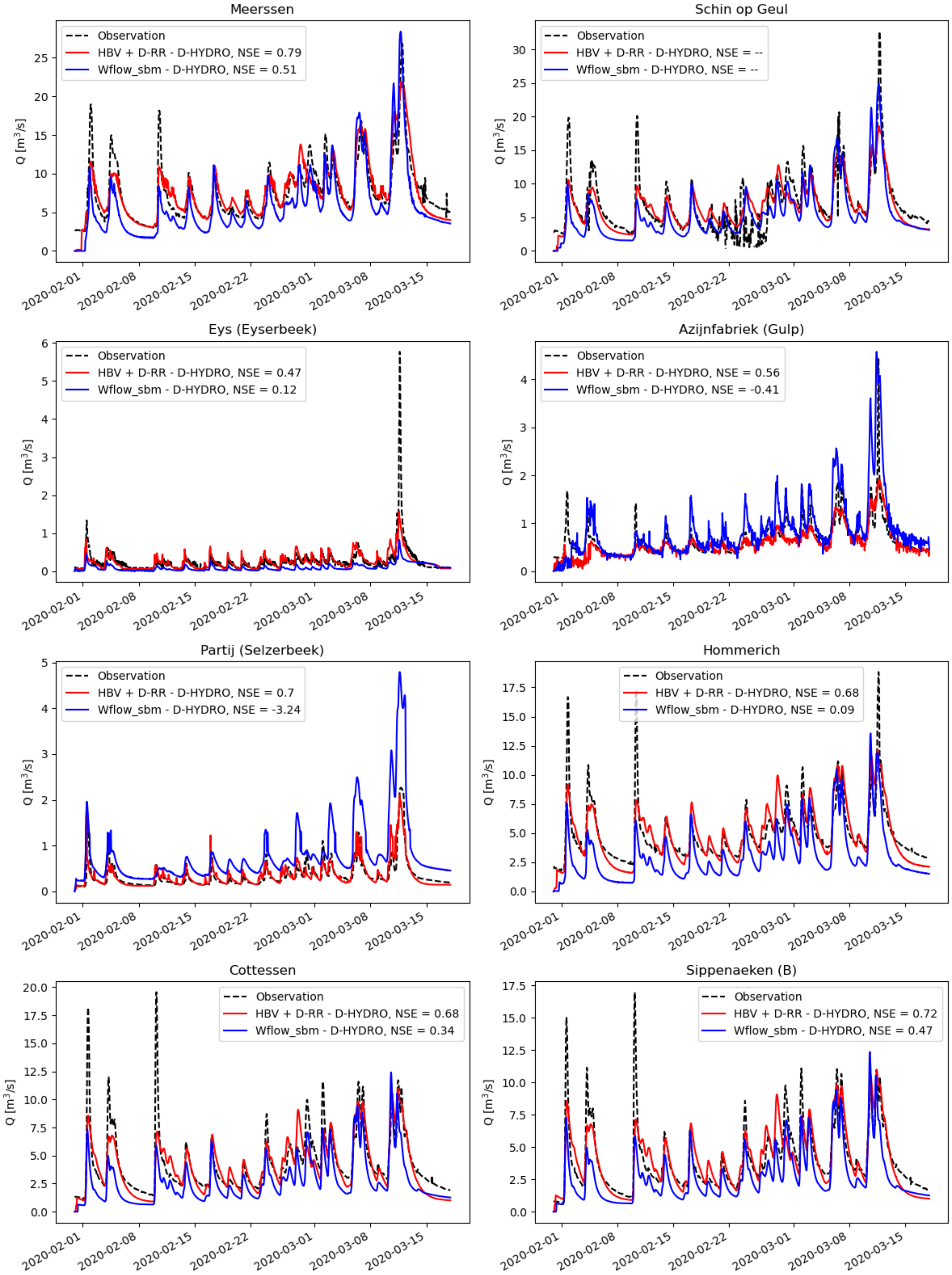


Figure 4.1: The hydrographs of the calibration period of the hydrological models in D-HYDRO.

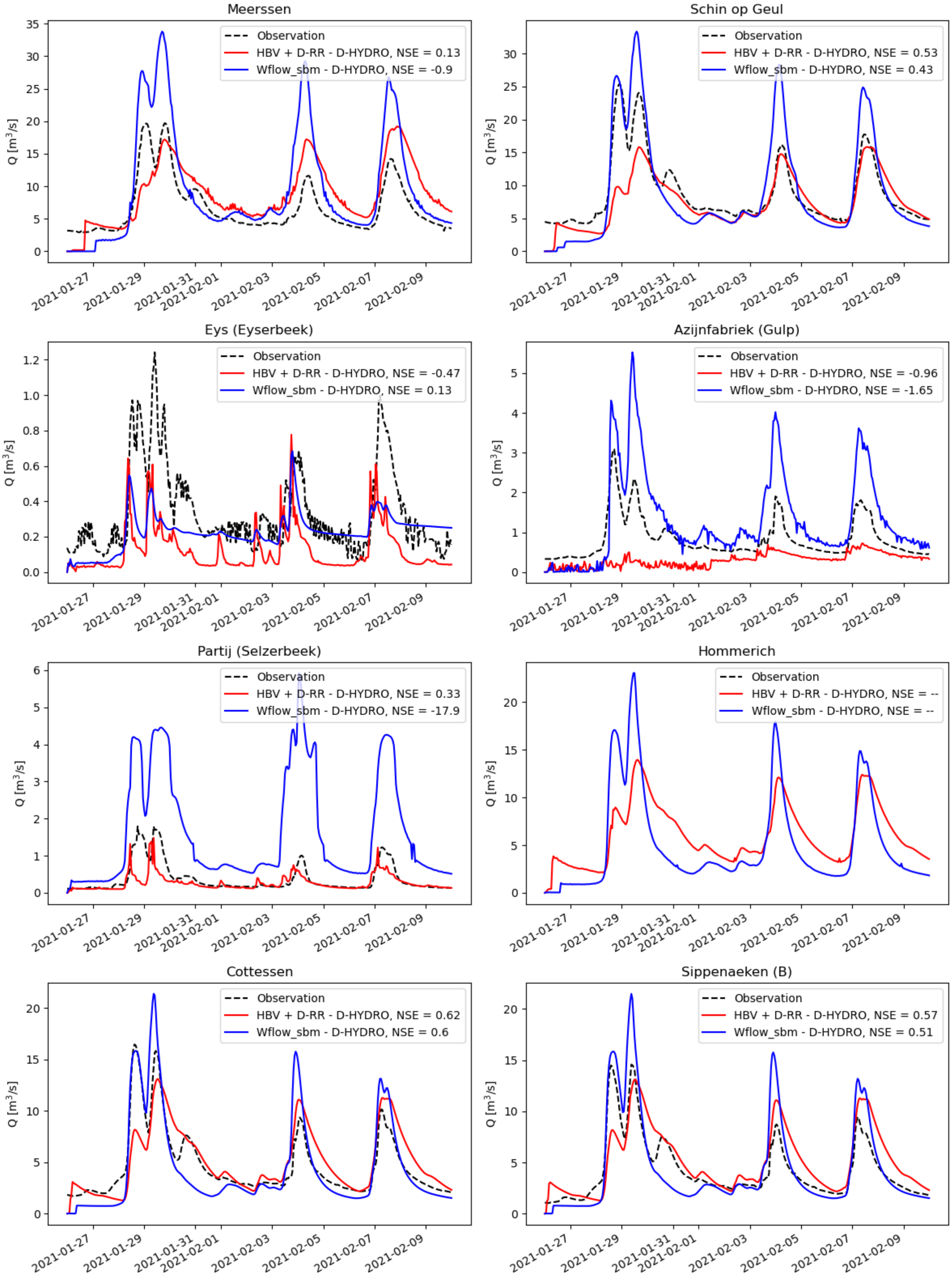


Figure 4.2: The hydrographs of the validation period of the hydrological models in D-HYDRO.

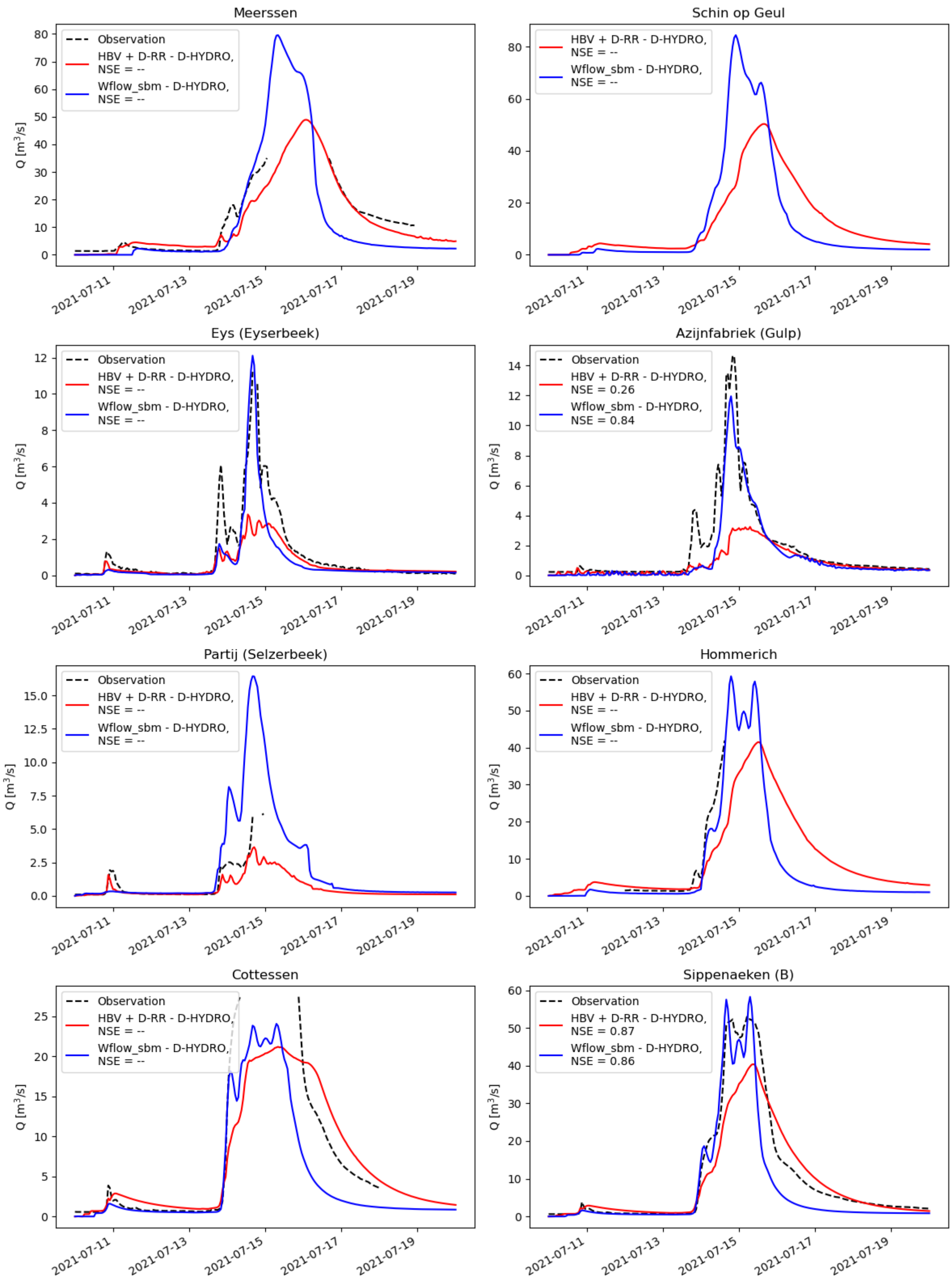


Figure 4.3: The hydrographs of the July 2021 flood event for the hydrological models in D-HYDRO.

## 4.2. July 2021 Flood extent

Slager et al. (2021) estimated the flood extent of the July 2021 flood event for the Dutch part of the Geul. D-HYDRO provides a flood extent of the July 2021 flood event for the hydrological models. The modelled flood extent is compared to the measured flood extent for Valkenburg in Figure 4.4 and for the confluence of the tributaries near Gulpen in Figure 4.5. It can be seen that Wflow_sbm is close to the measured flood extent. However, HBV and D-RR have a too small flood extent. The results show correspondence with the hydrographs during the event in Figure 4.3. The too small peak discharge of HBV and D-RR results in a too small flood extent in the figures. More water is needed to have a better representation of the flooded area. Wflow_sbm shows similarity with the flood event for both the hydrographs and flood extents.

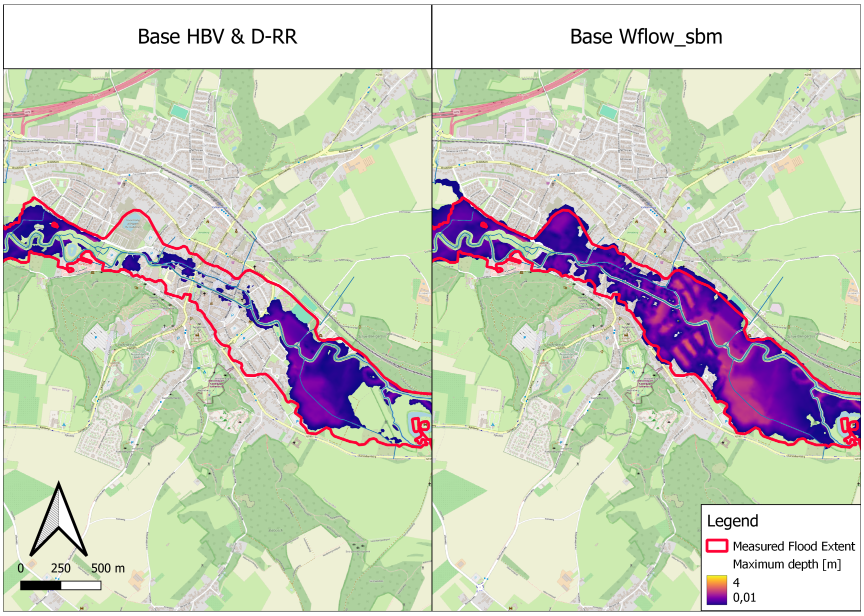


Figure 4.4: The modelled flood extents of the hydrological models in D-HYDRO of the July 2021 event, compared to the measured flood extent for the city of Valkenburg.

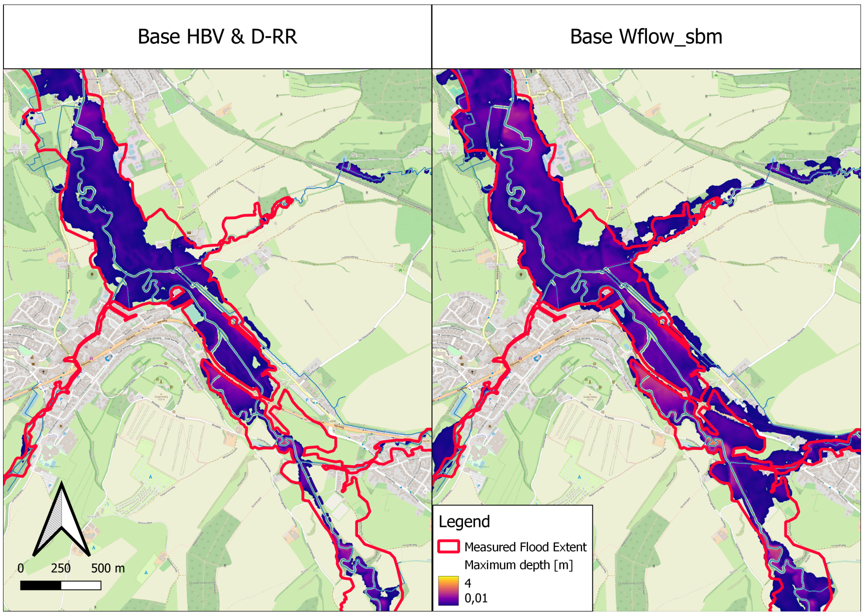


Figure 4.5: The modelled flood extents of the hydrological models in D-HYDRO of the July 2021 event, compared to the measured flood extent for the confluence of the tributaries near Gulpen.

## 4.3. Scenario Hydrographs

This section presents the hydrographs of the scenarios for the hydrological models. The change in the hydrological responses is discussed, based on the graphs.

### 4.3.1. Scenario 1a

Scenario 1a simulates the expansion of the villages Aken (Germany), Hombourg, and Kelmis (Belgium) by 6 $km^2$. This results in the hydrographs in Figure 4.6, compared to the base runs in Section 4.1. It can be seen that HBV and D-RR generate the slightly increased discharge peak faster. This is the result of an increase in overland flow by the extra paved areas. The largest change in behaviour can be seen at Azijnfabriek. The peak discharge increased by 0.6 $m^3$/s and arrived 14 hours earlier. The generation of the discharge peak becomes faster and starts at the same time as for Wflow_sbm. The hydrological response also changes at the other measurement locations for HBV and D-RR. An increased peak discharge of 0.5 $m^3$/s arrived 2 hours earlier at Sippenaeken. The peak at Cottessen arrived 1 hour earlier. The peak discharge at Hommerich increased by 0.5 $m^3$/s and arrived 2 hours earlier. The measurement location Partij has an increased peak discharge of 0.3 $m^3$/s, which arrived 3 hours later. But it can be seen that the peak discharge is spread over a longer time period and the generation of that peak occurs earlier than the base HBV and D-RR run. The timing did not change at Schin op Geul, but the discharge increased by 1 $m^3$/s. Lastly, the peak discharge increased by 0.8 $m^3$/s at Meerssen and the peak arrived 1 hour earlier. The addition of the houses does not influence the subsurface flow much, as change in the discharge after the event is very small for all measurement locations for HBV and D-RR.

The change in hydrological response is very small for Wflow_sbm. The peak discharge becomes a little larger at Sippenaeken, Hommerich, Azijnfabriek, Schin op Geul, and Meerssen. The increase in peak discharge is 1.5 $m^3$/s at Sippenaeken, 1 $m^3$/s at Hommerich, 0.4 $m^3$/s at Azijnfabriek, 1.5 $m^3$/s at Schin op Geul, and 1 $m^3$/s at Meerssen. The discharge peak arrived 2 hours earlier at Sippenaeken, and 1 hour earlier at Meerssen. The timing did not change at the other measurement locations. The extra houses at Aken does not result in a change of the peak discharge at Selzerbeek.

### 4.3.2. Scenario 1b

Scenario 1b simulates a completely paved Sippenaeken subcatchment. This results in the hydrographs in Figure 4.7. The measurement locations along the Geul show flashier behaviour for both models. The largest increase in peak discharges can be seen for HBV and D-RR. At Sippenaeken, the peak discharge increased from 40.4 $m^3$/s to 170.9 $m^3$/s. The change in timing of this peak cannot be captured, because the flashy behaviour results in for 4 discharge peaks greater than 100 $m^3$/s. This generates flooding in all the cases. The same happens for Wflow_sbm, however the magnitudes of the discharge peaks are smaller. The peak discharge for Wflow_sbm increased by 59 $m^3$/s to 119 $m^3$/s. This change in behaviour can be seen downstream at Cottessen, Hommerich, and Schin op Geul. The buffering and flooding in the Geul catchment reduce the flashy behaviour as can be seen at Meerssen. Here, HBV and D-RR and Wflow_sbm show similar hydrographs. The peak discharge of HBV and D-RR increased by 37 $m^3$/s and arrived 25 hours earlier. The peak discharge of Wflow_sbm increased by 7 $m^3$/s and arrived 7 hours earlier.

Further, the hydrological response at Azijnfabriek changes for Wflow_sbm, but does not for HBV and D-RR. This means that water from the Sippenaeken subcatchment flows to the Gulp subcatchment, where it enters the Gulp. This is not captured by HBV and D-RR. The reason for this is the topography in Belgium, which is included in Wflow_sbm, but not in HBV and D-RR. Water flows from the hills towards the valleys, where it is collected in a stream. This is the case for the areas around the border between the subcatchments Gulp and Sippenaeken. The increase at Azijnfabriek, results in less discharge at Sippenaeken for Wflow_sbm. Going more upstream, the difference between the models decreases as the water from Azijnfabriek joins the Geul.

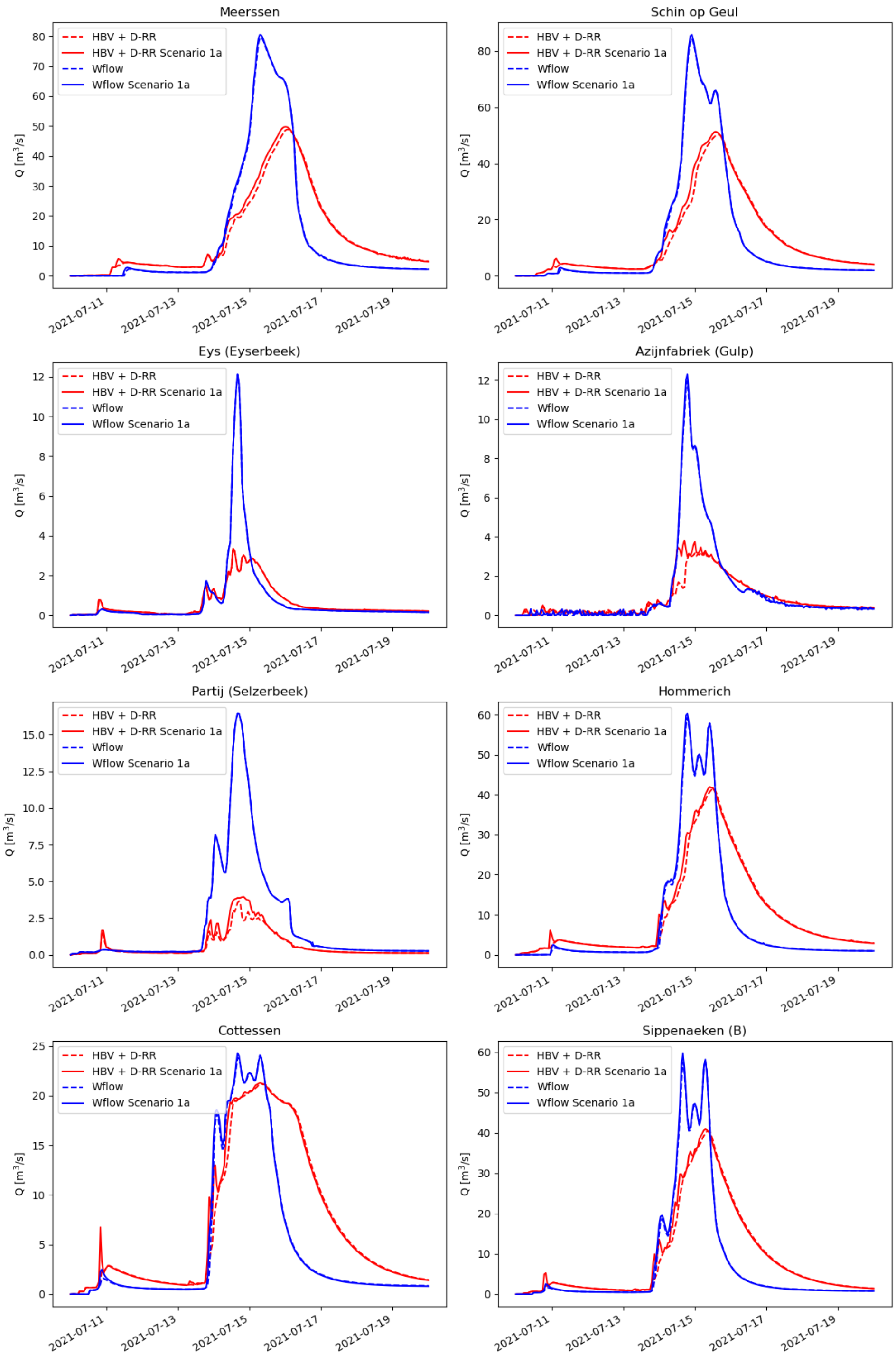


Figure 4.6: The hydrographs of Scenario 1a, compared to the base hydrological models.

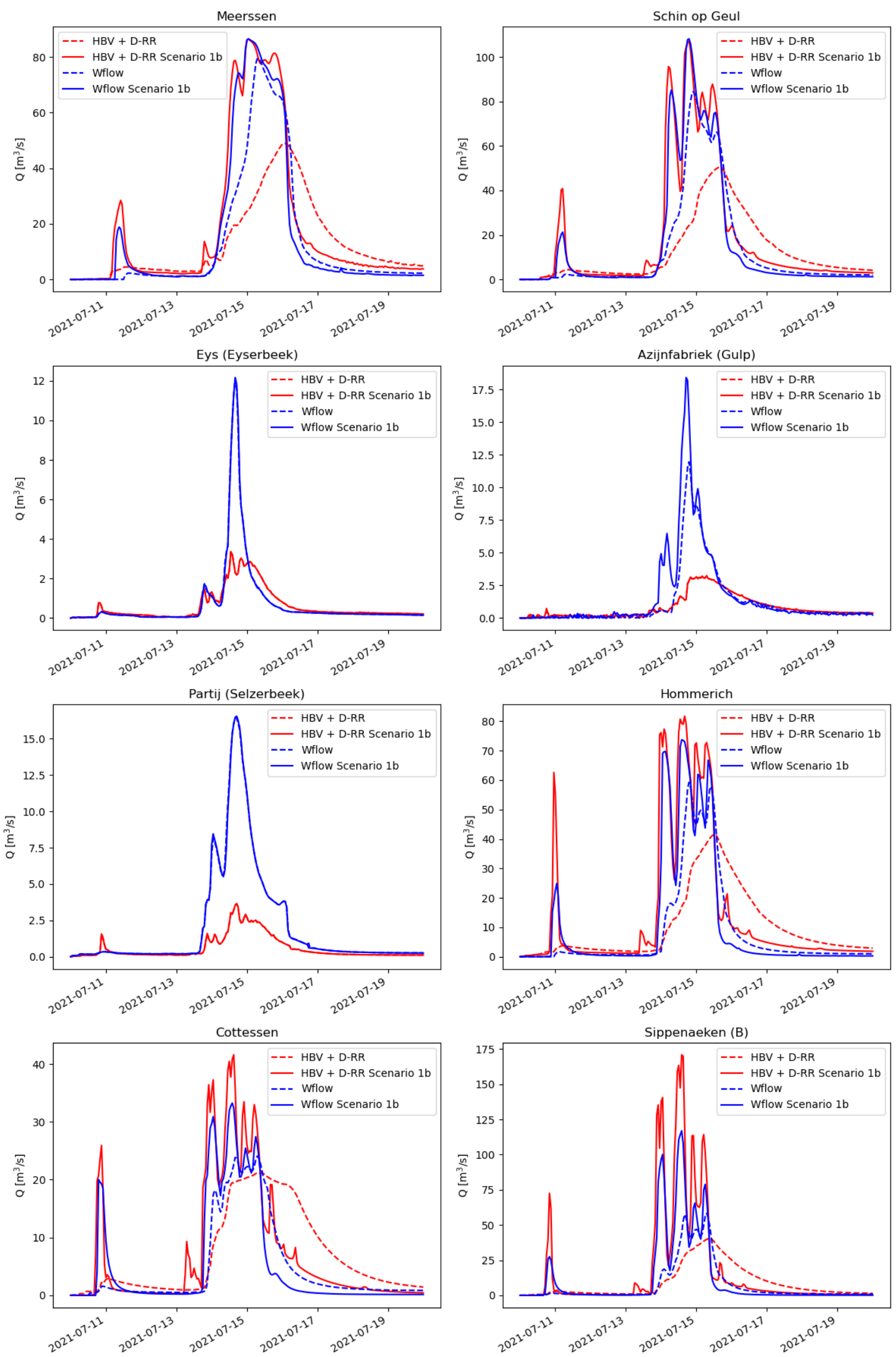


Figure 4.7: The hydrographs of Scenario 1b, compared to the base hydrological models.

### 4.3.3. Scenario 2a1 vs Scenario 2a2

Figure 4.8 presents the hydrographs for scenarios 2a1 and 2a2 at the discharge stations Meerssen and Schin op Geul. Both scenarios simulate an increase of 6 $km^2$ in the paved area of the Meerssen subcatchment. Scenario 2a1 simulates an increase close to the Geul river and Scenario 2a2 simulates an increase far from the river. The hydrographs per scenario are presented in Appendix G.1. The differences between the scenarios are very small. For Wflow_sbm the timing only differs at Meerssen, where the peak of Scenario 2a2 arrives 1 hour earlier. The timing for HBV and D-RR only differs at Schin op Geul, where the peak discharge of Scenario 2a2 arrived 1 hour earlier. The magnitude of the peak discharge is lower for Scenario 2a2 than for 2a1, except at Meerssen for Wflow_sbm. Here the peak discharge is 0.2 $m^3/s$ higher. The peak discharge is 0.1 - 0.3 $m^3/s$ lower for Scenario 2a2 at the other runs.

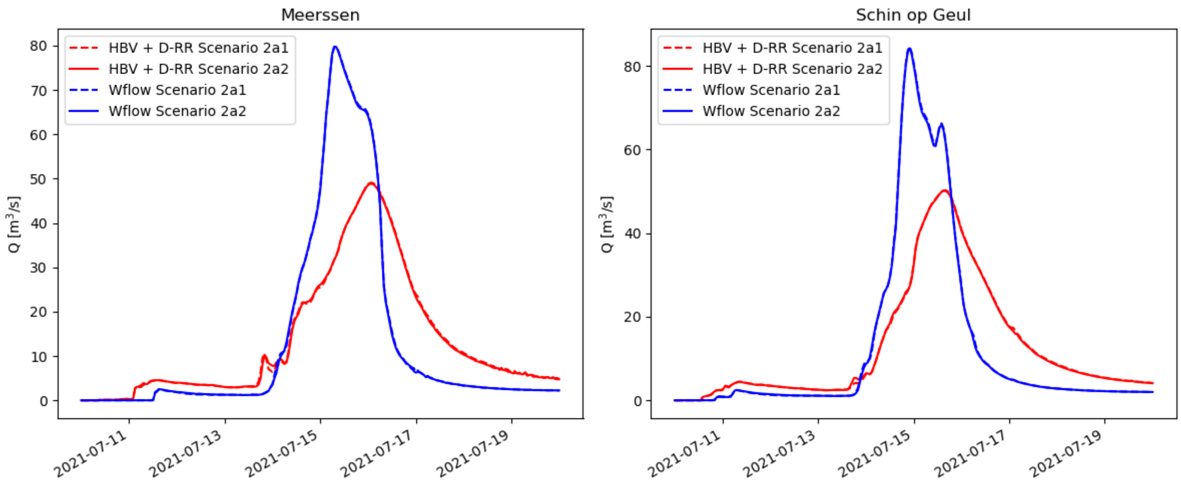


Figure 4.8: Comparison of the hydrographs of the Scenarios 2a1 and 2a2.

### 4.3.4. Scenario 2a3

Scenario 2a3 simulates a completely paved Meerssen subcatchment. This results in the hydrographs at Meerssen and Schin op Geul in Figure 4.9. It can be seen that the hydrological response of the sub-catchment changes. Section 2.2 describes that the Meerssen subcatchment contributes a little to the discharge in the Geul, compared to the other subcatchments. This behaviour is visible for Wflow_sbm, but not for HBV and D-RR. The shape of the hydrograph for Wflow_sbm only changes at the start of the precipitation event, while the behaviour of HBV and D-RR changes completely. One peak changes to multiple peaks, indicating a more flashy behaviour in Meerssen in this scenario.

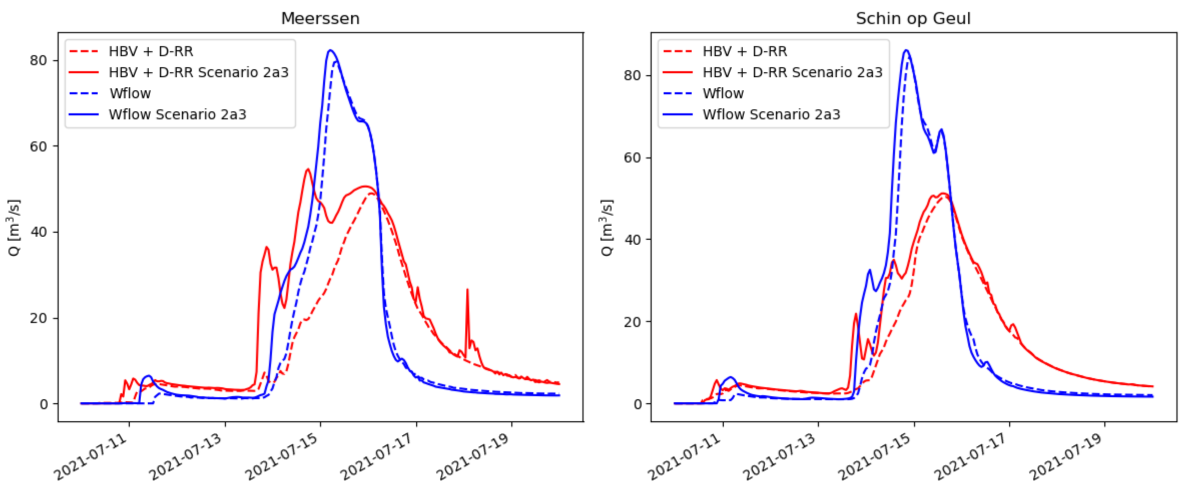


Figure 4.9: The hydrographs of Scenario 2a3, compared to the base hydrological models.

The peak discharge at Meerssen changes from 49 $m^3/s$ to 54.5 $m^3/s$ for HBV and D-RR. This peak occured 1.5 days earlier than in the base scenario. It can also be seen that when the peak of Wflow_sbm increases on 15 July, the discharge of HBV and D-RR drops. Indicating that the upstream discharge passes through Meerssen after the generated discharge in the subcatchment is discharged. The peak discharge at Meerssen increases by 0.8 $m^3/s$ and arrives one hour earlier. The hydropgraphs of Wflow_sbm show different discharge behaviour at the start of the event. The completely paved Meerssen subcatchment generates more overland flow, resulting in faster and more runoff. At Schin op Geul, the peak discharge occured 2 hours earlier and increased by 1.5 $m^3/s$. The peak discharge at Meerssen increased 2.5 $m^3/s$ and occured 3 hours earlier.

### 4.3.5. Scenario 2b1 vs Scenario 2b2

The results of the scenarios 2b1 and 2b2 are presented in Figure 4.10. Scenario 2b1 represents an increase in the paved area of 6 $km^2$ close to the Gulp stream and Scenario 2b2 represents the same increase far from the Gulp. The hydrological response changes at the measurement stations Azijnfabriek, Schin op Geul, and Meerssen. The discharge at the stations are lower for Scenario 2b2 than for Scenario 2b1 for Wflow_sbm. The differences are 0.5 $m^3/s$, 0.4 $m^3/$, and 0.2 $m^3/s$ at Azijnfabriek, Schin op Geul, and Meerssen respectively. The timing of the peak discharges does not change. HBV and D-RR also estimate lower peak discharges for Scenario 2b2. The magnitude of the peak discharge is 1.1 $m^3/s$ lower at Azijnfabriek, 0.4 $m^3/s$ lower at Schin op Geul, and 0.4 $m^3/s$ at Meerssen. The peak discharge of Scenario 2b1 is 2 hours earlier at Schin op Geul than that of Scenario 2b2. The other measurement locations do not contain a difference in timing for HBV and D-RR.

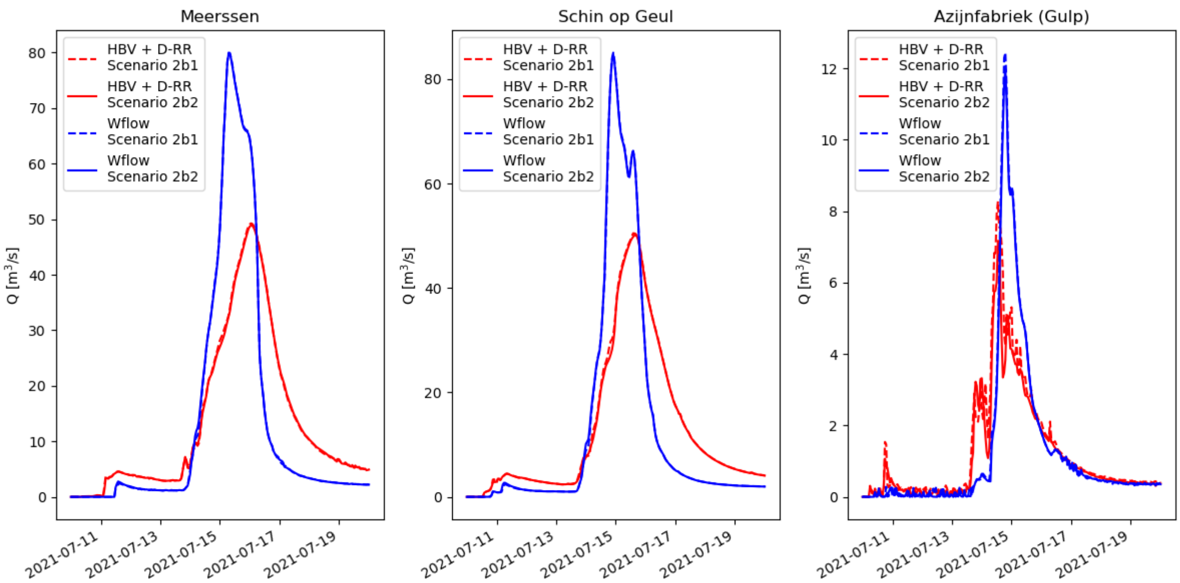


Figure 4.10: Comparison of the hydrographs of the scenarios 2b1 and 2b2.

### 4.3.6. Scenario 2b3

Scenario 2b3 simulates a completely paved Gulp subcatchment. This results in the hydrographs in Figure 4.11. It can be seen that the hydrological responses at Meerssen, Schin op Geul, and Azijnfabriek changed. The biggest change occured for HBV and D-RR. The peak discharge increased from 3.2 $m^3/s$ to 54.9 $m^3/s$ and occured 15 hours earlier. This results in a 19 $m^3/s$ higher discharge peak at Schin op Geul, which occured 23 hours earlier. The hydrograph shows similar behaviour to Wflow_sbm. This means that the overland flow flux of HBV and D-RR becomes similar to HBV and D-RR. The discharge peak at Meerssen occurred 21 hours earlier and increased by 11 $m^3/s$. The changed discharge behaviour of Wflow_sbm is smaller than HBV and D-RR. The discharge peak increased by 6 $m^3/s$ at Azijnfabriek and occurred 2 hours earlier. The peak discharge at Schin op Geul occurs 1 hour earlier and increases by 3 $m^3/s$. Lastly, the peak discharge increased at Meerssen by 3 $m^3/s$ and the peak occurred 2 hours earlier.

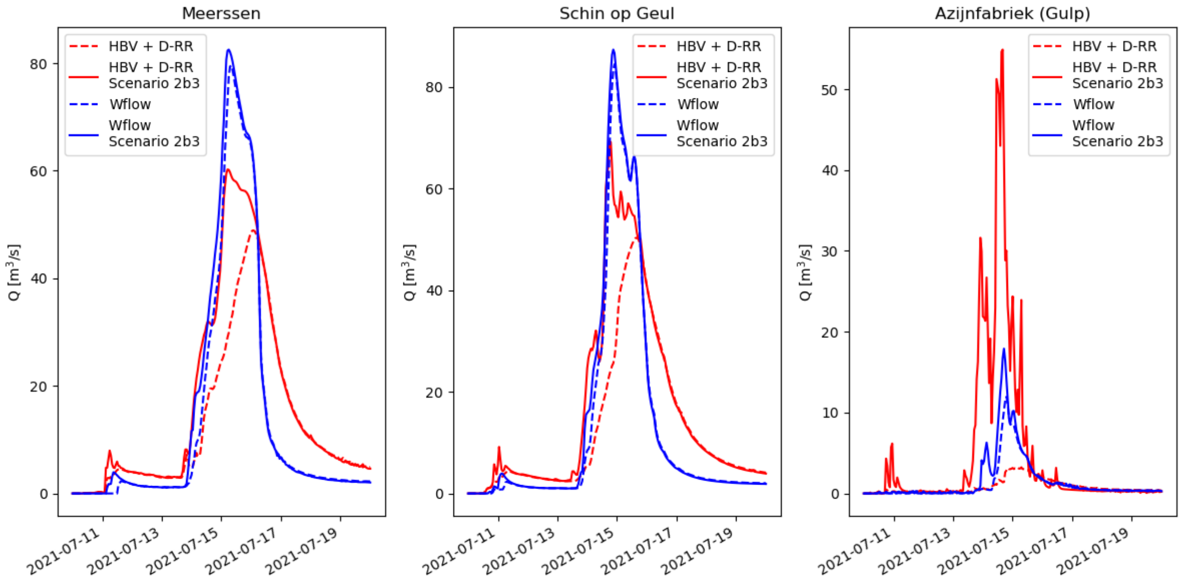


Figure 4.11: The hydrographs of Scenario 2b3, compared to the base hydrological models.

## 4.4. Flood Extent

In this section, the change in flood extent per scenario is investigated. The flooded area, the corresponding paved area, and flooded new paved area are determined per scenario and compared to the base hydrological models. An increase in flood extent is determined per scenario. An example of a changed flood extent is presented in Figure 4.12. In this figure, the flood extents of the base models are compared to Scenario 1a. It can be seen that the flood extent of HBV and D-RR changed, but Wflow_sbm did barely.

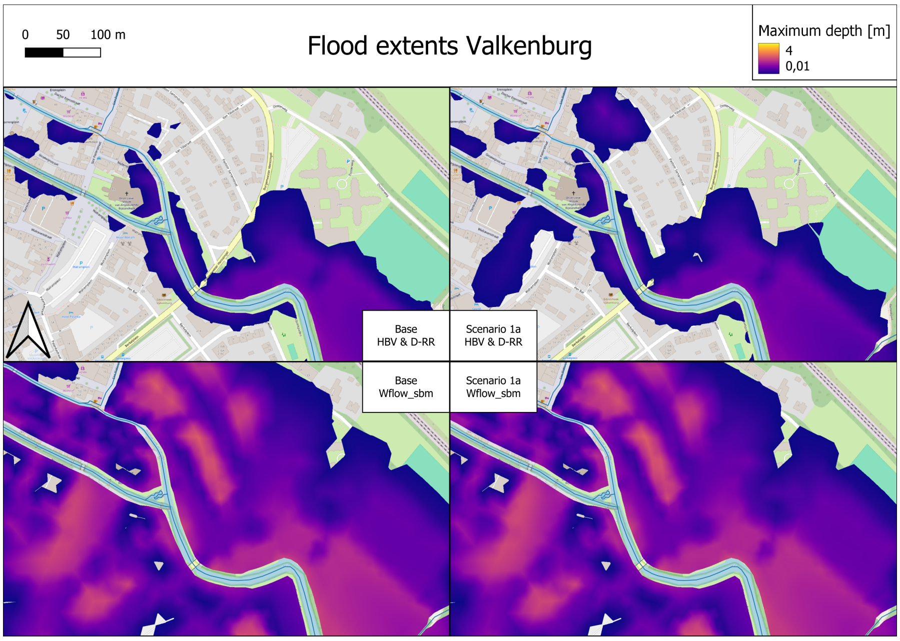


Figure 4.12: Comparison of the flood extents of the base hydrological models to Scenario 1a at the city of Valkenburg.

Table 4.1 presents the flooded areas per scenario and the differences to the base hydrological models. It can be seen that the flood extent of Wflow_sbm is almost twice the area of HBV and D-RR. This is the result of the underestimation of the discharge by HBV and D-RR, as explained and visualized in Section 4.2. HBV and D-RR have a relative larger change in flood extent for the scenarios than Wflow_sbm. This can be explained by the fact that HBV and D-RR do not represent the overland flow well. D-RR represents the urban runoff and is underestimated during the event. The increased paved area results in more direct runoff and therefore more overland flow. The change for D-RR is larger than for Wflow_sbm as Wflow_sbm already has a large overland flux. Changing the paved area leads therefore to a relatively smaller change in flood extent. The increase in overland flow results in more discharge in the river and in more flooding.

It can be seen that the scenarios containing 6 km$^2$ of new paved area do not show significant changes. The scenarios 2a1, 2a2, and 2b2 show no change in the flooded area and the scenarios 1a and 2b1 show a change of 5% or less. The scenarios containing a completely paved subcatchment show larger changes in the flooded area. The increase in flooded area shows correspondence to the contribution per subcatchment to the total flow in the Geul, as explained in Section 2.2. Sippenaeken contains one third of the total area of the Geul catchment and generates two third of the discharge at Valkenburg (Elmensdorp, 2023). On the other hand, Meerssen hardly contributes to the discharge in the Geul. The Gulp is the second largest contributor to the discharge at Valkenburg. The ratio of the contributions to the discharge can also be seen in the table. A completely paved Sippenaeken subcatchment in Scenario 1b shows the largest changed, followed by a completely paved Gulp subcatchment in Scenario 2b3. The smallest change occurs for a completely paved Meerssen subcatchment in Scenario 2b3.

| Scenario | Model | New Paved Area [ha] | Flooded Area: Area [ha] | Flooded Area: Increase [ha] | Flooded Area: Increase [%] |
|---|---|---|---|---|---|
| Base | HBV + D-RR | - | 513 | - | - |
| | Wflow_sbm | - | 997 | - | - |
| Scenario 1a | HBV + D-RR | 600 | 538 | 25 | 5 |
| | Wflow_sbm | 600 | 1010 | 13 | 1 |
| Scenario 1b | HBV + D-RR | 11008 | 1027 | 514 | 100 |
| | Wflow_sbm | 11008 | 1167 | 170 | 17 |
| Scenario 2a1 | HBV + D-RR | 600 | 513 | 0 | 0 |
| | Wflow_sbm | 600 | 999 | 2 | 0 |
| Scenario 2a2 | HBV + D-RR | 600 | 512 | -1 | 0 |
| | Wflow_sbm | 600 | 1000 | 3 | 0 |
| Scenario 2a3 | HBV + D-RR | 7327 | 559 | 46 | 9 |
| | Wflow_sbm | 7327 | 1041 | 528 | 4 |
| Scenario 2b1 | HBV + D-RR | 600 | 522 | 9 | 2 |
| | Wflow_sbm | 600 | 1004 | 7 | 1 |
| Scenario 2b2 | HBV + D-RR | 600 | 514 | 1 | 0 |
| | Wflow_sbm | 600 | 998 | 1 | 0 |
| Scenario 2b3 | HBV + D-RR | 4416 | 749 | 236 | 46 |
| | Wflow_sbm | 4416 | 1042 | 45 | 5 |

Table 4.1: The flooded areas per scenario, compared to the base hydrological models. The scenarios 1a, 2a1, 2a2, 2b1, and 2b2, simulate the planned increase of 6 $km^2$ in paved area in the South of Limburg. The scenarios 1b, 2a3, and 2b3 simulate a completely paved Sippenaeken, Meerssen, and Gulp subcatchment respectively.

The differences in the total flood extent between building close to and far from the river are very small for the scenarios 2a1 and 2a2 and for 2b1 and 2b2 in Table 4.1. The total flooded paved area is determined to investigate the differences in more detail. Table 4.2 presents the flooded paved areas, the flooded area of the new paved areas and their contribution to the increase of the total flooded paved area.

It can be seen that building close to or far from the river does make a difference for the total flooded paved area. The total flood extent did not differ much, but the land cover type of the flooded area changed. Scenario 2a1 resulted in 69 hectares more flooded paved area for HBV and D-RR and 91 hectares more for Wflow_sbm. The increase mostly contains the flooded area of the added paved area. This is 95% of the increase for both hydrological models. On the other hand, the flooded paved area did not change in Scenario 2a2. This can also be seen for the scenarios 2b1 and 2b2. Scenario 2b2 did not result in an increase of the flooded paved area, while the flooded paved area in Scenario 2b1 increased by 10 hectares for HBV and D-RR and by 23 hectares for Wflow_sbm. The new paved area is also in this scenario the largest contributor to the increase of the flooded area. The flooded new paved area is 84% of the increase in flooded paved area for HBV and D-RR and 91% of the increase for Wflow_sbm.

The flooded new paved area in Scenario 1a shows the smallest contribution to the increase of the flooded paved area. The increase of 5 hectares for HBV and D-RR comes for 25% by flooded new paved area. Wflow_sbm resulted in an increase of 3 hectares of which 70% is flooded new paved area. This results in relatively more downstream flooding of paved areas. This can also be seen for the completely paved Sippenaeken subcatchment in Scenario 1b. 61% of the 195 hectares increase of the flooded paved area resulted from flooded new paved area for HBV and D-RR. The increase of 132 hectares for Wflow_sbm contains 79% of flooded new paved areas. Therefore, downstream flood extent increased.

The completely paved Gulp subcatchment in Scenario 2b3 resulted in a large increase of the flooded paved area. The increase is 137 hectares for HBV and D-RR and 67 hectares for Wflow_sbm. This increase for Wflow_sbm is smaller than that of Scenario 2a1. This means that paved areas close to the Geul in the Meerssen subcatchment are more exposed to flooding than a completely paved Gulp subcatchment. This can also be seen for a completely paved Meerssen subcatchment in Scenario 2a3. This resulted in the largest flooded paved area. The flooded area increased by 415 hectares for HBV and D-RR and by 627 hectares for Wflow_sbm. Being at the downstream side, the Meerssen subcatchment is most vulnerable to flooding.

| Scenario | Model | Flooded Paved Area [ha] | Increase | | Flooded New Paved Area [ha] | Percentage Of Increase [%] |
|---|---|---|---|---|---|---|
| | | | Area [ha] | Perc. [%] | | |
| **Base** | HBV + D-RR | 15 | - | - | - | - |
| | Wflow_sbm | 83 | - | - | - | - |
| **Scenario 1a** | HBV + D-RR | 20 | 5 | 33 | 1 | 25 |
| | Wflow_sbm | 86 | 3 | 4 | 2 | 70 |
| **Scenario 1b** | HBV + D-RR | 210 | 195 | 1300 | 118 | 61 |
| | Wflow_sbm | 215 | 132 | 159 | 105 | 79 |
| **Scenario 2a1** | HBV + D-RR | 84 | 69 | 460 | 65 | 95 |
| | Wflow_sbm | 174 | 91 | 110 | 87 | 95 |
| **Scenario 2a2** | HBV + D-RR | 15 | 0 | 0 | 0 | 0 |
| | Wflow_sbm | 83 | 0 | 0 | 0 | 0 |
| **Scenario 2a3** | HBV + D-RR | 430 | 415 | 2767 | 411 | 99 |
| | Wflow_sbm | 710 | 627 | 755 | 611 | 98 |
| **Scenario 2b1** | HBV + D-RR | 25 | 10 | 67 | 8 | 84 |
| | Wflow_sbm | 106 | 23 | 28 | 21 | 91 |
| **Scenario 2b2** | HBV + D-RR | 15 | 0 | 0 | 0 | 0 |
| | Wflow_sbm | 83 | 0 | 0 | 0 | 0 |
| **Scenario 2b3** | HBV + D-RR | 152 | 137 | 913 | 108 | 79 |
| | Wflow_sbm | 150 | 67 | 81 | 60 | 90 |

Table 4.2: The flooded paved areas and flooded new paved areas per scenario, compared to the base hydrological models. The scenarios 1a, 2a1, 2a2, 2b1, and 2b2, simulate the planned increase of 6 km$^2$ in paved area in the South of Limburg. The scenarios 1b, 2a3, and 2b3 simulate a completely paved Sippenaeken, Meerssen, and Gulp subcatchment respectively. Flooded paved area is the total paved area that is flooded. The flooded new paved area is the increased area that is flooded. The percentage of increase is how much the flooded new area contributes to the increase in the total flooded paved area.

# 5 Discussion

This chapter discusses the implications of the research. Section 5.1 describes modelling assumptions and the model limitations. The implications of the used data is elaborated in Section 5.2. Section 5.3 discusses the assumptions for the scenarios. Lastly, Section 5.4 discusses the results.

## 5.1. Models

### 5.1.1. Modelled Areas

The D-HYDRO model of the Geul is focussed on the Netherlands, because the client was the Waterboard of Limburg and no data for Belgium were available (Hulsman et al., 2023). This affects the model representation of the Belgian part of the Geul catchment. D-RR did not contain paved areas in Belgium. To be able to simulate an expansion of paved areas in Belgium, villages are added to D-RR. These villages are based on the characteristics of surrounding Dutch villages. It was also assumed that the added villages do not contain a sewer system. This is not the case in reality, as manholes are observed on Belgian streets in Google Maps. Therefore, the flows from D-RR to the Geul in Belgium do not represent the reality. The sizes and sewer systems affect the outflow, but as there was no data, it is not possible to quantify the outflow.

Another implication of the Belgian part of the Geul catchment is the representation of the HBV laterals in the Gulp and Sippenaeken subcatchments. For the Gulp and Sippenaeken subcatchments, the laterals are equally divided over 3 and 7 laterals, respectively. The flood extent in these areas and the modelled discharge at Kelmis are, because of this, not completely correct. Only one lateral location is located before Kelmis, leading to an underestimation at this location. The flood extents will not represent reality. The real inflow will differ from an equally divided inflow. Another implication is that it is not possible to compare the total flooded area with the established flood extent of Slager et al. (2021). No flood extent is provided for Belgium and the tributaries.

### 5.1.2. HBV and D-RR

The Sippenaeken subcatchment is handled as one subsubcatchment in HBV. This is a large difference with the subcatchments in the Netherlands, where relatively small subsubcatchments are defined. Sippenaeken is one third of the Geul catchment and generates more than half of the downstream discharge in the Geul. But this subcatchment is calibrated by one measurement location, and a parameterset is derived for a large area. Sippenaeken is treated as a homogeneous area, which it is not in reality. First, the Sippenaeken subcatchment can be divided into two parts, as there are two measurement locations in this area; Sippenaeken and Kelmis. This could improve the coverarge of the heterogeneity of the subcatchment. Second, adding subsubcatchments to this area spreads the flow in a more realistic way and makes the use of spatially distributed forcing data possible. D-RR for the Geul is kept as it is, except for adding villages to Belgium. Hulsman et al. (2023) stated that the D-RR output for the Eyserbeek subcatchment could be optimized.

The results showed that HBV and D-RR represent the subsurface flow well, but do not represent the overland flow well. D-RR represents the overland flow by the urban areas, but HBV does not represent the overland flow of the unpaved areas. The output fluxes of HBV and D-RR are subsurface flow and groundwater flow. The subsurface flow is determined by the volume of the fast lateral store and not by the unsaturated store as in Wflow_sbm. Adding the overland flux to HBV would improve the representability of the hydrological response. The downside of this, is that extra parameters are included, which increases the possibility of equifinality. On the other side, the D-RR output could be increased by adjusting the paved areas. This would also improve the model representability.

### 5.1.3. Wflow_sbm

Wflow_sbm is built at a 1 km$^2$ resolution. The parameters are derived as the mean of the parameter within the grid cell (Eilander et al., 2023). A small change in land use can for example not result in a changed percentage paved area in a grid cell. This also affects the evaluation of the impact on the flood extent. It is hard to look at the impact on house level, with such large grid cells.

The Wflow_sbm Geul parameterset is adjusted to represent the July 2021 flood event. This results in a good performance for the event, but the results in the calibration and validation period could be improved. The peak discharge for the event drops too fast after the event, the discharge is underestimated in the calibration period, and overestimated in the validation period. This indicates that the subsurface flow is not presented correctly by the parameterset. The overland flow is compensated for this, which mainly can be seen in the validation period, where the discharge peaks are overestimated. It looks like that the Wflow_sbm Geul parameterset generates the peak discharge during the July 2021 flood event for the wrong reasons. Klein (2022) and Bouaziz (2022), also suggest to look deeper into the parameters. For example, the representation of the thick chalk layers in the catchment.

### 5.1.4. D-HYDRO

The D-HYDRO Geul model is built with the HBV-96 model of the Waterboard of Limburg, and not with the hydrological models in this research. D-HYDRO is not adjusted for the hydrological models. This results in longer calculation times for HBV and D-RR and Wflow_sbm than for the original HBV-96 model. On the other hand, D-HYDRO is calibrated with the HBV-96 model of the Waterboard. This means that roughnesses in the model are adjusted to improve the hydrographs at the measurement locations. This affects the modelled discharge with HBV and D-RR and Wflow_sbm. Ideally, D-HYDRO is calibrated for both hydrological models. However, this affects the comparison of the models. In this case, the hydrodynamic model will compensate for errors in the hydrological model, and you start to compare apples to oranges.

### 5.1.5. Coupling

The subsubcatchments and the laterals of HBV and D-RR are defined by the Waterboard of Limburg. The subsubcatchments and laterals of Wflow_sbm are built by HydroMT (Eilander et al., 2023). The input of this tool are the laterals of HBV. However, some laterals are combined into one lateral for Wflow_sbm, due to the resolution and underlying parameters as the DEM and flow direction map. This process was manually executed and leads to different subsubcatchment sizes over the Geul catchment. Next, the output of Wflow_sbm is equally divided over the HBV laterals within a subsubcatchment to prevent a sudden large volume of water at the lateral. This mainly affects the runtime of D-HYDRO, which becomes shorter because of this.

Creating the same subsubcatchments for HBV and Wflow_sbm allows a deeper comparison of the hydrological models. The fluxes can be compared for the same areas. This gives more insight in the behaviour of the models for certain land cover or hydrogeology types. It does not impact the hydrographs at the measurement locations. The total volume of water in the Geul remains the same, however local changes can occur. Changing the location or inflow of a lateral changes the volume of water in the downstream cross-sections. This change can result in a local flooding, which did not occur before.

### 5.1.6. Calibration

The calibration is done for HBV, which is combined with D-RR. The calibration strategy is based on getting the hydrographs right with the Nash Sutcliff Efficiency (NSE). This results in high NSE values in the calibration period, but the correspondence between the validation period and the July2021 flood event is low. The goal was to simulate peak discharges,especially the July 2021 flood event, but HBV and D-RR underestimate the peaks. The calibration strategy was therefore not extensive enough to simulate the flood event. A calibration indicator for high flows would increase the performance of HBV and D-RR.

Parameters are constraint for HBV based on literature and observations. However, some parameters needed to be adjusted; otherwise no good enough calibration hydrograph is calculated. The parameters for the maximum of the unsaturated zone, $S_{u,max}$ and the lag time $T_{lag}$, where changed for four of the six subcatchments. The main reason for the adjustment of $S_{u,max}$ is the fast succession of precipitation events in the calibration period. This requires a high storage value, as water needs to be stored and does not runoff completely. The drawback of this is that a precipitation event after a dry period is underestimated, as the large unsaturated storage needs to be filled first. In this case, a better NSE calibration value for a large $S_{u,max}$ does not result in a good representation of the July 2021 flood event. The adjustment of the $T_{lag}$ parameter is done for the subcatchments with high D-RR flow. A reason for this is that the lag function needs to account for D-RR output. The sewer outflow has different transport times than the HBV outflow. The sewer outflow is also recorded as one value per timestep, while there is spatial variability. The Meerssen subcatchment also accounts for the upstream observed discharge, resulting in a much higher value for $T_{lag}$. These reasons affect the calibration of the constraint parameters.

Another implication of the calibration is the calibration period. A calibration period of 6 months is quite short. The seasons in a year show different discharge behaviour, but are not completely included in the calibration period. The hydrological response is different for a precipitation event in the summer than in the winter. Season depended parameters could account for this and improve the model performance. The hydrological response can change over time. The calibration period is in this case one and a half years before the flood event, so this is not likely to be the case.

## 5.2. Data

Heavy precipitation events as the July 2021 flood event are hard to capture. A precipitation radar is unable to capture all the precipitation, as clutter occurs by the raindrops. The National Regenradar (NRR) provides calibrated data by three precipitation radars and ground measurement stations. This is a reliable precipitation data source, but uncertainty cannot be prevented. As a hydrological model is as good as the quality of the input data (Savenije, 2009), this effects the model results during the July 2021 event.

Another factor of uncertainty during heavy precipitation events are discharge measurements. During the flood in July 2021, most of the measurement devices failed, as can be seen in Section 4.1. The hydrological models are compared to the remaining available discharge data. These discharge data contain uncertainty, which increases with higher discharges, as is given in Appendix E.3. The discharges at Sippenaeken, Hommerich, and Azijnfabriek (Gulp) are estimated by a Q-H relationship. The peak discharges of the July 2021 flood event are outside of the measurement range, so extrapolation is needed. This extrapolation provides uncertainty, along with their uncertainty in the measurement range (Savenije, 2009). On the other hand, the discharge depends on the water level measurements, which also comes with uncertainty. The Waterboard of Limburg made estimations of the peak discharges at the measurement locations with no data. However, different peak discharges are found. For example at the Meerssen measurement location. The Waterboard of Limburg estimated a peak of 85 - 90 $m^3/s$ (Klein, 2022), while Bureau Stroming (2022) used a peak discharge of 55 $m^3/s$. The combination of all the discharge measurement uncertainties makes it hard to correctly model extreme flood events like the July 2021 flood event.

Potential evaporation data from the KNMI Maastricht weather station are used to force the hydrological models. Potential evaporation of the ERA5-Land was found to be not physically realistic. The evaporation at one location cannot represent the entire Geul catchment. However, it has no impact for large precipitation events, as there is no evaporation. However, on the other hand, the calibration period contains dry periods where point data have an impact on the results. Ideally, physical correct raster evaporation data is used to force the hydrological models.

The ERA5-Land actual evaporation data is used for the root zone storage capacity. This dataset corresponded to the potential evaporation of the KNMI Maastricht weather station. It is not used to force hydrological models, because the models were already run with the KNMI potential evaporation The large resolution could impact the results of the root zone storage capacity, as there are not so much grid cells in the Geul catchment. The different sources of evaporation could create ambiguity for the reader. Research in the different evaporation data sources could create clearness for hydrologists.

HBV and D-RR are forced with the same NRR data, but at a different scale. The mean precipitation in an area is calculated per timestep. This is on subsubcatchment scale for HBV and on subcatchment scale for D-RR. Differences in scale affect the model results. A local heavy precipitation event can be captured by HBV, but not by D-RR. This has the most effect on the Eyserbeek and Selzerbeek subcatchments, as they are largely dependent on discharge by paved areas. But it is difficult to say how large the effect is.

## 5.3. Scenarios

The scenarios are built using data provided by the Province of Limburg. However, assumptions were made during the process of constructing scenarios. The building plans for the South of Limburg are simulated in the Geul catchment. The added paved areas are overestimated, as the building plans are to a great extent planned in the city of Maastricht. The mean area of a house in Limburg is large compared to the national average, because of the low population density in the province. To take into account the gardens and *Water en Bodem sturend*, 70% of the added area is paved. This assumption is based on the land use categories of COPERNICUS and the corresponding paved/unpaved ratio in Wflow_sbm (Buitink, 2022). In reality, not all houses have that size or are free-standing. Apartments or flats are also built in the Geul catchment, resulting in an overestimation of the building area. Another assumption is in the area of infrastructure and services. It is assumed to be equal to the area to be built. This value is overestimated. New houses are, for example, built around existing infrastructure.

## 5.4. Results

The uncertainties described in the above sections come together in the produced results. These uncertainties cannot be quantified for extreme flooding like this, however the uncertainties can be interpreted by expert knowledge. The total uncertainty is estimated to be larger than the differences in the hydrographs for the scenarios containing 6 $km^2$ new paved area in Section 4.2. The changes in location resulted in small changes in the magnitude of the peak discharge. For example at Meerssen, where changes are estimated of 0.5 - 1 $m^3/s$ on a peak discharge of 80 $m^3/s$. This increase is not significant given a peak of this magnitude. Also, differences in the peak discharge magnitude between building close to and far from the river are not significant. For example Scenario 2b1 vs Scenario 2b2, where a change of 0.2 - 0.4 $m^3/s$ is estimated at Meerssen. The hydrographs of the scenarios containing a completely paved subcatchment show significant changes and a change in hydrological response can be seen. This is not the case for the other scenarios. So, conclusions cannot be drawn based on these small changes in the hydrographs.

The area of the flood extent cannot be determined per $m^2$, due to uncertainties. The cells in the mesh of the 2D grid vary from triangles with a base of 10 meters close to the river, to 30 meter far from the river. On the other hand, Wflow_sbm has grid cells of 1 by 1 kilometer. Combining the grid cells and the uncertainties, it is chosen to review the areas of the flood extent by hectares. This results in no change of the area of the flood extent in some cases.

The results of HBV and D-RR deemed to be less realistic than for Wflow_sbm. Adding paved areas to D-RR results in a change in discharge behaviour of HBV and D-RR. This behaviour becomes closer to the observations and Wflow_sbm. Overland flow is an important process of the hydrological response and the increased paved area results in a more realistic overland flow flux in HBV and D-RR. The estimated flood extent areas are therefore not realistic, but the change in area underlines the results of Wflow_sbm.

Lastly, the flooded paved area depends on the chosen land cover map. The land cover map of Wflow_sbm changed from CORINE to Openstreetmap, as this data source was more consistent to reality as explained in Section 2.4 (Bouaziz, 2022). Changing a land cover map affects the results of Wflow_sbm. Different categories containing different parameters, as the runoff coefficient or rooting depth, give different results. The results are also affected by the area classification. Areas can be paved or urban in one land cover map, but can have a different type in another land cover map. This affect the results of the determined flooded paved areas.

# 6 Conclusion

The goal of this research was to investigate the best suitable subcatchment for the construction of new residential houses in the Geul catchment, in terms of flooding. This is achieved by modelling the hydrological response of the Geul catchment with the hydrological models HBV + D-RR and Wflow_sbm, coupled to a D-HYDRO model of the Geul. The change in hydrological response is analysed for different scenarios of spatial development. The subquestions are answered to answer the research question.

1. *What is the current hydrological response of the Geul catchment?*

The main processes of the hydrological reponse are overland flow and subsurface flow. The hydrological response differs over the Geul catchment. The Belgium part of the Geul catchment reacts faster to a precipitation event than the Dutch part, due the geohydrology. The Belgian part contains thin soil and impermeable rocks, resulting in less storage and more subsurface flow. The Dutch part is characterized by chalk layers and acts as a sponge. The water infiltrates and is released slowly. Finally, the runoff is collected in the Geul river and its tributaries. The discharge varies highly and high water peaks often occur. The flood plains along the river act as a natural buffer and delay and spread out discharge peaks. The water retention basins in the catchment also reduce and spread out discharge peaks.

2. *How well do HBV + D-RR - D-HYDRO and Wflow_sbm - D-HYDRO describe the hydrological response of the Geul catchment?*

The hydrological response of the Geul catchment is modelled by HBV and D-RR and by Wflow_sbm. HBV and D-RR are set up in this research and Wflow_sbm is adopted from Klein (2022) and Bouaziz (2022). The hydrological models are coupled to the Geul D-HYDRO model of Hulsman et al. (2023). Both hydrological models describe a part of the hydrological response better than the other model. HBV and D-RR represent the subsurface flow better, while Wflow_sbm represents the overland flow better. Both models are calibrated on the same period, but Wflow_sbm is adjusted to improve the representation of the July 2021 flood event. This results in a better representation of the overland flow. However, the subsurface flow flux is affected and the discharge drops too fast to the base flow after the event. Wflow_sbm underestimates the consecutive precipitation events in the calibration period, where subsurface flow is important. On the other hand, HBV and D-RR represent the subsurface flow better. The performance in the calibration period indicates a good representation of the subsurface flow. This can also be seen for the July 2021 flood event. HBV and D-RR do not get the discharge peaks right, but the flow after the event is closer to the observations for HBV and D-RR than for Wflow_sbm. Lastly, the modelled flood extents during the July 2021 flood event are compared to the estimated extent by Slager et al. (2021). Wflow_sbm showed a better correspondence to the measured flood extent than HBV and D-RR.

So, HBV and D-RR better represent subsurface flow and describe the hydrological response during consecutive precipitation events. Wflow_sbm represents the overland flow flux better and therefore describes the hydrological response during the July 2021 flood event better.

3. *What are the building plans in the Geul catchment?*

The Province of Limburg wants to build 18,730 new houses in the South of Limburg. The planned houses in the Geul catchment are mostly built in existing cities, close to the Geul river. Scenarios of different spatial developments are constructed to evaluate the impact of the location of the new houses on the hydrological response of the Geul catchment. The following scenarios are evaluated:

- Scenario 1a: 6 $km^2$ extra paved area, divided over the villages Aken (Germany), Hombourg, and Kelmis (Belgium);
- Scenario 1b: completely paved Sippenaeken subcatchment;
- Scenario 2a1: 6 $km^2$ extra paved area, divided over areas close to the Geul river in the Meerssen subcatchment;
- Scenario 2a2: 6 $km^2$ extra paved area, divided over areas far from to the Geul river in the Meerssen subcatchment;
- Scenario 2a3: completely paved Meerssen subcatchment;
- Scenario 2b1: 6 $km^2$ extra paved area, divided over areas close to the Gulp tributary in the Gulp subcatchment;
- Scenario 2b2: 6 $km^2$ extra paved area, divided over areas far from to the Gulp tributary in the Gulp subcatchment;
- Scenario 2b3: completely paved Gulp subcatchment.

4. *How does the hydrological response of the Geul catchment change by building extra houses?*

The hydrographs of the scenarios containing 6 $km^2$ extra paved area did not show a significant change for both HBV and D-RR and Wflow_sbm. The magnitudes of the peak discharges of the measurement stations along the Geul river increased by a maximum of 1.5 $m^3$/s for the scenarios 1a, 2a1, 2a2, 2b1, and 2b2. The peak discharges occurred 0 to 3 hours earlier. The scenarios containing a completely paved subcatchment showed a significant change in the hydrological response. A completely paved Sippenaeken subcatchment in Scenario 1b resulted in a flashier response for the measurement locations along the Geul. The overland flow flux increased and the catchment reacts faster to the precipitation. Scenario 2a3, containing a completely paved Meerssen subcatchment, results in a faster responses in this subcatchment. The discharge increases faster and earlier and the magnitude of the peak discharge increased. Lastly, the completely paved Gulp subcatchment in Scenario 2b3 resulted in different behaviour in the Gulp subcatchment, which results in a faster and increased discharge peak downstream in Meerssen.

The flood extent provides more information on the change in the hydrological response in the Geul catchment. The flooded paved area and the flooded new paved area are determined per scenario. These areas increased for each scenario, except for the scenarios 2a2 and 2b2. Building in the hills, far from the river, did not result in a change of the flood extent. Building in the Sippenaeken catchment in scenarios 1a and 1b resulted in the smallest contribution to the increase in the flooded paved area. The increase in pavement results relatively in more extra flooded paved areas downstream. The subcatchment Meerssen is the most vulnerable to flooding. A completely paved subcatchment in Scenario 2a3 resulted in the largest flooded paved area. In Scenario 2a1, the increase in the flooded paved area was caused 95% by the flooding of the extra paved area close to the Geul. This also happened in the Gulp subcatchment for Scenario 2b1, where around 88% of the increase in flooded paved area is flooded new paved area. Lastly, a completely paved Gulp subcatchment in Scenario 2b3 resulted in a less flooded paved area than for extra houses close to the Geul in Meerssen in Scenario 2a1.
With the answered subquestions it is possible to answer the main research question of this research:

*Where can new houses be build in the Geul catchment, with the least amount of impact on peak discharge of the July 2021 flood?*

The goal of this research was to investigate best suitable location for the construction of new residential houses in the Geul catchment, in terms of flooding. The letter *Water en Bodem Sturend* and the housing shortage in the Netherlands are linked. The location of new houses is found to be important for the hydrological response. A relatively small increase in the paved area does not result in different discharge behaviour, and the total area of the flood extent showed a small difference. However, it impacts the flooded paved area. Building far from the river on the hills results in no increase of the flooded paved area. New houses in the valleys, close to the river, are more exposed to flooding. This is where the letter *Water en Bodem Sturend* is about, to build on sensible locations. It is also found that the Meerssen subcatchment is the most vulnerable to flooding. As this subcatchment contains the most paved area, more runoff will result in a more flooded paved area. Even a completely paved Gulp catchment results in less flooded paved area than building 6 $km^2$ close to the Geul in Meerssen. When the Belgians build new houses in the Sippenaeken subcatchment, the Netherlands will receive more water during an extreme event such as in July 2021. So, the Gulp subcatchment is the least vulnerable to flooding and can be considered the best building location for new houses among the three investigated subcatchments.

# 7
# Recommendations

**Recalibration**
The HBV parameterset could be improved. The model did not show good correspondence to the July 2021 flood event. A calibration strategy that focuses more on the peak discharges improves the model. A different and longer calibration period would also improve the results of HBV. The chosen calibration period contains a winter period with consecutive precipitation events. This affects the volume of the saturated store, as in this period the storage is full. But, when it starts to rain after a dry period, the store needs to be filled first, before it generates runoff. Further, accounting for a summer and winter period would tackle this problem. When the calibration strategy would take all this into account, the performance of HBV and D-RR would increase.

**Belgian Part**
The Belgian Part is not well represented in the D-HYDRO model. This part does not contain sewer areas in the models. During the research, sewer areas are added to D-RR, but these areas are not realistic. Also, the measurement station at Kelmis is not well represented in D-HYDRO. The location of the laterals results in an underestimation of the discharge at this location. As the discharge in the Netherlands largely depends on the Belgian part, a good representation is important.

**Resolution Wflow_sbm**
The Wflow_sbm Geul parameterset has a resolution of 1 $km^2$. Each cell contains a mean parameter value (Eilander et al., 2023). This affects the representation within the grid cell. A small change of land cover can be averaged out. On the other hand, a smaller resolution reduces the difference of scale to the D-HYDRO 2D grid. Aerts et al. (2022) found that a smaller resolution does not necessarily result in a better discharge estimation. However, the Wflow_sbm models were not coupled to D-HYDRO. It would be interesting to see if the resolution affects the discharges and flood extents in D-HYDRO.

**eWaterCycle**
The hydrological models HBV and Wflow_sbm are offline coupled to D-HYDRO. This means that the models are run separately. An online coupling would make the modelling processes clearer. Many actions were needed to postprocess the outputs to D-HYDRO input. During this process, many mistakes can be made and were made during the research. Redoing the postprocessing takes a lot of time, which can be reduced by an online coupling. This can be done via the eWaterCycle, where models built in different programming languages can be coupled and run. This was tried during this research, but the software was not ready. Building this online coupling improves the modelling process and less experienced programmers can use it.

**Investigate Different Land Covers**
The change in hydrological response is investigated for adding paved areas to the Geul catchment. The discharge behaviour and the total flood extent did not change much. In the Geul catchment, other land cover changes are possible, as forest to agriculture. The effect of future land cover changes to the hydrological response are also necessary to investigate.

# References


Aerts, J. P. M., Hut, R. W., van de Giesen, N. C., Drost, N., van Verseveld, W. J., Weerts, A. H., & Hazenberg, P. (2022, August). Large-sample assessment of varying spatial resolution on the streamflow estimates of the wflow_sbm hydrological model. *Hydrology and Earth System Sciences*, *26*(16), 4407–4430. Retrieved 2024-01-19, from https://hess.copernicus.org/articles/26/4407/2022/ doi: 10.5194/hess-26-4407-2022

Bergström, S. (1976). DEVELOPMENTAND APPLICATIONOF A CONCEPTUALRUNOFF MODEL FOR SCANDINAVIAN CATCHMENTS.

Bouaziz, L. (2022). *Samenvatting Wflow Geul.*

Bouaziz, L., Aalbers, E., Weerts, A. H., Hegnauer, M., Buiteveld, H., Lammersen, R., … Hrachowitz, M. (2022, March). Ecosystem adaptation to climate change: the sensitivity of hydrological predictions to time-dynamic model parameters. *Hydrology and Earth System Sciences*, *26*(5), 1295–1318. Retrieved 2023-10-23, from https://hess.copernicus.org/articles/26/1295/2022/ (Publisher: Copernicus GmbH) doi: 10.5194/hess-26-1295-2022

Breuer, L., Eckhardt, K., & Frede, H.-G. (2003, November). Plant parameter values for models in temperate climates. *Ecological Modelling*, *169*(2), 237–293. Retrieved 2023-10-23, from https://www.sciencedirect.com/science/article/pii/S0304380003002746 doi: 10.1016/S0304-3800(03)00274-6

Brooks, R. H., & Corey, A. T. (1963, dec). *Hydraulic properties of porous media.* Retrieved 2023-04-13, from https://mountainscholar.org/handle/10217/61288

Buitink, J. (2022). *hydromt_wflow/hydromt_wflow/data/lulc/corine_mapping.csv at main Deltares/hydromt_wflow GitHub.* Retrieved 17-12-2023, from https://github.com/Deltares/hydromt_wflow/blob/main/hydromt_wflow/data/lulc/corine_mapping.csv

Bureau Stroming. (2022). *Analyse functioneren klimaatbuffers in het Geul stroomgebied tijdens extreme neerslag in juli 2021.* Retrieved 23-06-2023, from https://www.stroming.nl/overzicht/natuurlijke-oplossingen-geuldal

Carlotto, T., & Chaffe, P. L. B. (2019, November). Master Recession Curve Parameterization Tool (MRCPtool): Different approaches to recession curve analysis. *Computers & Geosciences*, *132*, 1–8. Retrieved 2023-12-14, from https://www.sciencedirect.com/science/article/pii/S0098300419301025 doi: 10.1016/j.cageo.2019.06.016

Clarke, R. T. (1973, May). A review of some mathematical models used in hydrology, with observations on their calibration and use. *Journal of Hydrology*, *19*(1), 1–20. Retrieved 2023-03-15, from https://www.sciencedirect.com/science/article/pii/0022169473900899 doi: 10.1016/0022-1694(73)90089-9

Coron, L., Thirel, G., Delaigue, O., Perrin, C., & Andréassian, V. (2017, August). The suite of lumped GR hydrological models in an R package. *Environmental Modelling & Software*, *94*, 166–171. Retrieved 2023-03-15, from https://www.sciencedirect.com/science/article/pii/S1364815217300208 doi: 10.1016/j.envsoft.2017.05.002

Dautrebande, S., Leenaars, J. G., Schmitz, J., & Vanthournout, E. (2000). *Pilot Project for the Definition of Environment-Friendly Measures To Reduce the Risk for Flash Floods in the Geul River Catchment* (Tech. Rep.). Technum, University of Liège and CSO Environmental Consultancy. Retrieved 2023-08-16, from https://docslib.org/doc/4021354/pilot-project-for-the-definition-of-environment-friendly-measures-to

Deltares. (n.d.-a). *D-HYDRO Suite 1D2D - Deltares.* Retrieved 28-02-2023, from https://www.deltares.nl/nl/software/d-hydro-suite-1d2d/#features

Deltares. (n.d.-b). *wflow - Deltares.* Retrieved 15-3-2023, from https://www.deltares.nl/en/software/wflow-hydrology/

Deltares. (2022a). Delta Shell User Manual [Computer software manual].

Deltares. (2022b). D-Flow Flexible Mesh [Computer software manual].

Deltares. (2022c). D-Rainfall Runoff in Delta Shell [Computer software manual].

Deltares. (2022d). D-Real Time Control User Manual [Computer software manual].

de Moor, J. J. W., Kasse, C., van Balen, R., Vandenberghe, J., & Wallinga, J. (2008, June). Human and climate impact on catchment development during the Holocene — Geul River, the Netherlands. *Geomorphology*, *98*(3), 316–339. Retrieved 2023-08-18, from https://www.sciencedirect.com/science/article/pii/S0169555X07002371 doi: 10.1016/j.geomorph.2006.12.033

de Moor, J. J. W., & Verstraeten, G. (2008, March). Alluvial and colluvial sediment storage in the Geul River catchment (The Netherlands) — Combining field and modelling data to construct a Late Holocene sediment budget. *Geomorphology*, *95*(3), 487–503. Retrieved 2023-08-18, from https://www.sciencedirect.com/science/article/pii/S0169555X07003510 doi: 10.1016/j.geomorph.2007.07.012

Devia, G. K., Ganasri, B. P., & Dwarakish, G. S. (2015, January). A Review on Hydrological Models. *Aquatic Procedia*, *4*, 1001–1007. Retrieved 2023-03-15, from https://www.sciencedirect.com/science/article/pii/S2214241X15001273 doi: 10.1016/j.aqpro.2015.02.126

ECMWF. (2023). *ECMWF Reanalysis v5 | ECMWF.* Retrieved 02-10-2023, from https://www.ecmwf.int/en/forecasts/dataset/ecmwf-reanalysis-v5

Eilander, D., Boisgontier, H., van Verseveld, W., Bouaziz, L., Hegnauer, M., Buitink, J., & Dalmijn, B. (2023). *hydromt-wflow (v0.4.1).* Retrieved 08-12-2023, from https://doi.org/10.5281/zenodo.10185533

Elmensdorp, S. (2023). *Een watersysteemanalyse - wat leren we van het hoogwater van juli 2021?* Retrieved 07-03-2023, from https://pub.kennisbank.deltares.nl/Details/fullCatalogue/1000021132

European Environment Agency. (2017). *Copernicus Land Monitoring Service - EU-DEM | European Environment Agency.* (Data retrieved from EU-DEM, https://www.eea.europa.eu/data-and-maps/data/copernicus-land-monitoring-service-eu-dem)

Feddes, R. A. (1982). Simulation of field water use and crop yield. *Simulation of plant growth and crop production*, 194–209. Retrieved 2023-03-28, from https://research.wur.nl/en/publications/simulation-of-field-water-use-and-crop-yield

Fenicia, F., Savenije, H. H. G., Matgen, P., & Pfister, L. (2006, February). Is the groundwater reservoir linear? Learning from data in hydrological modelling. *Hydrology and Earth System Sciences*, *10*(1), 139–150. Retrieved 2023-10-25, from https://hess.copernicus.org/articles/10/139/2006/hess-10-139-2006.html (Publisher: Copernicus GmbH) doi: 10.5194/hess-10-139-2006

Gharari, S., Hrachowitz, M., Fenicia, F., Gao, H., & Savenije, H. H. G. (2014, December). Using expert knowledge to increase realism in environmental system models can dramatically reduce the need for calibration. *Hydrology and Earth System Sciences*, *18*(12), 4839–4859. Retrieved 2023-10-23, from https://hess.copernicus.org/articles/18/4839/2014/hess-18-4839-2014.html (Publisher: Copernicus GmbH) doi: 10.5194/hess-18-4839-2014

Google. (2023). Retrieved 04-12-2023, from https://www.google.nl/maps

H2O ACTUEEL. (2022). *Water en bodem sturend: met 33 structurerende keuzes zet kabinet in op herinrichting van Nederland.* Retrieved 09-08-2023, from https://www.h2owaternetwerk.nl/h2o-actueel/water-en-bodem-sturend-met-33-structurerende-keuzes-zet-kabinet-in-op-herinrichting-van-nederland

Harbers, M., & Heijnen, V. (2022). *Water en Bodem sturend.* Retrieved 06-03-2023, from https://open.overheid.nl/documenten/ronl-c35e65eba0903d738ae26dab222462337b0d8de7/pdf

Horton, P., Schaefli, B., & Kauzlaric, M. (2022). Why do we have so many different hydrological models? A review based on the case of Switzerland. *WIREs Water*, *9*(1), e1574. Retrieved 2023-02-28, from https://onlinelibrary.wiley.com/doi/abs/10.1002/wat2.1574 doi: 10.1002/wat2.1574

Hrachowitz, M. (2021). *Lecture 2 - Flow Paths 2021.* Technical University Delft. Retrieved 13-06-2023, from https://brightspace.tudelft.nl/d2l/le/content/399298/viewContent/2298342/View

Hrachowitz, M., Stockinger, M., Coenders-Gerrits, M., van der Ent, R., Bogena, H., Lücke, A., & Stumpp, C. (2021, September). Reduction of vegetation-accessible water storage capacity after deforestation affects catchment travel time distributions and increases young water fractions in a headwater catchment. *Hydrology and Earth System Sciences*, *25*(9), 4887–4915. Retrieved 2023-10-23, from https://hess.copernicus.org/articles/25/4887/2021/ (Publisher: Copernicus GmbH) doi: 10.5194/hess-25-4887-2021

Hulsman, R., Weijers, L., Verstegen, E., & Goedbloed, A. (2023). *Modelbouw D-HYDRO Geul* (Tech. Rep.). Royal HaskoningDHV.

Hut, R., Drost, N., van de Giesen, N., van Werkhoven, B., Abdollahi, B., Aerts, J., … Weel, B. (2022, July). The eWaterCycle platform for open and FAIR hydrological collaboration. *Geoscientific Model Development*, *15*(13), 5371–5390. Retrieved 2023-02-20, from https://gmd.copernicus.org/articles/15/5371/2022/ doi: 10.5194/gmd-15-5371-2022

Hutton, C., Wagener, T., Freer, J., Han, D., Duffy, C., & Arheimer, B. (2016). Most computational hydrology is not reproducible, so is it really science? *Water Resources Research*, *52*(10), 7548–7555. Retrieved 2023-03-01, from https://onlinelibrary.wiley.com/doi/abs/10.1002/2016WR019285 doi: 10.1002/2016WR019285

Idsinga, D. (2024). *Safely Building New Houses in the Geul Catchment.* Retrieved from https://github.com/DaanIdsinga/MscThesis doi: https://zenodo.org/doi/10.5281/zenodo.10572385

Informatiepunt Leefomgeving. (2023). *Beschermen van waterbelangen | Informatiepunt Leefomgeving.* Retrieved 30-11-2023, from https://iplo.nl/thema/water/water-ruimte/beschermen-waterbelangen//?utm_source=hdwater&utm_medium=link&utm_campaign=waterenruimte

Islam, Z. (2011). *A Review on Physically Based Hydrologic Modeling.* doi: 10.13140/2.1.4544.5924

Khakbaz, B., Imam, B., Hsu, K., & Sorooshian, S. (2012, February). From lumped to distributed via semi-distributed: Calibration strategies for semi-distributed hydrologic models. *Journal of Hydrology*, *418-419*, 61–77. Retrieved 2023-03-15, from https://www.sciencedirect.com/science/article/pii/S0022169409000894 doi: 10.1016/j.jhydrol.2009.02.021

Klein, A. (2022). *Hydrological Response of the Geul Catchment to the Rainfall in July 2021.* Retrieved 15-3-2023, from http://resolver.tudelft.nl/uuid:ee25d687-70af-4aca-ae41-78e3f83943bf

Klostermann, J., & Veraart, J. (2022). *Water en Ruimtelijke Ordening: instrumenten voor betere afstemming | STOWA.* Retrieved 30-11-2023, from https://www.stowa.nl/deltafacts/ruimtelijke-adaptatie/adaptief-deltamanagement/water-en-ruimtelijke-ordening

KNMI. (n.d.). *KNMI - Verdamping in Nederland.* Retrieved 09-10-2023, from https://www.knmi.nl/kennis-en-datacentrum/achtergrond/verdamping-in-nederland

KNMI. (2021). *KNMI - Het regent nu harder in Zuid-Limburg door klimaatverandering.* Retrieved 07-03-2023, from https://www.knmi.nl/over-het-knmi/nieuws/extreme-neerslag-in-zuid-limburg

KNMI. (2023a). *Dagwaarden van weerstations.* Retrieved 03-10-2023, from https://daggegevens.knmi.nl/

KNMI. (2023b). *KNMI - Uurgegevens van het weer in Nederland.* Retrieved 02-10-2023, from https://www.knmi.nl/nederland-nu/klimatologie/uurgegevens

L'hydrométrie en Wallonie. (2023). *L'hydrométrie en wallonie - précipitation.* Retrieved 02-10-2022, from https://hydrometrie.wallonie.be/home/observations/precipitation.html?station=DGH%2F5284&topic=Precip-hr

Muñoz Sabater, J. (2019). *ERA5-Land hourly data from 1950 to present.* doi: 10.24381/cds.e2161bac

Nash, J. E., & Sutcliffe, J. V. (1970, April). River flow forecasting through conceptual models part I — A discussion of principles. *Journal of Hydrology*, *10*(3), 282–290. Retrieved 2023-12-13, from https://www.sciencedirect.com/science/article/pii/0022169470902556 doi: 10.1016/0022-1694(70)90255-6

NOS Nieuws. (2021). *Onderzoek bevestigt link klimaat en watersnood door regen in juli.* Retrieved 14-08-2023, from https://nos.nl/collectie/13871/artikel/2394918-onderzoek-bevestigt-link-klimaat-en-watersnood-door-regen-in-juli

NOS Nieuws. (2023). *Woningtekort stijgt fors naar 390.000, pas vanaf 2028 minder krapte.* Retrieved 09-08-2023, from https://nos.nl/artikel/2482485-woningtekort-stijgt-fors-naar-390-000-pas-vanaf-2028-minder-krapte

Nota, D., & van de Weerd, B. (1978). *A hydrogeological study in the basin of the Gulp creek-a recon-*

*naissance in a small catchment area. I. Groundwater flow characteristics.* Landbouwhogeschool. Retrieved 04-05-2023, from https://research.wur.nl/en/publications/a-hydrogeological-study-in-the-basin-of-the-gulp-creek-a-reconnai

Pasquier, U., He, Y., Hooton, S., Goulden, M., & Hiscock, K. M. (2019). An integrated 1D–2D hydraulic modelling approach to assess the sensitivity of a coastal region to compound flooding hazard under climate change. *Natural Hazards*, *98*(3), 915–937. Retrieved 2023-11-30, from https://doi.org/10.1007/s11069-018-3462-1 doi: 10.1007/s11069-018-3462-1

*Plancapaciteitsmonitor Limburg.* (n.d.). Retrieved 15-12-2023, from https://www.pcmlimburg.nl/

Poppelier, E. (2023). *The impact of evaporation data calibration on regional hydrological model performance.* Retrieved 06-10-2023, from https://repository.tudelft.nl/islandora/object/uuid%3Aa885a1c7-d41f-4f96-8f58-d0ac65b62b96?collection=education

Prinsen, G., Hakvoort, H., & Dahm, R. (2009). Neerslag-afvoermodellering met SOBEK-RR. Retrieved 15-12-2023, from https://www.nhv.nu/stroming/nieuws/neerslagafvoermodellering-met-sobek-rr/

Provincie Limburg. (2021a). *Provincie Limburg - Testversie.* Retrieved from https://dataportaal-viewer.prvlimburg.nl/dashboard/dashboards/plancapaciteiten

Provincie Limburg. (2021b). *Provincie Limburg - Testversie.* Retrieved 15-12-2023, from https://dataportaal-viewer.prvlimburg.nl/dashboard/dashboards/woningvoorraad

Provincie Limburg. (2022). *Bijlagenboek Limburgse Woonmonitor van 2022.* Retrieved 15-12-2023, from https://www.limburg.nl/onderwerpen/wonen/woononderzoek/

Rijksoverheid. (2022). *Kabinet maakt water en bodem sturend bij ruimtelijke keuzes | Nieuwsbericht | Rijksoverheid.nl.* Retrieved 06-03-2023, from https://www.rijksoverheid.nl/actueel/nieuws/2022/11/25/kabinet-maakt-water-en-bodem-sturend-bij-ruimtelijke-keuzes

Rijksoverheid. (2023). *Omgevingswet | rijksoverheid.nl.* Retrieved 30-11-2023, from https://www.rijksoverheid.nl/onderwerpen/omgevingswet

Rijksoverheid.nl. (2023). *Woningbouwopgave stijgt naar 981.000 tot en met 2030 | Nieuwsbericht | Rijksoverheid.nl.* Retrieved 09-08-2023, from https://www.rijksoverheid.nl/actueel/nieuws/2023/07/12/woningbouwopgave-stijgt-naar-981.000-tot-en-met-2030

RTL Nieuws. (2022). *Hoogwaterpiek Geul bereikt Valkenburg: 'Gevaar is nog niet geweken' | RTL Nieuws.* Retrieved 04-05-2023, from https://www.rtlnieuws.nl/nieuws/nederland/artikel/5286365/hoogwaterpiek-geul-overstroming-valkenburg-limburg

RTL Nieuws. (2023). *Rapport: overstromingen Limburg niet te voorkomen, schade kan wel beperkt worden | RTL Nieuws.* Retrieved 07-03-2023, from https://www.rtlnieuws.nl/nieuws/nederland/artikel/5361798/overstroming-limburg-risicos-schade-verkleinen-rapport-deltares

Ruby, E. (2006). *How Urbanization Affects the Water Cycle.* Retrieved 09-08-2023, from https://oehha.ca.gov/ecotoxicology/fact-sheet/background-factsheet-effect-urbanization-water-cycle

Savenije, H. (2009). *CT4431 - Hydrological Modelling.* Retrieved 2023-06-15, from https://brightspace.tudelft.nl/d2l/le/content/399298/viewContent/2298278/View

Schaminée, J., Aggenbach, C., Crombaghs, B., de Haan, M., Hommel, P., Smolders, F., … Weeda, E. (2009). Preadvies Beekdalen Heuvellandschap.

Schellekens, J. (2022). *wflow documentation.* Retrieved 27-03-2023, from https://wflow.readthedocs.io/_/downloads/en/stable/pdf/

Schuurmans, H., & van Vossen, J. (2013). *Nationale Regenradar Toelichting operationele neerslagproducten* (Tech. Rep.). Retrieved 22-09-2023, from https://nationaleregenradar.nl/pdfs/hoofdrapport_NRR_definitief.pdf

Seibert, J., & Bergström, S. (2022, March). A retrospective on hydrological catchment modelling based on half a century with the HBV model. *Hydrology and Earth System Sciences*, *26*(5), 1371–1388. Retrieved 2023-06-08, from https://hess.copernicus.org/articles/26/1371/2022/ doi: 10.5194/hess-26-1371-2022

Sitterson, J., Knightes, C., Parmar, R., Wolfe, K., Muche, M., & Avant, B. (2017). An Overview of Rainfall-Runoff Model Types. Retrieved from https://cfpub.epa.gov/si/si_public_record_report.cfm?Lab=NERL&dirEntryId=339328

Slager, K., Becker, A., Bouaziz, L., & Kwadijk, J. (2022). *Rapid assessment study on the Geul river basin : screening of flood reduction measures.* Retrieved 06-10-2023, from https://www.deltares.nl/expertise/publicaties/rapid-assessment-study-on-the-geul-river-basin-screening-of-flood-reduction-measures

Slager, K., de Moel, H., & de Jong, J. (2021). *Maximum flood extents Limburg floods july 2021 (dataset).* Retrieved 16-12-2023, from https://data.4tu.nl/articles/_/16817389

SMHI. (n.d.). Integrated Hydrological Modelling System [Computer software manual].

Stam, M. H. (2002). Effects of Land-Use and Precipitation Changes on Floodplain Sedimentation in the Nineteenth and Twentieth Centuries (Geul River, The Netherlands). In *Flood and Megaflood Processes and Deposits.* John Wiley & Sons, Ltd. Retrieved 2023-10-06, from https://onlinelibrary.wiley.com/doi/abs/10.1002/9781444304299.ch14 doi: 10.1002/9781444304299.ch14

Stichting RIONED. (2024). *De koepelorganisatie voor stedelijk waterbeheer - RIONED.* Retrieved from https://www.riool.net/home

Thewissen, A. (2022). *Flood event of July 2021: How extreme were the floods in the Ahr, Vesdre and Geul?* Retrieved 16-3-2023, from http://resolver.tudelft.nl/uuid:a7436524-e11b-4922-8637-6a74a1868f04

Tsiokanos, A. (2022). *Investigation of the Impacts of Climate Variability and Land Use Changes on the Hydrology of the Geul River Catchment.* Retrieved 06-10-2023, from https://repository.tudelft.nl/islandora/object/uuid%3Abf03fedd-88a1-4cb0-a72a-1487dcf56402

van Dijk, A. I. J. M., & Bruijnzeel, L. A. (2001, July). Modelling rainfall interception by vegetation of variable density using an adapted analytical model. Part 2. Model validation for a tropical upland mixed cropping system. *Journal of Hydrology*, *247*(3), 239–262. Retrieved 2023-04-12, from https://www.sciencedirect.com/science/article/pii/S0022169401003936 doi: 10.1016/S0022-1694(01)00393-6

van Hattum, T., Blauw, M., Jensen, M. B., & de Bruin, K. (2016). *Op weg naar de waterslimme stad - WUR.* Retrieved 09-08-2023, from https://www.wur.nl/nl/project/op-weg-naar-de-waterslimme-stad.htm

van Heeringen, K.-J., Asselman, N., Beersma, J., Overeem, A., & Philip, S. (2022). *Analyse overstroming Valkenburg.*

van Verseveld, W., Visser, M., Boisgontier, H., Bootsma, H., Bouaziz, L., Buitink, J., … Hegnauer, M. (2023). *Wflow.jl.* Retrieved 28-03-2023, from https://zenodo.org/record/7687551#.ZCKpEcpByUk

Van Verseveld, W. J., Weerts, A. H., Visser, M., Buitink, J., Imhoff, R. O., Boisgontier, H., … Russell, B. (2022, August). Wflow_sbm v0.6.1, a spatially distributed hydrologic model: from global data to local applications. *Geoscientific Model Development Discussions*, 1–52. Retrieved 2023-03-09, from https://gmd.copernicus.org/preprints/gmd-2022-182/ (Publisher: Copernicus GmbH) doi: 10.5194/gmd-2022-182

van Wel, R. (2021). *'tegen vloedgolf Valkenburg kun je je niet wapenen' - 1Limburg.* Retrieved 21-08-2023, from https://www.1limburg.nl/nieuws/1466247/tegen-vloedgolf-valkenburg-kun-je-je-niet-wapenen

Vertessy, R. A., & Elsenbeer, H. (1999). Distributed modeling of storm flow generation in an Amazonian rain forest catchment: Effects of model parameterization. *Water Resources Research*, *35*(7), 2173–2187. Retrieved 2023-03-24, from https://onlinelibrary.wiley.com/doi/abs/10.1029/1999WR900051 doi: 10.1029/1999WR900051

Waterschap Limburg. (n.d.-a). *De actuele waterstand van Selzerbeek, Buffer Nijswiller.* Retrieved 24-08-2023, from https://www.waterstandlimburg.nl/Home/Waterstanden/226

Waterschap Limburg. (n.d.-b). *Volmolen Epen.* Retrieved 17-11-2023, from https://www.youtube.com/watch?v=DEltSW3TM34

Westenbrink, B. (2022). *Water en bodem sturend: 33 structurerende keuzes.* Retrieved 09-08-2023, from https://www.h2owaternetwerk.nl/h2o-podium/redactioneel/water-en-bodem-sturend-33-structurerende-keuzes

Wikipedia. (2021). *Oude Molen (Valkenburg) | Wikipedia.* Retrieved 16-08-2023, from https://

nl.wikipedia.org/wiki/Oude_Molen_(Valkenburg)

Wikipedia. (2022). *Eyserbeek - Wikipedia.* Retrieved 06-10-2023, from https://en.wikipedia.org/wiki/Eyserbeek#cite_note-1

Wikipedia. (2023a). *IJzeren Molen | Wikipedia.* Retrieved 16-08-2023, from https://nl.wikipedia.org/wiki/IJzeren_Molen

Wikipedia. (2023b). *Volmolen (Epen) | Wikipedia.* Retrieved 16-08-2023, from https://nl.wikipedia.org/wiki/Volmolen_(Epen)

Winteraeken, H. (2017). *Watermolenlandschappen, voorbeelden uit het Geuldal.* Retrieved 22-08-2023, from https://www.stichtingerm.nl/doc/waterbeheerenerfgoed30nov2017/Harry%20Winteraeken%20-%20Molenlandschappen%20vb%20Geuldal.pdf

Yang, L., Ni, G., Tian, F., & Niyogi, D. (2021). Urbanization Exacerbated Rainfall Over European Suburbs Under a Warming Climate. *Geophysical Research Letters*, *48*(21), e2021GL095987. Retrieved 2023-08-09, from https://onlinelibrary.wiley.com/doi/abs/10.1029/2021GL095987 doi: 10.1029/2021GL095987

# A

# D-RR

## A.1. Routines

D-RR represents a mixed sewer system in Figure A.1 (Deltares, 2022c). This model contains the storage on the streets and storage in the sewer system. Precipitation falls on the paved areas like roads and roofs and fills the street storage. When the storage is full, the excess water is discharged to the mixed sewer. The street storage decreases by evaporation. The water in the mixed sewer consists of this street excess water and dry weather flow (DWF), due to domestic water use. Next, the water in the sewer is pumped to a waste water treatment plant. When the sewer is full, the excess water is spilled into the Geul. The state and flux variables of D-RR are presented in Appendix A.2. The corresponding parameters and forcing are presented in Appendix A.3.

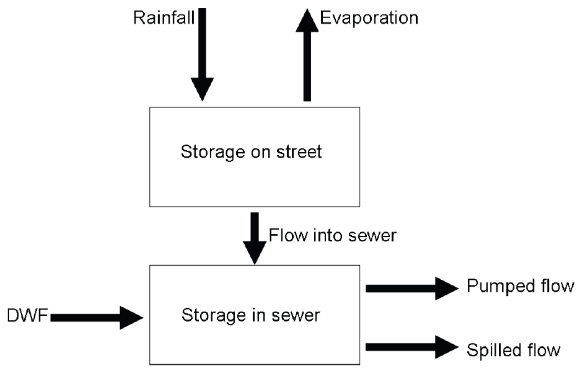


Figure A.1: Schematization of the D-RR model (Deltares, 2022c).

## A.2. State and Flux Variables

| Variable | Description | Unit |
|---|---|---|
| Storage on Street | Amount of street storage | mm |
| Flow into Sewer | Flow from street to sewer | mm/h |
| Storage in Sewer | Amount of sewer storage | mm |

## A.3. Parameters and Forcing

| Parameter | Description | Unit |
|---|---|---|
| Runoff Area | Calculation area of the paved part | $m^2$ |
| Surface Level | Level of the sewer outflow | m AD |
| Runoff Coefficient | Delay factor of the spilled water | 1/min |
| Capacity (mixed/rainfall) | Pump capacity for mixed/rain water | mm/h |
| Capacity (dry weather flow) | Pump capacity for dry weather flow | mm/h |
| Pump Discharge Target | Location where the water is directed to | - |
| Storage on Street | Available street storage | mm |
| Storage in Sewer (mixed/rainfall) | Available mixed/rainfall sewer storage | mm |
| Storage in Sewer (dry weather flow) | Available dry weather sewer storage | mm |
| Meteo Station Name | Corresponding meteo station containing precipitation and potential evaporation data | - |

# B
# HBV

## B.1. Routines

Figure B.1 presents the used semi-distributed HBV model in this research. The model is adapted from the course CIE4431 Hydrologic Models (Hrachowitz, 2021). The HBV model consists of four storages and depends on 8 parameters. The routines of the model are presented in this section. Appendix B.2 presents the state and flux variables and Appendix B.3 presents the parameters and forcing.

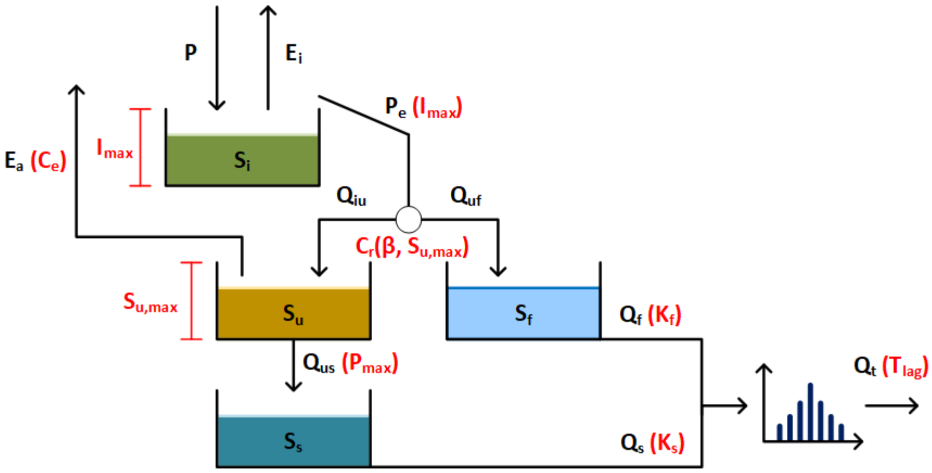


Figure B.1: Schematization of the HBV model, including the 8 parameters.

### B.1.1. Interception

The canopy store receives precipitation, $P$, and potential evaporation, $E_p$, as input. The volume of the canopy storage $S_i$ increases with the amount of precipitation. The available water can be evaporated as interception, which is limited by the potential evaporation. Interception only occurs when there is no rainfall in the time step. The interception flux is defined as:

$$E_i = min\left(E_p, \frac{S_i}{dt}\right) \tag{B.1}$$

### B.1.2. Throughfall

The maximum storage of the canopy store is defined by $I_{max}$. When the maximum is exceeded, the excess water is released as throughfall. This water infiltrates in the unsaturated zone or is drained to the fast lateral store. The throughfall $P_e$ is calculated by:

$$P_e = max\left(0, \frac{S_i - I_{max}}{dt}\right) \tag{B.2}$$

The available throughfall is partitioned in infiltration and fast lateral recharge, based on the runoff coefficient $C_r$. This coefficient is the fraction of the catchment in which the water content in the unsaturated store, $S_u$, exceeds its capacity $S_{u,max}$. The shape of $C_r$ is controlled by the shape parameter $\beta$. $C_r$ is defined as:

$$C_r = \left(\frac{S_u}{S_{u,max}}\right)^{\beta} \tag{B.3}$$

The amount of infiltration $Q_{iu}$ is determined by the above runoff coefficient. The larger the unsaturated storage, the larger the runoff coefficient, and the smaller the amount of infiltration. The infiltration flux is defined as:

$$Q_{iu} = (1 - C_r)\, P_e \tag{B.4}$$

The water that cannot be stored in the unsaturated store, is drained to the fast lateral store. The fast lateral recharge $Q_{uf}$ increases for a higher runoff coefficient and is defined as:

$$Q_{uf} = C_r P_e \tag{B.5}$$

### B.1.3. Transpiration

The plant transpiration $E_a$ depends on the available energy after interception, the available water in the unsaturated store, and the relative soil moisture, $C_e$ for which the vegetation starts to experience water stress. When all the potential evaporation is intercepted, or when no water is available in the unsaturated store, the transpiration becomes zero. $E_a$ is calculated by:

$$E_a = min\left(\left(E_p - E_i\right) \frac{S_u}{S_{u,max} C_e}, S_u\right) \tag{B.6}$$

### B.1.4. Percolation

Water percolates from the unsaturated zone to the saturated zone. The percolation $Q_{us}$ depends on the maximum percolation rate $P_{max}$ and the volume of the saturated zone $S_u$. The percolation flux is defined as:

$$Q_{us} = P_{max} \frac{S_u}{S_{u,max}} \tag{B.7}$$

### B.1.5. Total Flow

The fast lateral recharge is routed through a fast responding lateral flow component, the fast lateral store. Subsurface flow $Q_f$ is released from this store, based on a storage coefficient $K_f$ and the fast lateral storage $S_f$. $Q_f$ is calculated by:

$$Q_f = K_f S_f \tag{B.8}$$

Groundwater flow $Q_s$ is released from the saturated zone. The flow depends on a storage coefficient $K_s$ and the saturated storage $S_s$. The groundwater flow is defined as:

$$Q_s = K_s S_s \tag{B.9}$$

The total flow $Q_t$ is the sum of the subsurface and groundwater flow. This water is released to the river. The flow is delayed by a transformation function, based on $T_{lag}$. The total flow is spread as a symmetrical triangle over $T_{lag}$ time steps, based on a weighting function. This lag function accounts for the travelling times of the water in the catchment.

$$Q_t = Q_f + Q_s \tag{B.10}$$

# B.2. State and Flux Variables

| Symbol | Description | Unit |
|---|---|---|
| $S_i$ | Canopy storage | mm |
| $S_u$ | Unsaturated root-zone storage | mm |
| $S_f$ | Fast lateral flow storage | mm |
| $S_s$ | Saturated storage | mm |
| $P_e$ | Throughfall | mm $t^{-1}$ |
| $Q_{iu}$ | Infiltration | mm $t^{-1}$ |
| $Q_{uf}$ | Fast lateral recharge | mm $t^{-1}$ |
| $E_a$ | Transpiration | mm $t^{-1}$ |
| $Q_{us}$ | Percolation | mm $t^{-1}$ |
| $Q_f$ | Subsurface flow | mm $t^{-1}$ |
| $Q_s$ | Groundwater flow | mm $t^{-1}$ |
| $Q_t$ | Total flow | mm $t^{-1}$ |

# B.3. Parameters and Forcing

| Symbol | Description | Unit |
|---|---|---|
| $P$ | Precipitation | mm $t^{-1}$ |
| $E_p$ | Potential evaporation | mm $t^{-1}$ |
| $I_{max}$ | Maximum of the interception storage | mm |
| $S_{u,max}$ | Maximum of the unsaturated storage | mm |
| $\beta$ | Shape parameter of the runoff coefficient | - |
| $C_e$ | Relative soil moisture when vegetation starts to experience water stress | - |
| $P_{max}$ | Maximum percolation recharge rate | mm $t^{-1}$ |
| $K_f$ | Fast lateral storage coefficient | $t^{-1}$ |
| $K_s$ | Saturated storage coefficient | $t^{-1}$ |
| $T_{lag}$ | Time delay of the released discharge | t |

# C

# Wflow_sbm

## C.1. Routines

Figure C.1 presents the wflow_sbm with its main routines, indicated with the colored boxes. The main routines are Interception, Snow and glaciers, Soil module and evapotranspiration, Lateral subsurface flow, Surface routing, and Reservoirs and lakes. Glaciers are not taken into account in the Snow and glaciers routine, because there are no glaciers in the Geul catchment. The Reservoirs and lakes are also not reviewed, because they are in the river part, which is determined by D-HYDRO. This section describes these main routines in detail with the corresponding equations. Appendix C.2 presents the state and flux variables and Appendix C.3 presents the parameters and forcing.

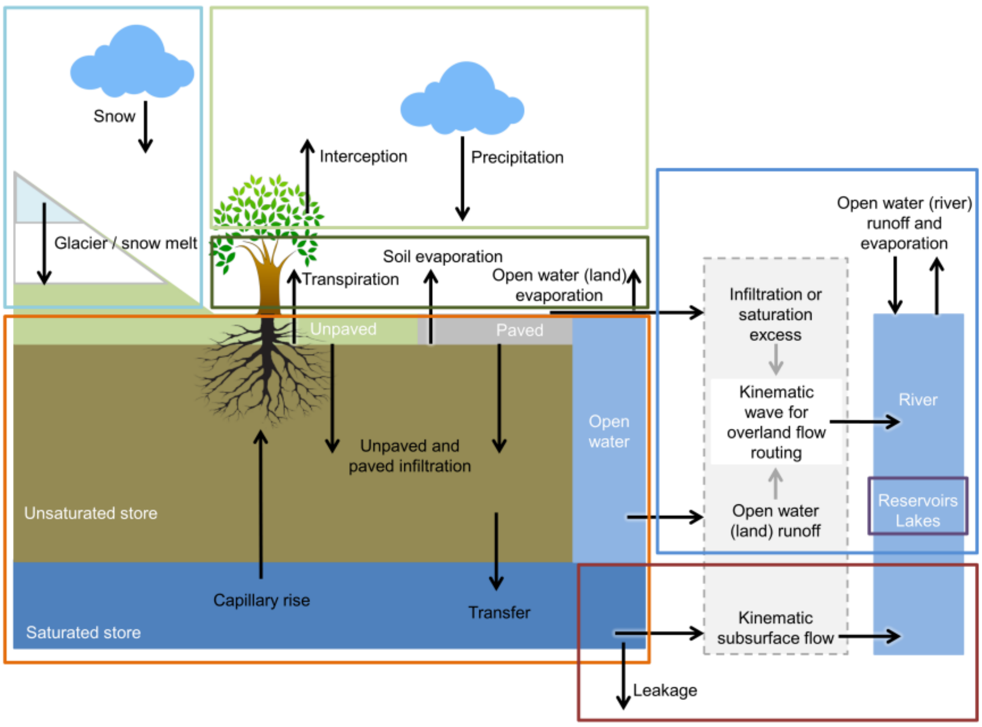


Figure C.1: An overview of the wflow_sbm model (Van Verseveld et al., 2022). The routines in the model are: green, Interception; light blue, Snow; orange, Soil module and evapotranspiration; brown, Lateral subsurface flow; dark blue, Surface routing; and black, Reservoirs and lakes.

### C.1.1. Interception

The interception flux is calculated by two different models: the analytical Gash model, and the modified Rutter model. The model choice is made by the simulation time step. The Gash model is used for daily (or larger) time steps, and the modified Rutter model is used for time steps smaller than daily time steps. Hourly time steps are used in this research, so the modified Rutter model is reviewed in detail. A simplification of the Rutter model is used to calculate the interception. The simplified model does not take drainage from the canopy into account.

*Modified Rutter Model*

The interception parameters can be estimated based on the monthly Leaf Area Index (LAI) [-]. This estimation is under the assumption that the canopy capacity for leaves $S^t_{leaf,max}$ [mm] is linearly related to the LAI with the specific leaf storage $S_{leaf}$ [mm]:

$$S^t_{leaf,max} = S_{leaf} LAI^t \tag{C.1}$$

The specific leaf storage is related to the land cover type. The canopy gap fraction $f^t_{canopygap}$ [-] at time step $t$ is determined by the extinction coefficient $k$ [-] based on (van Dijk & Bruijnzeel, 2001):

$$f^t_{canopygap} = e^{\left(-kLAI^t\right)} \tag{C.2}$$

The stemflow $P^t_{stemflow}$ [mm] at time step $t$ is calculated as a fraction of the amount of precipitation $P^t$ [mm] at that time step. The stemflow fraction $f_{stemflow}$ [-] is equal to 0.1 of the canopy gap fraction $f_{canopygap}$ [-].

$$P^t_{stemflow} = f_{stemflow} P^t \tag{C.3}$$

The amount of precipitation that falls on the canopy $P^t_{canopy}$ [mm] at time step $t$ is a function of the total precipitation amount and the canopy gap and stemflow fractions:

$$P^t_{canopy} = \max\left(\left(1 - f_{canopygap} - f_{stemflow}\right), 0\right) P^t \tag{C.4}$$

The initial drainage $D^t_{canopy,s1}$ [mm] from the canopy storage at time step $t$ is the excess canopy storage at the previous time step, compared to the storage capacity of the canopy $S_{canopy,max}$ [mm]:

$$D^t_{canopy,s1} = \begin{cases} \left(S^{t-1}_{canopy} - S_{canopy,max}\right), & \text{if } S^{t-1}_{canopy} > S_{canopy,max} \\ 0, & \text{else} \end{cases} \tag{C.5}$$

Next, the canopy storage is updated based on the initial canopy drainage, precipitation on the canopy, and the evaporation from the canopy storage:

$$S^t_{canopy} = S^{t-1}_{canopy} + P^t_{canopy} - D^t_{canopy,s1} \tag{C.6}$$

$$S^t_{canopy} = S^t_{canopy} - \min(S^t_{canopy}, E^t_{pot,total}) \tag{C.7}$$

The remaining potential evaporation $E^t_{pot,remainder}$ [mm] at time step $t$ is returned by:

$$E^t_{pot,remainder} = E^t_{pot,total} - \min\left(S^t_{canopy}, E^t_{pot,total}\right) \tag{C.8}$$

If required, the canopy storage is drained again with $D^t_{canopy,s2}$ [mm] at time step $t$:

$$D^t_{canopy,s2} = \begin{cases} \left(S^{t-1}_{canopy} - S_{canopy,max}\right), & \text{if } S^{t-1}_{canopy} > S_{canopy,max} \\ 0, & \text{else} \end{cases} \tag{C.9}$$

This results in the final canopy storage:

$$S^t_{canopy} = S^{t-1}_{canopy} - D^t_{canopy,s2} \tag{C.10}$$

The throughfall $P^t_{throughfall}$ [mm] at time step $t$ is the sum of the total drainage from the canopy and the precipitation amount that directly falls on the ground:

$$P^t_{throughfall} = D^t_{canopy,s1} + D^t_{canopy,s2} + f_{canopygap} P^t \tag{C.11}$$

The total interception $I^t_{total}$ [mm] at time step $t$ is given by:

$$I^t_{total} = P^t - P^t_{stemflow} - P^t_{throughfall} \tag{C.12}$$

### C.1.2. Snow

The effective precipitation $P^t_{effective}$ [mm] consists of throughfall and stemflow. The effective precipitation occurs as snowfall $P^t_{snow}$ [mm] at time step $t$, if the air temperature $T^t_{air}$ [°C] is below the temperature threshold $s_{fall,Tthreshold}$ [°C]. The range over which the precipitation is partly snow, and partly rain is defined by an interval parameter $s_{fall,Tinterval}$ [°C]. This visualised in Figure C.2, with $tt$ as $s_{fall,Tthreshold}$ and $tti$ as $s_{fall,Tinterval}$.

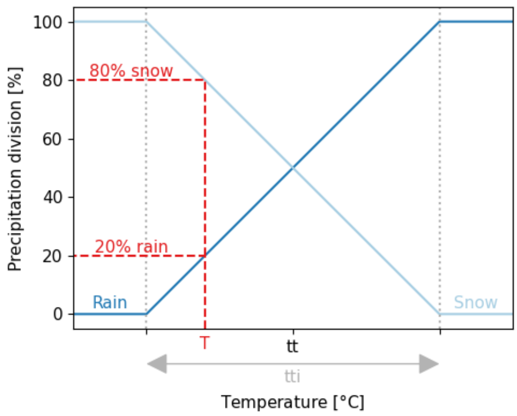


Figure C.2: The division between snow and rainfall is based on the threshold temperature (van Verseveld et al., 2023). tt ($s_{fall,Tthreshold}$) is the threshold temperature for snow and tti ($s_{fall,Tinterval}$) is the interval over which the precipitation falls partly as snow and rain.

The fraction of the precipitation that occurs as rainfall $f^t_{rain}$ [-] at time step $t$ is calculated by:

$$f^t_{rain} = \begin{cases} 0, & \text{if } s_{fall,Tinterval} = 0 \;\&\; T^t_{air} \leq s_{fall,Tthreshold} \\ 1, & \text{if } s_{fall,Tinterval} = 0 \;\&\; T^t_{air} > s_{fall,Tthreshold} \\ \max\left(\min\left(\frac{T^t_{air} - s_{fall,Tthreshold} - 0.5 s_{fall,Tinterval}}{s_{fall,Tinterval}}, 1\right), 0\right) & \text{if } s_{fall,Tinterval} \neq 0 \end{cases} \tag{C.13}$$

The rainfall fraction is used to calculate the amount of snowfall $P^t_{snow}$ [mm] and the amount of rain $P^t_{rain}$ [mm] at time step $t$:

$$P^t_{snow} = \left(1 - f^t_{rain} P^t_{effective}\right) \tag{C.14}$$

$$P^t_{rain} = f^t_{rain} P^t_{effective} \tag{C.15}$$

Snowmelt occurs when the air temperature $T^t_{air}$ is above the melting temperature threshold $s_{melt,Tthreshold}$ [°C]. The potential snow melt $M^t_{snow,pot}$ [mm] at time step $t$ is determined by the degree-day factor $s_{ddf}$ [mm t$^{-1}$ °C]:

$$M^t_{snow,pot} = \begin{cases} s_{ddf}\left(T^t_{air} - s_{melt,Tthreshold}\right), & \text{if } T^t_{air} > s_{melt,Tthreshold} \\ 0, & \text{else} \end{cases} \tag{C.16}$$

The actual snow melt $M^t_{melt,act}$ [mm] at time step $t$ is limited by the snow storage $S^{t-1}_{snow}$ at the previous time step. The actual snow melt is equal to the minimum of $M^t_{snow,pot}$ and $S^{t-1}_{snow}$. Water that can refreeze retains in the snow pack if $T^t_{air}$ is below $s_{melt,Tthreshold}$. The potential amount of water that can refreeze $M^t_{refreeze,pot}$ [mm] at time step $t$ is calculated with $s_{ddf}$, a refreezing coefficient $s_{refreeze}$ [-], $T^t_{air}$, and $s_{melt,Tthreshold}$:

$$M^t_{refreeze,pot} = \begin{cases} s_{ddf} s_{refreeze} \left( s_{melt,Tthreshold} - T^t_{air} \right), & \text{if } T^t_{air} < s_{melt,Tthreshold} \\ 0, & \text{else} \end{cases} \tag{C.17}$$

The actual amount of water that can refreeze $M^t_{refreeze,act}$ [mm] is determined by taking the minimum of $M^t_{refreeze,pot}$ [mm] and the amount of snow water at the previous time step $S^{t-1}_{snow,liquid}$ [mm]. The storage in the snow pack $S^t_{snow}$ [mm] at time step $t$ is a function of the storage in the snow pack at the previous time step, amount of snowfall, actual refreezing and actual snow melt:

$$S^t_{snow} = S^{t-1}_{snow} + P^t_{snow} + M^t_{refreeze,act} - M^t_{snow,act} \tag{C.18}$$

The liquid water content of the snow $S^t_{snow,liquid}$ [mm] at time step $t$ is a function of the liquid water content at the previous time step, actual refreezing, actual snow melt, and amount of rainfall. The liquid water content is limited by the maximum amount of water that the snow pack can hold, controlled by the water holding capacity $s_{whc}$ [-] and the snow pack storage. The liquid water content of the snow is determined by:

$$S^t_{snow,liquid} = S^{t-1}_{snow,liquid} - M^t_{refreeze,act} + M^t_{snow,act} + P^t_{rain} \tag{C.19}$$

$$S^t_{snow,liquid} = S^t_{snow,liquid} - \max\left( S^t_{snow,liquid} - S^t_{snow} s_{whc}, 0 \right) \tag{C.20}$$

The amount that exceeds the fraction of the current snow pack, $\max\left( S^t_{snow,liquid} - S^t_{snow} s_{whc} \right)$, becomes available as rainfall.

## C.1.3. Soil Module and Evapotranspiration

**Infiltration**

The available water for infiltration $F^t_{available}$ [mm] at time step $t$ consists of throughfall, stemflow, and snow melt. $F^t_{available}$ is first added to the river flow and overland flow components. The river flow component is based on the river fraction $f_{fraction}$ and the overland flow component is based on the open water fraction $f_{open\,water}$, excluding rivers:

$$R^t_{river} = f_{river} f^t_{available} \tag{C.21}$$

$$R^t_{open\,water} = f_{open\,water} F^t_{available} \tag{C.22}$$

$R^t_{river}$ [mm] is the runoff from the river fraction and $R^t_{open\,water}$ [mm] is the runoff from the open water fraction at time step $t$. $R^t_{river}$ and $R^t_{open\,water}$ are later added to the river and overland flow components. The remaining available water for infiltration is equal to:

$$F^t_{available} = F^t_{available} - R^t_{river} - R^t_{open\,water} \tag{C.23}$$

The soil has a depth $z_{soil}$ [mm] and is divided into a saturated store $S_{sat}$ [mm] and an unsaturated store $S_{unsat}$ [mm]. The top of the saturated store forms a pseudo-water table at depth $z_{watertable}$ [mm]. $S_{sat}$ depends on $z_{soil}$, $z_{watertable}$, the saturated soil water content $\theta_s$, and the residual water content $\theta_r$ [mm mm$^{-1}$]:

$$S_{sat} = (z_{soil} - z_{watertable})\,(\theta_s - \theta_r) \tag{C.24}$$

The initial storage capacity of the unsaturated zone $S^t_{unsat,max}$ [mm] at time step $t$ is based on $S^{t-1}_{sat}$, the sum of the unsaturated storage for $n$ unsaturated soil layers $S^{t-1}_{unsat,n}$ [mm] at the previous time step, and the total soil water capacity of the soil. $S^t_{unsat,max}$ is calculated by:

$$S^t_{unsat,max} = z_{soil}\,(\theta_s - \theta_r) - S^{t-1}_{sat} - \sum S^{t-1}_{unsat,n} \tag{C.25}$$

The total available water for infiltration is split into infiltration for the paved areas and for the unpaved areas. The maximum amount of water that can infiltrate in paved areas $F^t_{paved}$ [mm] at time step $t$ depends on the infiltration capacity $c_{infiltration,paved}$ [mm day$^{-1}$] of the paved areas, reduction factor for snow $f_{frozen}$ [-], $F^t_{available}$, and the fraction of paved area $f_{paved}$ [-]:

$$F^t_{paved} = \min\left(c_{infiltration,paved} f^t_{frozen}, f_{paved} F^t_{available}\right) \tag{C.26}$$

The maximum amount of water that can infiltrate in unpaved areas $F^t_{umpaved}$ [mm] at time step $t$ depends on the infiltration capacity $c_{infiltration,unpaved}$ [mm day$^{-1}$] of the unpaved areas, $f_{frozen}$ [-], $F^t_{available}$, and the fraction of unpaved area $(1 - f_{paved})$ [-]:

$$F^t_{unpaved} = \min\left(c_{infiltration,unpaved} f^t_{frozen}, (1 - f_{paved})\, F^t_{available}\right) \tag{C.27}$$

The reduction factor $f_{frozen}$ depends on the soil temperature at the near-surface $T^t_{soil}$ [°C] at time step $t$. $T^t_{soil}$ depends on the near-surface soil temperature at the previous time step, the air temperature at time step $t$, and a weighting coefficient $w$ [-]:

$$T^t_{soil} = T^{t-1}_{soil} + w\left(T^t_{air} - T^{t-1}_{soil}\right) \tag{C.28}$$

$f^t_{frozen}$ at time step $t$ is determined with the model parameter $f_{red,frozen}$ [-] and $T^t_{soil}$ as follows:

$$f^t_{frozen} = \begin{cases} \frac{1.0}{b + e^{\left(-c\left(T^t_{soil} - a\right)\right)}} + f_{red,frozen}, & \text{if snow \& soilinfreduction} \\ 1, & \text{else} \end{cases} \tag{C.29}$$

With:

$$a = 0.0, b = \frac{1.0}{1.0 - f_{red,frozen}}, c = 8.0$$

The actually infiltrating water $F^t_{total}$ [mm] is limited by initial unsaturated storage capacity:

$$F^t_{total} = \min\left(F^t_{paved} + F^t_{unpaved}, S_{unsat,max}\right) \tag{C.30}$$

The amount of infiltration excess water $F^t_{excess}$ [mm] at time step $t$ is determined by:

$$F^t_{excess} = \left(f_{paved} F^t_{available} - F^t_{paved}\right) + (1 - f_{paved})\left(F^t_{available} - F^t_{unpaved}\right) \tag{C.31}$$

**Soil Water Accounting Scheme**

The water in a unsaturated store layer can be transferred to another unsaturated store layer or to the saturated store. The transfer of water $Q^t_{transfer,n}$ [mm t$^{-1}$] is controlled by the vertical saturated hydraulic conductivity $K_{vz}$ [mm t$^{-1}$] at depth $z$ of the bottom layer for transfer between unsaturated soil layers or at $z_{watertable}$ for transfer to the saturated store. It also depends on the effective saturation degree of the layer, and a Brooks-Corey power coefficient $c_n$:

$$Q_{transfer,n} = K_{vz}\left(\frac{\theta - \theta_r}{\theta_s - \theta_r}\right)^{c_n} \tag{C.32}$$

$c_n$ depends on the pore size distribution index $\lambda$:

$$c_n = \frac{2 + 3\lambda}{\lambda} \tag{C.33}$$

$K_{vz}$ declines with soil depth $z$ and depends on the vertical saturated conductivity at the soil surface $K_{v0}$ $[mmt^{-1}]$ and scaling parameter $f_{Kv}$, Figure C.3.:

$$K_{vz} = K_{v0} e^{(-f_{Kv} z)} \tag{C.34}$$

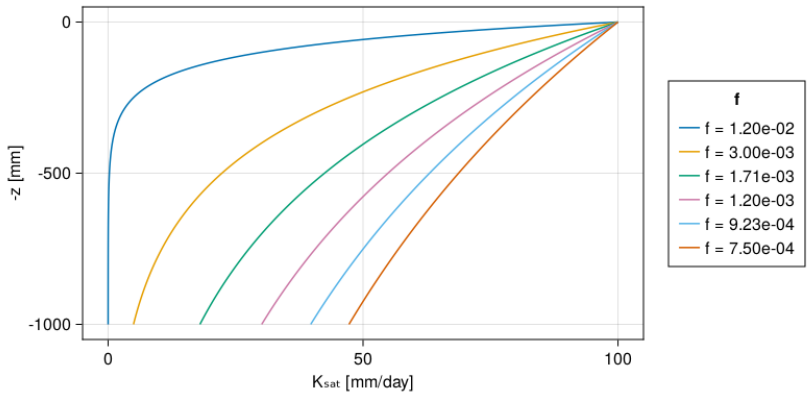


Figure C.3: Relation between the soil depth and the saturated hydraulic conductivity $K_{sat}$ ($K_{vz}$) (van Verseveld et al., 2023).

For $n$ unsaturated soil layers, the transfer of water is calculated by:

$$S^t_{unsat,n} = S^{t-1}_{unsat,n} + Q^t_{in,n} \tag{C.35}$$

$$Q^t_{transfer,n} = f_{Kv,n}\left(K_{v0}\right) e^{(-f_{Kv} z_n)} \min\left(\left(\frac{S^t_{unsat,n}}{z_{n,thickness}\left(\theta_s - \theta_r\right)}\right)^{c_n}, 1\right) \tag{C.36}$$

$$S^t_{unsat,n} = S^t_{unsat,n} - \min\left(Q^t_{transfer,n}, S^t_{unsat,n}\right) \tag{C.37}$$

$$Q^t_{in,n} = \begin{cases} F^t_{total} & \text{if } n = 1 \\ \min\left(Q^t_{transfer,n-1}, S^t_{unsat,n-1}\right) & \text{if } n > 1 \end{cases} \tag{C.38}$$

When the soil consists of one layer, the transfer of water from the unsaturated store to the saturated store, is controlled by $K_{vz}$ at depth $z^{t-1}_{watertable}$ and the ratio between the unsaturated store and saturation deficit $S^t_{deficit}$ [mm] at time step $t$:

$$S^t_{deficit} = \left(\theta_s - \theta_r\right) z_{soil} - S^{t-1}_{sat} \tag{C.39}$$

$$Q^t_{transfer,n} = f_{Kv,1}\left(K_{v0}\right) e^{(-f_{Kv} z^{t-1}_{watertable})} \frac{S^t_{unsat,1}}{S^t_{deficit}} \tag{C.40}$$

**Evapotranspiration**

The open water evaporation from water bodies $E^t_{open\,water}$ [mm] at time step $t$ is based on the open water fraction, the water level in the kinematic reservoir of the overland flow component $S^{t-1}_{w1,land}$ at the previous time step, and the remaining potential evaporation after interception:

$$E^t_{open\,water} = \min\left(f_{open\,water} S^{t-1}_{w1,land}, f_{open\,water} E^t_{pot,remainder}\right) \tag{C.41}$$

The open water evaporation from the rivers $E^t_{river}$ [mm] at time step $t$ is determined in the same way as the open water evaporation from water bodies. For the river, the fraction of rivers and the water level in the kinematic wave reservoir of the river flow component are used.

$$E^t_{river} = \min\left(f_{river} S^{t-1}_{w1,river}, f_{river} E^t_{pot,remainder}\right) \tag{C.42}$$

The remaining potential evaporation after interception and open water evaporation is given by:

$$E^t_{pot,remainder} = E^t_{pot,remainder} - E^t_{river} - E^t_{open\,water} \tag{C.43}$$

The potential evaporation of the soil $E^t_{pot,soil}$ [mm] at time step $t$ is based on $E^t_{pot,remainder}$ and the canopy gap fraction $f^t_{canopygap}$ [-]. When the soil consists of one layer, the soil evaporation $E^t_{act,soil}$ [mm] is determined by:

$$E^t_{pot,soil} = f^t_{canopygap} E^t_{pot,remainder} \tag{C.44}$$

$$E^t_{act,soil} = \min\left(E^t_{pot,soil} \frac{S^t_{deficit}}{z_{soil}\,(\theta_s - \theta_r)}, S^t_{unsat,1}\right) \tag{C.45}$$

The soil evaporation is equal to the potential evaporation, when the soil is fully saturated. If this is not the case, the soil evaporation decreases linearly with increasing soil moisture deficit.

If the soil consists of different layers, the soil evaporation is determined for the upper layer. The soil evaporation is calculated by:

$$E^t_{act,soil} = \begin{cases} \min\left(E^t_{pot,soil} \frac{S^t_{unsat,1}}{z^{t-1}_{watertable}(\theta_s - \theta_r)}, S^t_{unsat,1}\right), & \text{if } z^{t-1}_{watertable} \leq z_{1,thickness} \\ \min\left(E^t_{pot,soil} \frac{S^t_{unsat,1}}{z_{1,thickness}(\theta_s - \theta_r)}, S^t_{unsat,1}\right), & \text{if } z^{t-1}_{watertable} > z_{1,thickness} \end{cases} \tag{C.46}$$

The remaining potential soil evaporation and the storage in the upper layer of the unsaturated store at time step $t$ are determined by:

$$E^t_{remainder,soil} = E^t_{pot,soil} - E^t_{act,soil} \tag{C.47}$$

$$S^t_{unsat,1} = S^t_{unsat,1} - E^t_{act,soil} \tag{C.48}$$

When the soil contains different layers and the water table is present in the upper soil layer, soil evaporation from the saturated store $E^t_{act,soil,sat}$ [mm] is possible:

$$E^t_{act,soil,sat} = \min\left(E^t_{remainder,soil} \frac{z_{1,thickness} - z^{t-1}_{watertable}}{z_{1,thickness}}, \left(z_{1,thickness} - z^{t-1}_{watertable}\right)(\theta_s - \theta_r)\right) \tag{C.49}$$

The saturated store becomes:

$$S^t_{sat} = S^{t-1}_{sat} - E^t_{act,soil,sat} \tag{C.50}$$

The available potential evaporation for transpiration is determined by the remaining potential evaporation after interception and open water evaporation and the canopy gap fraction:

$$E^t_{pot,remainder} = E^t_{pot,remainder}\left(1.0 - f^t_{canopygap}\right) \tag{C.51}$$

When the roots reach the water table at the previous time step, first, the transpiration is taken from the saturated store. The fraction of the wet roots $f_{wet\,roots}$ [-] is determined by a sigmoid function, the model parameter $c_{rd}$ and the rooting depth $z_{rooting}$ [mm]. $f_{wet\,roots}$ defines how sharp the transition is between fully wet and fully dry roots. $c_{rd}$ controls the sharpness of the sigmoid function. The wet roots fraction is determined by:

$$f_{wet\,roots} = \frac{1.0}{1.0 + e^{\left(-c_{rd}\left(z^{t-1}_{watertable} - z_{rooting}\right)\right)}} \tag{C.52}$$

The transpiration from the saturated store $E^t_{trans,sat}$ at time step $t$ is determined by:

$$E^t_{trans,sat} = \begin{cases} \min\left(f_{wet\,roots} E^t_{pot,remainder}, S^t_{sat}\right), & \text{if multiple soil layers} \\ \min\left(f_{wet\,roots} E^t_{pot,remainder}, S^{t-1}_{sat}\right), & \text{else} \end{cases} \tag{C.53}$$

Next, the saturated store is updated:

$$S^t_{sat} = \begin{cases} S^t_{sat} - E^t_{trans,sat}, & \text{if multiple soil layers} \\ S^{t-1}_{sat} - E^t_{trans,sat}, & \text{else} \end{cases} \tag{C.54}$$

The remaining available potential evaporation for transpiration from the unsaturated store becomes:

$$E^t_{pot,remainder} = E^t_{pot,remainder} - E^t_{trans,sat} \tag{C.55}$$

The maximum water extraction by roots $E_{root,max,n}$ per unsaturated soil layer $n$ at time step $t$ depends on the fraction of roots $f^t_{roots,n}$ [-] and the unsaturated store:

$$E^t_{root,max,n} = f^t_{roots,n} S^t_{unsat} \tag{C.56}$$

The soil matric suction $h$ [cm] is calculated by Brooks and Corey (1963) with the air entry value $h_b$ [cm]:

$$\frac{(\theta - \theta_r)}{(\theta_s - \theta_r)} = \begin{cases} \left(\frac{h_b}{h}\right)^{\lambda}, & h > h_b \\ 1, & h \le h_b \end{cases} \tag{C.57}$$

The soil matric suction $h^t_n$ for each unsaturated soil layer $n$ at time step $t$ is determined by:

$$h^t_n = \frac{h_b}{\left(\frac{S^t_{unsat,n}/z^t_{n,thickness}}{(\theta_s - \theta_r)}\right)^{\lambda_n^{-1}}} \tag{C.58}$$

The root water uptake model is based on Feddes (1982) and is visualized in Figure C.4. When the soil water pressure drops below the wilting point, $h4$, the root water uptake is zero. The ideal condition for the root water uptake is a soil water pressure equal to the critical soil moisture content, $h3$. Between $h3$ and $h4$, $f^t_{root\,uptake,n}$ declines linearly from 1 to 0. $h2$ is the field capacity and $h1$ (default: 10 cm) is the air entry pressure, which can be defined as input of the model.

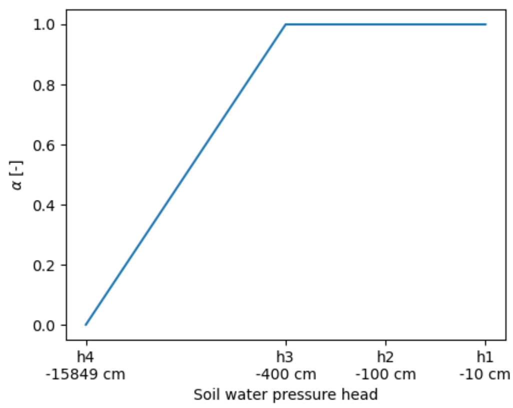


Figure C.4: Root water uptake reduction coefficient as a function of soil water pressure. (van Verseveld et al., 2023).

The transpiration of an unsaturated soil layer $n$ $E^t_{trans,unsat,n}$ [mm] depends on $E_{root,max,n}$, $E^t_{pot,remainder}$, $S^t_{unsat}$, and $f^t_{root\,uptake,n}$:

$$E^t_{trans,unsat,n} = \min\left(E^t_{root,max,n}, E^t_{pot,remainder}, S^t_{unsat,n}\right) f^t_{root\,uptake,n} \tag{C.59}$$

Next, the unsaturated storage and the remaining potential evaporation are updated:

$$S^t_{unsat,n} = S^t_{unsat,n} - E^t_{trans,unsat,n} \tag{C.60}$$

$$E^t_{pot,remainder} = E^t_{pot,remainder} - E^t_{trans,unsat,n} \tag{C.61}$$

The soil water balance is calculated after the soil water transfer, evaporation, and transpiration are determined. When the maximum unsaturated storage per layer is exceeded, the excess water is transferred to the layer above or to the surface. The actually infiltration $F^t_{act}$ [mm] is determined by subtracting the excess water at the surface $R^t_{excess,unsat}$ [mm]:

$$F^t_{act} = F^t_{total} - R^t_{excess,unsat} \tag{C.62}$$

To determine the capillary rise, first $K^t_{vz_{watertable}}$ [mm t$^{-1}$]at time step $t$ is determined:

$$K^t_{vz_{watertable}} = f_{Kv,n}\,(K_{v0})\,e^{\left(-f_{Kv}z^{t-1}_{watertable}\right)} \tag{C.63}$$

The unsaturated store capacity $S^t_{unsat,max}$ [mm] is calculated by:

$$S^t_{unsat,max} = z_{soil}\,(\theta_s - \theta_r) - S^t_{sat} - \sum S^t_{unsat,n} \tag{C.64}$$

Next, the maximum capillary rise $C^t_{max}$ [mm] is determined by $K^t_{vz_{watertable}}$, the actual transpiration from the unsaturated zone, $S^t_{sat}$, and $S^t_{unsat,max}$:

$$C^t_{max} = \max\left(0.0, \min\left(K_{vz^t_{watertable}}, \sum E^t_{trans,unsat,n}, S^t_{unsat,max}, S^t_{sat}\right)\right) \tag{C.65}$$

The actual capillary rise $C^t_{act}$ [mm] at time step $t$ is determined by scaling the maximum capillary rise by an empirical equation. $C^t_{act}$ depends on the critical water depth beyond which capillary rise ceases $z_{cap,maxdepth}$ [mm] and an empirical coefficient $m$ [-], which is related to soil properties and climate. When the soil consists of multiple layers, $C^t_{act}$ is divided over the unsaturated soil layers, from the bottom to the top soil layer, without exceeding $\theta_s$. $C^t_{act}$ is determined by:

$$C^t_{act} = \begin{cases} C^t_{max}\left(1 - \frac{z^{t-1}_{watertable}}{z_{cap,maxdepth}}\right)^m, & \text{if } z^{t-1}_{watertable} < z_{cap,maxdepth} \\ 0, & \text{else} \end{cases} \tag{C.66}$$

**Leakage**

When the maximum leakage parameter $L_{max}$ is set larger than zero, water leaves the model. The leakage $L^t$ [mm] at time step $t$ from the saturated store to the deeper groundwater is determined by:

$$L^t = \min\left(K_{v0}e^{(-f_{Kv}z_{zoil})}, S^t_{sat}, L_{max}\right) \tag{C.67}$$

### C.1.4. Lateral Subsurface Flow

The subsurface flow is routed by the kinematic wave approach. The saturated zone can be drained laterally by saturated downslope subsurface flow $Q_{subsurface}$ [m$^{-3}$t$^{-1}$] for the land slope $c_{land\ slope}$ [-] with width $w$ [m]. The horizontal saturated hydraulic conductivity at the soil surface $K_{h0}$ [m day$^{-1}$] depends on the vertical saturated hydraulic conductivity at the soil surface $K_{v0}$, a multiplication factor $f_{Kh0}$, the water table depth $z_{ssf,watertable}$, and the soil depth $z_{ssf,soil}$:

$$K_{h0} = 0.001 f_{Kh0} K_{v0} \frac{t_b}{t} \tag{C.68}$$

$Q_{subsurface}$ [m$^3$ t$^{-1}$] is determined by:

$$Q_{subsurface} = \frac{K_{h0}c_{land\ slope}}{f_{Kv}}\left(e^{\left(-f_{Kv}z_{ssf,watertable}\right)} - e^{\left(-f_{Kv}z_{ssf,soil}\right)}\right)w \tag{C.69}$$

The following continuity equation is set up:

$$(\theta_s - \theta_r)\, w \frac{\partial h}{\partial t} = -\frac{\partial Q_{subsurface}}{\partial x} + wR_{input} \tag{C.70}$$

With water table height $h$ [m], distance downslope $x$ [m], and the netto input rate to the saturated zone $R_{input}$ [m t$^{-1}$]. Substituting for $h\left(\frac{\partial q}{\partial h}\right)$ gives:

$$\frac{\partial Q_{subsurface}}{\partial t} = -c\frac{\partial Q_{subsurface}}{\partial x} + cwR_{input} \tag{C.71}$$

$$c = \frac{K_{h0} c_{land\,slope}}{(\theta_s - \theta_r)} e^{\left(-f_{Kv} z_{ssf,watertable}\right)} \tag{C.72}$$

The continuity equation is solved iteratively with Newton's method. The flow width $w$ of for each grid cell is calculated by dividing the cell area with the distance downslope $x$, based on the length in the x and y direction of each grid cell and the flow direction. The netto input rate $R_{input}$ consists of the transfer of water from the unsaturated soil layer above the water table, capillary rise, transpiration from the saturated zone, leakage and soil evaporation from the saturated store.

The exfiltration of the saturated store $R^t_{exfilt,sat}$ during saturated conditions depends subsurface flow in and out of a cell $Q^t_{subsurface,in}$ and $Q^t_{subsurface,out}$ [m$^3$ day$^{-1}$], the water table depth $z^t_{ssf,watertable}$, $R_{input}$, $w$, $x$, $\theta_s$, and $\theta_r$:

$$R^t_{exfilt,sat} = \max\left(0, \frac{\left(Q^t_{subsurface,in} + R_{input} wx - Q^t_{subsurface,out}\right)}{wx} - z^t_{ssf,watertable}\,(\theta_s - \theta_r)\right) \tag{C.73}$$

After the subsurface flow calculation, it is checked if exfiltration of the unsaturated store to the surface occurs, because of a water table depth change. The check is performed from the bottom to the top of the unsaturated layer. The excess water of each unsaturated soil layer is transferred from the bottom to the top unsaturated layer, and can result in exfiltration of water to the surface.

### C.1.5. Surface Flow Routing

The kinematic wave approach is also used for the river and surface flow routing. The river routing is not reviewed in detail, because this is determined by the D-HYDRO Suite. The kinematic wave equations for surface flow routing are given by:

$$\frac{dQ}{dx} + \frac{dA}{dt} = Q_{inflow} \tag{C.74}$$

$$A = \alpha Q^{\beta} \tag{C.75}$$

Combining the equations gives:

$$\frac{dQ}{dx} + \alpha\beta Q^{\beta-1}\frac{dQ}{dt} = Q_{inflow} \tag{C.76}$$

With surface runoff $Q$ [m$^3$ s$^{-1}$], runoff pathway length $x$ [m], cross-section area of the runoff pathway $A$ [m$^2$], lateral inflow per unit length $Q_{inflow}$ [m$^2$ s$^{-1}$], and the integration time step $t$ [s]. The coefficients $\alpha$ and $\beta$ are determined with Manning's equation:

$$\alpha = \left(\frac{nP^{\frac{2}{3}}}{\sqrt{c_{slope}}}\right)^{\beta};\ \beta = 0.6 \tag{C.77}$$

With wetted perimeter $P$ [m], the slope $c_{land\,slope}$ [m m$^{-1}$], and Manning's coefficient $n_{land}$ for overland flow. The wetted perimeter $P$ is equal to the effective flow width, which is determined by dividing the grid cell area by the flow length and subtracting the river width $w_{river}$.

The lateral inflow per unit flow length for overland flow routing $Q_{inflow}$ consists of:

- Infiltration excess water $F_{excess}^{t}$;
- Saturation excess water during infiltration $F_{excess,sat}^{t}$;
- Exfiltration water from the unsaturated zone $R_{exfilt,unsat}^{t}$;
- Water exfiltrating during saturated conditions $R_{exfilt,sat}^{t}$;
- Runoff from open water $R_{open\,water}^{t}$;
- Open water evaporation loss $E_{open\,water}^{t}$.

The lateral inflow per unit length for river flow routing $Q_{inflow}$ consists of:

- Overland flow;
- Lateral subsurface flow;
- Runoff from the river $R_{river}^{t}$;
- River evaporation loss $E_{river}^{t}$.

The Courant number $C$ determines the number of iterations within a time step $t$. $C$ is determined by:

$$C = \frac{c_k dt}{dx} \tag{C.78}$$

$$c_k = \frac{1}{\alpha\beta Q^{\beta-1}} \tag{C.79}$$

The number of iterations within a time step $t$ is calculated by multiplying the 95th percentile of $C$ with 1.25. The number of iterations can also be fixed to a specific sub time step [s] in the configuration file. When overland and river flow are present in a river cell, the cell is partitioned based on the land slope of the river cell $c_{land\,slope,river}$ and the land slope of the upstream cell $c_{land\,slope,upstream}$. The fraction of lateral subsurface or overland flow from an upstream cell into the river $f_{to\,river}$ is determined by:

$$f_{to\,river} = \frac{c_{land\,slope,upstream}}{c_{land\,slope,upstream}+c_{land\,slope,river}} \tag{C.80}$$

The fraction of lateral subsurface or overland flow from an upstream cell that flows into the downstream kinematic reservoir of lateral subsurface or overland flow $f_{to\,land}$ is determined by:

$$f_{to\,land} = 1 - f_{to\,river} \tag{C.81}$$

## C.2. State and Flux Variables

| Symbol | Description | Unit | Wflow.jl name |
|---|---|---|---|
| $S_{canopy}$ | Canopy storage | mm | canopystorage |
| $S_{snow}$ | Snow storage | mm | snow |
| $S_{snow,liquid}$ | Amount of liquid water in the snow pack | mm | snowwater |
| $S_{unsat,n}$ | Amount of water in the unsaturated zone, for layer $n$ | mm | ustorelayerdepth |
| $S_{sat}$ | Amount of water in saturated zone | mm | satwaterdepth |
| $P$ | Precipitation | mm $t^{-1}$ | precipitation |
| $I_{total}$ | Total interception | mm $t^{-1}$ | interception |
| $P_{throughfall}$ | Throughfall | mm $t^{-1}$ | throughfall |
| $F_{available}$ | Water available for infiltration | mm $t^{-1}$ | avail_forinfilt |
| $F_{excess}$ | Infiltration excess | mm $t^{-1}$ | infiltexcess |
| $F_{excess,sat}$ | Water that cannot infiltrate due to saturated soil | mm $t^{-1}$ | waterexcess |
| $F_{act}$ | Actual infiltration | mm $t^{-1}$ | actinfilt |
| $R_{exfilt,sat}$ | Water exfiltrating during saturation excess conditions | m $t^{-1}$ | exfiltwater |
| $R_{exfilt,unsat}$ | Water exfiltrating from unsaturated store by change of water table | mm $t^{-1}$ | exfiltustore |
| $R_{river}$ | Runoff from river fraction | mm $t^{-1}$ | runoff_river |
| $R_{open\,water}$ | Runoff from open water fraction (excluding rivers) | mm $t^{-1}$ | runoff_land |
| $E_{open\,water}$ | Evaporation from open water bodies (excluding rivers) | mm $t^{-1}$ | ae_openw_l |
| $E_{river}$ | Evaporation from rivers | mm $t^{-1}$ | ae_openw_r |
| $E_{act,sat}$ | Soil evaporation from the saturated store | mm $t^{-1}$ | soilevapsat |
| $E_{act,soil}$ | Soil evaporation form the unsaturated store | mm $t^{-1}$ | - |
| $E_{trans,sat}$ | Transpiration from the saturated store | mm $t^{-1}$ | actevapsat |
| $\sum E_{trans,unsat,n}$ | Transpiration from the unsaturated store | mm $t^{-1}$ | ae_ustore |
| $C_{act}$ | Actual capillary rise | mm $t^{-1}$ | actcapflux |
| $L$ | Leakage | mm $t^{-1}$ | actleakage |
| $R_{input}$ | Net recharge to the saturated store | m $t^{-1}$ | recharge |
| $Q_{subsurface}$ | Subsurface flow | $m^3$ $day^{-1}$ | ssf |
| $Q_{transfer,n}$ | Transfer of water from unsaturated store layer to saturated store | mm $t^{-1}$ | transfer |
| $Q$ | Surface runoff in the kinematic wave | $m^3$ $s^{-1}$ | q and q_av |

# C.3. Parameters and Forcing

| Symbol | Description | Unit | Wflow.jl name | Default |
|---|---|---|---|---|
| $P$ | Precipitation | mm $t^{-1}$ | precipitation | - |
| $E_{pot,total}$ | Potential evapotranspiration | mm $t^{-1}$ | potential_evaporation | - |
| $T_{air}$ | Air temperature | °C | temperature | - |
| $z_{soil}$ | Soil depth | mm | soilthickness | 2000.0 |
| $\theta_s$ | Saturated soil water content | mm $mm^{-1}$ | $\theta_s$ | 0.6 |
| $\theta_r$ | Residual soil water content | mm $mm^{-1}$ | $\theta_r$ | 0.01 |
| $f_{paved}$ | Fraction of paved soil | - | pathfrac | 0.01 |
| $f_{open\,water}$ | Open water body fraction (excluding rivers) | - | waterfrac | 0.0 |
| $c_{infiltration,unpaved}$ | Infiltration capacity of unpaved soil | mm $t^{-1}$ | infiltcapsoil | 100.0 mm $day^{-1}$ |
| $c_{infiltration,paved}$ | Infiltration capacity of paved soil | mm $t^{-1}$ | infiltcappath | 10.0 mm $day^{-1}$ |
| $z_{rooting}$ | Rooting depth | mm | rootingdepth | 750.0 |
| $\frac{E_{sat}}{P_{sat}}$ | Gash interception model parameter | - | e_r | 0.1 |
| $LAI$ | Leaf area index | - | leaf_area_index | - |
| $S_{leaf}$ | Specific leaf storage | mm | sl | - |
| $S_{canopy,max}$ | Canopy storage capacity | mm | cmax | 1.0 |
| $f_{canopygap}$ | Canopy gap fraction | - | canopygapfraction | 0.1 |
| $S_{wood,max}$ | Storage capacity woody parts of vegetation | mm | swood | - |
| $k$ | Extinction coefficient | - | kext | - |
| $c_{rd}$ | Model parameter controlling the sigmoid function, for the wet roots fraction | - | rootdistpar | -500.0 |
| $z_{cap,maxdepth}$ | Critical water depth which capillary rise ceases | mm | cap_hmax | 2000.0 |
| $m$ | Empirical coefficient controlling capillary rise | - | cap_n | 2.0 |
| $K_{v0}$ | Vertical saturated hydraulic conductivity at the soil surface | mm $t^{-1}$ | $kv_0$ | 3000.0 mm $day^{-1}$ |
| $f_{Kv}$ | Scaling parameter for saturated hydraulic conductivity | $mm^{-1}$ | f | 0.001 |

| Symbol | Description | Unit | Wflow.jl name | Default |
|---|---|---|---|---|
| $c_n$ | Brooks-Corey power coefficient | - | c | 10.0 |
| $h_b$ | Air entry value | cm | hb | 10.0 |
| $L_{max}$ | Maximum allowed leakage | mm t$^{-1}$ | maxleakage | 0.0 mm day$^{-1}$ |
| $f_{Kh0}$ | Multiplication factor applied to $K_{v0}$ (for lateral subsurface flow) | - | - | 1.0 |
| $f_{Kv,n}$ | Multiplication factor (correcting vertical hydraulic conductivity) | - | kvfrac | 1.0 |
| $s_{ddf}$ | Degree-day-melt factor snow | mm °C$^{-1}$ t$^{-1}$ | cfmax | 3.75653 mm °C$^{-1}$ day$^{-1}$ |
| $s_{fall,Tthreshold}$ | Temperature threshold for snowfall | °C | tt | 0.0 |
| $s_{fall,Tinterval}$ | Temperature threshold interval for snowfall | °C | tti | 1.0 |
| $s_{melt,Tthreshold}$ | Temperature threshold for snowmelt | °C | ttm | 0.0 |
| $s_{whc}$ | Water holding capacity of snow | - | whc | 0.1 |
| $w$ | Weighting coefficient | - | w_soil | 0.1125 |
| $f_{red,frozen}$ | Controlling infiltration reduction factor | - | cf_soil | 0.038 |
| $c_{land\ slope}$ | Slope of the land surface | m m$^{-1}$ | $\beta_1$ | - |
| $c_{river\ slope}$ | Slope of river | m m$^{-1}$ | sl | - |
| $\beta$ | Rating curve coefficient | - | b | - |
| $\alpha$ | Rating curve exponent | - | e | - |
| $n_{land}$ | Manning's roughness (overland flow) | $c_{land\ slope}$ m$^{-\frac{1}{3}}$ | | 0.072 |
| $n_{river}$ | Manning's roughness (river flow) | $c_{river\ slope}$ m$^{-\frac{1}{3}}$ | | 0.036 |
| $x_{river}$ | River length | m | dl | - |
| $w_{river}$ | River width | m | width | - |
| $h_{bankfull}$ | River bankfull depth | m | bankfull_depth | 1.0 |

# D
# Paved and Unpaved Areas

## D.1. Adding Paved Areas

The Belgian part of the Geul catchment does not contain paved areas in the original model (Hulsman et al., 2023). These areas are manually added to D-RR to enable the simulation of housing and improve the model performance in Belgium. The villages Gemmenich, Hombourg, Kelmis, Montzen, and Plombieres are added to D-RR. There is no sewerage data available for these villages, so assumptions have to be made.

First, the paved areas of these villages are determined. The areas are estimated, based on the paved areas in the Netherlands in D-RR. The paved area of Kelmis is assumed to be equal to Vaals. It can be seen in Figure D.1 that Kelmis and Vaals are the largest villages in the figure domain. Vaals is a little smaller than Kelmis, but Vaals is more densely build than Kelmis. Based on this, Kelmis has been assigned the same paved area as Vaals, 516680 $m^2$. The paved area of Kelmis is split in kelmis1 and kelmis2 with an equal area of 253840 $m^2$. The other villages, Gemmenich, Hombourg, Montzen, and Plombieres have been assigned the same paved area as Epen of 39900 $m^2$. These villages are in the same order of magnitude, as can be seen in Figure D.1.

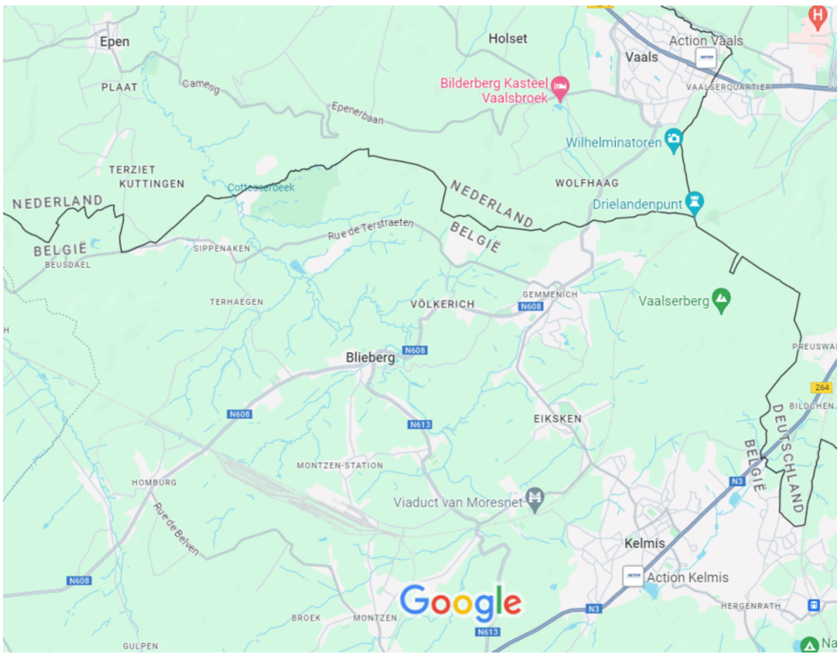


Figure D.1: Overview of the added villages and the compared Dutch villages (Google, 2023). The added villages are Gemmenich, Hombourg (Homburg), Kelmis, Montzen, and Plombieres (Blieberg). The compared Dutch villages are Epen and Vaals.

Next, the sewer systems of the paved areas are determined. In the Netherlands, values are available for the storage in the sewer and the pump-overcapacity in the case of no data. A mixed sewer system contains 7 millimeters storage and has a pump-overcapacity of 0.7 millimeters per hour (Stichting RIONED, 2024). Applying this to kelmis1, leads to the overflow timeseries in Figure D.2a. It can be seen that there is once an overflow event, which is too little compared to other paved areas in D-RR, where there are at least 5-7 overflow events. Finetuning of this sewer system is not possible, as there is no sewerage data. It is assumed to have no sewer system in the added paved areas, to encounter the lack of overflows. In Figure D.2b, the flow to the Geul timeseries is shown in the case without a sewer. Logically, it can be seen that all the water flows directly to the Geul, when there is precipitation. However, this is not realistic, but otherwise the sewer overflows are underestimated. The high amount of overflow events compensates for the not added villages in Belgium, so the high amount of overflow events with no sewer system is valid. Applying these changes are processed in a workflow in Idsinga (2024).

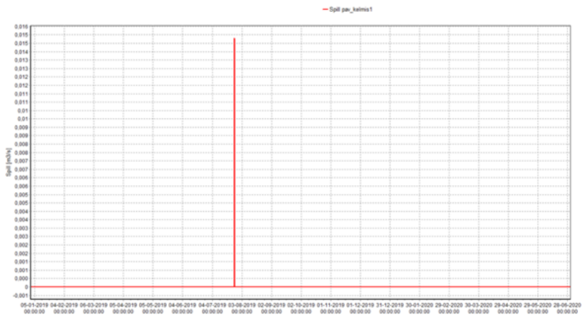

(a) Applying the standard values of a mixed sewer system to kelmis1.

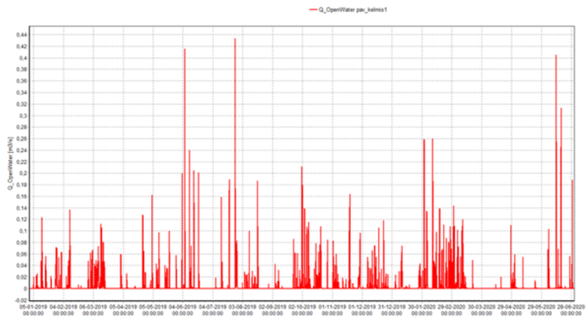

(b) Applying no sewer system to kelmis1.

Figure D.2: The difference between the case with a mixed sewer system (Figure D.2a) and the case without no sewer system (Figure D.2b) for kelmis1, the halve of the paved area of Kelmis.

## D.2. Paved and Unpaved Areas

The determined paved and unpaved areas per subsubcatchment are given in this section. The areas are determined by the Jupyter Notebooks in Idsinga (2024). The subsubcatchments are sorted per subcatchment, which are defined in Section 2.5. A figure with the subsubcatchments and a table with the areas is given per subcatchment.

### D.2.1. Gulp

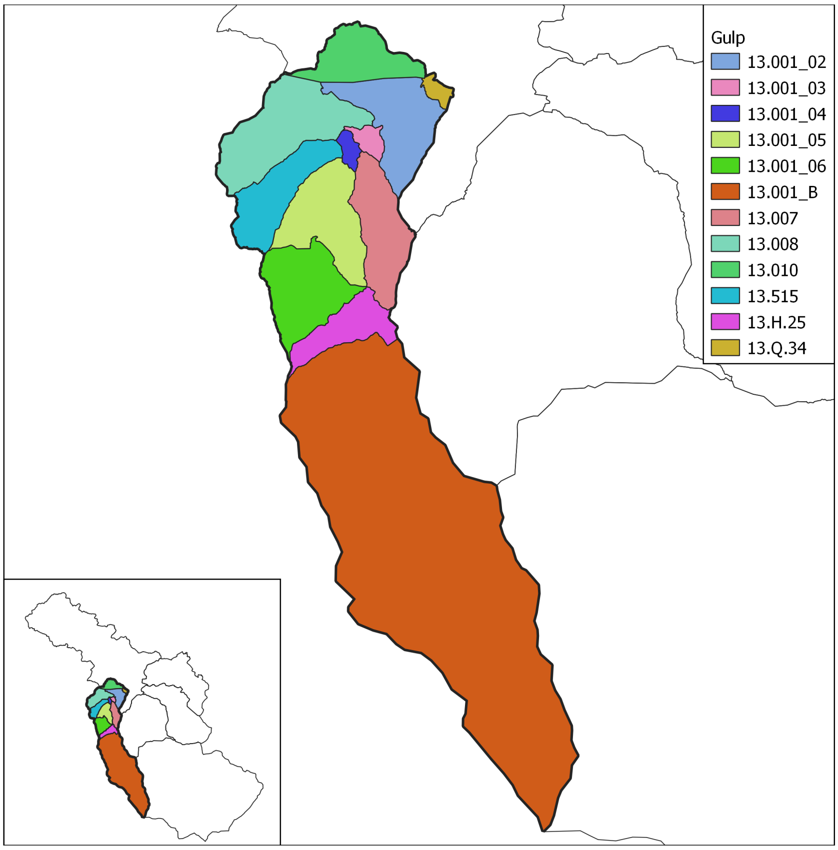


Figure D.3: Overview of the subsubcatchments in the Gulp subcatchment.

| Subsubcatchment | Total Area $m^2$ | Paved Area $m^2$ | Unpaved Area $m^2$ |
|---|---|---|---|
| 13.001_01 | 528134 | 114387 | 413747 |
| 13.001_02 | 2698891 | 37560 | 2661331 |
| 13.001_03 | 334383 | 10298 | 324085 |
| 13.001_04 | 246536 | 2950 | 243586 |
| 13.001_05 | 2731432 | 6033 | 2725399 |
| 13.001_06 | 2644107 | 25565 | 2618542 |
| 13.001_B | 25852012 | 39900 | 25812112 |
| 13.007 | 2327870 | 12636 | 2315235 |
| 13.008 | 3580046 | 61028 | 3519017 |
| 13.010 | 1823680 | 65261 | 1758419 |
| 13.515 | 2098109 | 429 | 2097680 |
| 13.H.25 | 1481408 | 12649 | 1468758 |
| 13.Q.34 | 229363 | 21157 | 208206 |

Table D.1: Areas of the subsubcatchments in the Gulp subcatchment.

### D.2.2. Eyserbeek

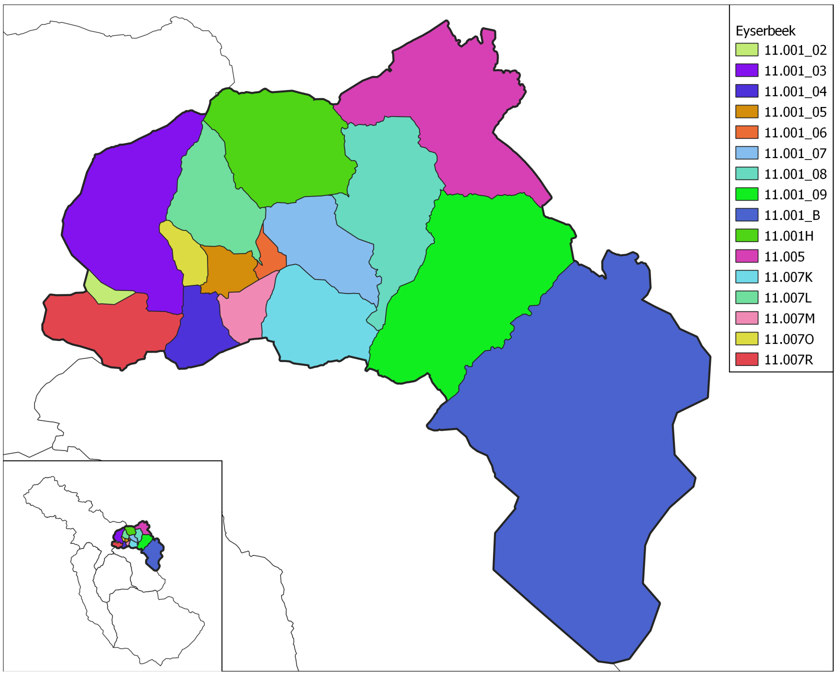


Figure D.4: Overview of the subsubcatchments in the Eyserbeek subcatchment.

| Subsubcatchment | Total Area m$^2$ | Paved Area m$^2$ | Unpaved Area m$^2$ |
|---|---|---|---|
| 11.001_01 | 1092266 | 752 | 1091514 |
| 11.001_02 | 941533 | 9656 | 931877 |
| 11.001_03 | 2252207 | 74391 | 2177816 |
| 11.001_04 | 494868 | 7585 | 487283 |
| 11.001_05 | 299294 | 5411 | 293882 |
| 11.001_06 | 128176 | 3378 | 124799 |
| 11.001_07 | 1019719 | 23626 | 996093 |
| 11.001_08 | 1875953 | 237356 | 1638598 |
| 11.001_09 | 3479255 | 145258 | 3333997 |
| 11.001_B | 9188622 | 193871 | 8994750 |
| 11.001H | 1843039 | 53056 | 1789983 |
| 11.005 | 2636829 | 50293 | 2586536 |
| 11.007K | 1165376 | 10722 | 1154654 |
| 11.007L | 1056024 | 4423 | 1051600 |
| 11.007M | 345314 | 450 | 344864 |
| 11.007O | 249308 | 874 | 248434 |
| 11.007R | 972753 | 7786 | 964967 |

Table D.2: Areas of the subsubcatchments in the Eyserbeek subcatchment.

### D.2.3. Selzerbeek

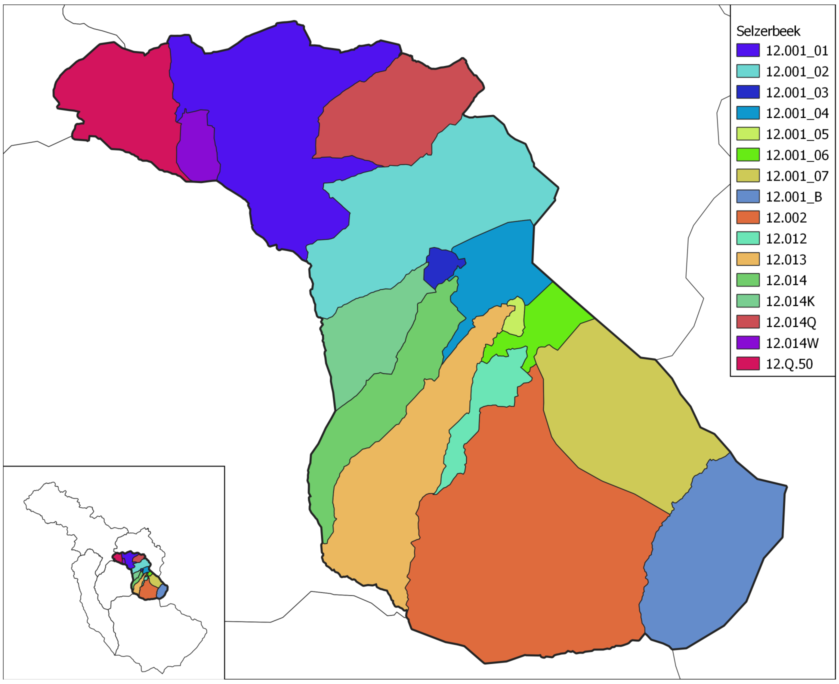


Figure D.5: Overview of the subsubcatchments in the Selzerbeek subcatchment.

| Subsubcatchment | Total Area $m^2$ | Paved Area $m^2$ | Unpaved Area $m^2$ |
|---|---|---|---|
| 12.001_01 | 3703439 | 47835 | 3655604 |
| 12.001_02 | 3265449 | 50679 | 3214770 |
| 12.001_03 | 136206 | 3737 | 132468 |
| 12.001_04 | 907759 | 6475 | 901284 |
| 12.001_05 | 79688 | 2150 | 77538 |
| 12.001_06 | 502509 | 6909 | 495599 |
| 12.001_07 | 2749118 | 338846 | 2410272 |
| 12.001_B | 2362858 | 575002 | 1787856 |
| 12.002 | 6170239 | 169226 | 6001013 |
| 12.012 | 537619 | 14280 | 523339 |
| 12.013 | 2495111 | 4680 | 2490431 |
| 12.014 | 1433483 | 22932 | 1410551 |
| 12.014K | 1034315 | 26495 | 1007821 |
| 12.014Q | 1588035 | 389 | 1587647 |
| 12.014W | 321247 | 379 | 320868 |
| 12.Q.31 | 181919 | 27178 | 154741 |
| 12.Q.50 | 1452260 | 22330 | 1429930 |

Table D.3: Areas of the subsubcatchments in the Selzerbeek subcatchment.

### D.2.4. Sippenaeken

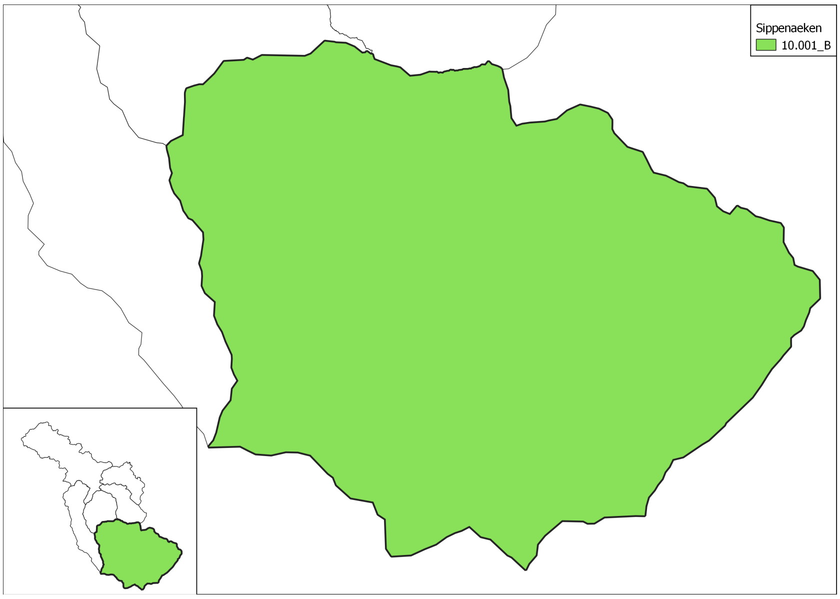


Figure D.6: Overview of the subsubcatchment in the Sippenaeken subcatchment.

| Subsubcatchment | Total Area $m^2$ | Paved Area $m^2$ | Unpaved Area $m^2$ |
|---|---|---|---|
| 10.001_B | 123287219 | 636380 | 122650839 |

Table D.4: Areas of the subsubcatchment in the Sippenaeken subcatchment.

### D.2.5. Hommerich

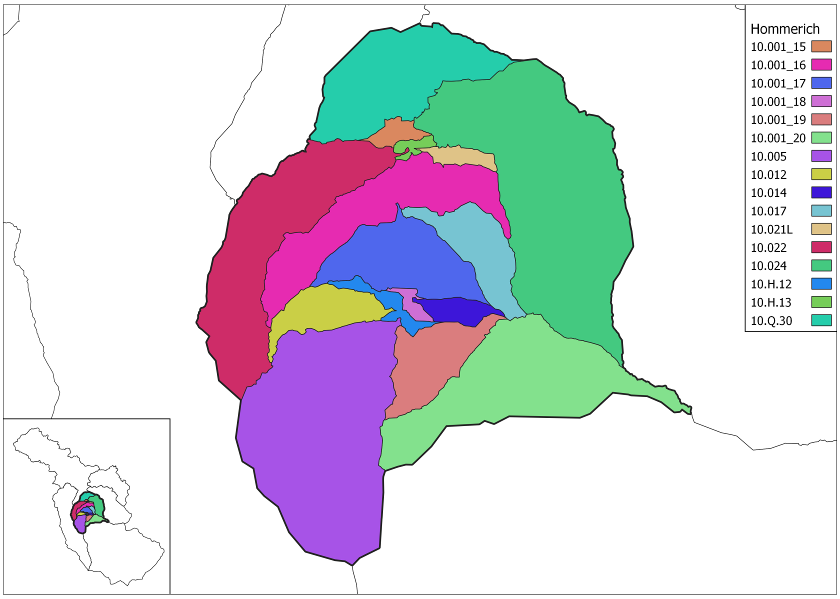


Figure D.7: Overview of the subsubcatchments in the Hommerich subcatchment.

| Subsubcatchment | Total Area $m^2$ | Paved Area $m^2$ | Unpaved Area $m^2$ |
|---|---|---|---|
| 10.001_15 | 212975 | 5938 | 207037 |
| 10.001_16 | 2466547 | 57130 | 2409416 |
| 10.001_17 | 1765008 | 34841 | 1730166 |
| 10.001_18 | 125747 | 1064 | 124683 |
| 10.001_19 | 1181012 | 698 | 1180314 |
| 10.001_20 | 3586159 | 0 | 3586159 |
| 10.005 | 5734466 | 18615 | 5715851 |
| 10.012 | 830549 | 9859 | 820690 |
| 10.014 | 317390 | 0 | 317390 |
| 10.017 | 1099644 | 2291 | 1097352 |
| 10.021L | 224674 | 22236 | 202438 |
| 10.022 | 3634507 | 33421 | 3601086 |
| 10.024 | 6663527 | 138631 | 6524896 |
| 10.H.12 | 278325 | 7145 | 271181 |
| 10.H.13 | 112579 | 3265 | 109314 |
| 10.Q.30 | 2949332 | 17695 | 2931636 |

Table D.5: Areas of the subsubcatchments in the Hommerich subcatchment.

### D.2.6. Meerssen

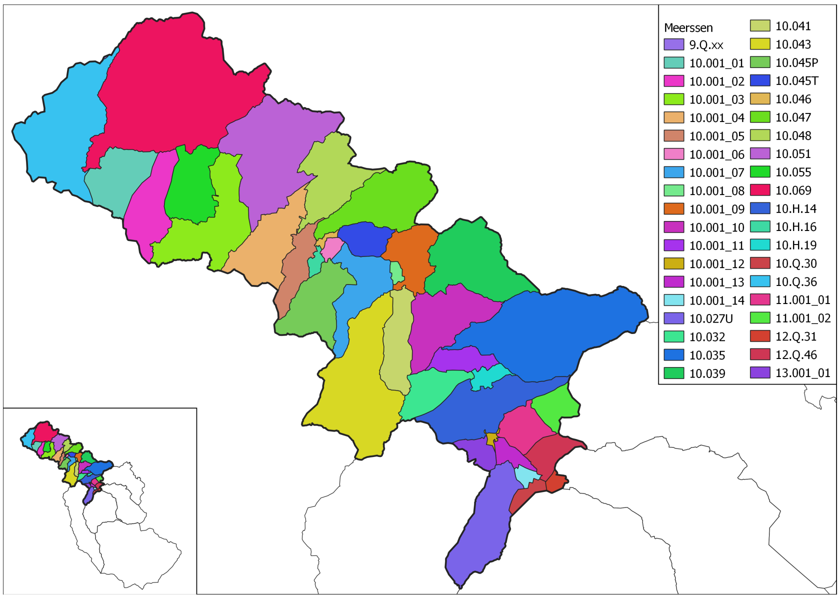


Figure D.8: Overview of the subsubcatchments in the Meerssen subcatchment.

| **Subsubcatchment** | **Total Area m$^2$** | **Paved Area m$^2$** | **Unpaved Area m$^2$** |
|---|---|---|---|
| 9.Q.xx | 6445029 | 538715 | 5906314 |
| 10.001_01 | 2029174 | 198634 | 1830540 |
| 10.001_02 | 2086911 | 47521 | 2039391 |
| 10.001_03 | 3432818 | 265871 | 3166946 |
| 10.001_04 | 2564134 | 416052 | 2148082 |
| 10.001_05 | 1240018 | 187127 | 1052892 |
| 10.001_06 | 231976 | 27989 | 203987 |
| 10.001_07 | 2050989 | 35232 | 2015757 |
| 10.001_08 | 153098 | 0 | 153098 |
| 10.001_09 | 1567204 | 30040 | 1537164 |
| 10.001_10 | 2808159 | 41012 | 2767147 |
| 10.001_11 | 832998 | 48106 | 784892 |
| 10.001_12 | 90111 | 2312 | 87798 |
| 10.001_13 | 438155 | 21548 | 416607 |
| 10.001_14 | 222857 | 220 | 222637 |
| 10.027U | 2857087 | 1338 | 2855748 |
| 10.032 | 1358716 | 11808 | 1346908 |
| 10.035 | 7109878 | 143246 | 6966632 |
| 10.039 | 3551058 | 154775 | 3396283 |
| 10.041 | 1710652 | 83649 | 1627004 |
| 10.043 | 5402804 | 60402 | 5342402 |
| 10.045P | 2241956 | 73488 | 2168468 |
| 10.045T | 915494 | 0 | 915494 |
| 10.046 | 100794 | 27942 | 72852 |
| 10.047 | 3147868 | 68255 | 3079613 |
| 10.048 | 2547051 | 169387 | 2377664 |
| 10.051 | 5461070 | 139495 | 5321575 |
| 10.055 | 2059563 | 155851 | 1903712 |
| 10.069 | 10919046 | 462819 | 10456228 |
| 10.H.14 | 3154815 | 36324 | 3118490 |
| 10.H.16 | 196491 | 56139 | 140352 |
| 10.Q.30 | 2949332 | 17695 | 2931636 |
| 12.Q.46 | 847905 | 4062 | 843844 |
| 10.H.19 | 414997 | 44824 | 370174 |

Table D.6: Areas of the subsubcatchments in the Meerssen subcatchment.

# E

# Data

## E.1. Forcing Analysis

The input data of the HBV and Wflow_sbm should ideally be the same to be able to compare the models. The HBV model requires one data value per time step for an entire catchment, while Wflow_sbm contains spatially distributed data. Representative data values for the HBV model are needed to give reliable model results. Analysis is done to find the most representative forcing source for a subcatchment. These analyses can be reproduced by the Jupyter Notebooks in Idsinga (2024).

### E.1.1. Precipitation

Four different precipitation data sources are compared to the NRR data input of Wflow_sbm. The most representative precipitation data source for the NRR data will be chosen. The data sources are listed below and the locations are shown in Figure E.1. The data sources are compared for two different precipitation events. The different types of events makes it possible to draw a conclusion about the data sources. The compared precipitation data sources are:

- KNMI weather station Maastricht, the Netherlands: measures precipitation hourly and potential evaporation daily (KNMI, 2023a, 2023b);
- NRR data at the discharge measurement locations: data is subtracted from the NRR data at the discharge locations;
- Mean per subcatchment of NRR data: for each subcatchment the mean of the NRR data per time step is calculated.
- SPW precipitation station Gemmenich, Belgium: contains hourly measured precipitation data (L'hydrométrie en Wallonie, 2023);

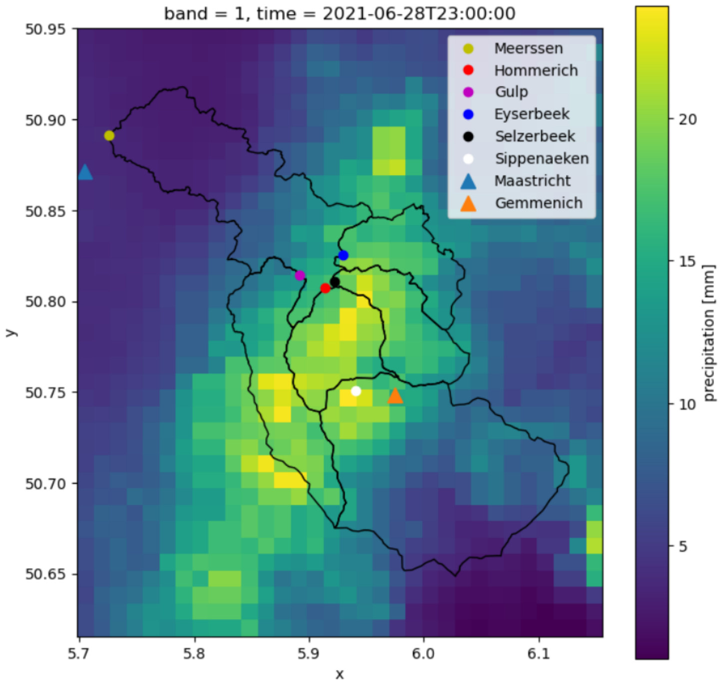


Figure E.1: Map of the locations of the data sources with the NRR data as background on 23:00 at 28.06.2021. The subcatchments are drawn in black.

The precipitation event in Figure E.2a occurs locally in the North-West of the Geul catchment. Also, a diagonal strip of precipitation is visible in the middle of the catchment. The precipitation event in Figure E.2b has a different shape. In this figure, a wide vertical strip of precipitation passes the Geul catchment. Based on the shapes of the precipitation events, point values will not give representative values. For example the subcatchment Meerssen in the North-West of the Geul catchment. In Figure E.2a, a high value at the Maastricht weather station and at the Meerssen discharge station, does not mean that there is a high amount of precipitation in the east part of the subcatchment. So, the spatial variability can not be covered with a point value.

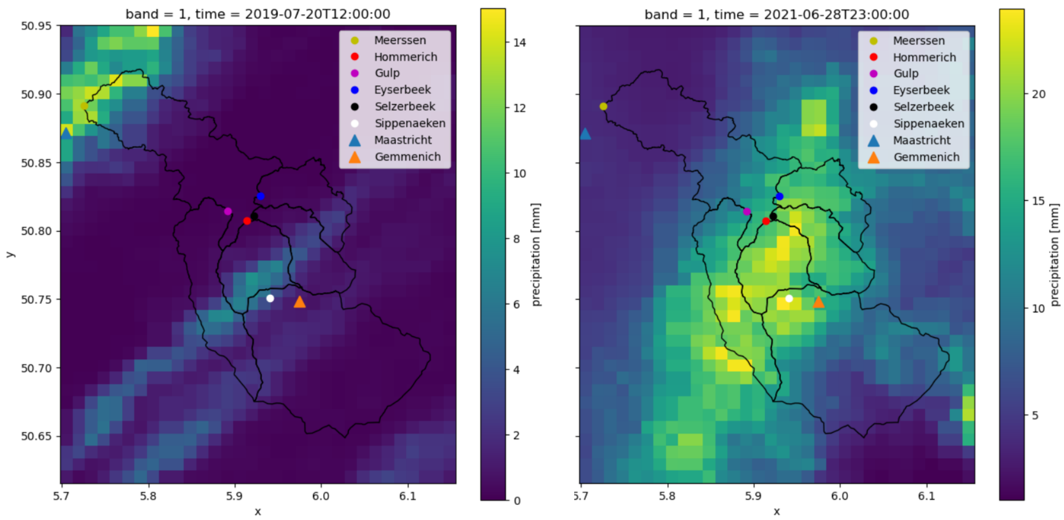


(a) Precipitation event on 12:00 20.07.2019.

(b) Precipitation event on 23:00 28.06.2021.

Figure E.2: Reviewed precipitation events for the HBV input analysis.

To account for spatial variability, the mean NRR data per subcatchment will be used. In this case, local precipitation is averaged out over the subcatchment. An advantage is that local precipitation will not lead to an overestimation of the total precipitation within the catchment. A disadvantage is that precipitation peaks in the HBV model are lower than reality, because of the averaging. To tackle this, the mean of each subsubcatchment is used for the HBV model runs, because this allows to have some spatial variability in the model.

### E.1.2. Potential Evaporation

The ERA5 land potential evaporation is compared to the KNMI weather station in Maastricht in Figure E.3. It can be seen that there is a difference of a factor of two between the two data sources. The ERA5 land potential evaporation is based on open water evaporation (Muñoz Sabater, 2019). According to KNMI (n.d.), no more than 7 millimetres can evaporate on a hot summer day. The figure shows that the ERA5 land data exceeds this physical limit in the Meerssen subcatchment. Because of this, in this research the potential evaporation of the KNMI Maastricht weather station is used.

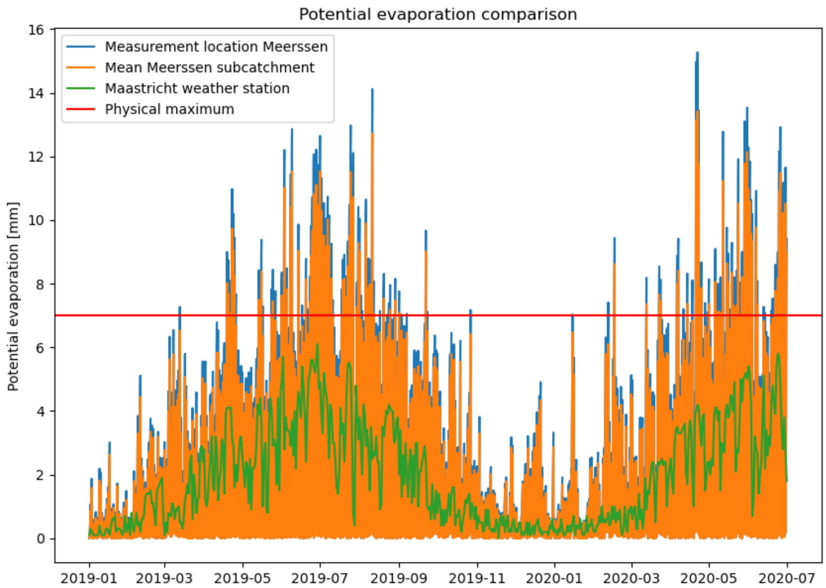


Figure E.3: Comparison of the ERA5 and the KNMI Maastricht weather station evaporation for the Meerssen subcatchment with the physical maximum of 7 mm/day.

## E.2. Forcing Preprocessing

The original forcing data cannot directly be used and preprocessing is required. Preprocessing of HBV + D-RR forcing is described in Appendix E.2.1. The forcing preprocessing for Wflow_sbm is described in Appendix E.2.2. The corresponding Jupyter Notebooks can be found in Idsinga (2024).

### E.2.1. HBV + D-RR

The forcing of HBV and D-RR consists of precipitation and potential evaporation. Both types of forcing are described by an array of values per catchment. In the case of HBV subsubcatchments and of D-RR subcatchments. The precipitation forcing is the NRR data averaged per (sub)subcatchment as visualized in Figure E.4.

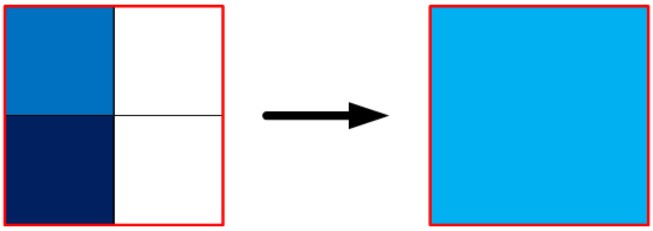

Figure E.4: The HBV and D-RR precipitation value in a (sub)subcatchment is estimated as the average of the radar data in that area.

The potential evaporation consists of the potential evaporation at the KNMI Maastricht weather station, which is the same for each (sub)subcatchment. The potential evaporation is given per 0.1 millimeter and is converted to per 1 millimeter. The timezone is also changed. The data is given in UTC +1 and is converted to UTC +0, to be consistent with the other data sources. Lastly, the potential evaporation data is converted from daily to hourly values, where it is equally spread over 24 hours.

### E.2.2. Wflow_sbm

The forcing of Wflow_sbm consists of potential evaporation, precipitation, and temperature. First, the potential evaporation of the KNMI Maastricht weather station is adjusted like in Appendix E.2.1. Next the potential evaporation values are translated to rasterdata. This means that each raster cell has the same potential evaporation value at a time step. The preprocessing of the NRR precipitation requires two steps for Wflow_sbm. In the first step, the data is translated from mm/5min to mm/h. Next, the coordinates of each forcing source are reprojected to the coordinates of Wflow_sbm. This is visualized in Figure E.5a. The ERA5-Land temperature data is given in Kelvin and is converted to degrees Celsius. Next, the coordinates are translated to the Wflow_sbm coordinates. The final step is combining the KNMI Maastricht potential evaporation, NRR precipitation, and ERA5-Land temperature datasets into one dataset. This is visualized in Figure E.5b.

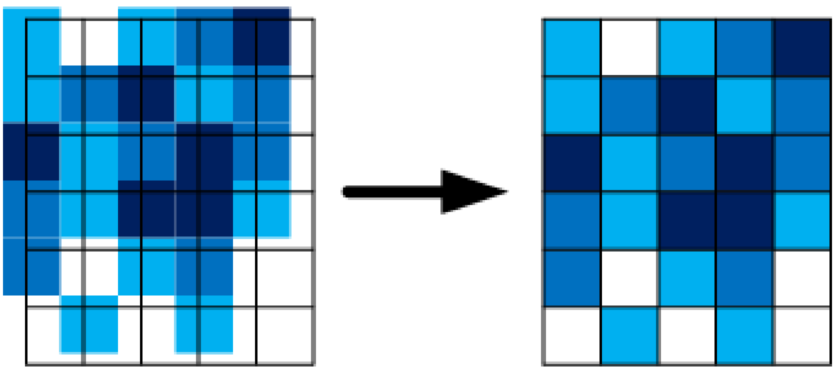

(a) Example of reprojecting the precipitation data to the Wflow_sbm coordinates.

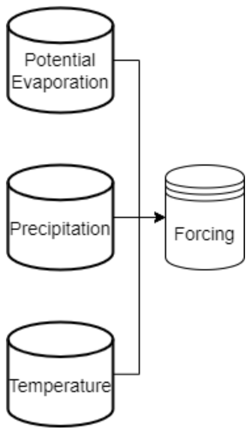


(b) Create one dataset.

Figure E.5

## E.3. Discharge Data

Overview of the used discharge measurement locations and their corresponding information. HBV is calibrated on the stations Sippenaeken, Hommerich, Meerssen, Eyserbeek, Selzerbeek, and Gulp. The other measurement stations are reviewed in the D-HYDRO model.

| **Station Name** | **Station ID** | **Frequency** | **Type** | **Data Start** | **Measurement Range** |
|---|---|---|---|---|---|
| Sippenaeken | L6660 | Hourly | Q-H Relationship | 13.06.1996 | 0.165 - 25 $m^3/s$ with 10% uncertainty |
| Cottessen | 10.Q.29 | 15 Minutes | Measurement Weir | 01.08.1991 | 0.5 - 20 $m^3/s$ with 5 - 15% uncertainty; 20 - 25 $m^3/s$ with 15 - 20% uncertainty |
| Hommerich | 10.Q.30 | 15 Minutes | Q-H Relationship | 01.01.1970 | 1 - 60 $m^3/s$ with 10 - 30% uncertainty |
| Meerssen | 10.Q.36 | 15 Minutes | ADCP | 03.09.1969 | 1 - 55 $m^3/s$ with 5 - 25% uncertainty |
| Schin op Geul | 10.Q.63 | 15 Minutes | ADCP | 17.02.2016 | - |
| Eyserbeek | 11.Q.32 | 15 Minutes | Measurement Weir | 01.07.1991 | 0.01 - 0.08 $m^3/s$ with 10 - 25% uncertainty; 0.08 - 7.75 $m^3/s$ with 5 - 15% uncertainty |
| Selzerbeek | 12.Q.31 | 15 Minutes | Measurement Weir | 31.07.1991 | 0 - 6.5 $m^3/s$ with 10 - 20% uncertainty |
| Gulp | 13.Q.34 | 15 Minutes | Q-H Relationship | 15.04.1972 | 0.2 - 12 $m^3/s$ with 15 - 25% uncertainty |

Table E.1: Overview of the used discharge stations in the Geul catchment in this research (Klein, 2022)

# F Calibration

The HBV calibration consists of three runs. The HBV output is compared to the measured discharge. An overview of the observations is given in Appendix F.1. The parameter intervals in the first run in Appendix F.2 are not adjusted. The second and last runs contain parameter constraints, based on literature and observations in Appendix F.3. The parameter intervals are optimized by the Nash Sutcliff Efficiency (NSE) objective function in Appendix F.4. Lastly, the calibration and validations of HBV and D-RR and wflow_sbm are compared in D-HYDRO in Chapter 4 and Appendix G.

## F.1. Observed Discharge

The discharge observations of the 8 used measurement locations are presented in this section. The location in Kelmis is excluded, as it is not well represented in the Geul D-HYDRO model. The measurement location Selzerbeek; Molentak is excluded. This research did not go into detail of the real time control structures. Figure F.1 presents the observations during the calibration period. The observations during the validation period are presented in Figure F.2. Lastly, Figure F.3 presents the observations of the July 2021 event. As can be seen, multiple measurement locations failed during the event.

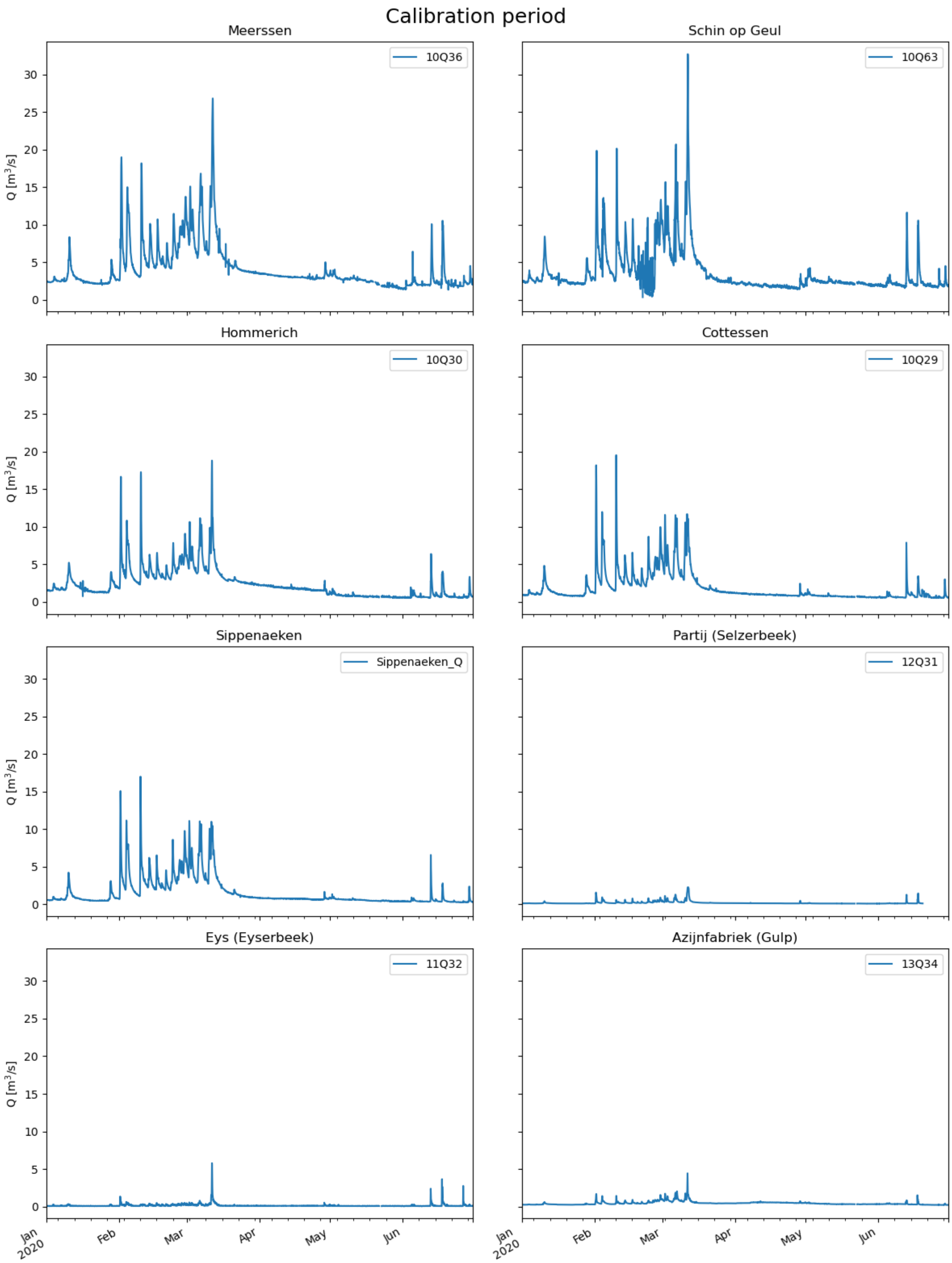


Figure F.1: Discharge observations during the calibration period.

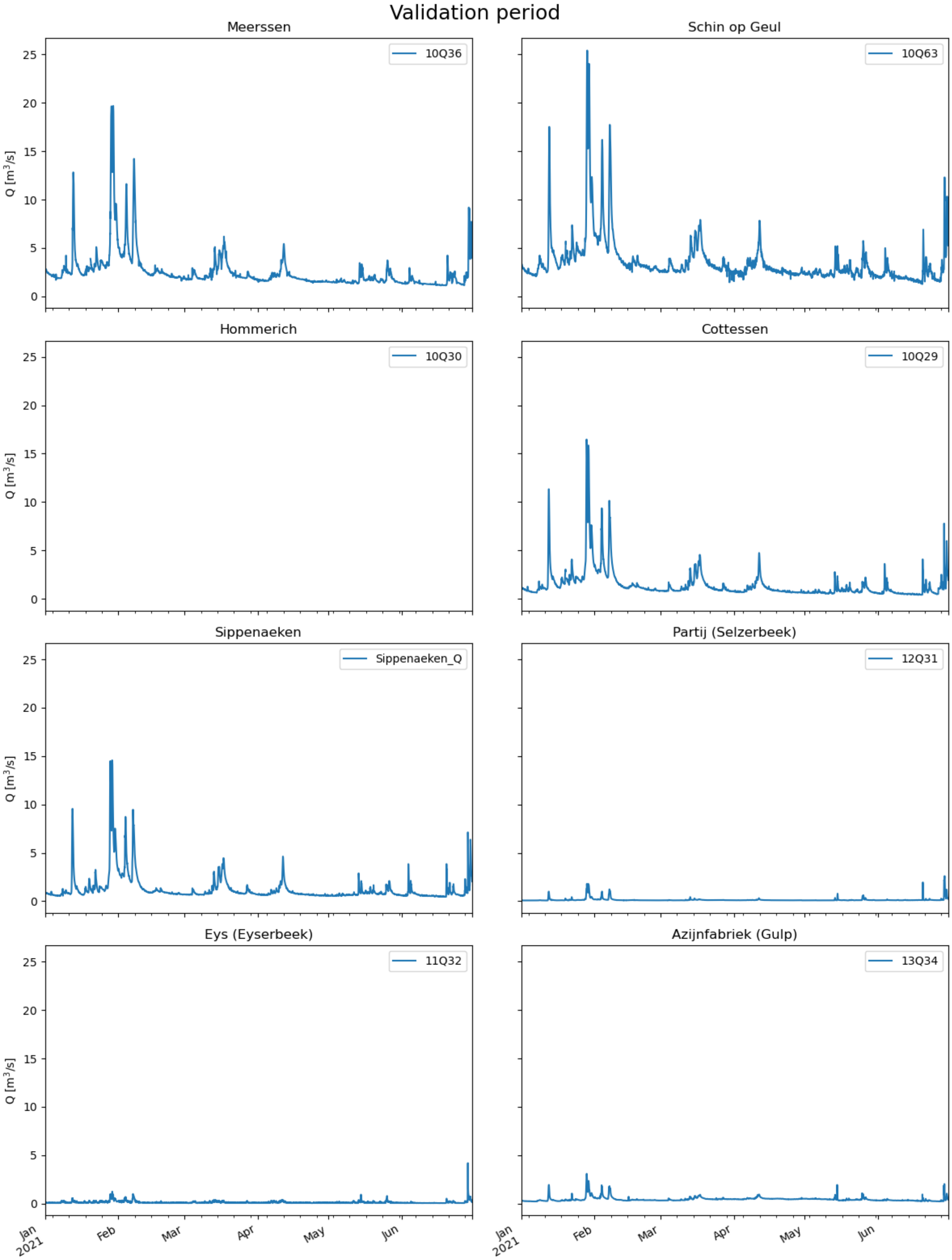


Figure F.2: Discharge observations during the validation period.

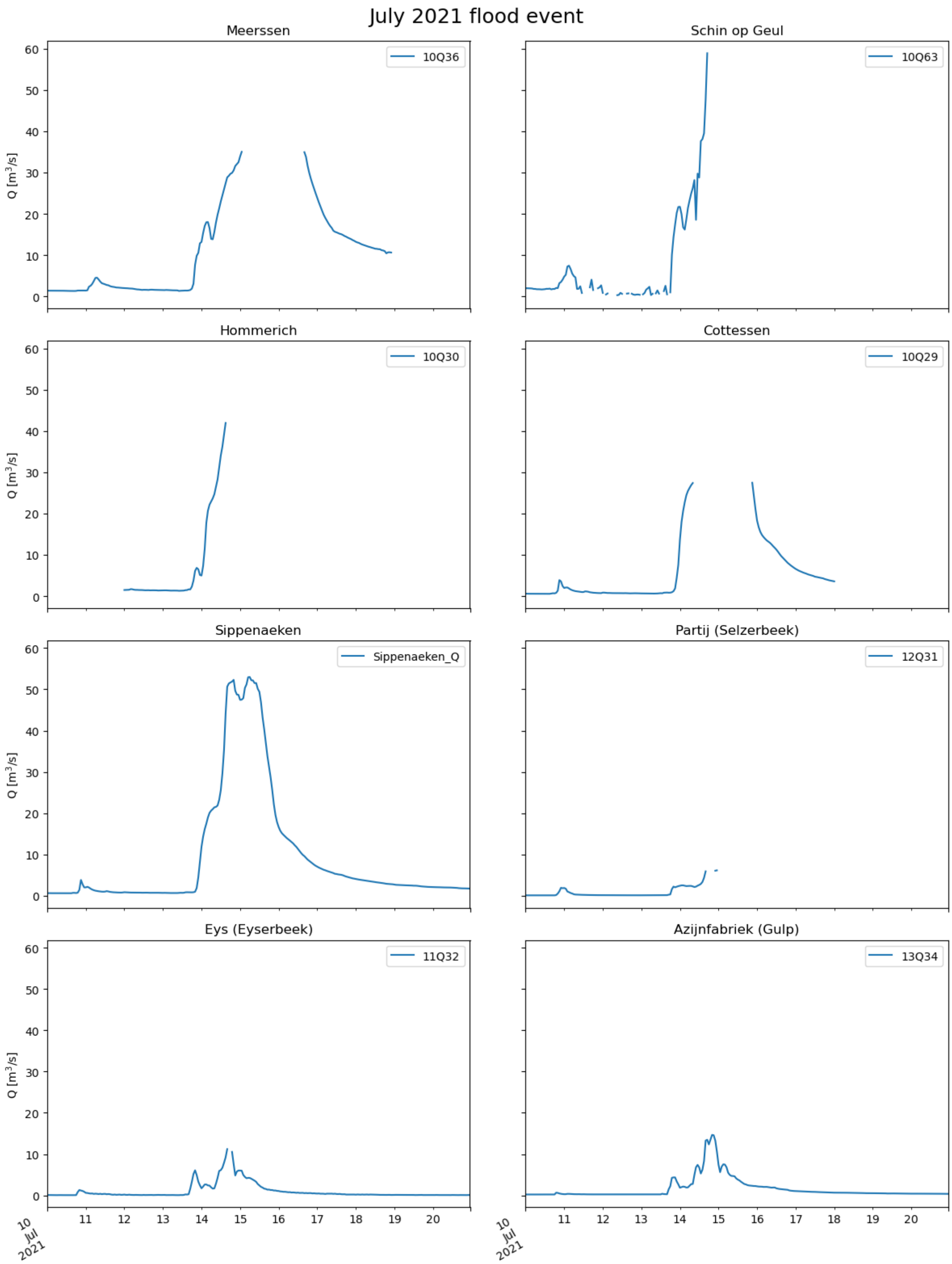


Figure F.3: Discharge observations during the July 2021 flood event.

## F.2. Run 1: First Estimate

The first run contains widely chosen parameter intervals. The intervals are based on Hrachowitz (2021) and Thewissen (2022). The chosen parameter intervals are shown in Appendix F.2.

| | $I_{max}$ | $C_e$ | $S_{u,max}$ | $\beta$ | $P_{max}$ | $T_{lag}$ | $K_f$ | $K_s$ |
|---|---|---|---|---|---|---|---|---|
| **Min** | 0 | 0.2 | 40 | 0.5 | 0.001 | 0 | 0.01 | 0.0001 |
| **Max** | 10 | 1.0 | 800 | 5.0 | 0.30 | 10 | 0.10 | 0.05 |

Table F.1: Parameter intervals for the first HBV calibration run.

The first estimate caused low NSE values for the subcatchments Eyserbeek and Selzerbeek, compared to the other subcatchments, as can be seen for NSEcal 1a in Table F.2. The inflow in these subcatchments are largely urban-driven and depends on the D-RR output. The D-RR output is added to the lag function of HBV to improve the modelled discharge. The changes by adding the D-RR output to the HBV lag function, 1b, are given in Table F.2. This results in a large increase of the NSE calibration value for the Selzerbeek, however the NSE calibration value for the Eyserbeek changes slightly. But for the validation periods, the NSE validation value descreases much. The NSE calibration value of the other subcatchments do not change much and the NSE validation value for Gulp and Sippenaeken increase. There is no measured data for Hommerich in the validation period and the NSE can not be calculated. The observed discharge of Hommerich is added to the output of Meerssen, as Hommerich is upstream of Meerssen, so the validation NSE of Hommerich can not be calculated.

| | NSEcal 1a | NSEcal 1b | NSEval 1a | NSEval 1b |
|---|---|---|---|---|
| **Gulp** | 0.735 | 0.736 | 0.306 | 0.418 |
| **Eyserbeek** | 0.567 | 0.575 | 0.347 | 0.340 |
| **Selzerbeek** | 0.598 | 0.804 | 0.327 | 0.113 |
| **Sippenaeken** | 0.865 | 0.870 | 0.583 | 0.620 |
| **Hommerich** | 0.845 | 0.844 | - | - |
| **Meerssen** | 0.771 | 0.774 | - | - |

Table F.2: The differences in the NSE values between adding the D-RR output directly to the HBV output (1a) and adding the D-RR output to the HBV lag function (1b).

The best parameterset, the calibration period, parameters plot, and validation period per subcatchment are given in the next subsections.

### F.2.1. Gulp

| $I_{max}$ | $C_e$ | $S_{u,max}$ | $\beta$ | $P_{max}$ | $T_{lag}$ | $K_f$ | $K_s$ |
|---|---|---|---|---|---|---|---|
| 6.89 | 0.666 | 747.3 | 3.19 | 0.0584 | 7.22 | 0.0598 | 0.00693 |

Table F.3: Best parameterset for the Gulp subcatchment for run 1.

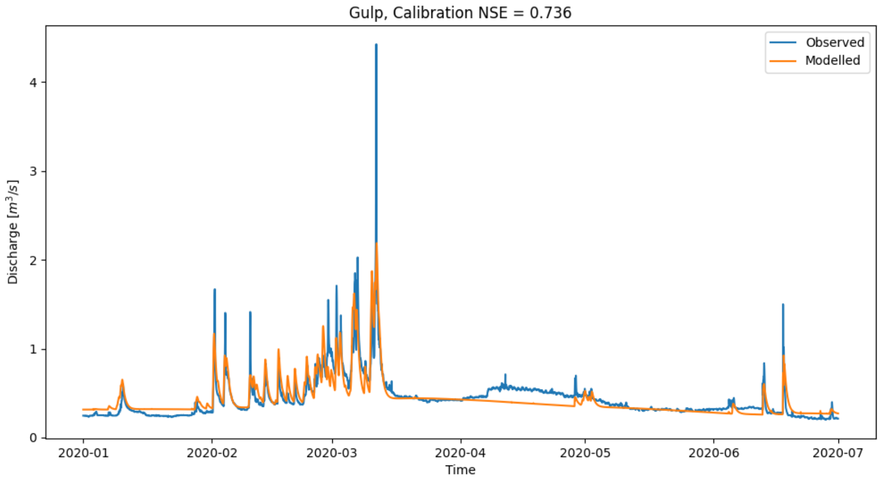


Figure F.4: Modelled discharge in the calibration period for the Gulp subcatchment for run 1.

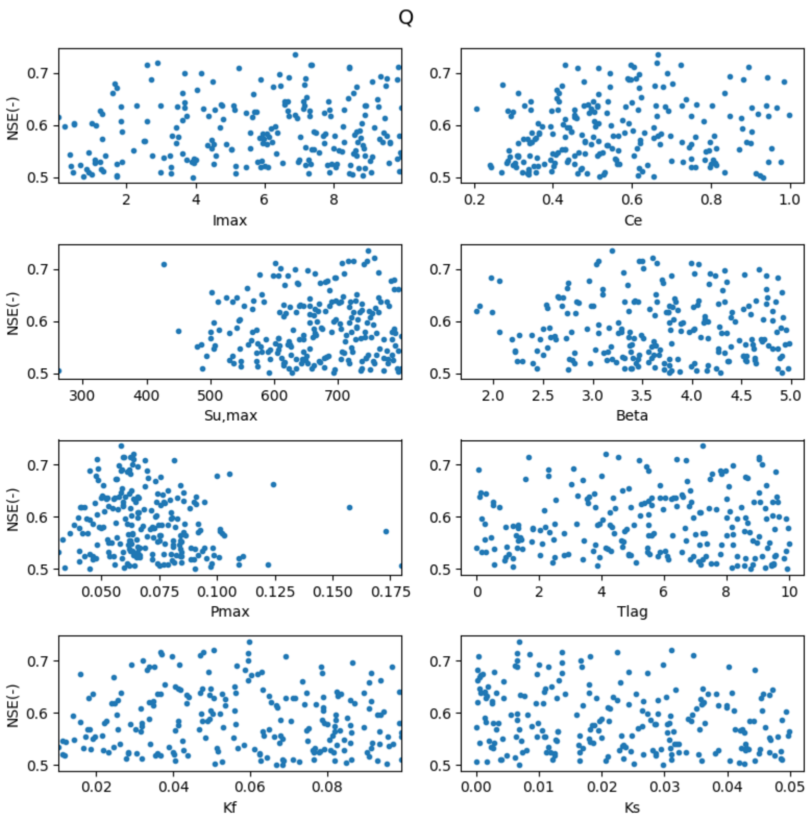


Figure F.5: Dotty plots for the Gulp subcatchment for run 1.

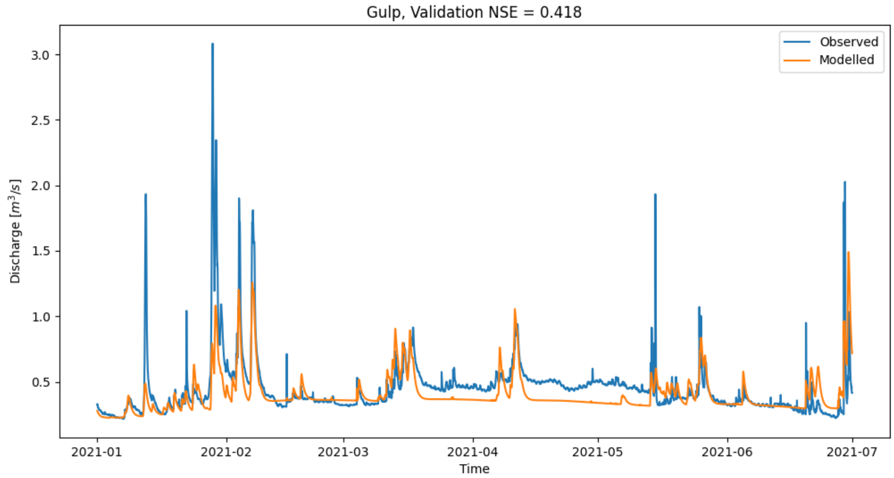


Figure F.6: Modelled discharge in the validation period for the Gulp subcatchment for run 1.

### F.2.2. Eyserbeek

| $I_{max}$ | $C_e$ | $S_{u,max}$ | $\beta$ | $P_{max}$ | $T_{lag}$ | $K_f$ | $K_s$ |
|---|---|---|---|---|---|---|---|
| 5.35 | 0.493 | 690.4 | 4.98 | 0.0195 | 5.47 | 0.0593 | 0.0135 |

Table F.4: Best parameterset for the Eyserbeek subcatchment for run 1.

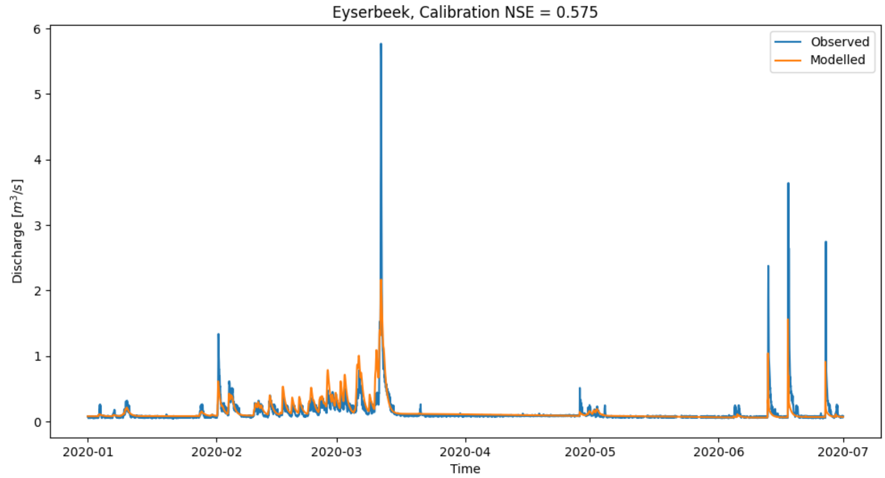


Figure F.7: Modelled discharge in the calibration period for the Eyserbeek subcatchment for run 1.

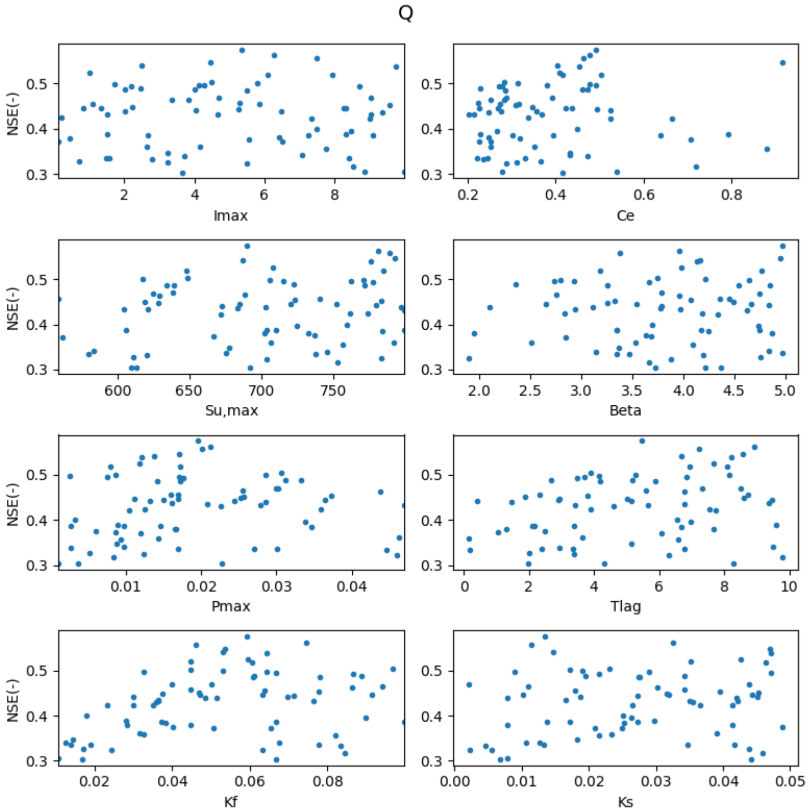


Figure F.8: Dotty plots for the Eyserbeek subcatchment for run 1.

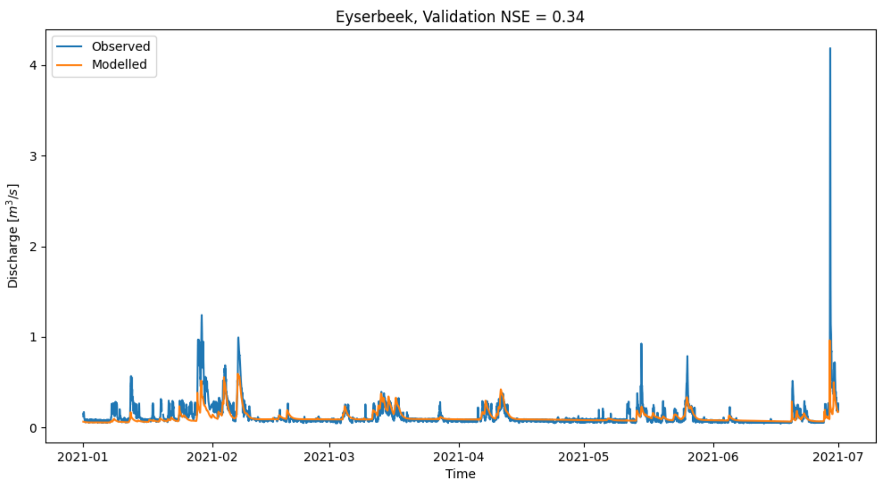


Figure F.9: Modelled discharge in the validation period for the Eyserbeek subcatchment for run 1.

### F.2.3. Selzerbeek

| $I_{max}$ | $C_e$ | $S_{u,max}$ | $\beta$ | $P_{max}$ | $T_{lag}$ | $K_f$ | $K_s$ |
|---|---|---|---|---|---|---|---|
| 8.58 | 0.310 | 581.3 | 4.90 | 0.0431 | 9.16 | 0.0814 | 0.0481 |

Table F.5: Best parameterset for the Selzerbeek subcatchment for run 1.

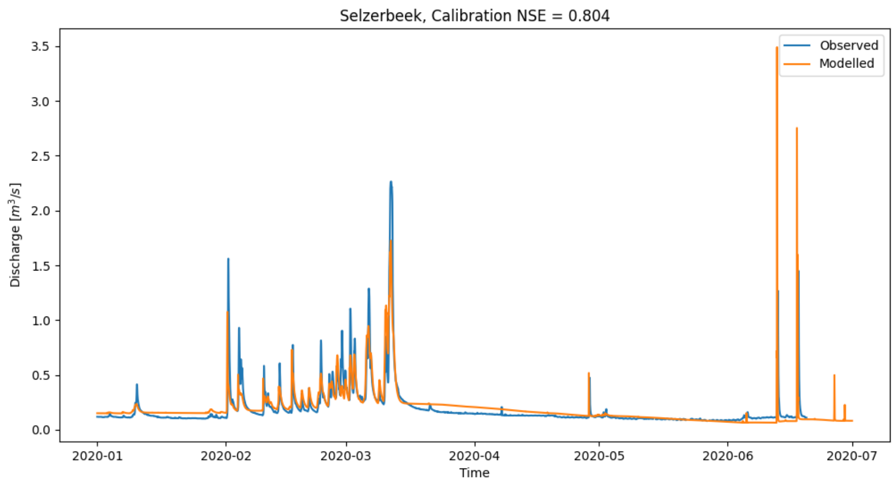


Figure F.10: Modelled discharge in the calibration period for the Selzerbeek subcatchment for run 1.

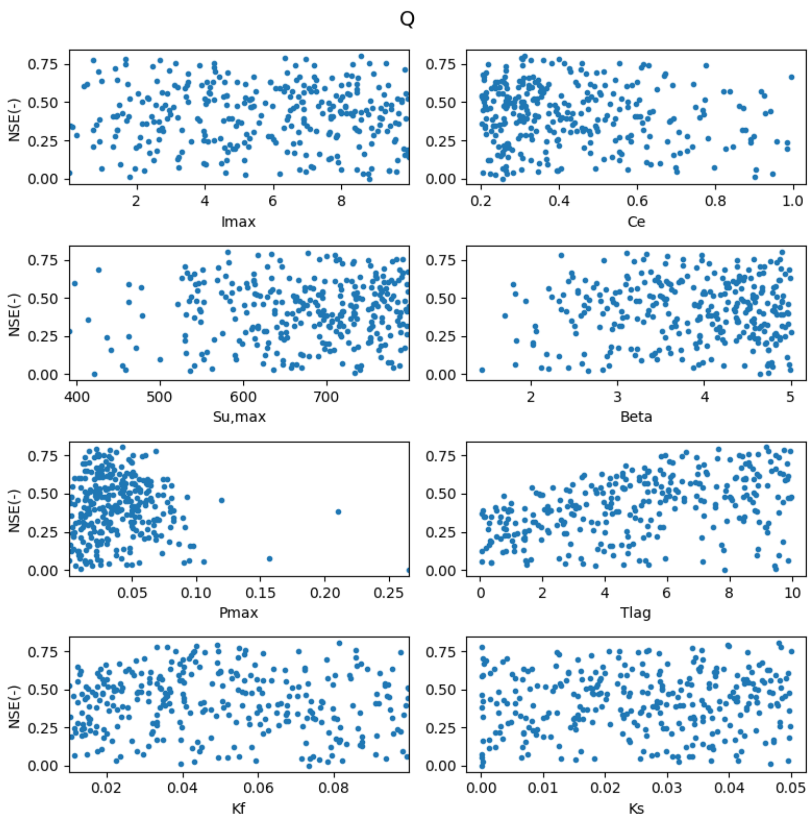


Figure F.11: Dotty plots for the Selzerbeek subcatchment for run 1.

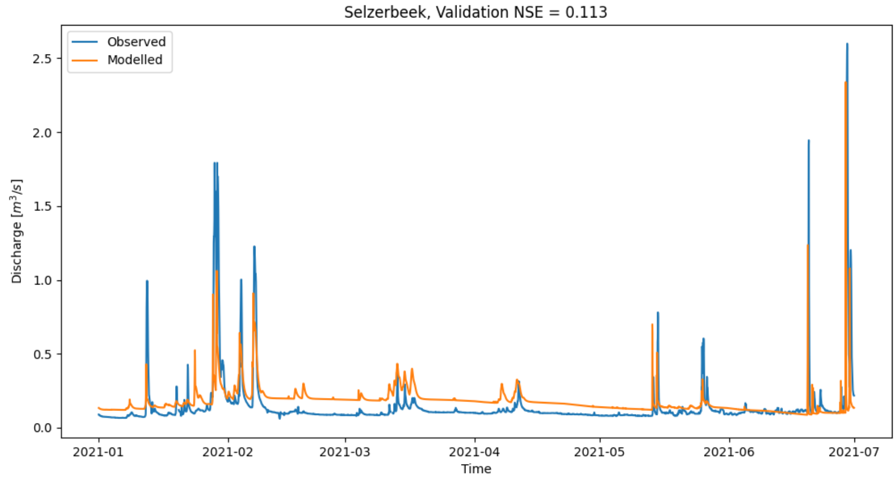


Figure F.12: Modelled discharge in the validation period for the Selzerbeek subcatchment for run 1.

### F.2.4. Sippenaeken

| $I_{max}$ | $C_e$ | $S_{u,max}$ | $\beta$ | $P_{max}$ | $T_{lag}$ | $K_f$ | $K_s$ |
|---|---|---|---|---|---|---|---|
| 0.207 | 0.599 | 299.5 | 3.89 | 0.0196 | 6.45 | 0.0288 | 0.00343 |

Table F.6: Best parameterset for the Sippenaeken subcatchment for run 1.

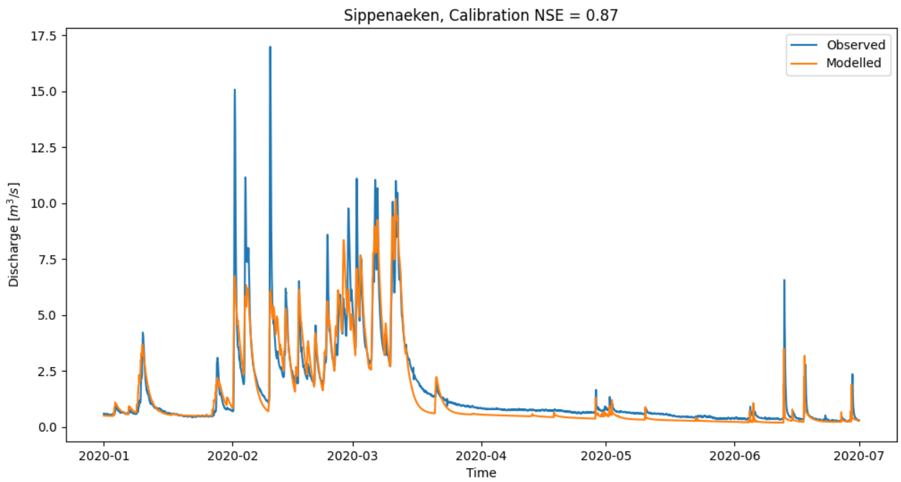


Figure F.13: Modelled discharge in the calibration period for the Sippenaeken subcatchment for run 1.

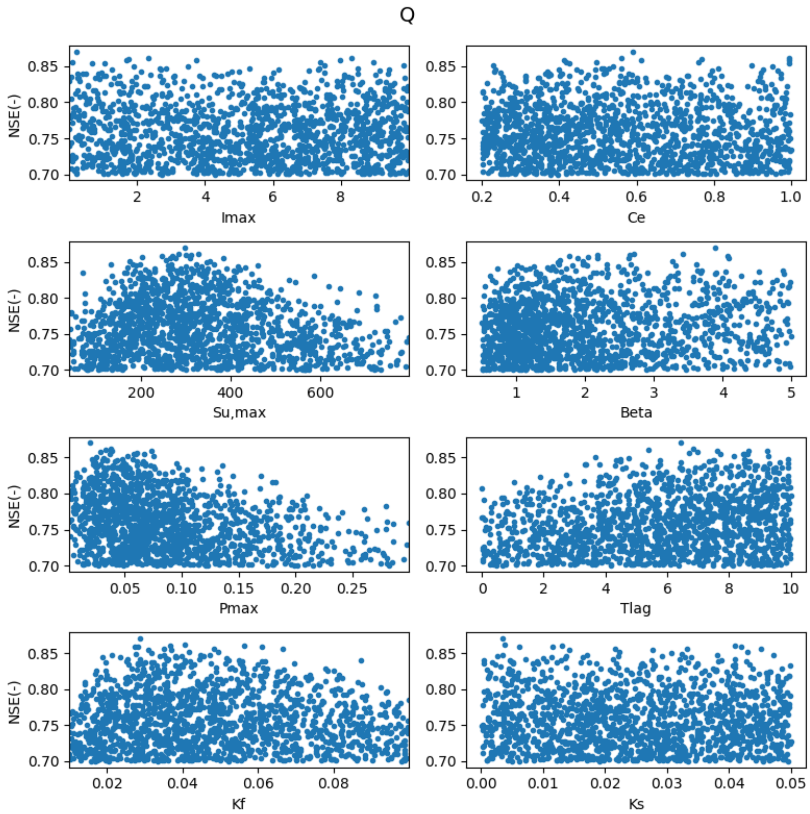


Figure F.14: Dotty plots for the Sippenaeken subcatchment for run 1.

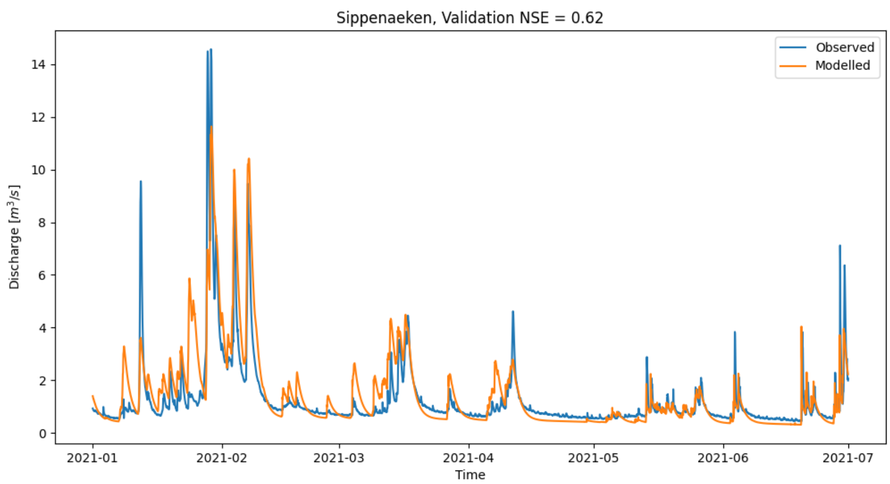


Figure F.15: Modelled discharge in the validation period for the Sippenaeken subcatchment for run 1.

### F.2.5. Hommerich

| $I_{max}$ | $C_e$ | $S_{u,max}$ | $\beta$ | $P_{max}$ | $T_{lag}$ | $K_f$ | $K_s$ |
|---|---|---|---|---|---|---|---|
| 2.85 | 0.605 | 170.0 | 4.59 | 0.277 | 2.97 | 0.0858 | 0.00121 |

Table F.7: Best parameterset for the Hommerich subcatchment for run 1.

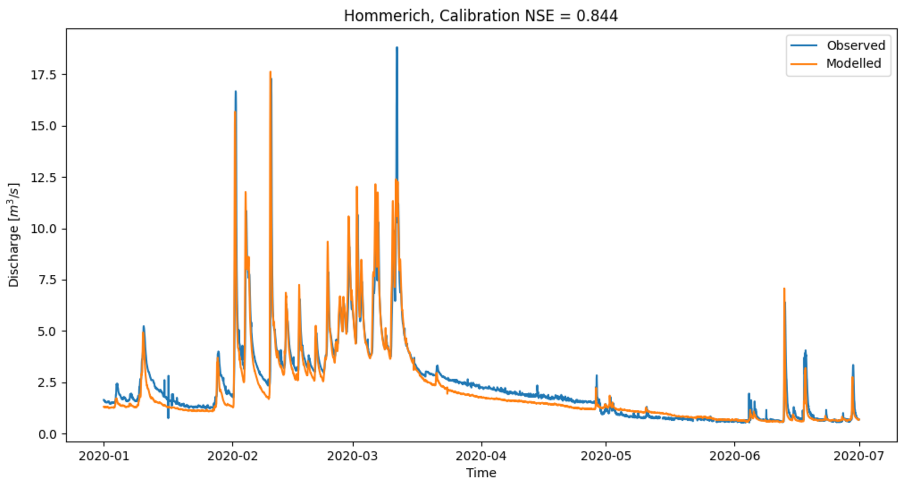


Figure F.16: Modelled discharge in the calibration period for the Hommerich subcatchment for run 1.

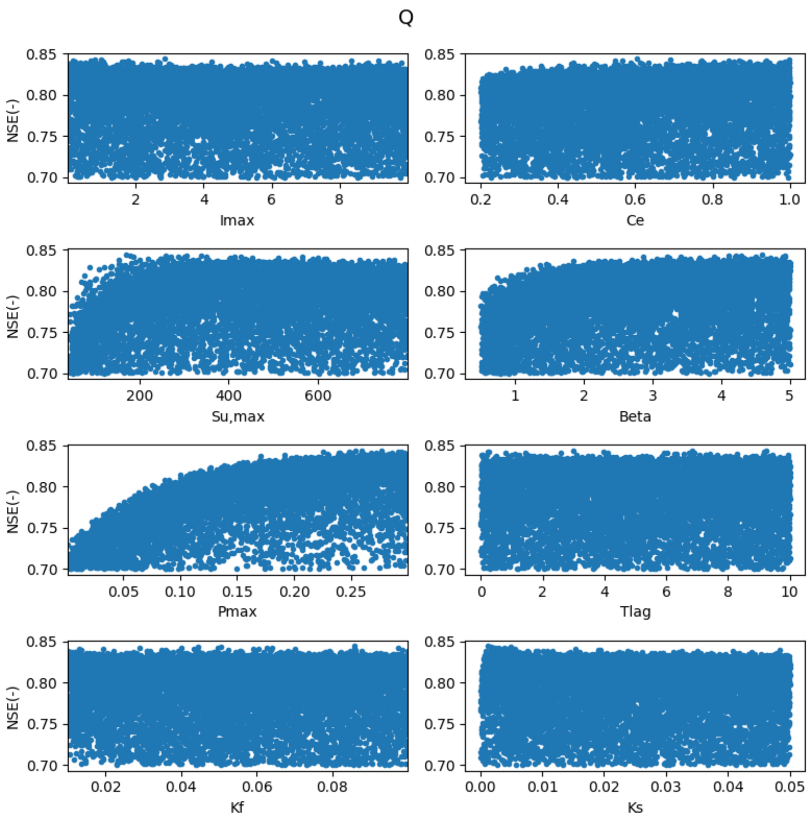


Figure F.17: Dotty plots for the Hommerich subcatchment for run 1.

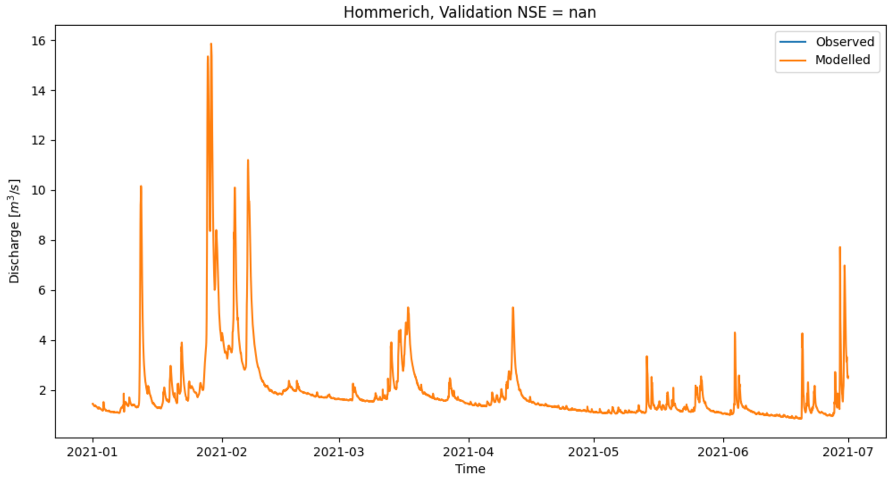


Figure F.18: Modelled discharge in the validation period for the Hommerich subcatchment for run 1.

### F.2.6. Meerssen

| $I_{max}$ | $C_e$ | $S_{u,max}$ | $\beta$ | $P_{max}$ | $T_{lag}$ | $K_f$ | $K_s$ |
|---|---|---|---|---|---|---|---|
| 7.84 | 0.967 | 537.4 | 3.43 | 0.0504 | 9.98 | 0.0132 | 0.00642 |

Table F.8: Best parameterset for the Meerssen subcatchment for run 1.

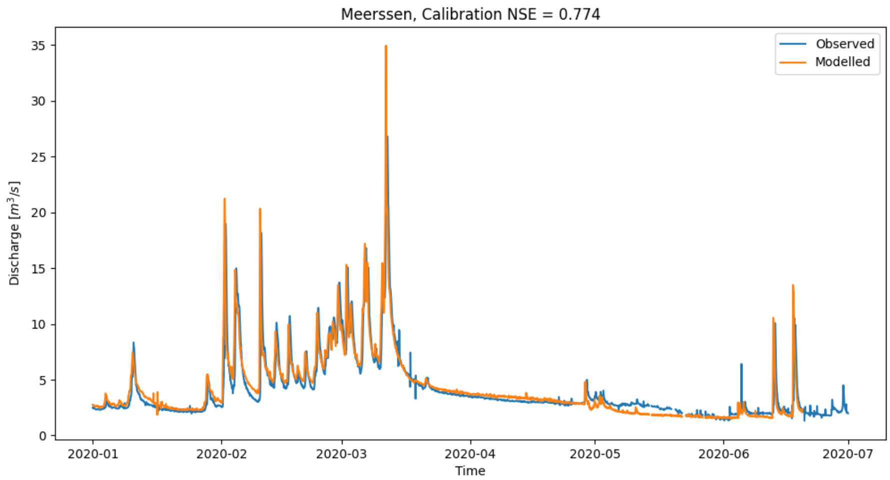


Figure F.19: Modelled discharge in the calibration period for the Meerssen subcatchment for run 1.

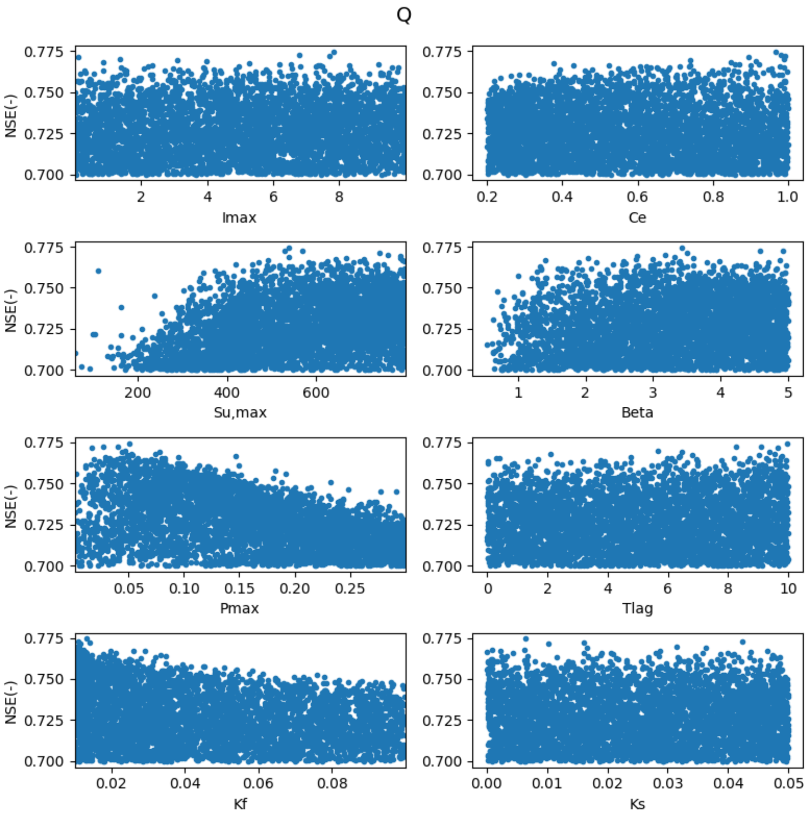


Figure F.20: Dotty plots for the Meerssen subcatchment for run 1.

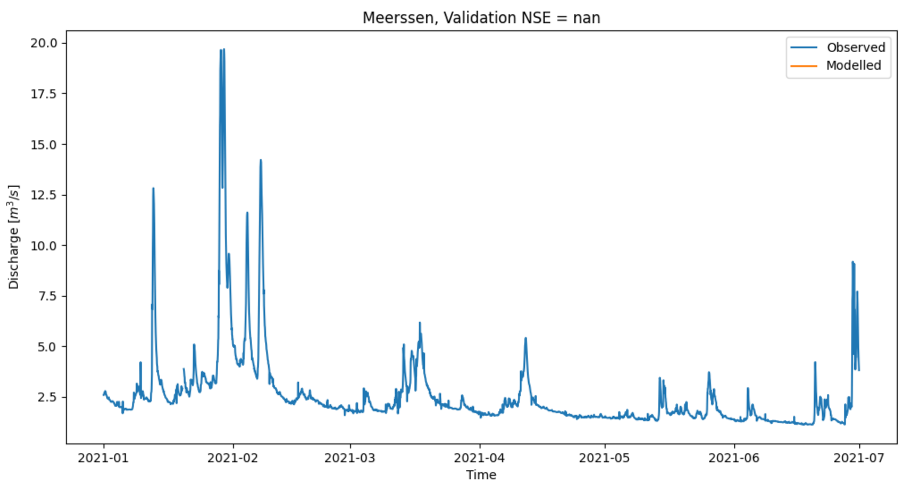


Figure F.21: Modelled discharge in the validation period for the Meerssen subcatchment for run 1.

## F.3. Parameter Intervals

The parameter intervals are based on definitions, literature, or observations. The parameters $I_{max}$, $S_{u,max}$, $T_{lag}$, and $K_s$ are constraint by literature and observations. The derivation of these parameter intervals is given in the next subsections.

### F.3.1. $I_{max}$

The interception is limited by the maximum storage in the interception reservoir. This maximum depends on the landcover in the subcatchment (Gharari, Hrachowitz, Fenicia, Gao, & Savenije, 2014). A forest will have more interception than cropland and grassland (Breuer, Eckhardt, & Frede, 2003). The parameter $I_{max}$ is derived by the equation in Equation (F.1) (Gharari et al., 2014). The value is estimated by the percentage of the landcover class and their maximum interception capacity. The percentage forest is defined as $\alpha$ and the percentage cropland and grassland is defined as $\beta$.

$$I_{max} = \alpha I_{forest} + \beta I_{crop,grass} \tag{F.1}$$

A forest has an interception storage of 2-5 millimeter and cropland and grassland have a storage of 1-3 millimeter (Breuer et al., 2003). The percentages forest and cropland and grassland per subcatchment are derived in Section 2.4. This results in the parameter intervals for the $I_{max}$ parameter in Table F.9.

| **Subcatchment** | $\alpha$ (%) | $\beta$ (%) | $I_{max}$ |
|---|---|---|---|
| Gulp | 15 | 78 | 1.08 - 3.09 |
| Eyserbeek | 5 | 76 | 0.86 - 2.53 |
| Selzerbeek | 20 | 65 | 1.05 - 2.95 |
| Sippenaeken | 22 | 61 | 1.05 - 2.93 |
| Hommerich | 33 | 60 | 1.26 - 3.45 |
| Meerssen | 19 | 64 | 1.02 - 2.87 |

Table F.9: The $I_{max}$ parameter interval derived per subcatchment. $\alpha$ is the percentage of forest in the subcatchemnt and $\beta$ is the percentage of cropland and grassland.

### F.3.2. $S_{u,max}$

The root zone storage capacity is the maximum volume of water that can be held against gravity in the pores of the the unsaturated zone and which is accessible for the roots of vegetation (Bouaziz et al., 2022). The roots of the plants ensure access to water in case of dry spells (Hrachowitz et al., 2021). The water use of the vegetation can be measured by evaporation, as vegetation uses water to transpire (Bouaziz et al., 2022). The root zone storage capacity can be calculated by the water balance of the soil. The capacity can be estimated by calculating the maximum yearly water deficit. The storage deficit is estimated by calculating the cumulative difference between daily precipitation and evaporation data. The corresponding equation is presented in Equation (F.2). The storage deficit can not be larger than zero, because excess water is released when the soil is full. The maximum root zone capacity is determined by the minimum value of the cumulative storage deficit, as in Equation (F.3).

$$S_{u,t} = min\left(0, \int_{T_0}^{T_1} (P_E(t) - E_R(t))\, dt\right) \tag{F.2}$$

$$S_{u,max} = min(S_{u,t}) \tag{F.3}$$

Daily precipitation data per subcatchment is used from the Nationale Regenradar (NRR) (Schuurmans & van Vossen, 2013). ERA5 actual evaporation data is used for the daily evaporation (Muñoz Sabater, 2019). This data showed correspondence to the potential evaporation data of the KNMI Maastricht weather station. The ERA5 data accounts for spatial variability over the subcatchments. The result of the maximum root zone storage capacities per subcatchment is presented in Figure F.22. It can clearly be seen that 2018 and 2019 were dry years in the Netherlands, as the maximum storage defecit occurs in these years.

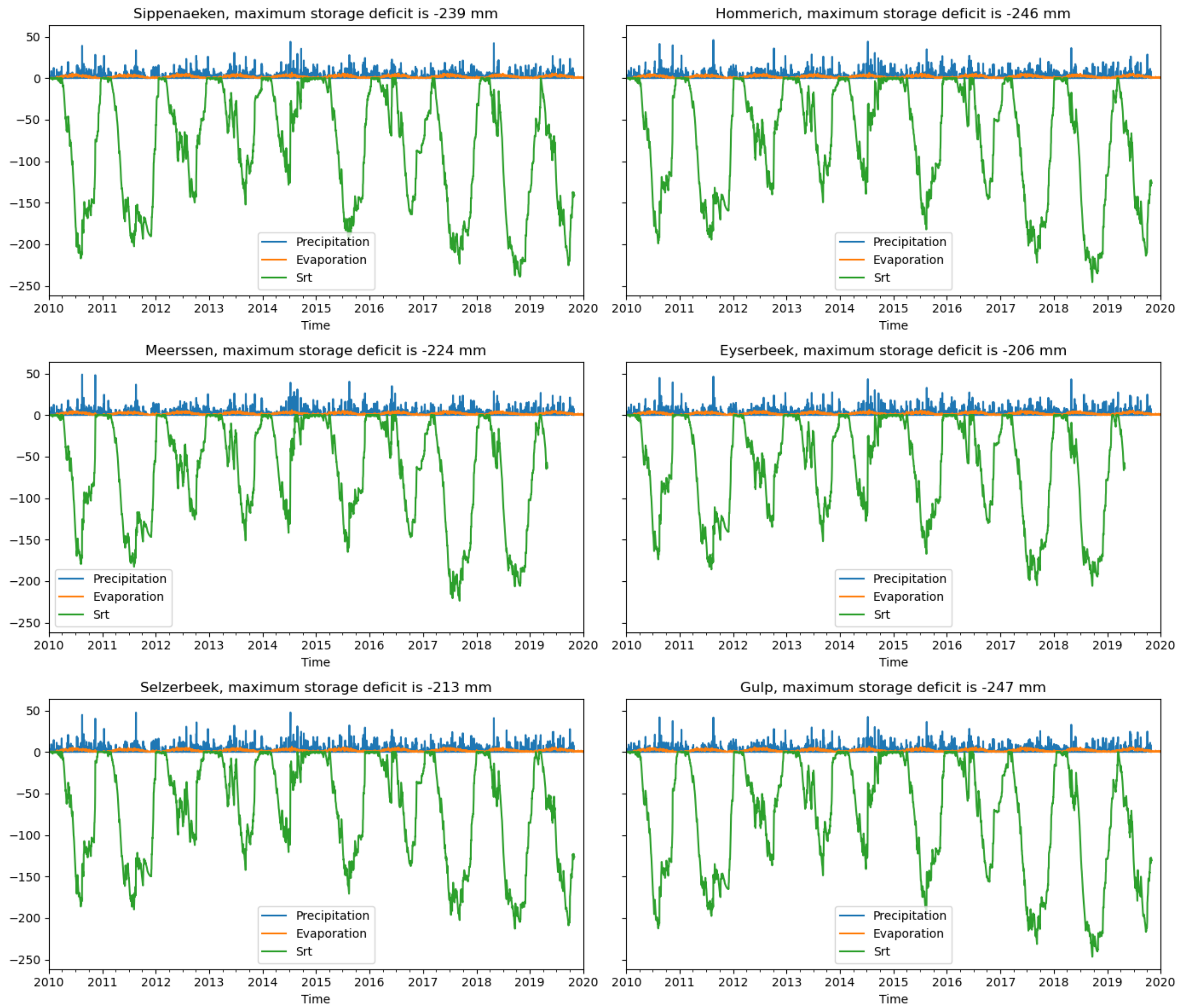


Figure F.22: Maximum storage deficit calculation per subcatchment.

The root zone capacities varies a little over the subcatchments. The difference between Eyserbeek and Gulp is 41 millimeter, which is 25% of the deficit of the Eyserbeek subcatchment. To account for uncertainties in the observations and radar resolutions and to give calibration freedom, a range of ±25% is applied to the estimated maximum storage deficits. The intervals for the $S_{u,max}$ parameter are given in Table F.10.

| | Gulp | Eyserbeek | Selzerbeek | Sippenaeken | Hommerich | Meerssen |
|---|---|---|---|---|---|---|
| **Minimum** | 185 | 155 | 160 | 179 | 185 | 168 |
| **Estimated** | 247 | 206 | 213 | 239 | 246 | 224 |
| **Maximum** | 309 | 258 | 266 | 299 | 308 | 280 |

Table F.10: Parameter intervals per subcatchment for the $S_{u,max}$ parameter.

### F.3.3. $K_s$

The saturated storage coefficient, $K_s$, determines the outflow from the saturated reservoir. The larger the parameter, the larger the groundwater flow per timestep. The slow reacting subcatchments Meerssen and Hommerich, will have a larger $K_s$ value than the fast reacting subcatchments as Eyserbeek and Selzerbeek. The saturated storage coefficient can be estimated by a Master Recession Curve (MRC) (Fenicia, Savenije, Matgen, & Pfister, 2006). A MRC contains all recession curves on top of each other in a graph and a pattern emerges. The recession curves are the declining parts of the hydrographs, where no precipitation occurs. The $K_s$ parameter is determined by the slope of the pattern line. The parameters per subcatchment are derived by the measured discharge and the Matlab tool of Carlotto and Chaffe (2019). The graphs and the corresponding estimated values are visualized in Figure F.23. A uncertainty range of 10% is applied to the $K_s$ interval to account for uncertainties in the parameter estimation. The parameter interval per subcatchment is given in Table F.11.

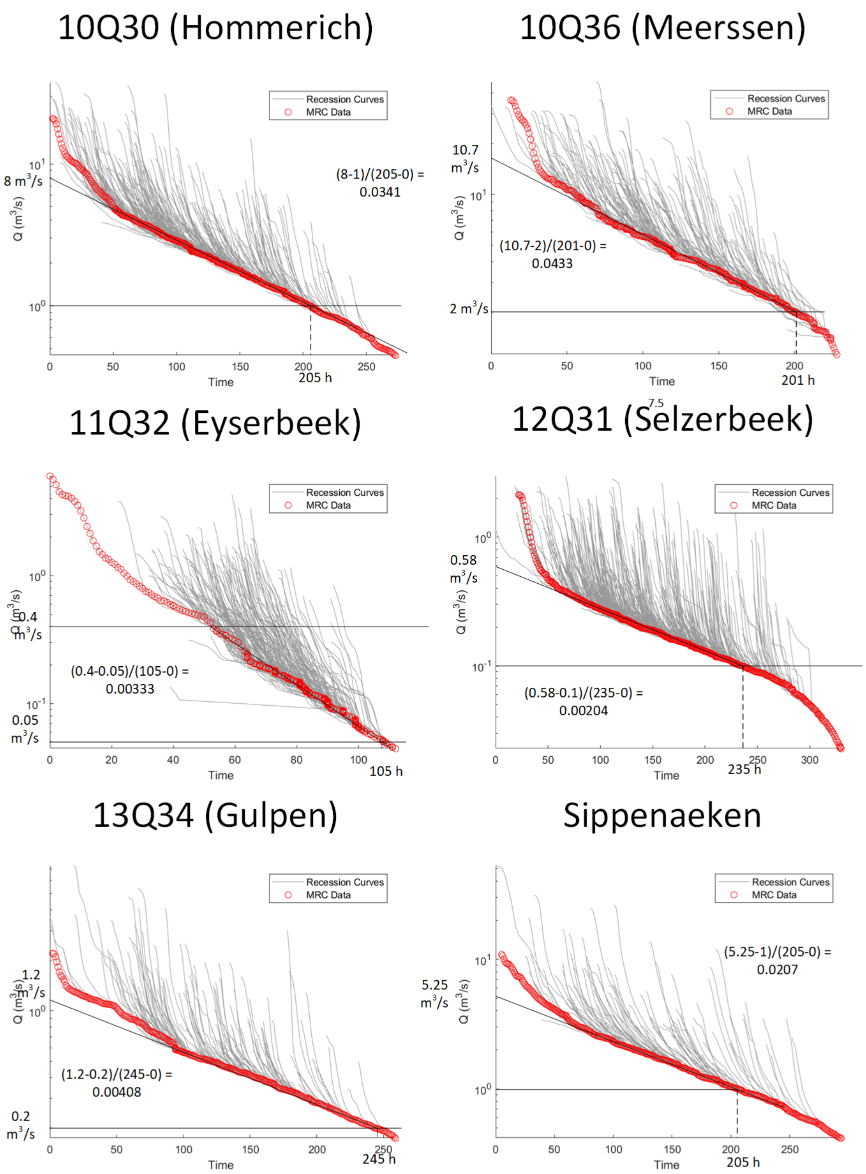


Figure F.23: MRC plots per subcatchment and their derived $K_s$ value.

| | Gulp | Eyserbeek | Selzerbeek | Sippenaeken | Hommerich | Meerssen |
|---|---|---|---|---|---|---|
| **Minimum** | 0.00367 | 0.00300 | 0.00184 | 0.0186 | 0.0307 | 0.0390 |
| **Estimated** | 0.00408 | 0.00333 | 0.00204 | 0.0207 | 0.0341 | 0.0433 |
| **Maximum** | 0.00449 | 0.00366 | 0.00224 | 0.0228 | 0.0375 | 0.0476 |

Table F.11: Parameter intervals per subcatchment for the $K_s$ parameter.

### F.3.4. $T_{lag}$

The parameter $T_{lag}$ determines how the calculated discharge is released over time to account for travelling times. The parameter estimation is based on the response times per subcatchment in Section 2.5. Figure F.24 visualises the derivation. The response time is given as the time between the peak of a precipitation event and the corresponding discharge peak. $T_{lag}$ is equal to two times the response time. The result per subcatchment is given in Table F.12. The range for Gulp, Eyserbeek, and Selzerbeek are increased to account for uncertainty.

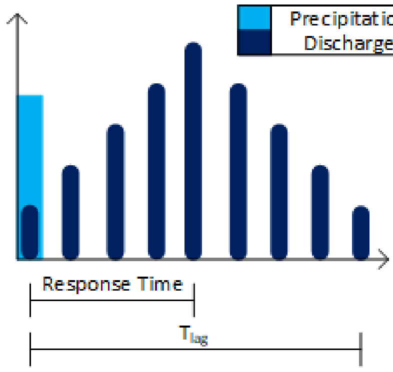


Figure F.24: Derivation of the $T_{lag}$ parameter, based on the response time.

| Subcatchment | Response Time | $T_{lag}$ |
|---|---|---|
| Gulp | 2 | 3 - 5 |
| Eyserbeek | 1 | 1 - 3 |
| Selzerbeek | 1 | 1 - 3 |
| Sippenaeken | 2 - 4 | 4 - 8 |
| Hommerich | ? | 4 - 10 |
| Meerssen | 4 - 10 | 8 - 20 |

Table F.12: $T_{lag}$ estimation per subcatchment.

### F.3.5. Final Parameter Intervals

Table F.13 presents the final parameter intervals for the second calibration run. The above described parameter constraints by literature and observations are added to the table. These parameters are $I_{max}$, $S_{u,max}$, $T_{lag}$, and $K_s$. The other parameters are constraint by the calculated NSE in the dotty plots. It can be seen that some parameters in Table F.13 are red colored. This means that the estimated parameter intervals are adjusted and are no longer equal to the determined intervals. An example is given in Figure F.25. It can be seen that for consecutive precipitation events, the outflow is overestimated for the subcatchment Selzerbeek. This is the result of a too small root zone capacity parameter and the parameter interval is adjusted.

| | | $I_{max}$ | $C_e$ | $S_{u,max}$ | $\beta$ | $P_{max}$ | $T_{lag}$ | $K_f$ | $K_s$ |
|---|---|---|---|---|---|---|---|---|---|
| **Gulp** | Min | 1.08 | 0.4 | 500 | 3.0 | 0.04 | 3.0 | 0.02 | 0.00367 |
| | Max | 3.09 | 1.0 | 900 | 6.0 | 0.07 | 10 | 0.07 | 0.00449 |
| **Eyserbeek** | Min | 0.86 | 0.8 | 800 | 4.0 | 0.005 | 4.0 | 0.05 | 0.003 |
| | Max | 2.53 | 1.0 | 1200 | 8.0 | 0.02 | 7.0 | 0.15 | 0.00366 |
| **Selzerbeek** | Min | 1.05 | 0.2 | 500 | 2.0 | 0.01 | 8.0 | 0.03 | 0.00184 |
| | Max | 2.95 | 0.8 | 800 | 8.0 | 0.05 | 14 | 0.10 | 0.00224 |
| **Sippenaeken** | Min | 1.05 | 0.5 | 179 | 2.5 | 0.02 | 4.0 | 0.03 | 0.0186 |
| | Max | 2.93 | 0.7 | 299 | 3.5 | 0.06 | 8.0 | 0.06 | 0.0228 |
| **Hommerich** | Min | 1.26 | 0.7 | 500 | 4.0 | 0.30 | 4.0 | 0.01 | 0.0307 |
| | Max | 3.45 | 1.0 | 800 | 10 | 0.60 | 10 | 0.01 | 0.10 |
| **Meerssen** | Min | 1.02 | 0.1 | 168 | 2.0 | 0.002 | 16 | 0.05 | 0.039 |
| | Max | 2.87 | 0.5 | 280 | 10 | 0.10 | 60 | 0.10 | 0.0476 |

Table F.13: The final parameter intervals for run 2. The parameters in red are constraint by literature or observations, but the modelled result did not match the observations and the interval is changed.

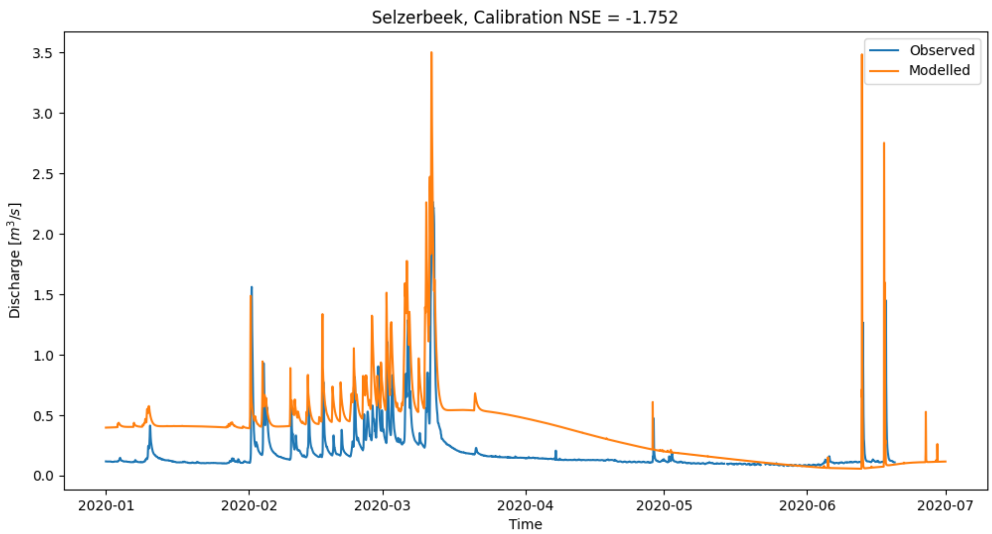


Figure F.25: Example of parameter constraints for the Selzerbeek. It can be seen that a too small $S_{u,max}$ parameter lead to an overestimation of the modelled discharge in wet periods.

# F.4. Run 2: Parameter Constraints

The results of the second run after applying parameter constraints is given in Table F.14. It can be seen that the NSE calibration values clearly improved, except for Hommerich. However, this results in lower NSE validation values. The best parameterset, the calibration period, parameters plot, and validation period per subcatchment are given in the next subsections.

| | NSEcal 1 | NSEcal 2 | NSEval 1 | NSEval 2 |
|---|---|---|---|---|
| **Gulp** | 0.736 | 0.753 | 0.418 | 0.289 |
| **Eyserbeek** | 0.575 | 0.704 | 0.340 | 0.166 |
| **Selzerbeek** | 0.804 | 0.864 | 0.113 | 0.253 |
| **Sippenaeken** | 0.870 | 0.879 | 0.620 | 0.526 |
| **Hommerich** | 0.844 | 0.840 | - | - |
| **Meerssen** | 0.774 | 0.782 | - | - |

Table F.14: The differences in the NSE values between the random parameter intervals in run 1 and the constraint parameter intervals in run 2.

### F.4.1. Gulp

| $I_{max}$ | $C_e$ | $S_{u,max}$ | $\beta$ | $P_{max}$ | $T_{lag}$ | $K_f$ | $K_s$ |
|---|---|---|---|---|---|---|---|
| 2.02 | 0.747 | 631.7 | 5.23 | 0.0483 | 6.39 | 0.0438 | 0.00394 |

Table F.15: Best parameterset for the Gulp subcatchment for run 2.

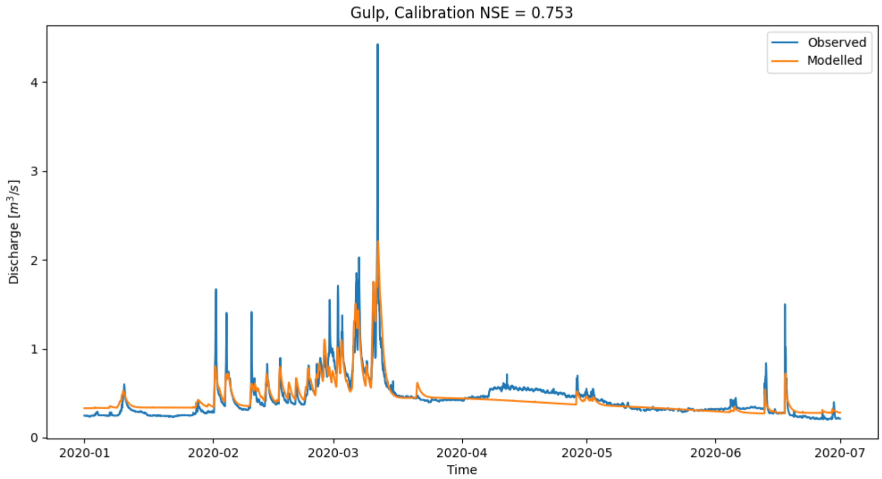


Figure F.26: Modelled discharge in the calibration period for the Gulp subcatchment for run 2.

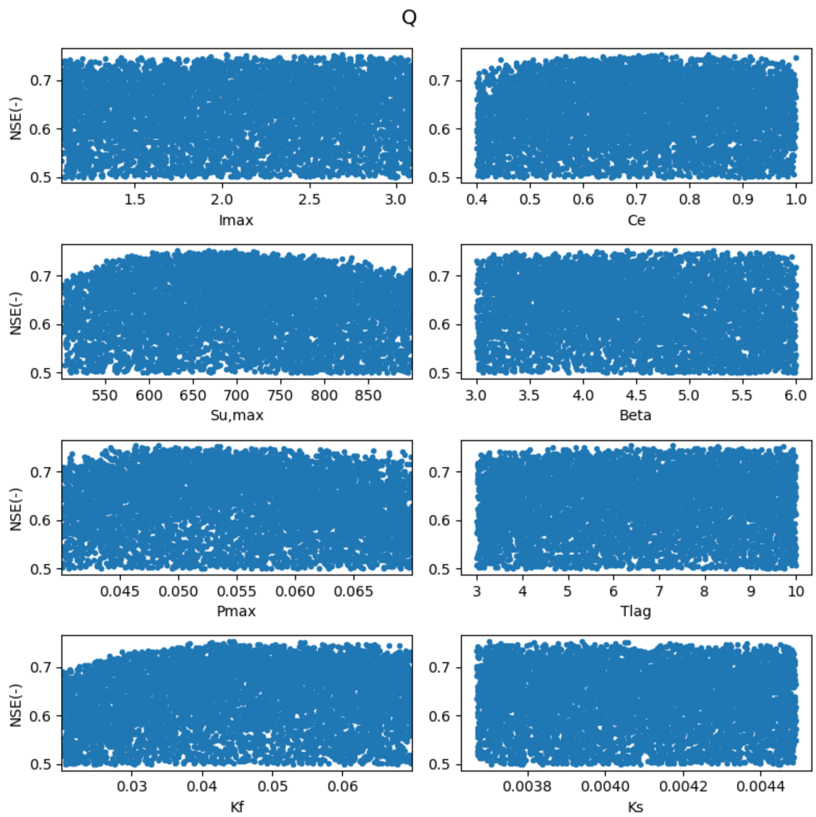


Figure F.27: Dotty plots for the Gulp subcatchment for run 2.

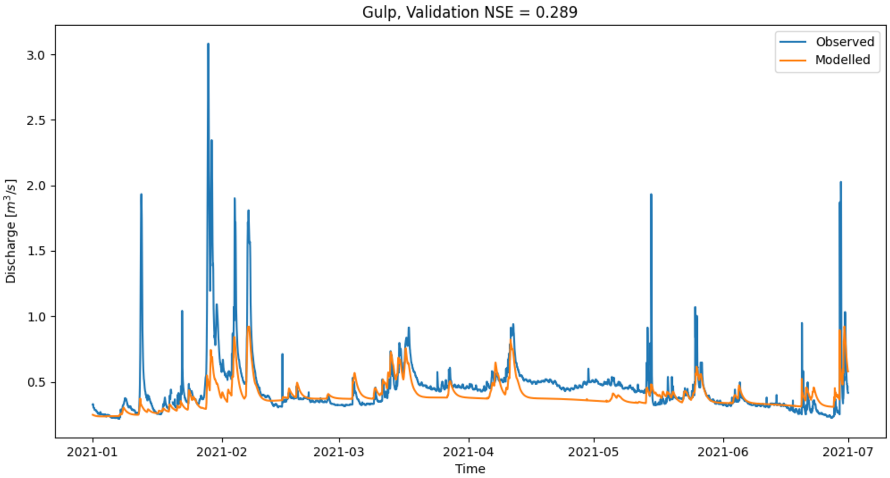


Figure F.28: Modelled discharge in the validation period for the Gulp subcatchment for run 2.

## F.4.2. Eyserbeek

| $I_{max}$ | $C_e$ | $S_{u,max}$ | $\beta$ | $P_{max}$ | $T_{lag}$ | $K_f$ | $K_s$ |
|---|---|---|---|---|---|---|---|
| 1.24 | 0.995 | 922.5 | 6.14 | 0.0140 | 5.05 | 0.0954 | 0.00330 |

Table F.16: Best parameterset for the Eyserbeek subcatchment for run 2.

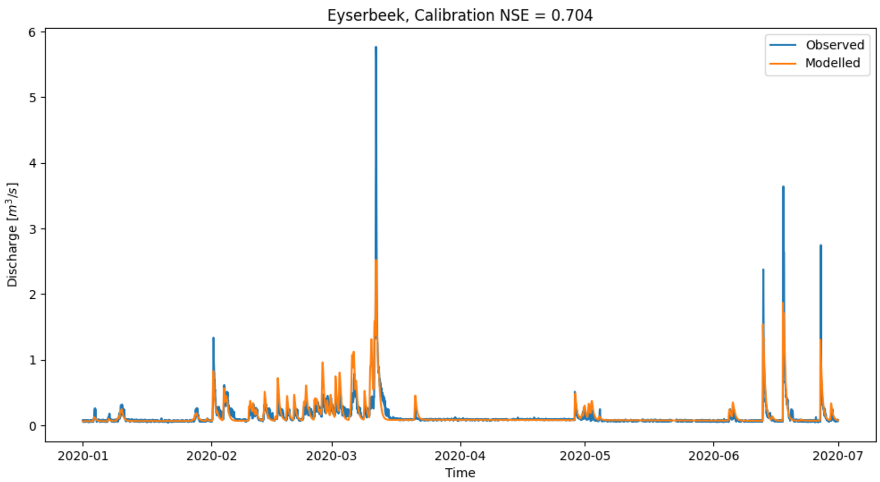


Figure F.29: Modelled discharge in the calibration period for the Eyserbeek subcatchment for run 2.

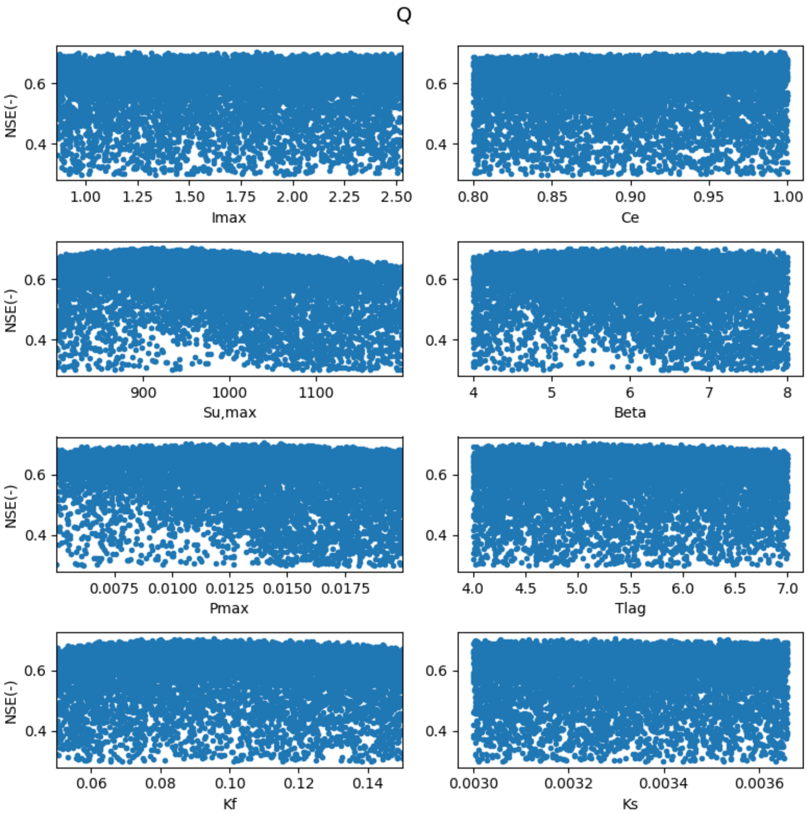


Figure F.30: Dotty plots for the Eyserbeek subcatchment for run 2.

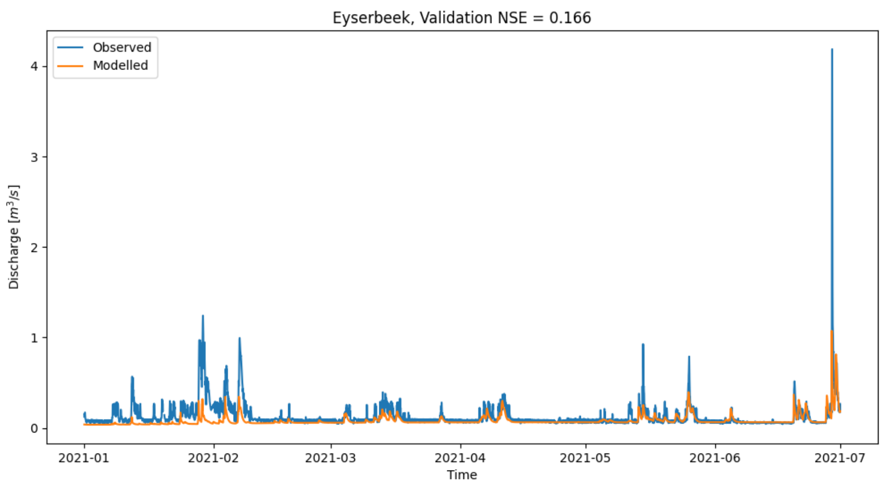


Figure F.31: Modelled discharge in the validation period for the Eyserbeek subcatchment for run 2.

### F.4.3. Selzerbeek

| $I_{max}$ | $C_e$ | $S_{u,max}$ | $\beta$ | $P_{max}$ | $T_{lag}$ | $K_f$ | $K_s$ |
|---|---|---|---|---|---|---|---|
| 1.12 | 0.412 | 703.6 | 4.20 | 0.0298 | 10.6 | 0.0622 | 0.00221 |

Table F.17: Best parameterset for the Selzerbeek subcatchment for run 2.

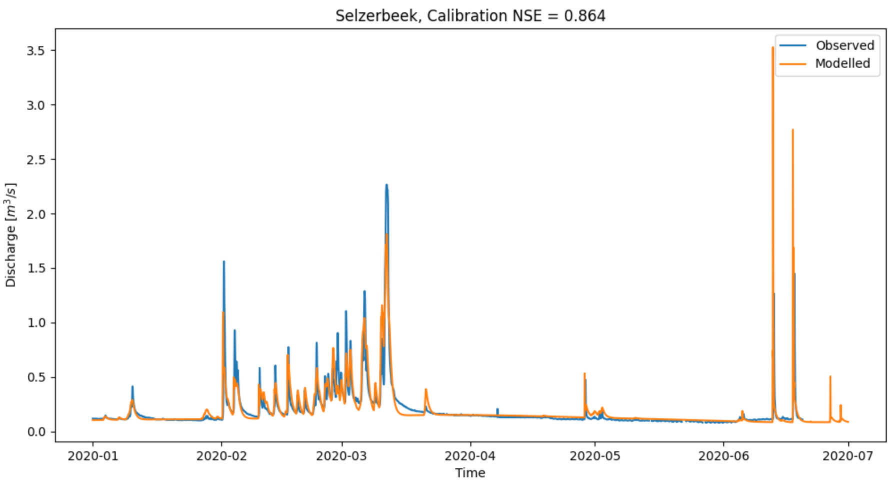


Figure F.32: Modelled discharge in the calibration period for the Selzerbeek subcatchment for run 2.

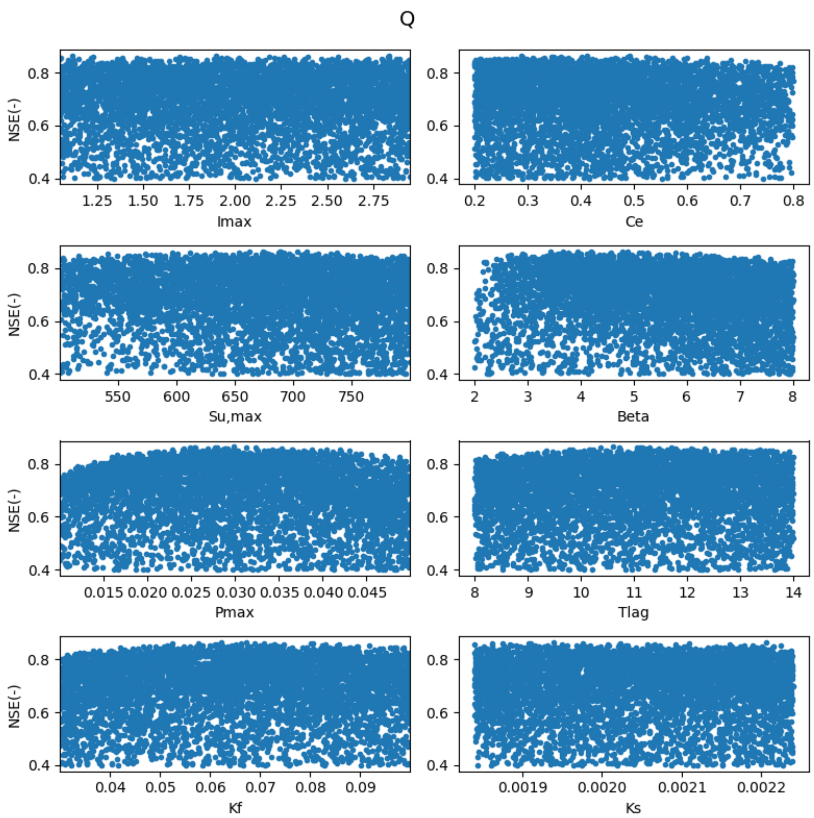


Figure F.33: Dotty plots for the Selzerbeek subcatchment for run 2.

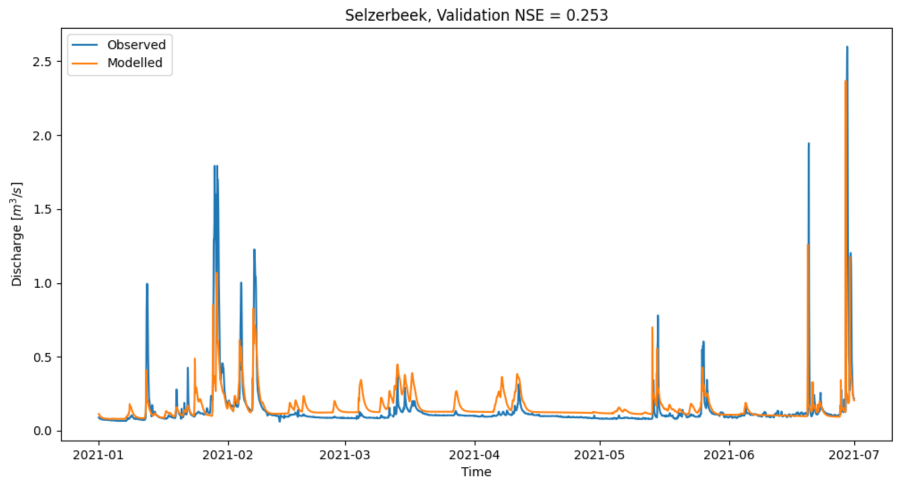


Figure F.34: Modelled discharge in the validation period for the Selzerbeek subcatchment for run 2.

## F.4.4. Sippenaeken

| $I_{max}$ | $C_e$ | $S_{u,max}$ | $\beta$ | $P_{max}$ | $T_{lag}$ | $K_f$ | $K_s$ |
|---|---|---|---|---|---|---|---|
| 1.17 | 0.609 | 274.4 | 2.64 | 0.0347 | 7.75 | 0.0398 | 0.0196 |

Table F.18: Best parameterset for the Sippenaeken subcatchment for run 2.

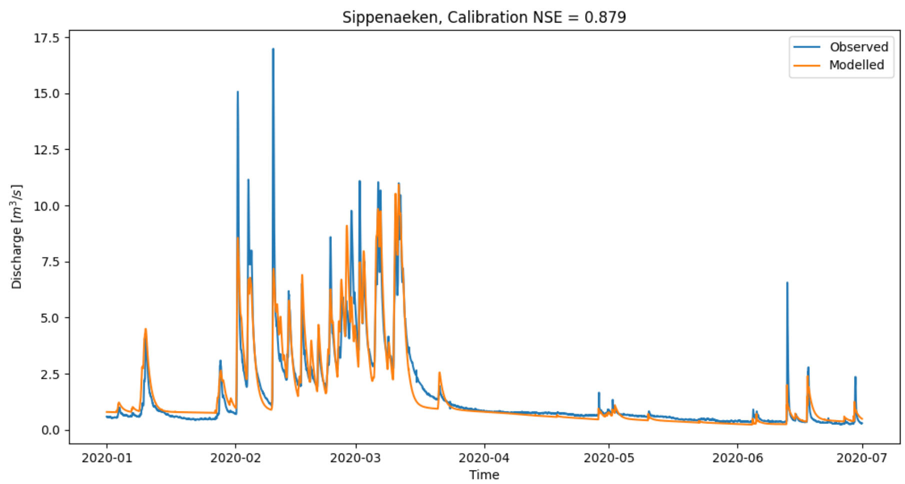


Figure F.35: Modelled discharge in the calibration period for the Sippenaeken subcatchment for run 2.

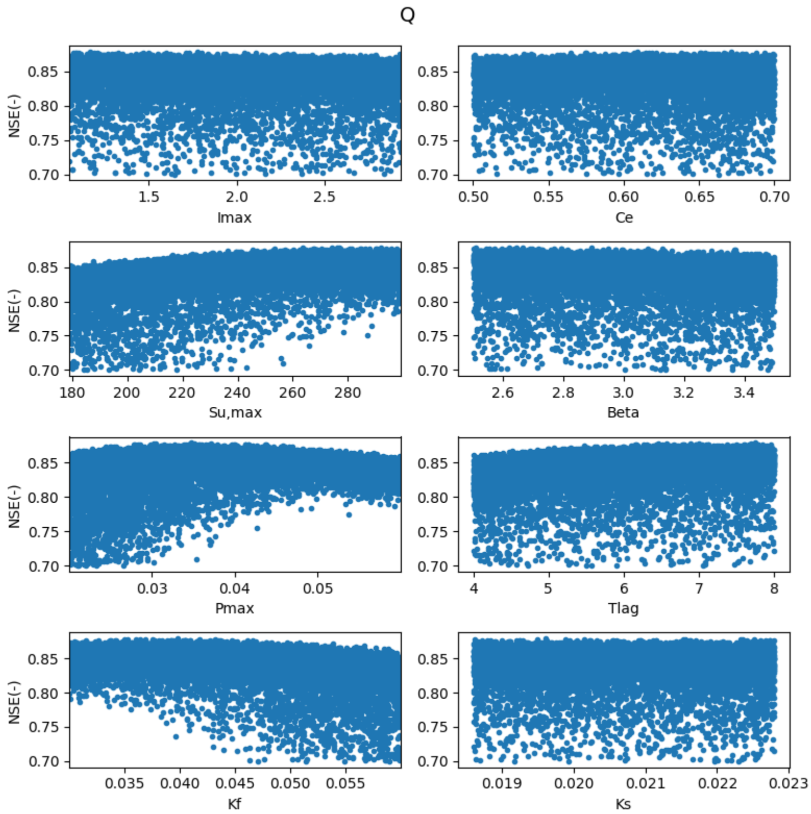


Figure F.36: Dotty plots for the Sippenaeken subcatchment for run 2.

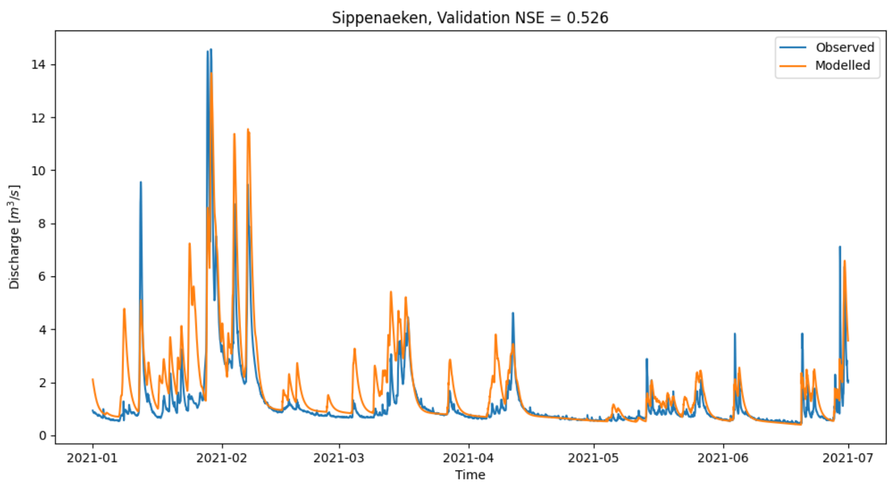


Figure F.37: Modelled discharge in the validation period for the Sippenaeken subcatchment for run 2.

### F.4.5. Hommerich

| $I_{max}$ | $C_e$ | $S_{u,max}$ | $\beta$ | $P_{max}$ | $T_{lag}$ | $K_f$ | $K_s$ |
|---|---|---|---|---|---|---|---|
| 1.28 | 0.905 | 794.0 | 7.28 | 0.512 | 9.51 | 0.0942 | 0.0321 |

Table F.19: Best parameterset for the Hommerich subcatchment for run 2.

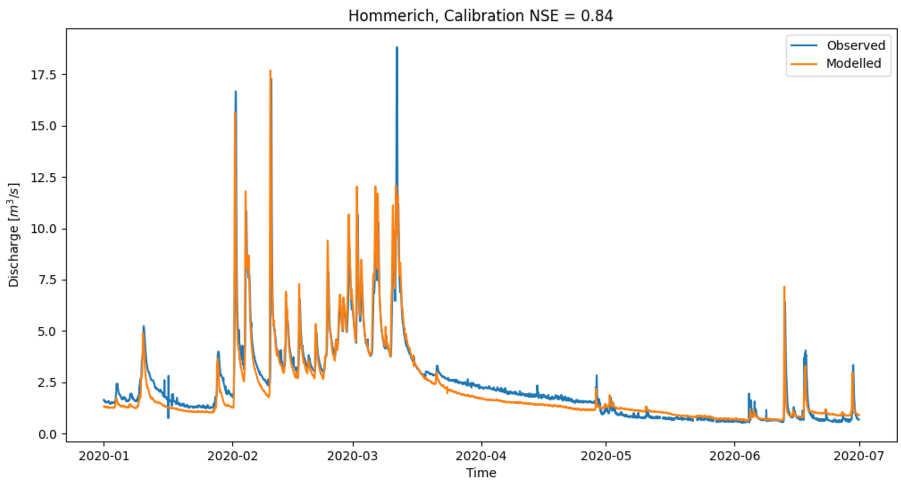


Figure F.38: Modelled discharge in the calibration period for the Hommerich subcatchment for run 2.

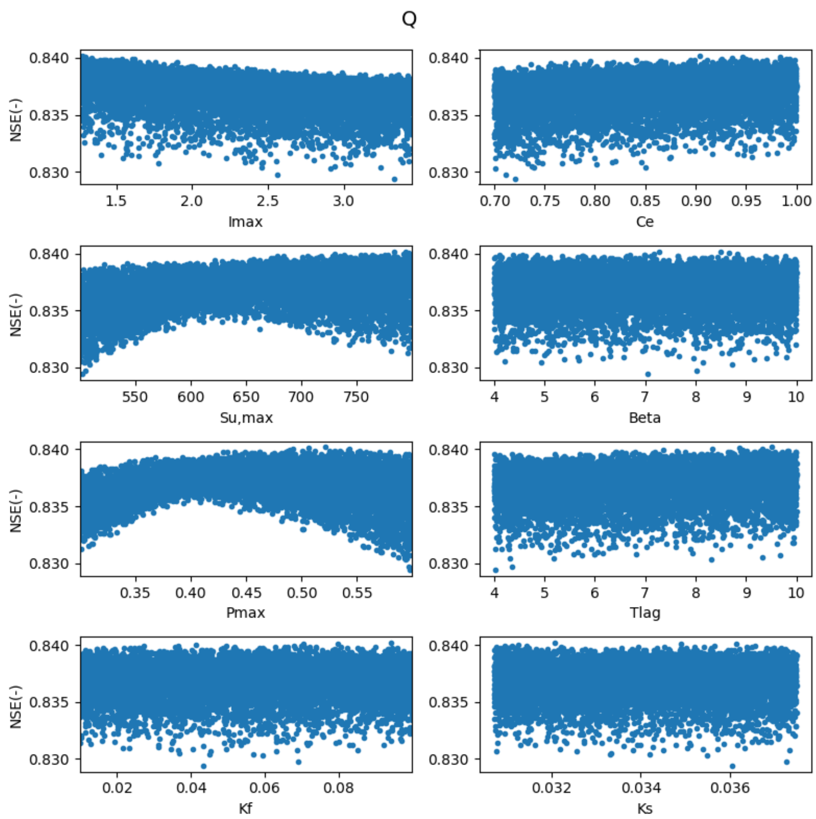


Figure F.39: Dotty plots for the Hommerich subcatchment for run 2.

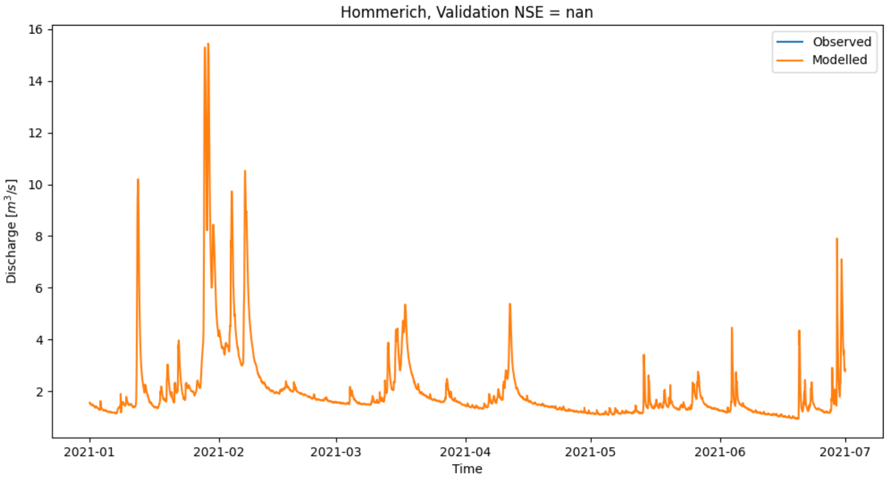


Figure F.40: Modelled discharge in the validation period for the Hommerich subcatchment for run 2.

### F.4.6. Meerssen

| $I_{max}$ | $C_e$ | $S_{u,max}$ | $\beta$ | $P_{max}$ | $T_{lag}$ | $K_f$ | $K_s$ |
|---|---|---|---|---|---|---|---|
| 1.78 | 0.276 | 276.4 | 7.52 | 0.0678 | 33.4 | 0.0643 | 0.0450 |

Table F.20: Best parameterset for the Meerssen subcatchment for run 1.

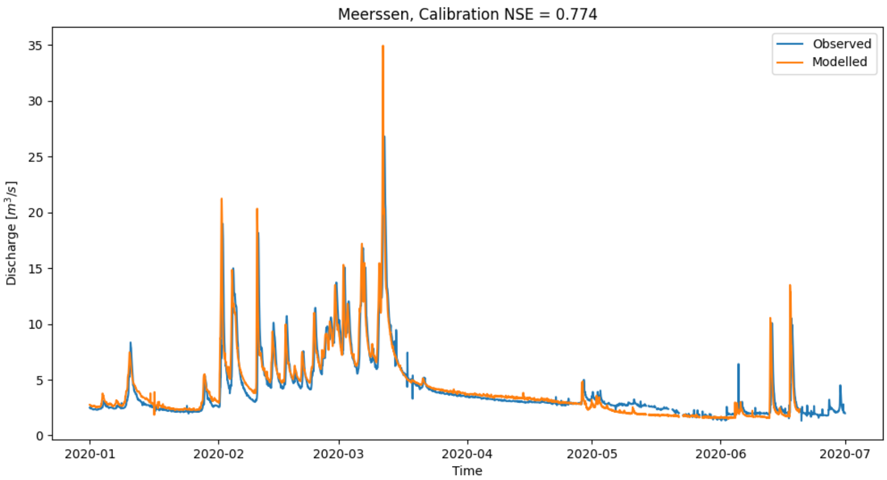


Figure F.41: Modelled discharge in the calibration period for the Meerssen subcatchment for run 1.

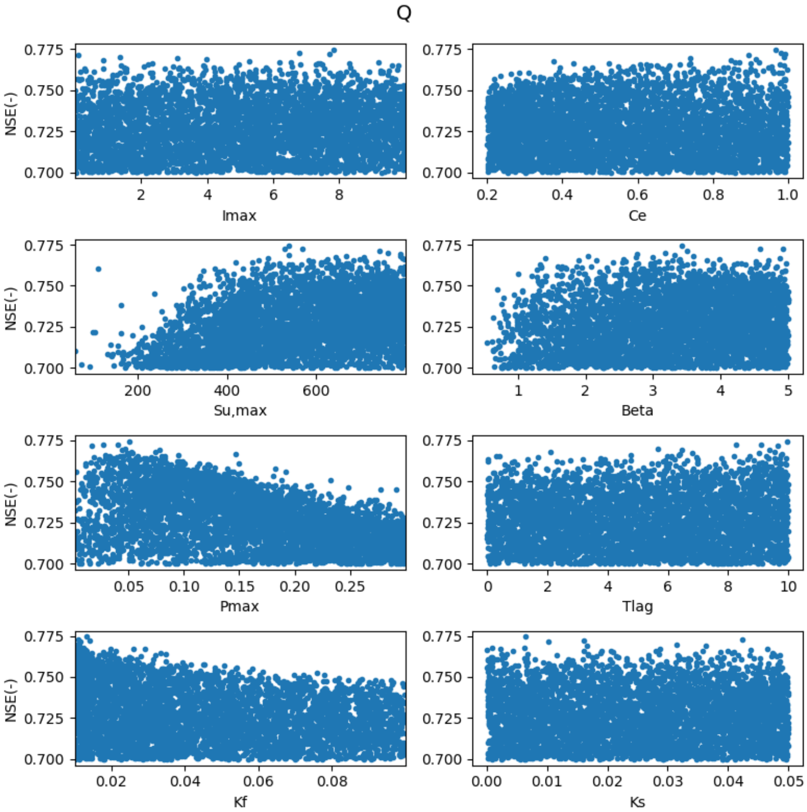


Figure F.42: Dotty plots for the Meerssen subcatchment for run 1.

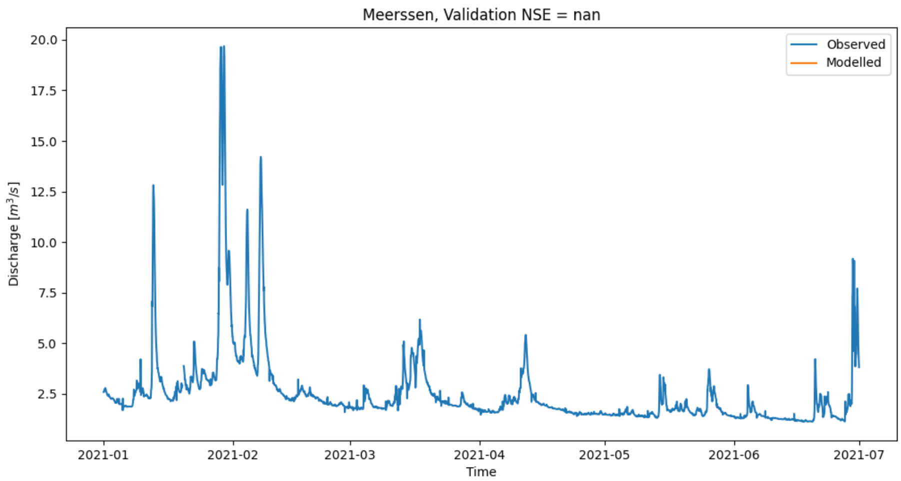


Figure F.43: Modelled discharge in the validation period for the Meerssen subcatchment for run 1.

# G Results

This appendix shows the results per scenario. Appendix G.1 contains the hydrographs per scenario. Chapter 4 summarizes the results and describes the differences between the scenarios.

## G.1. Scenario Hydrographs

### G.1.1. Scenario 2a1

Scenario 2a1 simulates an increase of 6 $km^2$ paved area to the villages close to the Geul in the Meerssen subcatchment. This results in the hydrographs in Figure G.1, where only the discharge at Meerssen and Schin op Geul changes. The increase in paved area results in more discharge and faster reacting at the start of the July2021 precipitation event for HBV and D-RR. The results for Wflow_sbm show little change. The timing of the peak discharge does not change for the models, but it can be seen that the discharge is faster generated at Meerssen for HBV and D-RR. The peak discharge increased by 0.2 $m^3/s$ for Wflow_sbm at both measurement locations. On the other hand, the peak discharge decreased at Meerssen by 0.8 $m^3/s$ for HBV and D-RR. The peak discharge depends mostly on subsurface flow for HBV and D-RR. The increased paved area results in less infiltration and therefore less subsurface flow.

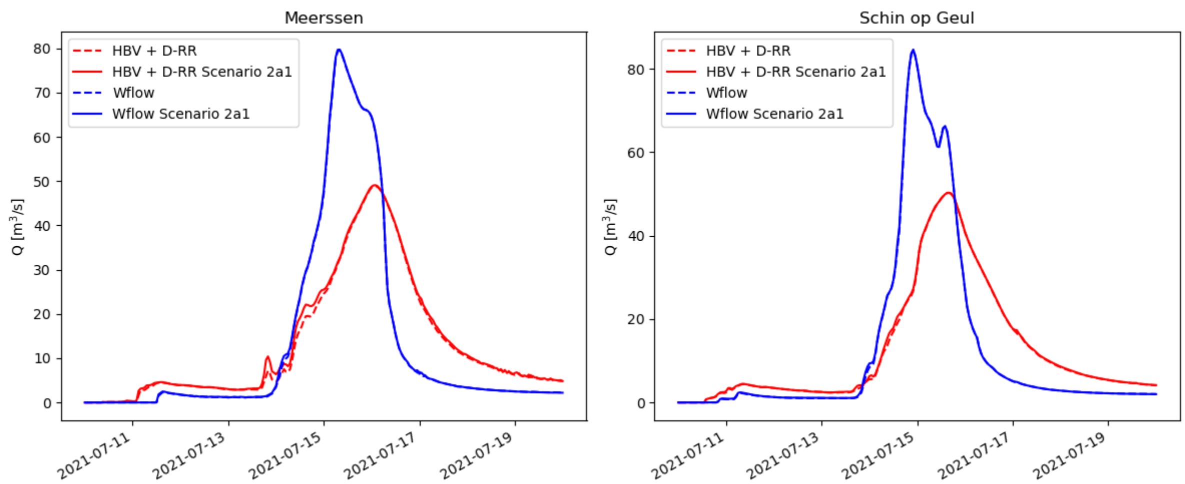


Figure G.1: Hydrographs of Scenario 2a1 compared to the base hydrological models.

### G.1.2. Scenario 2a2

Scenario 2a2 simulates an increase of 6 km$^2$ paved area to the villages far from the Geul in the Meerssen subcatchment. This results in the hydrographs in Figure G.2 The increase in paved area results, like scenario 2a1, in more discharge and faster reacting at the start of the July2021 precipitation event for HBV and D-RR. The peak discharges decreases by 0.1 - 0.2 m$^3$/s at the measurement locations and arrives 1 hour earlier at Schin op Geul. For Wflow_sbm, the peak discharge at Meerssen increases by 0.2 m$^3$/s and arrives 1 hour earlier. The peak discharge at Schin op Geul decreases by 0.2 m$^3$/s and the timing does not change.

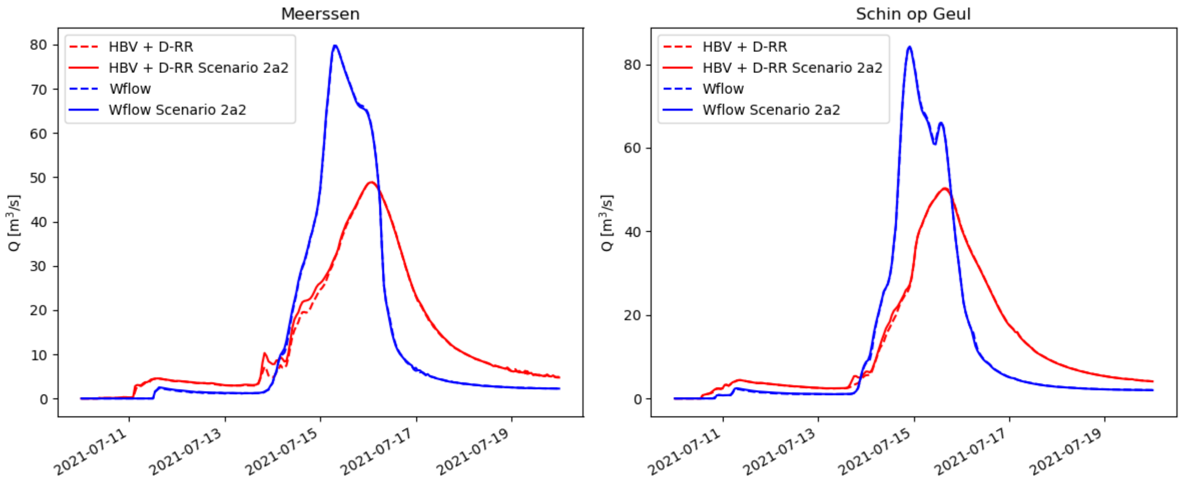


Figure G.2: Hydrographs of Scenario 2a2 compared to the base hydrological models.

### G.1.3. Scenario 2b1

Scenario 2b1 simulates an increase of 6 km$^2$ paved area to villages close to the Gulp tributary in the Gulp subcatchment. This results in the hydrographs in Figure G.3 for Meerssen, Schin op Geul, and Azijnfabriek. The discharge behaviour of the Gulp completely changes for HBV and D-RR and shows more similar behaviour to Wflow_sbm. The reason for this is the increased overland flow by the increased paved area. The peak discharge at Azijnfabriek increases by 5 m$^3$/s and occurs 18 hours earlier than in the base HBV and D-RR. This results in a faster discharge generation at Schin op Geul and Meerssen. The peak discharge occurs 2 hours earlier at Schin op Geul and 1 hour earlier at Meerssen. The peak discharges increase by 0.2 m$^3$/s at Schin op Geul and 0.4 m$^3$/s at Meerssen. Wflow_sbm shows an increase of 0.4 m$^3$/s at Azijnfabriek, without a change in timing of the peak. The peak discharge at Schin op Geul increases by 0.5 m$^3$/s, with no change in timing. Lastly, the peak discharge at Meerssen increases by 0.4 m$^3$/s and occurs 1 hour earlier. The change in peak discharge at Schin op Geul is larger than at Azijnfabriek, while the paved area is increases in the Gulp subcatchment. This is, because the city of Gulpen is next to the Gulp and Geul and therefore directly runoffs to Geul. Because of this, an expansion of Gulpen will result in an increased discharge in the Geul at Schin op Geul.

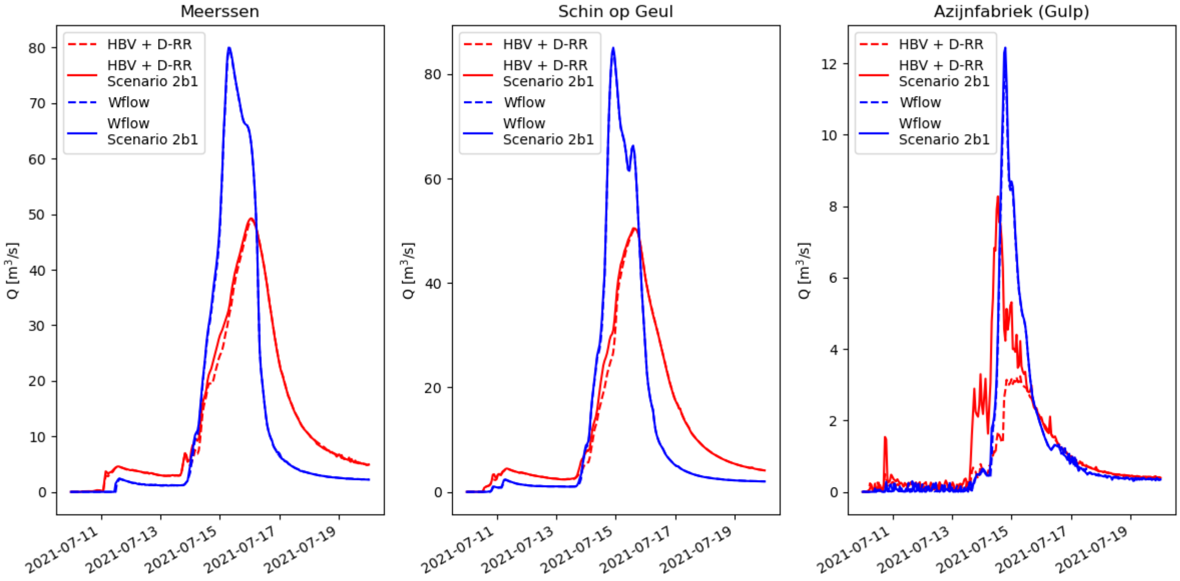


Figure G.3: Hydrographs of Scenario 2b1 compared to the base hydrological models.

## G.1.4. Scenario 2b2

Scenario 2b2 simulates an increase of 6 km$^2$ paved area to the villages far from the Gulp tributary in the Gulp subcatchment. This results in the hydrographs in Figure G.4. For HBV and D-RR, the discharge behaviour at Azijnfabriek changes completely, and the discharge generation is faster at Schin op Geul and Meerssen. The changes in the response for Wflow_sbm are visibly small. The change in discharge behaviour is the same as for Scenario 2b1, however the change in the magnitude and timing of the peak discharges is different. The peak discharge at Azijnfabriek increased by 4 m$^3$/s and occurs 18 hours earlier for HBV and D-RR. The change of the peak discharge is negligible small for Wflow_sbm. At Schin op Geul, the peak discharge decreased by 0.2 m$^3$/s for HBV and D-RR, while the peak discharge increased by 0.2 m$^3$/s for Wflow_sbm. The timing of both peak discharges did not change. The peak discharge occurs 1 hour earlier at Meerssen for both models. However, the peak discharge increases by 0.2 m$^3$/s for Wflow_sbm and is approximately the same for HBV and D-RR.

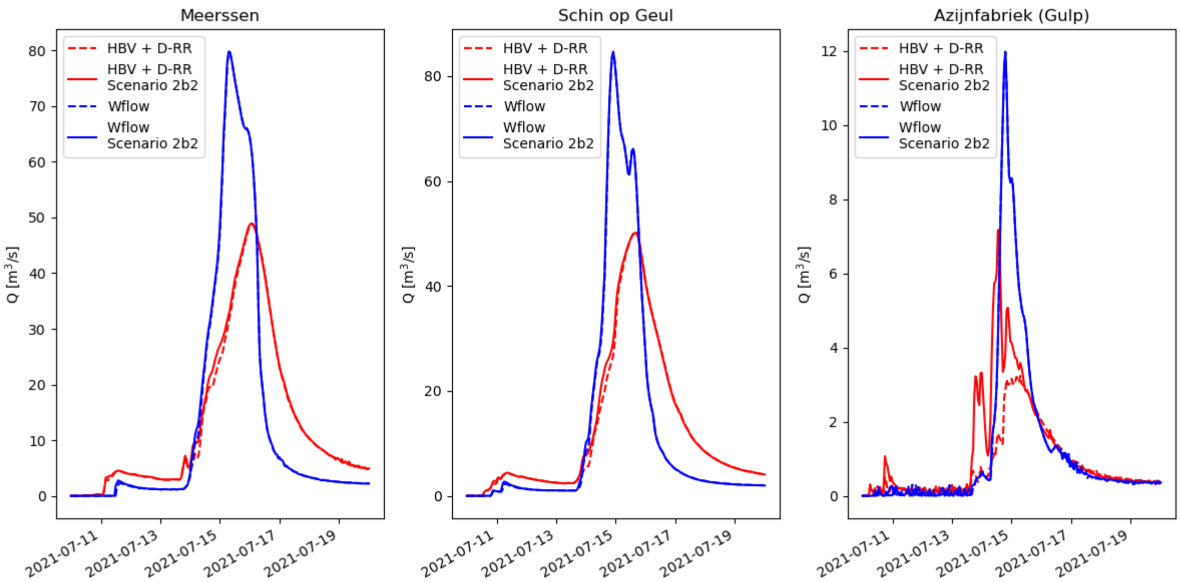


Figure G.4: Hydrographs of scenario 2b2 compared to the base hydrological models.